



UNIVERSIDADE DE LISBOA

INSTITUTO SUPERIOR TÉCNICO

Real-time control for long ohmic alternate current discharges

Ivo Samuel Lages Militão da Silva Carvalho

Supervisor: Doctor Horácio João Matos Fernandes

Co-supervisor: Doctor Carlos Alberto Nogueira Garcia da Silva

Thesis approved in public session to obtain the PhD Degree in

Technological Physics Engineering

Jury final classification: Pass with Merit

Jury

Chairperson: Chairman of the IST Scientific Board

Members of the Committee:

Doctor Carlos António Abreu Fonseca Varandas
Doctor Leonardo Giudicotti
Doctor Horácio João Matos Fernandes
Doctor Bernardo Brotas de Carvalho
Doctor Martin Hron

2013



UNIVERSIDADE DE LISBOA

INSTITUTO SUPERIOR TÉCNICO

Università degli Studi di Padova
Joint European Research Doctorate in Fusion Science and Engineering

Real-time control for long ohmic alternate current discharges

Ivo Samuel Lages Militão da Silva Carvalho

Supervisor: Doctor Horácio João Matos Fernandes

Co-supervisor: Doctor Carlos Alberto Nogueira Garcia da Silva

Thesis approved in public session to obtain the PhD Degree in

Technological Physics Engineering

Jury final classification: Pass with Merit

Jury

Chairperson: Chairman of the IST Scientific Board

Members of the Committee:

Doctor Carlos António Abreu Fonseca Varandas, Professor Catedrático do Instituto Superior Técnico, da Universidade de Lisboa;

Doctor Leonardo Giudicotti, Professor Associado, Università degli Studi di Padova, Itália;

Doctor Horácio João Matos Fernandes, Professor Auxiliar (com Agregação) do Instituto Superior Técnico, da Universidade de Lisboa;

Doctor Bernardo Brotas de Carvalho, Professor Auxiliar do Instituto Superior Técnico, da Universidade de Lisboa;

Doctor Martin Hron, Senior Researcher, Institute of Plasma Physics, Academy of Sciences, Czech Republic.

Abstract

The ISTTOK tokamak ($I_p = 4\text{-}8 \text{ kA}$, $B_T = 0.4\text{-}0.8 \text{ T}$, $R = 0.46 \text{ m}$, $a = 0.085 \text{ m}$) is one of the few tokamaks with a regular alternate plasma current (AC) discharges scientific programme. In order to improve the discharge stability and to increase the number and duration of AC discharge cycles a novel control system was developed.

The previous ISTTOK real-time control system based in the PCI hardware was only able to control the plasma position based on the information provided by the Mirnov probes diagnostic. The main aim for this thesis is the upgrade of the ISTTOK control system which was completely redesigned. The novel control system integrates all real-time diagnostics and actuators in order to optimise the plasma discharge parameters by controlling the plasma current, plasma position and gas puffing in real-time during ISTTOK plasma discharges.

The controller acquires data from 50 analogue-to-digital converter (ADC) channels of real-time diagnostics and measurements: tomography, Mirnov coils, interferometer, electric probes, sine and cosine probes, bolometer, current in the power supplies, loop voltage and plasma current. The system has a control cycle of $100 \mu\text{s}$ during which it reads all the diagnostics connected to the Advanced Telecommunications Computing Architecture (ATCA) digitizers and sends the control reference to ISTTOK actuators. The controller algorithms are executed on an Intel Q8200 chip with 4 cores running at 2.33 GHz and connected to the I/O interfaces through an ATCA based environment. The real-time control system was programmed in C++ on top of the Multi-threaded Application Real-Time executor (MARTE). The system also features a user-friendly interface based on HyperText Markup Language (HTML) and JavaScript to configure the controller parameters.

As part of this thesis, the power supplies upgrade is also included. This upgrade consisted in the power increase of the vertical field power supply, the design and construction of a controllable magnetising field power supply and the design of a new control module for all the power supplies.

This update improved the reliability of the AC discharges allowing ISTTOK to operate during more than 1 s with 40 semi-cycles of 25 ms each. The key factors for this achievement were the construction of a controllable magnetising field power supply and the integrated control of several boards on a single crate in an ATCA based environment.

Resumo

O Tokamak ISTTOK ($I_p = 4$ kA, $B_T = 0,5$ T, $R = 0,46$ m, $a = 0,085$ m) é um dos poucos tokamaks com um programa científico regular de descargas com corrente de plasma alternada (AC). A fim de melhorar a estabilidade das descargas e aumentar o número de ciclos por descarga AC foi desenvolvido um novo sistema de controlo. Agora, o sistema de controlo integra todos os diagnósticos e actuadores em tempo real, a fim de optimizar os parâmetros de descarga de plasma, controlando a corrente de plasma, a posição do plasma e a injecção de gás em tempo real durante as descargas do ISTTOK.

O novo sistema de controlo adquire dados de 50 conversores analógico-digitais (ADC) incluindo os diagnósticos de tempo real e as outras medições auxiliares: tomografia, bobinas de Mirnov, interferómetro, sondas elétricas, sondas magnéticas seno e cosseno, bolômetro, corrente nas fontes de alimentação, a tensão de enlace e corrente de plasma. O sistema tem um ciclo de controlo de 100 μ s durante o qual lê todos os diagnósticos ligados aos digitalizadores baseados na tecnologia Advanced Telecommunications Computing Architecture (ATCA) e envia a referência de controlo para os actuadores do ISTTOK. Os algoritmos do controlador são executados num processador Intel Q8200 com 4 núcleos a 2,33 GHz e ligados a um ambiente baseado na tecnologia ATCA. O sistema de controlo em tempo real foi programado em C++ sobre a plataforma de tempo real chamada Multi-threaded Application Real-Time executor (Marte). O sistema possui também uma interface baseada em HyperText Markup Language (HTML) e JavaScript para configurar os parâmetros do controlador.

Como parte integrante desta tese, a atualização fontes de alimentação também está incluída. Esta atualização consiste no aumento das especificações da fonte do campo vertical, a concepção e construção de uma fonte do campo primário e no projeto de um novo módulo de controlo para todas as fontes de corrente do ISTTOK.

Esta atualização melhorou a confiabilidade e estabilidade das descargas AC, permitindo o ISTTOK funcionar durante mais de 1 segundo, com 40 semi-ciclos de aproximadamente 26 ms cada um. Os principais fatores para essa conquista foi a construção de uma fonte de corrente controlável para o campo do primário e o controle integrado dos diagnósticos e actuadores de tempo real num ambiente baseado em ATCA.

Sommario

Il Tokamak ISTTOK ($I_p = 4 \text{ kA}$, $B_T = 0.5 \text{ T}$, $R = 0.46 \text{ m}$, $a = 0.085 \text{ m}$) è uno dei pochi tokamak con un programma scientifico regolare di scariche con corrente di plasma alternata (AC). Per migliorare la stabilità della scarica ed aumentare il numero di cicli di AC per scarica, è stato sviluppato un nuovo sistema di controllo.

Il precedente sistema di controllo in tempo reale di ISTTOK si basava su hardware PCI controllando soltanto un'unica posizione del plasma sulla base delle informazioni fornite dalla diagnostica di sonde Mirnov, mentre tutti gli altri parametri della scarica erano preprogrammati.

Il tema principale di questa tesi è quello di aggiornare il sistema di controllo di ISTTOK che è stato completamente ridisegnato . Il sistema di controllo integra, adesso, tutte le diagnostiche e gli attuatori in tempo reale per ottimizzare i parametri di scarica di plasma, attraverso il controllo della corrente di plasma, della posizione del plasma e d' iniezione di gas in tempo reale durante la scarica di ISTTOK .

Il nuovo sistema di controllo acquisisce dati da 50 convertitori analogico-digitali (ADC), comprese la diagnostica in tempo reale e altre misure connesse: tomografia, bobine di Mirnov, interferometro, sonde elettriche, sonde magnetiche seno e coseno, bolometro, corrente nelle fonti di alimentazione, tensione di collegamento e corrente di plasma . Il sistema ha un ciclo di controllo 100 μs durante il quale legge tutti le diagnostiche collegate a scanner che si basano sulla tecnologia Advanced Telecommunications Computing Architecture (ATCA) e invia il riferimento di controllo agli attuatori ISTTOK. Gli algoritmi del controllore vengono eseguiti su un processore Intel Q8200 con 4 core a 2,33 GHz e collegati ad un ambiente basato sulla tecnologia ATCA. Il sistema di controllo in tempo reale è stato programmato in C ++ su piattaforma in tempo reale chiamata Multi-threaded Application Real-time Executor (MARTE).

Il sistema dispone, inoltre, di un'interfaccia basata su HyperText Markup Language (HTML) e JavaScript per configurare i parametri del controllore.

L'aggiornamento delle fonti di alimentazione è parte integrante della tesi e consiste nell'aumento delle specifiche della fonte del campo verticale, nella progettazione e costruzione di una fonte del campo primario e la progettazione di un nuovo modulo di controllo per tutte le attuali fonti di corrente di ISTTOK .

Questo aggiornamento migliora l' affidabilità e la stabilità delle scariche AC, consentendo che l'ISTTOK funzioni per più di 1 secondo, con 40 semicicli di circa 26 ms ciascuno. I principali fattori per questo risultato è stata la realizzazione di una fonte di corrente controllabile per il campo del primario ed il controllo integrato delle diagnostiche e degli attuatori in un ambiente in tempo reale basato sulla tecnologia ATCA.

Keywords

Palavras chave

Nuclear fusion

Fusão nuclear

Real-time

Tempo-real

Tokamak

Tokamak

ISTTOK

ISTTOK

Control

Controlo

Power supplies

Fontes de corrente

ATCA

ATCA

Alternate current discharges

Descargas alternadas

Contents

ABSTRACT	I
RESUMO	III
SOMMARIO	V
KEYWORDS / PALAVRAS CHAVE	VII
CONTENTS	IX
FIGURE LIST.....	XI
TABLE LIST	XV
CHAPTER 1 - INTRODUCTION	1
1.1. NUCLEAR FUSION	2
1.2. MAGNETIC CONFINEMENT	8
1.3. TOKAMAK OPERATION	14
1.4. ALTERNATE CURRENT DISCHARGES	18
1.5. ISTTOK DESCRIPTION	23
CHAPTER 2 - DIAGNOSTICS	25
2.1. ISTTOK DIAGNOSTICS	27
2.2. DIAGNOSTICS INTEGRATION ON THE REAL-TIME PLATFORM	39
CHAPTER 3 - ISTTOK ACTUATORS.....	41
3.1. ISTTOK CONFIGURATION	42
3.2. ISTTOK POWER SUPPLIES	43
3.3. POWER SUPPLIES CONTROL	49
3.4. OTHER ACTUATORS.....	55
CHAPTER 4 - DESIGN OF THE ATCA CONTROL AND DATA ACQUISITION SYSTEM.	57
4.1. SYSTEM LAYOUT	58
4.2. ATCA CRATE HARDWARE.....	61
4.3. MARTE FRAMEWORK	68
4.4. REAL-TIME CONTROL.....	77
4.5. ISTTOK GENERIC APPLICATION MODULES (GAMs).....	82
CHAPTER 5 - SYSTEM CONFIGURATION.....	95
5.1. REMOTE CONFIGURATION LAYOUT	96
5.2. USER-LEVEL CONFIGURATION.....	100
5.3. SYSTEM OPERATION	112
CHAPTER 6 – RESULTS	119
6.1. ALTERNATE CURRENT RESULTS	120
6.2. MACHINE OPERATION RESULTS	124
CHAPTER 7 – CONCLUSIONS.....	131
ACKNOWLEDGEMENTS	133
BIBLIOGRAPHY.....	135

ACRONYMS	141
ANNEXES	143
ISTTOK POWER SUPPLIES COMMUNICATION PROTOCOL:	143
SCHEMATICS (POWER SUPPLIES CONTROLLER).....	148

Figure list

Figure 1 – Binding energy per particle as a function of the mass number	2
Figure 2 – Fusion reaction between deuterium and tritium	3
Figure 3 – Fusion reactions cross section versus temperature	3
Figure 4 – Inertial fusion process	4
Figure 5 – JET Tokamak schematic	5
Figure 6 – Image from the MAST spherical tokamak during a plasma discharge	6
Figure 7 – Wendelstein 7-X magnetic configuration schematic	6
Figure 8 – International Thermonuclear Experiment Reactor (ITER)	7
Figure 9 – IFMIF accelerator schematic	7
Figure 10 – Helical trajectory of ions and electrons in a uniform magnetic field	8
Figure 11 – Necessary currents to form a toroidal field	9
Figure 12 – Two models for driving plasma current in tokamaks	10
Figure 13 – Force between two straight parallel wires	10
Figure 14 – Effect of the vertical field on the plasma	11
Figure 15 – Effect of the horizontal field on the plasma	12
Figure 16 – Effect of an elongation field in the plasma shape	12
Figure 17 – Magnetic field arrangement to create plasma with a high triangularity	13
Figure 18 – X-point operation by adding a divertor field coil	13
Figure 19 – Fusion sequence in a tokamak for energy production	14
Figure 20 – Operation sequence envisaged for ITER	14
Figure 21 – Transformer magnetisation hysteresis curve	18
Figure 22 – Pulsed discharge versus AC discharge schematic	19
Figure 23 – Pulse #16713, 13 semi-cycle AC discharge with the old control system	20
Figure 24 – JET AC pulse #24807	21
Figure 25 – AC operation at HT-7 tokamak, pulse # 83352	22
Figure 26 – ISTTOK tokamak geometry including all coils and port plugs	23
Figure 27 – Poloidal cut evidencing the ISTTOK vertical field and horizontal field mapping	24
Figure 28 – JET tokamak diagnostics and their location	25
Figure 29 – Position of the 12 magnetic probes inside the vacuum chamber	27
Figure 30 – ISTTOK analogue integrators schematic	28
Figure 31 – Rogowski coil	29
Figure 32 – ISTTOK cross-section displaying the equatorial tomography camera	30
Figure 33 – Responsivity of the photodiode versus radiation wavelength	30
Figure 34 – Tomography diagnostic schematic	31
Figure 35 – Photodiode amplifier schematic	31
Figure 36 – ISTTOK electric probes used for real-time control	32
Figure 37 – ISTTOK floating potential measurement	32
Figure 38 – ISTTOK interferometer based on the heterodyne detection principle	33
Figure 39 – Hydrogen excitation levels and radiation wavelength	34
Figure 40 – ISTTOK Heavy Ion Beam schematic	35
Figure 41 – ISTTOK Retarding field energy analyser	36
Figure 42 – Electric probe arrays	37

Figure 43 – Location of the ISTTOK diagnostics around the torus	38
Figure 44 – ISTTOK Diagnostics contribution to the measured quantities	39
Figure 45 – Data path schematic from the acquisition up to the controller board memory	40
Figure 46 – Old and new configuration of the primary field circuit	42
Figure 47 – ISTTOK operation mode selection circuit schematic	42
Figure 48 – Horizontal and Vertical field power supplies schematic	43
Figure 49 – Primary field power supply without the connecting wires	44
Figure 50 – Power supplies control module	44
Figure 51 – Backplane of the power supplies control module	44
Figure 52 – Power supplies controller board	45
Figure 53 – Driver board (without front panel)	46
Figure 54 – COMPASS tokamak fast amplifiers control module	46
Figure 55 – Equivalent power supplies circuit used for simulating the PS behaviour	49
Figure 56 – Simulink model for the Horizontal field power supply control	50
Figure 57 – Horizontal field power supply reference tracking	51
Figure 58 – Detail of the Horizontal field power supply reference tracking	51
Figure 59 – Vertical field power supply reference tracking	52
Figure 60 – Primary field power supply reference tracking	52
Figure 61 – Differences in reference following between scenario control and current control	54
Figure 62 – Puffing feedback on H_α radiation in a long AC discharge (pulse 34332)	55
Figure 63 – Puffing tests with 800 mbar on the gas puffing reservoir	56
Figure 64 – Overview of the new ISTTOK control system	57
Figure 65 – Old ISTTOK real-time control system schematic	58
Figure 66 – FireSignal schematic	59
Figure 67 – ISTTOK overall control schematic	59
Figure 68 – ATCA crate image	62
Figure 69 – ATCA acquisition board and the RTM module	63
Figure 70 – Connections to the FPGA in the acquisition board	64
Figure 71 – Acquisition modules	64
Figure 72 – FPGA digital 100 tabs FIR filter response in frequency	65
Figure 73 – ATCA controller board	66
Figure 74 – PCI quad serial port	66
Figure 75 – ATCA controller board simplified schematic	67
Figure 76 – BaseLib2 abstraction levels	70
Figure 77 – MARTe control cycle sequence	73
Figure 78 – MARTe objects	74
Figure 79 – IOGAM interface with the hardware	75
Figure 80 – MARTe services (ISTTOK configuration)	78
Figure 81 – Control cycle histogram for pulse #34729	78
Figure 82 – The full controller scheme in macro blocks	79
Figure 83 – AC discharge sequence schematic	81
Figure 84 – Pulse #34135, pre-programmed parts of on AC discharge	81
Figure 85 – Execution time histograms for the FireSignalDischargeStatusGAM, ControllerGAM, CosineProbeGAM, DataCollectionGAM, ElectricProbesGAM and HAlphaGAM	83

Figure 86 – InterferometryGAM, MachineProtectionGAM, MagneticsGAM, PlasmaStatusGAM, PowerSupplyCommunicatorGAM and MainRogowskiGAM execution time histograms	84
Figure 87 – SineProbeGAM, TechnicalSignalsGAM, TimeWindowsGAM, TomographyGAM and WaveformGAM Execution time histograms	84
Figure 88 – Discharge time and waveform time in an AC discharge	86
Figure 89 – Plasma current, discharge status and waveform time	87
Figure 90 – Comparison between the total tomography intensity and the H _{α} radiation	88
Figure 91 – Discharge configuration webpage in edit mode	96
Figure 92 – Discharge configurator webpage after submitting all the changes	97
Figure 93 – Advanced configuration webpage in edit mode	98
Figure 94 – Advanced configuration webpage in display mode	99
Figure 95 – Discharge configurator HTML webpage with labels	100
Figure 96 – Detail of the discharge configurator time-windows editor	103
Figure 97 – Detail of the waveform selection for the discharge configurator	105
Figure 98 – Advanced configuration webpage with labels	106
Figure 99 – Advanced configuration waveform selection drop-down menu	109
Figure 100 – Comparison between the old and the new control system.....	119
Figure 101 – Pulse #33001, 20 cycles AC discharge without gas puffing feedback control	120
Figure 102 – Pulse #34261, 22 cycles AC discharge with gas puffing real-time control	120
Figure 103 – Pulse #34332 – 40 semi-cycles AC discharge at ±4kA	121
Figure 104 – Plot of 14 AC discharges, discharge reproducibility	122
Figure 105 – Detail of 14 different current inversions	123
Figure 106 – Detail of 14 different breakdowns	123
Figure 107 – Pulse #34104. Simultaneous feedback control	124
Figure 108 – Horizontal and Vertical field PS currents in plasma position control	125
Figure 109 – Pulse #34037. Plasma current control at 6 kA	126
Figure 110 – Pulse #34531, 40 semi-cycles AC discharge, C _{III} to H _{α} normalized radiation	127
Figure 111 – Pulse #34531. Detail of the C _{III} and H _{α} radiation	127
Figure 112 – Pulse #35044, 20 cycles AC discharge with a tungsten probe (r = 65 mm)	128
Figure 113 – Pulse #35047, 24 cycles AC discharge with a tungsten probe (r=70 mm)	129
Figure 114 – Partial meltdown of a tungsten piece	132

Table List

Table 1 – Main advantages and disadvantages by energy source.....	1
Table 2 - ISTTOK tokamak parameters.....	23
Table 3 – ISTTOK interferometer parameters.....	34
Table 4 – ISTTOK power supplies characteristics.....	48
Table 5 – MARTe worldwide footprint. List of working systems using MARTe framework and list of test with the MARTe framework.	68
Table 6 – BaseLib2 levels and relative position on the abstraction	70
Table 7 – CPU load distribution per CPU core in a quad core CPU.....	77
Table 8 – Association between GAMs and instances running on the ISTTOK control system. The table is ordered by the sequence in the control cycle, from “ATCAAdc” (first instance to run) to “Codac” (last before end of cycle). WaveformGAM is instantiated five times and PowerSupplyCommunicatorGAM is instantiated tree times.....	83
Table 9 – ISTTOK GAMs mean execution times and standard deviation.....	84
Table 10 – TimeInputGAM inputs and outputs.....	85
Table 11 – TimeWindowsGAM inputs and outputs.	85
Table 12 – TomographyGAM inputs and outputs.....	87
Table 13 – ElectricProbesGAM inputs and outputs.	88
Table 14 – MagneticsGAM inputs and outputs.....	89
Table 15 – SineProbeGAM inputs and outputs.....	89
Table 16 – CosineProbeGAM inputs and outputs.	89
Table 17 – MainRogowskyGAM inputs and outputs.....	89
Table 18 – InterferometryGAM inputs and outputs.	90
Table 19 – HAlphaGAM inputs and outputs.....	90
Table 20 – TechnicalSignalsGAM inputs and outputs.	90
Table 21 – PlasmaStatusGAM inputs and outputs.....	91
Table 22 – MachineProtectionGAM inputs and outputs.	91
Table 23 – WaveformGAM inputs and outputs.	92
Table 24 – ControllerGAM inputs and outputs.	92
Table 25 – PowerSupplyCommunicatorGAM inputs and outputs.	93
Table 26 – TomographyGAM inputs and outputs.	93
Table 27 - DataCollectionGAM inputs and outputs.	93
Table 28 - FireSignalDischargeStatusGAM inputs and outputs.....	94

Chapter 1 - Introduction

Energy is one of the key elements for mankind. In a world where the energy demand is expanding year over year is fundamental to assure a regular energy supply over the years to come. About 80% of the consumed energy is provided by fossil fuels which produce greenhouse effect gases, their replacement posts a great challenge since their usage has also includes many advantages as Table 1 suggests.

As a subset of the world energy mix, the electric energy has seen a regular increase in demand throughout the years. Since electric energy is mostly generated by coal and natural gas, their replacement by either renewable energy or nuclear energy would decrease the atmosphere pollution. In particular, nuclear fusion offers a set of future benefits that can be useful to complement the energy mix. Unlike fission, the fusion energy production has intrinsic safety features (no possibility of a run-away reaction or explosion). Although radioactive materials will be generated in the walls of a fusion power plant they would decay with half-lives of about 10 years and the whole plant could be re-cycled within 100 years. In principle this gives fusion significant advantages over nuclear fission.

The nuclear fusion raw fuels are abundant around the globe and would last for thousands of years (millions if sea water lithium is included) at the actual energy consumption rate. Fusion is a very efficient form of energy production, 1 kg of deuterium and tritium (nuclear fusion raw materials best candidates) would supply the same amount of energy as 10 million kg of coal.

With such good promises in mind, nuclear fusion research and development is fundamental to complement the word energy mix for the years to come.

Advantages	Energy source	Disadvantages
- High energy density. - Very good energetic vector. - Relative low investment needed.	Oil	- Produces greenhouse gas. - Limited reserves and unevenly distributed around the world.
- High energy density. - Relative low investment needed.	Gas	- Produces greenhouse gas. - Lower energy concentration than oil.
- Large availability. - Low cost energy production.	Coal	- Most pollutant of fossil fuels. - May send low radioactive particles to atmosphere.
- Low running cost. - Renewable energy, no emissions. - High energy storage.	Hydroelectric	- Requires a high initial investment. - Landscape impact. - Limited favourable localizations.
- Low running cost. - Renewable energy, no emissions.	Wind	- Irregular production. - In large quantities unbalances grid.
- Renewable energy, no emissions.	Photoelectric	- Not cost effective (for now). - Weather dependant.
- Low running costs. - No greenhouse gas emissions.	Fission	- Requires a high initial investment. - High radioactivity (waste management). - Possibility of dangerous accidents.
- Low running costs. - No greenhouse gas emissions. - Low radioactivity. - Safe intrinsic process.	Fusion (when available)	- Requires a high initial investment. - Still produces radioactivity, but in a much lower scale than fission. - Not available, still in research phase.

Table 1 – Main advantages and disadvantages by energy source.

1.1. Nuclear fusion

The aim of fusion research is to achieve the conditions required for plasma to start producing energy from the fusion of light nuclei such as deuterium and tritium (both hydrogen isotopes). Nuclear fusion is the process of binding two atomic nuclei generating a heavier particle. For obtaining energy with such a process, the two atomic nuclei must have a low atomic mass as Figure 1 suggests. The referred figure also indicates that the energy released by a fusion reaction of two light nuclei such as deuterium and tritium is greater than the energy released by a fission reaction of a heavy atom.

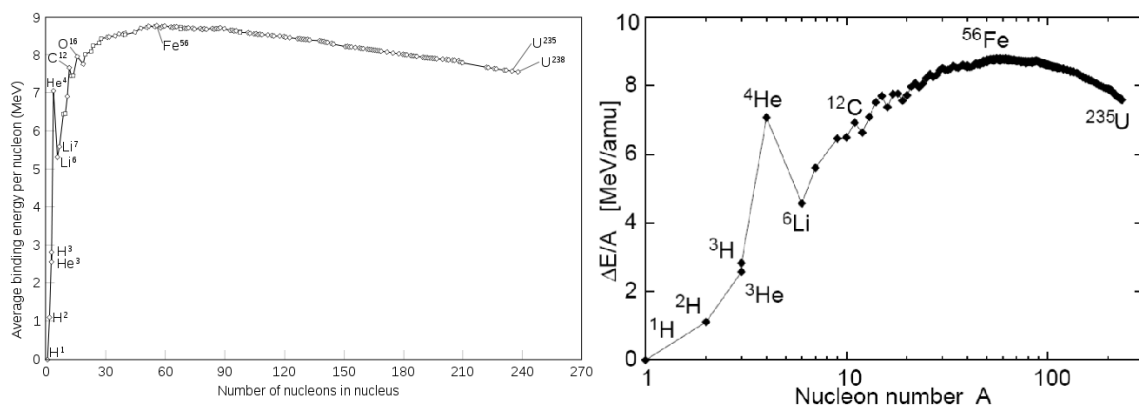
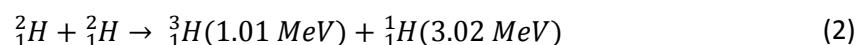
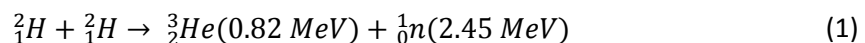


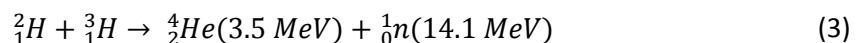
Figure 1 – Binding energy (in MeV) per particle as a function of the mass number (A), left image in linear scale, image on the right in logarithmic scale. This figure evidences the energy released by nuclear fusion reactions such as the fusion of deuterium and tritium into helium plus a neutron.

There are several energy producing fusion reactions between low atomic mass nuclei, some of the possible fusion reactions are described below:

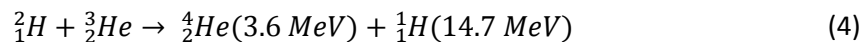
Deuterium – Deuterium:



Deuterium - Tritium:



Deuterium – Helium 3:



The fusion reaction that holds most potential is the Deuterium-Tritium fusion (equation 3) into Helium 4 plus one energetic neutron (Figure 2). Since the mass of the neutron is about four times smaller than the alpha particle, by moment conservation, the alpha particle resulting from the fusion reaction will have about one fifth of the total energy (3.5 MeV) and the neutron will have the remaining energy, about four fifths of the total energy (14.1 MeV).

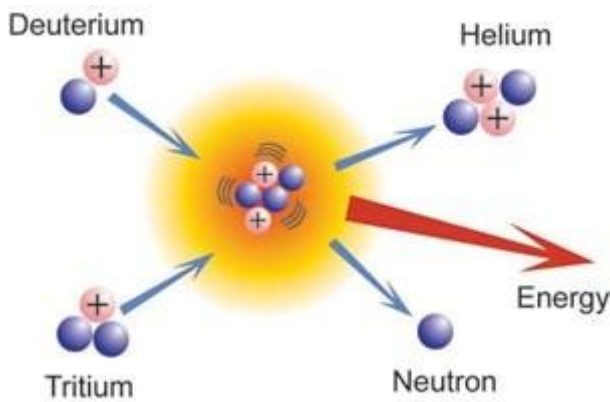


Figure 2 – Fusion reaction between deuterium and tritium, this reaction produces an alpha particle (Helium nucleus) with 3.5MeV and a 14.1 MeV neutron (image obtained from the ITER website)

Since atomic nuclei have the same positive charge, they repel each other, in order to overcome this repelling force (Coulomb barrier) and bind them together, the two nuclei must possess enough kinetic energy. One of the reasons for selecting the deuterium-tritium fusion reaction as the most promising for the initial fusion experiments is the cross-section of the reaction. As it can be observed in Figure 3, the Deuterium-Tritium reaction has the highest cross-section on a relative low temperature compared with the other fusion reactions.

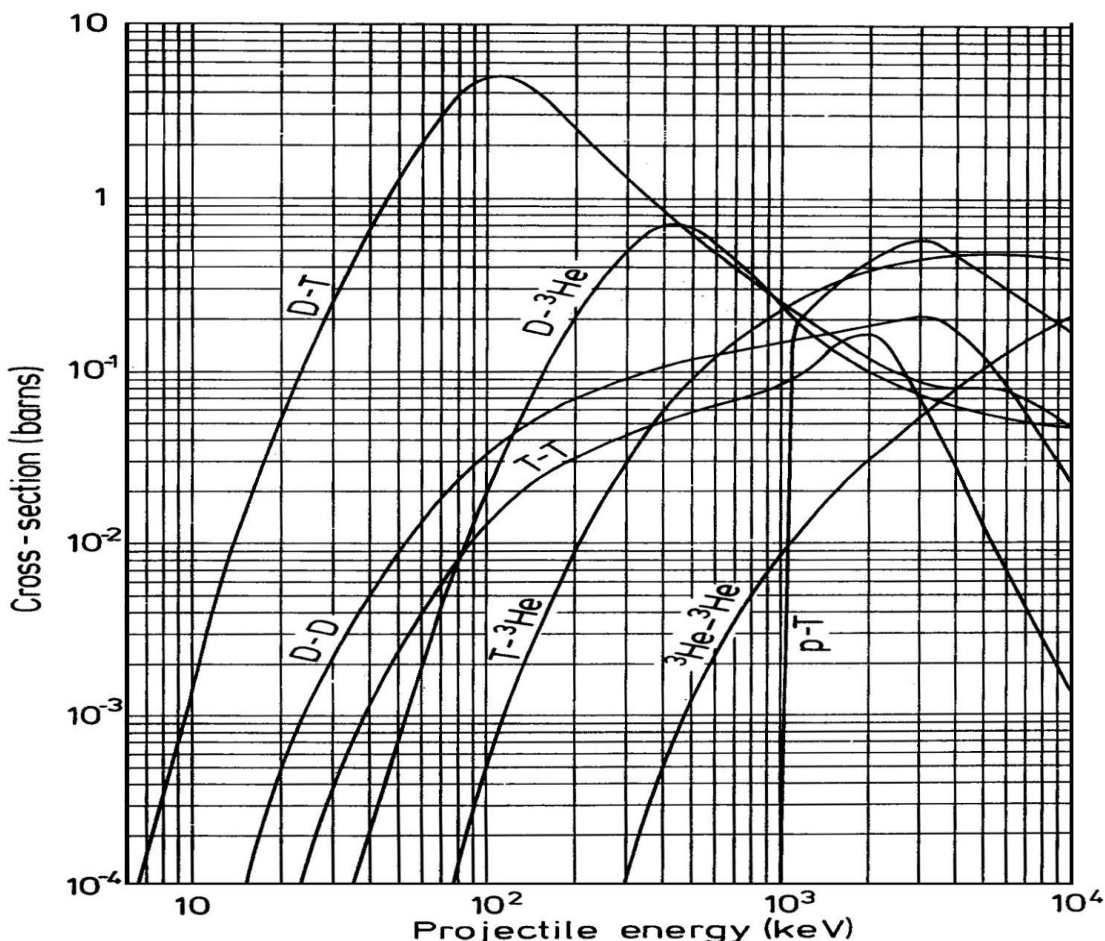
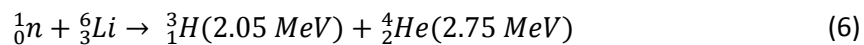
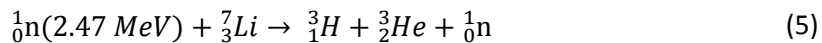


Figure 3 – Fusion reactions cross section versus temperature. As it can be observed the most promising fusion reaction is deuterium with tritium, with a cross section peak at about 100 keV (image from http://www.kayelaby.npl.co.uk/atomic_and_nuclear_physics/4_7/4_7_4.html).

The deuterium part of the fusion fuel is very common and has a global footprint since deuterium can be obtained from the seawater. About 1 part in 5000 of the hydrogen from water is deuterium which is enough for providing electric energy for millions of years at the present consumption rate. The tritium part of the fuel is more problematic, although present in seawater, the concentration of tritium in the seawater is much lower than deuterium concentration. There is no other sizable natural source since tritium decay with a half-life of about 10 years. The most viable alternative to obtain tritium is by breeding the tritium from lithium. It can either be bred from lithium-7 or from lithium-6, breeding lithium 7 into tritium plus helium-3 requires a 2.47 MeV neutron (equation 5) and breeding lithium 6 into tritium produces about 4.8 MeV (equation 6) but lithium-6 makes up 7.4% of natural lithium.

Breeding lithium into tritium reactions:



If the fusion triple product defined by the plasma temperature, plasma density and confinement time is greater than the value defined by equation 7 (valid for a 50%-50% deuterium-tritium mix) the plasma has the necessary conditions to enter the ignition state. As an example the JET tokamak [1] has already reached a value over $1 \times 10^{21} \text{ m}^{-3} \text{ s keV}$.

$$n \tau T \geq 5 \times 10^{21} \text{ m}^{-3} \text{ s KeV} \quad (7)$$

There are two main alternatives to produce fusion reactions on earth, inertial confinement and magnetic confinement (described in detail in the next sub-section).

The inertial confinement technique uses a laser-driven implosion of a small pellets containing frozen deuterium-tritium mix. A large number of laser beams are fired at the same time converging on a small target (Figure 4), this process heats the surface of the pellet into plasma state, thus producing a pressure directed to the centre of the pellet squeezing the remaining fuel. The rapid blow off also creates a shock wave that travels toward the centre of the compressed fuel from all sides. The implosion inertia confines the fuel for a fraction of time at fusion temperatures and with a high density. The intense heat and pressure forces the deuterium-tritium mix to fuse.

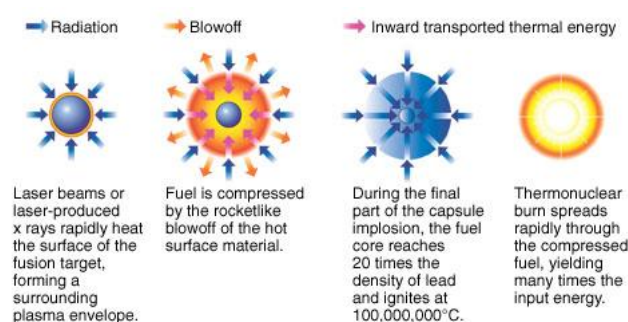


Figure 4 – Inertial fusion process (image obtained from the Lawrence Livermore National Laboratory website).

Regarding the state of the art of the inertial fusion, the National Ignition Facility (NIF) [2][3] machine was upgraded (2009) in order to demonstrate the feasibility of the inertial fusion. The High Power laser for Energy Research project (HiPER) [4][5] will be constructed as a large scale laser system designed to demonstrate significant energy production from inertial confinement fusion.

The magnetic confinement consists in trapping particles using the magnetic field configuration. This particle confinement can be achieved by ionizing the particles into plasma state and then produce an ordered movement of the plasma, by creating a plasma current. As any other electronic current, the plasma current column can be attracted or repelled by parallel electric currents in the same direction or in the opposite direction respectively. The magnetic confinement is described in detail in the next sub-chapter (1.2 - magnetic confinement). The main objective for the magnetic confinement is to avoid plasma contact with the wall. This enables the plasma to be heated to millions of degrees without losing all the energy to the wall.

There are two promising families of machine configurations for magnetic plasma confinement namely the tokamak family (including tokamaks, spherical tokamaks) and the stellarators family (including the Torsatron, Heliotron, Heliac and Helias configurations).

The tokamak is a device with a torus shape (see Figure 5), the toroidal field coils are wrapped around the vacuum chamber creating a toroidal magnetic field to confine the ionized particles. The central solenoid is used to create plasma current around the toroidal direction and the poloidal field coils are used to control the plasma position and shape. The main advantage of the tokamak over the stellarator configuration is the relative simplicity of the coil arrangement.

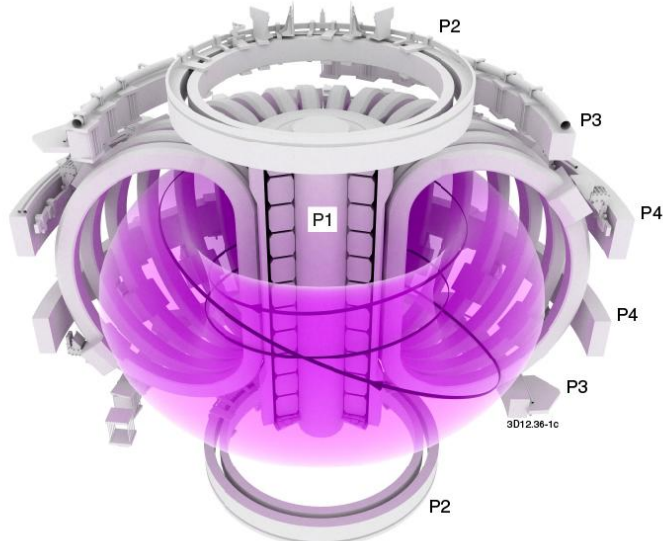


[Figure 5 – JET Tokamak schematic \(image obtained from CCFE\).](#)

As a subset of the tokamaks, there are also the spherical tokamaks such as MAST [6], which have a low aspect ratio and almost resemble a sphere due to the lack of a central solenoid for driving plasma current (plasma current is driven by external poloidal coils). Figure 6 depicts the

aspect of a spherical tokamak, although the performance of these devices is lower than the tokamak performance, the spherical tokamaks have the advantage of having compact and less complicated design.

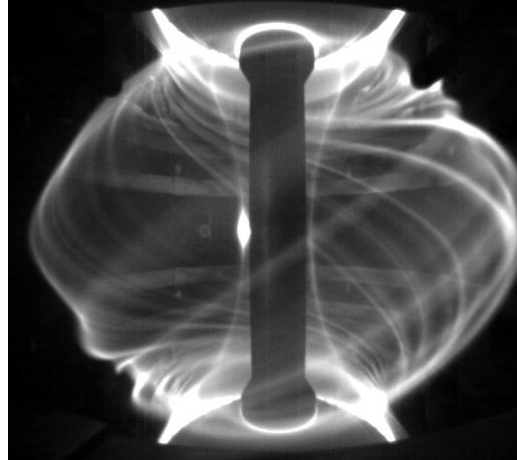


Figure 6 – Image from the MAST spherical tokamak during a plasma discharge (image obtained from CCFE).

The stellarator has a relatively complex [7] magnetic configuration (Figure 7) which prevents the plasma from contacting with the vacuum vessel wall while requiring much lower plasma current to confine the plasma than a tokamak. The main advantage of the stellarator is their stability without having to drive plasma current while their biggest disadvantage is the complexity of the design and lower confinement time.

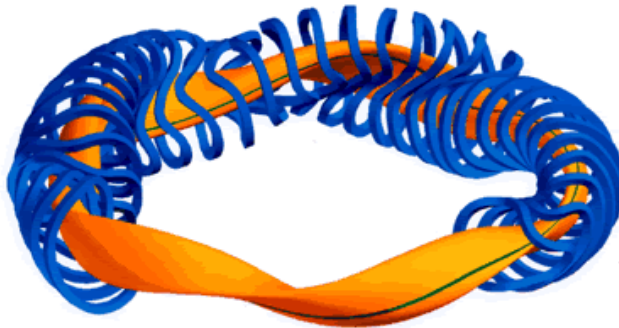


Figure 7 – Wendelstein 7-X magnetic configuration schematic (image from the IPP website).

Regarding the state of the art of nuclear fusion by magnetic confinement, the tokamak concept (at the date of this thesis) appears to be closer to achieving energy production from fusion reaction since there is a clear roadmap for the design of such reactor. The stellarator configuration is also making progress towards nuclear fusion, at the date of this thesis, the stellarator Wendelstein 7-X [8] is in the final construction phase and is aimed at producing fusion reactions at near steady-state. The stellarator concept main advantage is the ability to work in a steady-state basis, but since W7-X will not have enough cooling power, the operation at full power will be restricted at about 30 minutes due to temperature limitations.

The tokamak for nuclear fusion roadmap starts with ITER [9][10][11][12][13] (Figure 8) which is currently under construction. This device is aimed to produce fusion power with a ratio of the power in fusion products to that used to heat the plasma (Q) up to 10[9].

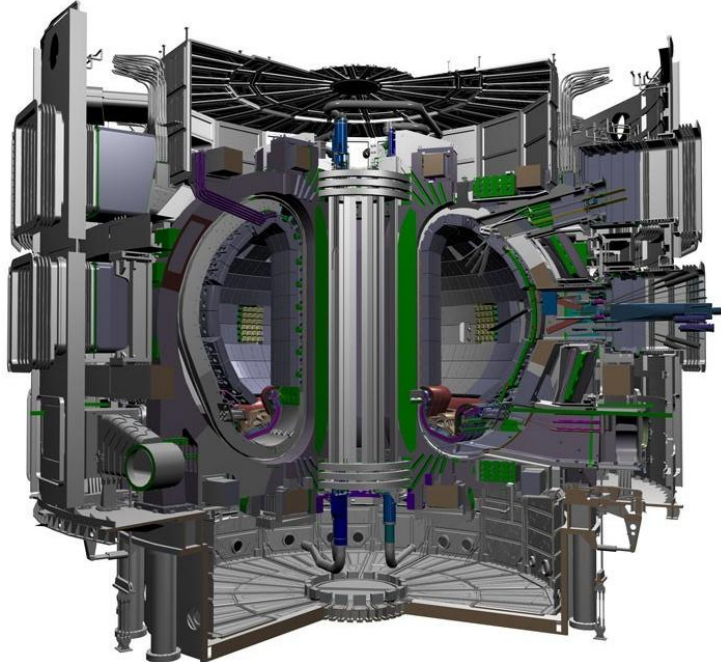


Figure 8 – International Thermonuclear Experiment Reactor (ITER), image from the ITER website.

Parallel to ITER construction and operation, the International Fusion Materials Irradiation Facility (IFMIF) will have an extremely important role in the material development. The IFMIF[14] (Figure 9) facility consists in an accelerator-based neutron source that will use Deuterium-Lithium stripping reactions to simulate 14 MeV neutrons from Deuterium-Tritium fusion reactions. This will enable to test materials with neutrons with the same energy as the neutrons produced by D-T fusion reaction.

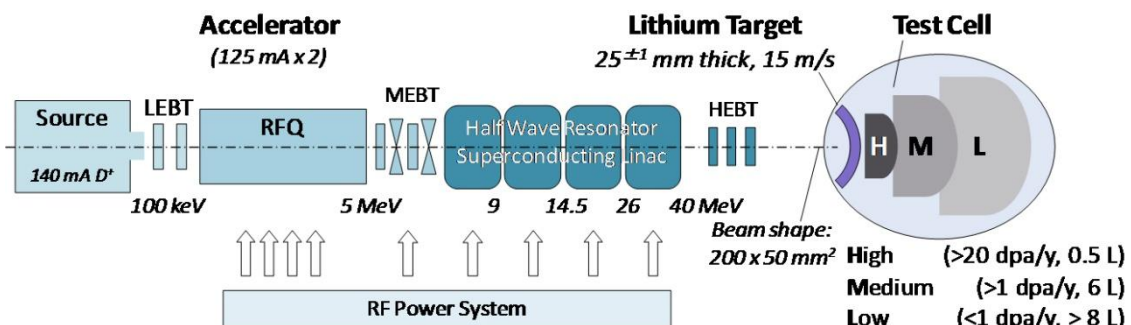


Figure 9 – IFMIF accelerator schematic. Two parallel 125 mA Deuteron beams at 40 MeV will collide on a liquid Li screen to produce a flux of neutrons (image obtained from the IFMIF website).

The DEMO tokamak will be designed by leveraging on the knowledge gained from ITER and IFMIF operation. The DEMO reactor is aimed to demonstrate the electricity production capability from nuclear fusion.

1.2. Magnetic confinement

Plasma is one of the four states of the matter which is obtained by heating a gas until the particles are ionized. Since plasma is at an even higher temperature than the gas, it tends to expand to all the available space. When the plasma particles contact their container wall, they transfer their energy to the wall, so the particles lose their energy. In order to maintain the required plasma temperature for fusion, the particles need to be confined to avoid energy losses.

There are several possibilities to confine plasma; (i) gravitational confinement, (ii) magnetic confinement and (iii) inertial confinement (described in the previous sub-chapter). In the stars such as the sun the hot plasma is confined by the large gravitational field. This gravitational field compresses the plasma and forces the light atoms to fuse producing nuclear fusion energy. The plasma thermal expansion is compensated by the large gravitational pressure.

Since plasma is composed by charged particles it is possible to confine the plasma by applying a magnetic field with the proper geometry. When a uniform magnetic field is applied the charged particles will follow spiral paths along the magnetic field lines (Figure 10) due to the Lorentz force. The motion of the charged particles across the magnetic field lines is restricted, so the hot plasma is contained within this magnetic field lines avoiding plasma wall interaction that would cool down the plasma.

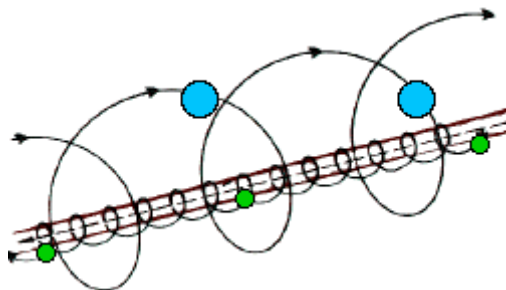


Figure 10 – Helical trajectory of ions (blue) and electrons (green) in a uniform magnetic field.

There are two main candidates for a magnetic confinement fusion device, the tokamak [15] and the stellarator [16]. The tokamak configuration is based on a torus shape and requires a combination of coils to generate the required magnetic equilibrium field, the macroscopic equilibrium of fusion plasma is described by the magneto hydro dynamics (MHD) model [17]. A toroidal magnetic field is used to confine the plasma particles. To generate a toroidal field the current has to be in the poloidal direction (toroidal field coils) as detailed in Figure 11. This magnetic field arrangement directs the plasma particles in a spiral movement around a closed circle (a toroidal loop).

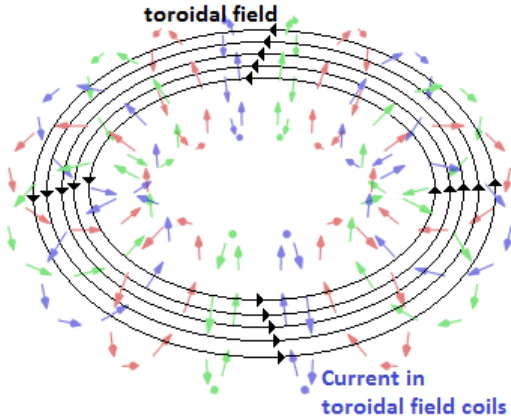


Figure 11 – Necessary currents to form a toroidal field.

After ionization the plasma particles can travel in a loop, if the loop is closed it is possible to induce a current using the Faraday principle (equation 8) this phenomena can also be described by the Maxwell-Faraday equation (equation 9). It can also be written in an integral form by the Kelvin-Stokes theorem (equation 10). These equations state that in order to create the necessary electromotive force (EMF) for the plasma particles acceleration in a loop it is necessary to have a varying magnetic flux inside the surface of the correspondent plasma particles loop. If this varying magnetic field is created the plasma particles will have an EMF to accelerate them in their toroidal movement, thus creating a plasma current.

$$\text{EMF} = -\frac{\partial \mathbf{B}}{\partial t} \quad (8)$$

$$\nabla \times \mathbf{E} = -\frac{\partial \mathbf{B}}{\partial t} \quad (9)$$

$$\oint_{\partial\text{surf}} \vec{E} \cdot d\vec{l} = - \int_{\text{surf}} \frac{\partial \mathbf{B}}{\partial t} \cdot d\mathbf{A} \quad (10)$$

In tokamaks, the plasma current is inducted by a special coil arrangement perpendicular to the loop surface or redirected through an iron core as a regular transformer, if the coils are in the centre the coil arrangement is called the central solenoid (Figure 12). This schema is equivalent to a regular transformer circuit, with the secondary of the transformer being the plasma. As in a transformer the current generated in the secondary is driven by the current variation on the primary coil. Nevertheless, there is one fundamental difference between the tokamak plasma current drive and a transformer, since the secondary of a tokamak is the plasma itself, the resistance and inductance of the secondary circuit (plasma) changes according to the plasma characteristics, for example, when there is low plasma current the plasma is resistive and when the plasma current is higher, the electron temperature is also higher and the plasma resistivity drops to very low levels. The plasma internal inductance mainly depends on the plasma current distribution inside the vacuum vessel. When modelling the plasma current drive in a tokamak, these effects must be taken into account.

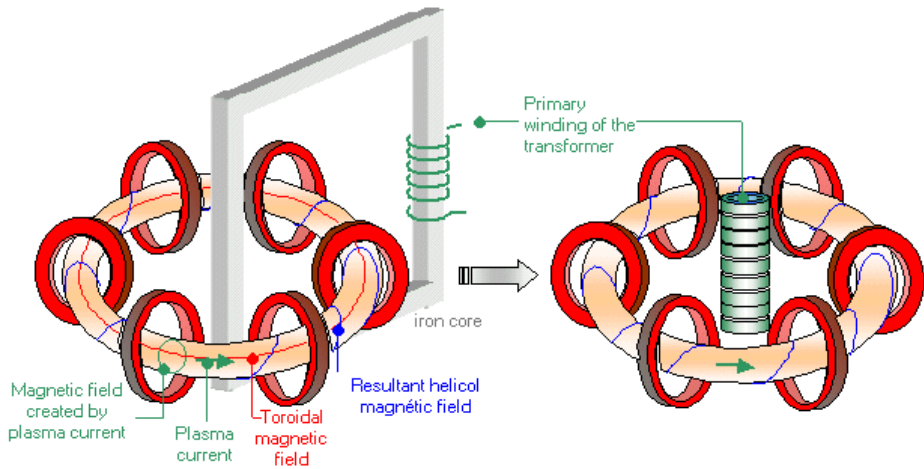


Figure 12 – Two models for driving plasma current in tokamaks. On the left side of the figure, the resulting magnetic flux change driven by the primary circuit is redirected through a high magnetic permeability material (normally iron) and on the right side, the primary circuit is inserted directly in the middle of the tokamak structure producing directly the necessary dB/dt inside the loop surface. (Image obtained from the Institut de Recherche sur la Fusion Magnétique website).

The plasma current along the toroidal direction produces a poloidal field and together with the toroidal field result in a helicoidal field (Figure 12) which is essential to counteract the plasma pressure. Without the poloidal field the plasma particles would be free to drift along the different toroidal field lines, the poloidal field produces a twist in the magnetic field lines that effectively trap the plasma particles. The number of toroidal turns (m number) per poloidal turns (n number) is called safety factor (q). The safety factor name comes from the fact that larger values of q are associated with higher ratios of toroidal field to plasma current and consequently less risk of current-driven plasma instabilities. Normally tokamaks operate with a q of one in the plasma centre and a q at the plasma edge of 2-8, a q below two at the edge implies that the plasma is MHD unstable.

Additional poloidal field coils (parallel to the plasma current) are necessary to control the plasma position and shape inside de vacuum vessel [18]. The Ampere law (equation 11) provides the tools to analyse the force between 2 conductors (Figure 13), the magnetic field generated by an infinite long straight wire is given by equation 12 and the force between two parallel straight wires is given by equation 13.

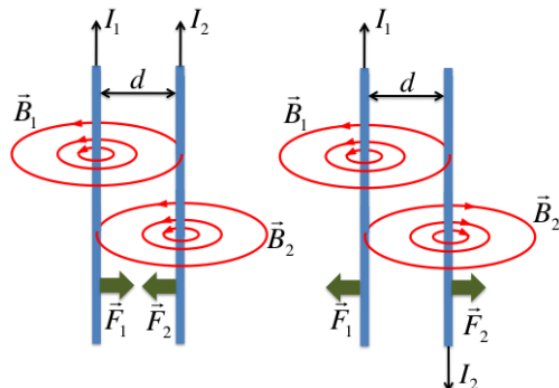


Figure 13 – Force between two straight parallel wires. The wires are attracted when the current travels in the same direction on both wires and they are repelled when the currents are in opposite directions.

$$\nabla \times H = J + \frac{\partial D}{\partial t} \quad (11)$$

$$B = \frac{\mu I}{2 \pi r} \quad (12)$$

$$\frac{F}{\Delta L} = \frac{\mu I_1 I_2}{2 \pi r} \quad (13)$$

When the plasma particles are accelerated to provide the plasma current they are likely to expand radially due to the hoop force generated by their toroidal movement. To counteract the hoop force it is necessary to provide a vertical field such as Figure 14 to provide a volumetric inward force (Newton per cubic meter) in the plasma corresponding to the external product of the current density (J) with the magnetic field (B) generated by the current passing in the coils according to equation 14.

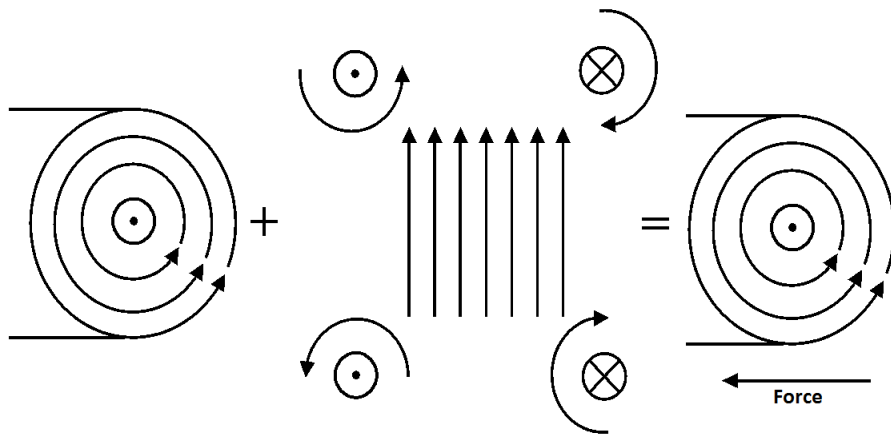


Figure 14 – Effect of the vertical field on the plasma (toroidal cut view). The vertical field produces a radial force in the plasma used to counteract the plasma hoop force and to control the plasma radial position inside the vacuum vessel.

$$f = J \times B \left(\frac{N}{m^3} \right) \quad (14)$$

According to the MHD equations, the required vertical field to stabilize the hoop force generated by the plasma current [19] is described by equation 15 according to the virial theorem.

$$B_v = \frac{\mu_0 I_\phi}{4 \pi R_0} \left(\beta_p + \ln \left(\frac{8 R_0}{a} \right) + \frac{1}{2} l_i - \frac{3}{2} \right) \quad (15)$$

Where B_v is the equilibrium vertical field, I_ϕ is the toroidal plasma current, a is the minor radius, β_p is the average plasma pressure compared to the magnetic pressure of the poloidal field at the plasma boundary, R_0 is the major radius and l_i is a positive quantity of order unity which depends on the distribution of the current.

The plasma column vertical position can be controlled by providing a horizontal field. This horizontal field will create a vertical force depending on the direction of the horizontal field according to equation 14. The horizontal field effect on the plasma is depicted in Figure 15.

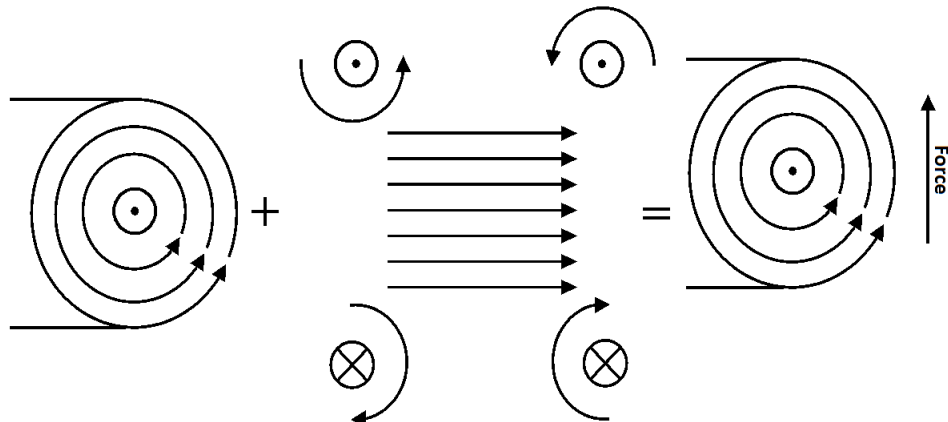


Figure 15 - Effect of the horizontal field on the plasma. The horizontal field produces a vertical force in the plasma used to counteract the plasma hoop force and to control the plasma radial position inside the vacuum vessel.

In order to optimize the plasma distribution and performance, modern tokamaks use an elongated plasma shape. This elongation can be achieved by applying a magnetic field as depicted in Figure 16. Since currents in the same direction attract themselves, the plasma is attracted to the top and to the bottom of the machine in an unstable balance because the force between the plasma and the coils producing the field depend on the distance between them according to equation 12. This inverse relation between the force and the distance causes the plasma to be attracted to the coil that is less distant (with the current on top similar to the current on the bottom of the elongation field), causing an exponential movement towards the nearest coil [20][21]. To prevent this catastrophic vertical displacement event [22] it is necessary to take action as quick as possible by applying a horizontal field and consequently applying a vertical force to counteract the displacement: for example the JET vertical stabilization system [23] is decoupled for the shape controller [24] and has dedicated coils and power supply with a control cycle of 50 μ s [25] for the sole purpose of stopping the plasma vertical velocity (the JET shape controller controls the vertical position at a higher time scale). The plasma elongation is defined by the ratio of the height of the plasma shape by the width of the plasma column.

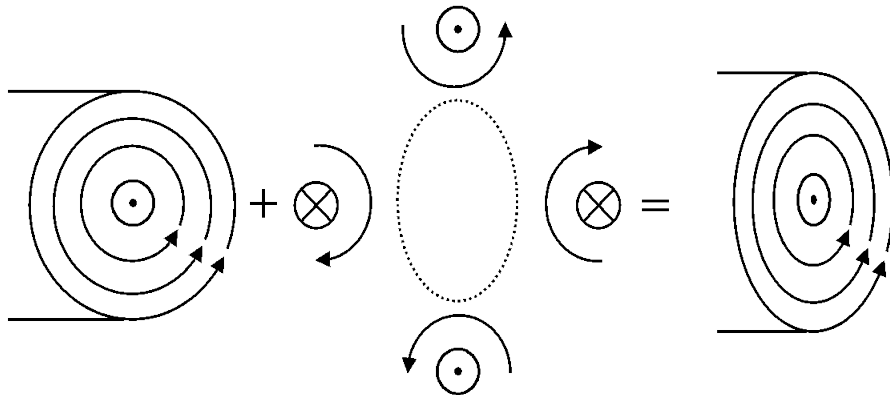


Figure 16 – Effect of an elongation field in the plasma shape.

To further optimize the plasma operation, the plasma surface near the high toroidal field side (inner side) can flattened with a magnetic field arrangement such as Figure 17. This field leads to plasma with a high triangularity. The plasma triangularity is defined by the ratio of the

horizontal distance from the top of the plasma to the plasma centre by the plasma minor radius.

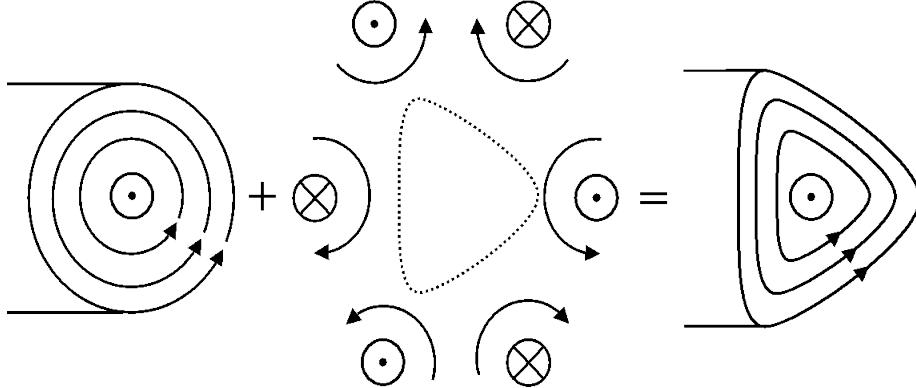


Figure 17 – Magnetic field arrangement to create plasma with a high triangularity.

To avoid the contact of the last closed flux surface (LCFS) with the vacuum vessel wall, a divertor field is added as depicted in Figure 18. Without this field the LCFS is determined by the contact with the wall. With divertor operation the LCFS is isolated in respect to the wall and this fact dramatically increases the plasma performance. As Figure 18 suggests, by applying this divertor field an x-point is formed. The x-point is where the poloidal magnetic field is null in such a way that two flux surfaces appear to cross. The x-point and the lower field lines redirect most of the particles and power flux to the lower part of the wall named divertor (represented in blue in Figure 18). The divertor is responsible for the main part of the power deposition on the wall without counting with the neutrons produced by the fusion reactions.

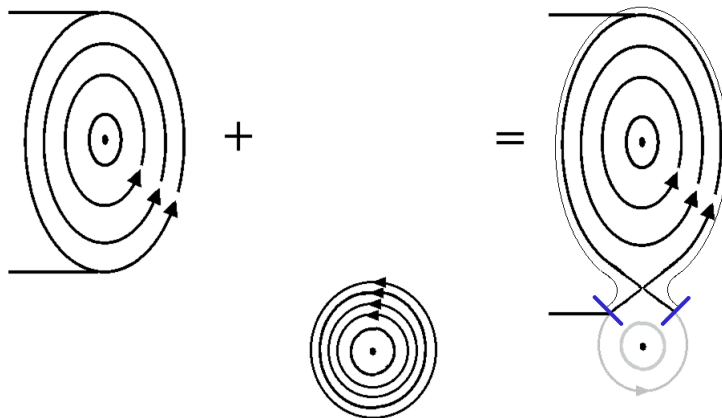


Figure 18 – X-point operation by adding a divertor field coil. With the divertor field the plasma the last closed flux surface does not interact with the wall, most of the power deposition is sent to the divertor (represented in blue). With this field an x-point is created corresponding to a null poloidal field point.

All these poloidal fields are magnetically coupled (current variation in one coil can generate current in other coils by magnetic coupling), so all the magnetic fields must have an integrated controller with multiple-input-multiple-output (MIMO) capabilities that deals with the mutual inductances of the circuits.

1.3. Tokamak operation

In a tokamak, to generate plasma, the vacuum vessel is pumped down and with the right magnetic field configuration [26], loop voltage and a controlled gas injection the gas inside the vacuum vessel breaks-down in avalanche and plasma is formed. Then the plasma current is ramped up with the correct magnetic setup for controlling the plasma position and shape. In D-T burn experiments a mixture of these two gases (ideally a 50%-50%) is inserted in the vessel and the plasma is heated up to fusion temperatures with auxiliary heating such as neutral beam injection or radio-frequency heating. The exit from the power phase is a critical process since when the additional heating is turned off and the plasma continues to radiate losing a lot of power (depending on the radiation level, which depends on the impurity content), when this happens the plasma is prone to mode lock events that can lead to plasma disruption. After safely exiting from the power phase the plasma current has to be ramped down and finally the plasma is extinguished. A normal discharge sequence is depicted in Figure 19.

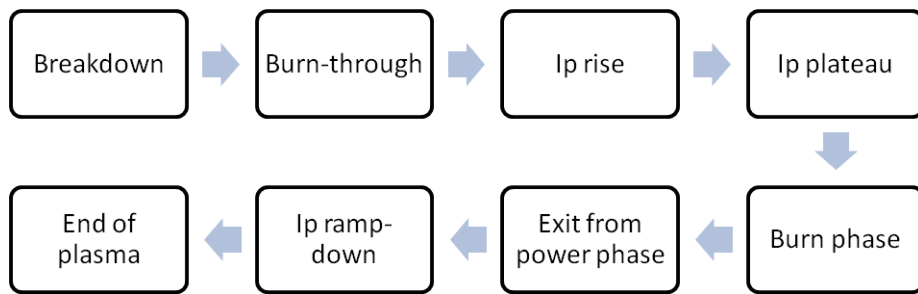


Figure 19 – Fusion sequence in a tokamak for energy production.

Since tokamak operation is normally in a pulsed regime there is some dwell time between discharges, this time is used for post-pulse checks, safety operation checks and for uploading the next experiment configuration, the envisaged operation flowchart for the ITER tokamak can be observed in Figure 20.

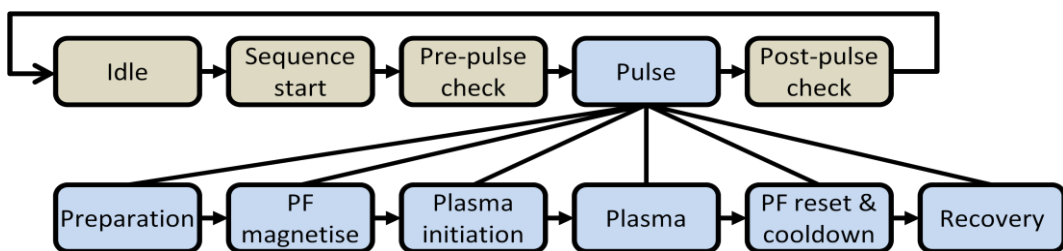


Figure 20 – Operation sequence envisaged for ITER. Since the ITER tokamak will have super conducting coils, the toroidal field will be always working throughout the experimental campaign.

As stated in chapter 1.1 there is a minimum fusion triple product (equation (7)) for D-T fusion. This triple product has 3 components, the temperature, the density and the confinement time. These variables are normally interdependent but the temperature mainly depends on the plasma heating power and confinement, the density is generally (with peaked density profile this limit can be slightly surpassed) limited by the plasma current per cross section area (Greenwald limit, equation 16, where I_p is the plasma current and "a" is the minor radius). The confinement time is defined by the length of time for which particles are confined within the plasma.

$$n_G(10^{20} \text{ m}^{-3}) = \frac{I_p}{\pi a^2} (\text{MA/m}^2) \quad (16)$$

The plasma can be heated by several different methods, each with different characteristics. Usually, in large tokamak devices a combination of several heating methods is used.

List of heating methods:

1. Ohmic heating

The ohmic field power supply is used to create plasma current, when a current passes through a resistive medium the medium is heated by Joule effect. This heating mode is always present in a tokamak but as the plasma is heated the plasma resistance drops, because of this effect the ohmic heating loses efficiency as the plasma temperature rises (lowering plasma resistivity), so this method is only suitable for initial heating.

2. High frequency heating

High frequency electromagnetic wave heating consists in the same principle as the microwave oven. When these waveforms are sent to the plasma, the plasma particles absorb the energy from the electromagnetic field and then transfer the energy to the other plasma particles through collisions. The circular motions of the ions and electrons around the magnetic field lines are used as resonant frequencies for electro-cyclotron heating and ion-cyclotron heating respectively. Another frequency also used for radio frequency heating is the lower hybrid frequency which is a combination of the previously referred frequency. The lower hybrid has a component of electric field parallel to the magnetic field, so it can also be used to accelerate electrons moving along the field lines.

The ion-cyclotron heating has a broad effect on the plasma but requires coupling between the antenna and the plasma for the power deposition to be effective.

The electron-cyclotron heating has a localized effect on the plasma and can be used for localized current drive that is very useful for heating magnetic islands and control of plasma instabilities. Due to higher frequency of operation, the coupling requirements between the antenna and the plasma are less strict than the ion-cyclotron.

3. Neutral beam injection (NBI) heating

Particles with high kinetic energy that are injected into the plasma transfer their energy to the plasma particles through collisions and heat them. This particle injection also has the side effect of fuelling the plasma since after the collisions the neutral particles are ionized and stay inside plasma (until naturally ejected). Normally a deuterium beam is used since other species would contaminate the plasma with impurities.

In order to produce this neutral beam of fast particles first it is necessary to produce ions and then accelerate them to a high energy. After these ions are accelerated, they need to be neutralised before entering the plasma to avoid deflection by the magnetic field inside the torus. For tokamaks constructed up to date, the ions produced are positive ions, but for ITER,

because of the neutralization process efficiency at very high ion energies (1 MeV for ITER NBI), the accelerated ions will be negative ions.

Methods of operation:

The nuclear fusion ultimate goal is to produce commercially viable electric power. In order to optimize the energy production of a tokamak fusion reactor several paths can be taken and a basic problem has to be addressed, the natural pulsed operation due to ohmic field flux consumption. A list of operation methods can be found below:

1. Pulsed operation

The tokamak concept has naturally a pulsed operation. This is due to the fact that to create plasma current by ohmic means, the magnetic field flux inside the circular surface defined by the plasma has to be increasing all the time to produce a positive loop voltage to drive plasma current by ohmic means. Since this flux cannot be increased to infinity, the plasma discharge has a finite duration, and after the discharge is finished it is necessary to regenerate this flux by driving current into the opposite direction. This leads to a pulsed operation with a considerable dwell time without energy production.

Advantages:

- Full power discharge.
- Maximum plasma current.
- Optimization of the machine for peak fusion energy.

Disadvantages:

- Pulsed operation with a considerable dwell time in the energy production.

2. Hybrid operation / Steady-state operation

The discharge duration can be extended by usage of special plasma configurations that optimise the non-inductive current drive. With this configuration a meaningful fraction of the plasma current is driven by the bootstrap current of the particles captured in banana orbits, the remaining part of the current drive can be obtained by a combination of non-inductive plasma current actuators such as the NBI, electron-cyclotron current drive and lower-hybrid current drive.

Advantages:

- Longer plasma duration.
- Potential steady-state operation if all the plasma current is driven by non-inductive means.

Disadvantages:

- Usually lower power than pulsed operation at the maximum plasma current.
- More unstable operation scenario.

3. Alternate current (AC) operation

When the ohmic flux is exhausted, instead of safely terminate the discharge, there is the option of driving the plasma current to the opposite direction. If the transition is fast enough, the ionization is not lost [27][28][29][30] the plasma current can be inverted safely, thus jump-starting another cycle with the reverse plasma current. This allows the tokamak to operate in a quasi-steady state similar to a standard transformer operation mode (with current flat-tops). This mode of operation does not yield a 100% duty cycle in the energy production since when the plasma current inverts there is not enough energy in the plasma for fusion reaction to occur. Nevertheless the dwell time in energy production would be insignificant in relation to the overall period with energy production for a large machine.

This subject is further developed in the next sub-chapter.

Advantages:

- Full power discharge.
- Combines the advantages of the pulsed operation while having a low dwell time in the energy production.
- Possible optimization for energy production per unit of capital invested.

Disadvantages:

- Non-axisymmetric actuators namely tangential NBI need to be redesigned.
- Forces between coils during the plasma current reversal process.
- Confinement loss and power deposition during inversion.

4. Low dwell time pulsed operation

As the AC operation regime, it drives plasma currents in both directions, but it differs to the previous regime because the ionisation is lost right before a cycle in the opposite direction starts. In fact each cycle can be considered an individual pulse since it has all the pulsed discharge phases [31].

This mode of operation is easier to obtain than a plasma current reversal without loss of ionization and causes less stress in the machine since it can be viewed as different discharges since the discharge in fact ends before the discharge in the opposite direction starts. The dwell time for this mode of operation can be very low, approximating the fusion production duty cycle to the power production duty cycle of the AC operation regime.

Advantages:

- Same advantages as the AC operation.

Disadvantages:

- Same disadvantages as the AC operation and a slight increase in the dwell time between energy production periods.

1.4. Alternate current discharges

The traditional and more effective method to drive plasma current inside a tokamak is induction process similar to a transformer. The primary of the transformer is the central solenoid and the secondary of the transformer is the plasma itself. Since the plasma changes configuration with time the secondary of the transformer can be seen as a resistance and inductance in function of the time. For example if the plasma changes the q profile the inductance changes and the plasma resistance depends on the temperature. Although the plasma resistance is very low at high plasma temperatures it is still different from zero, implying that there is power loss in the transformer circuit (power transfer for plasma heating). Since the flux driven by the primary field power supply is limited, this implies that, without additional current drive, the tokamak operation is limited in time. A typical transformer flux curve is depicted on Figure 21.

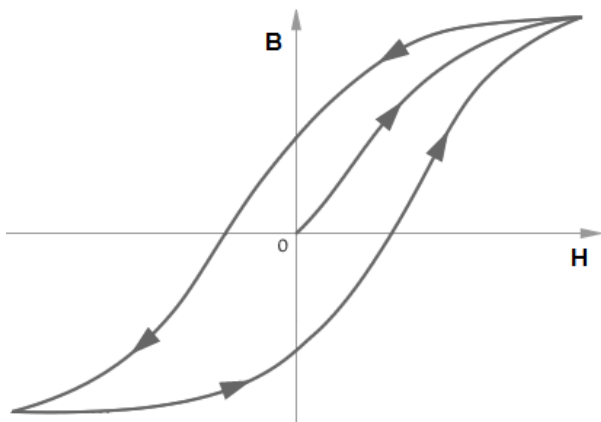


Figure 21 – Transformer magnetisation hysteresis curve. Magnetic flux density versus magnetising field strength

When the flux reaches saturation the μ value (equation 17) declines sharply and it is not possible to drive more flux efficiently. Without flux variation and without non-inductive current drive the loop voltage will drop and consequently the plasma current will also drop.

$$\mu = B / H \quad (17)$$

The magnetic core saturation time depends on the machine design and on the flux consumption to sustain the amount of plasma current. This value ranges from a few milliseconds to a few minutes (without additional current drive generation). These time scales are obviously not enough for a fusion power plant which is supposed to generate large and continuous amounts of energy. There are two different approaches to solve this problem; one is to generate current from non-inductive sources (neutral beam and electromagnetic waves) while optimizing the natural bootstrap current due to particles trapped in banana orbits. The other alternative approach is to invert the plasma current direction when the magnetic flux in the core is approaching saturation. This operation regime is similar to a transformer working in alternate current (AC) as depicted in Figure 22. This can be considered as a quasi-steady state regime. This process is found in literature as (AC) discharge.

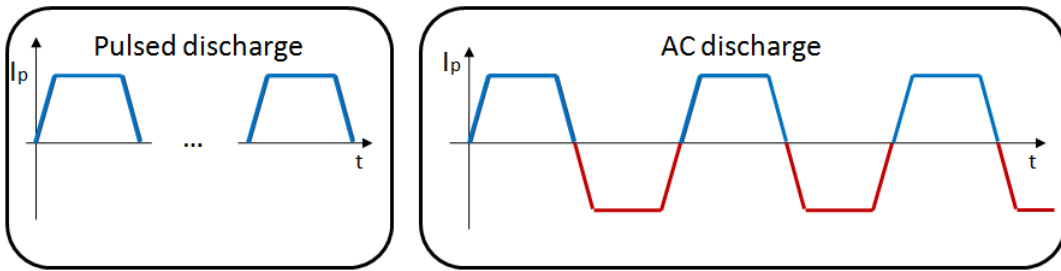


Figure 22 – Pulsed discharge versus AC discharge schematic.

Tokamak operation in a stationary regime (with non-inductive current drive) has some important technological disadvantages:

- The efficiencies of the non-inductive current drive are usually low, if taken in account the internal efficiency of the generating device.
- Some current drive technologies require good coupling between the antenna and the plasma which may not be always possible. As a result there is an additional loss in the power transmission.
- The extended operation time and large power can cause serious technological problems to the neutral beam and gyrotron design (large power device used to generate high power electromagnetic waves with micro-wave frequency to be injected in the plasma).
- A solution with several current drive devices is more complicated and requires more maintenance costs.

Operation on the AC regime has several theoretical advantages, as described below:

- AC discharges are technically simpler to produce, more viable and more efficient.
- Ability to operate the machine at full power with lower dwell time between energy production cycles.
- Operation in alternate regime allows reducing the duty-cycle between energy production cycles, optimizing the operation of a fusion power plant. The only period without energy production is the plasma current inversion phase, including ramp-down and ramp-up.
- The use of AC inductive current drive for a tokamak fusion reactor allows the reactor to operate with a minimum plant recirculating power. It further allows more flexibility in the optimization of the fusion power per unit capital investment.

Nevertheless AC discharges also have the following challenges/drawbacks:

- The plasma current has an important role in the balance/position of the plasma column. Plasma position becomes uncontrolled when the plasma current crosses zero, so this transition needs to be very fast to avoid loss of confinement (power deposition on the tokamak walls).
- The H-mode plasma operation in AC discharges has to be rebuilt every time the plasma current inverts the direction. This can lead to some power dissipation in the machine.

- The change in the plasma current direction and consequently the vertical magnetic field leads to some mechanical stress in the machine which could lead to material fatigue and deterioration. This issue could be addressed by a correct mechanical dimensioning of the machine and also by increasing the flattop duration.
- For future tokamak reactors, the ohmic coils will be superconducting and a limited coil current change rate can be applied on them during the plasma current transition time, which means the transition time will be longer, causing a loss in the plasma parameters. This problem can be mitigated by using an auxiliary heating system to maintain plasma ionization during low plasma current phase.

The lack of control of the ISTTOK AC discharges was the main motivation for this thesis. One of the “best” ISTTOK AC discharge with the old control system is depicted in Figure 23. As it can be observed the AC discharges with the old control system were very far from stable, the plasma current was decaying along time and there were no plasma current flat-top. The old control system only controlled the plasma position and the primary field power supply was pre-programmed without any feedback control. The gas injection was also regulated at a fixed value during all the discharge without any feedback system. These restrictions on control can help to explain the obtained results with the old control system. The new ISTTOK control system is the main theme for this thesis.

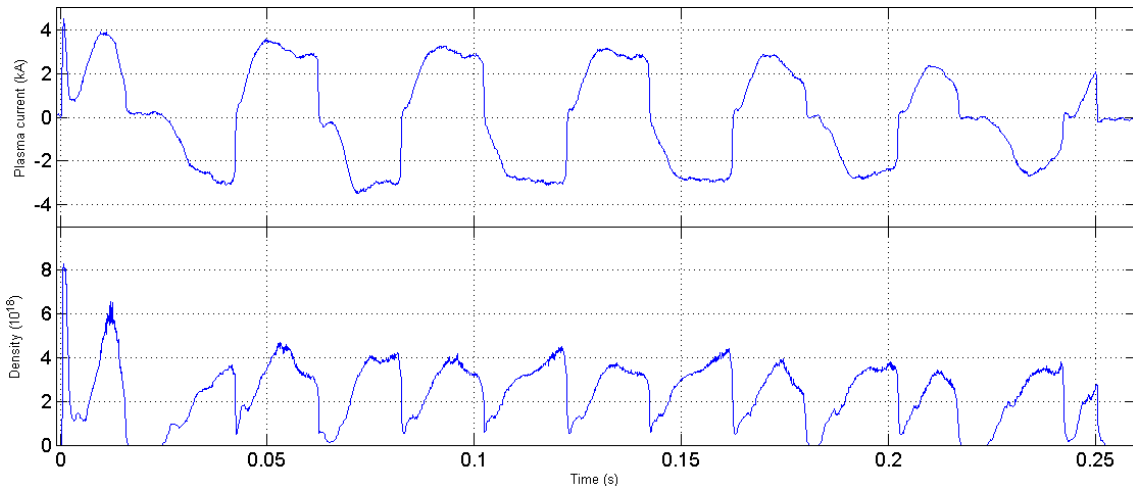


Figure 23 – ISTTOK pulse #16713, 13 semi-cycle AC discharge with the old control system. The feedback was only on the vertical and horizontal magnetic field, there was no feedback on either gas injection or plasma current. For the breakdown, the old system used a high voltage discharge on the primary field obtained from a high voltage capacitor bank. The initial spike in current is due to this phenomenon.

Like breakdown [26], the current reversal also requires a near zero poloidal field in the centre of the vacuum vessel in order to decrease the reconnection length and to avoid loss of ionization. If the power supplies produce the required magnetic field, the plasma current reversal is successful without using additional heating methods to sustain ionization.

Regarding the state of the art of the AC discharges, this type of discharge was investigated in several machines, a summary of the results obtained by small (ISTTOK), medium (HT-7) and large size (JET) tokamaks is presented below.

AC operation results in JET tokamak:

The JET tokamak was able to produce a full cycle of AC operation with 2MA of plasma current [31] for each direction but with loss of ionization between semi-cycles. Dwell times between the two plasmas (one for each direction) ranged between 50 ms and 6 s were obtained. Since there was a loss of ionization between semi-cycles a plasma breakdown was also necessary for the second semi-cycle, nevertheless the dwell time was much smaller than two JET consecutive discharges that usually have a dwell time not smaller than 15 minutes (normally around 30m), if absolutely necessary this time could be shorted but secure operation checks and component cool down require this minimum time between two consecutive discharges.

Experiments in JET successfully demonstrated that in a large tokamak AC operation is a feasible current drive mode for a tokamak fusion reactor. These two semi-cycles operation showed no difference in plasma characteristics from a normal JET discharge. The two half cycles are characterized by the same Z_{eff} , the same radiated power at the same density, and the same reaction rate for the same ICRH power. No degradation of plasma purity in the second plasma with respect to the first one was observed. The range of pre-fill pressure in which second breakdown can be achieved is not substantially different from that for normal breakdown, indicating that the possible presence of impurity gases in the wall gas release does not have a major effect.

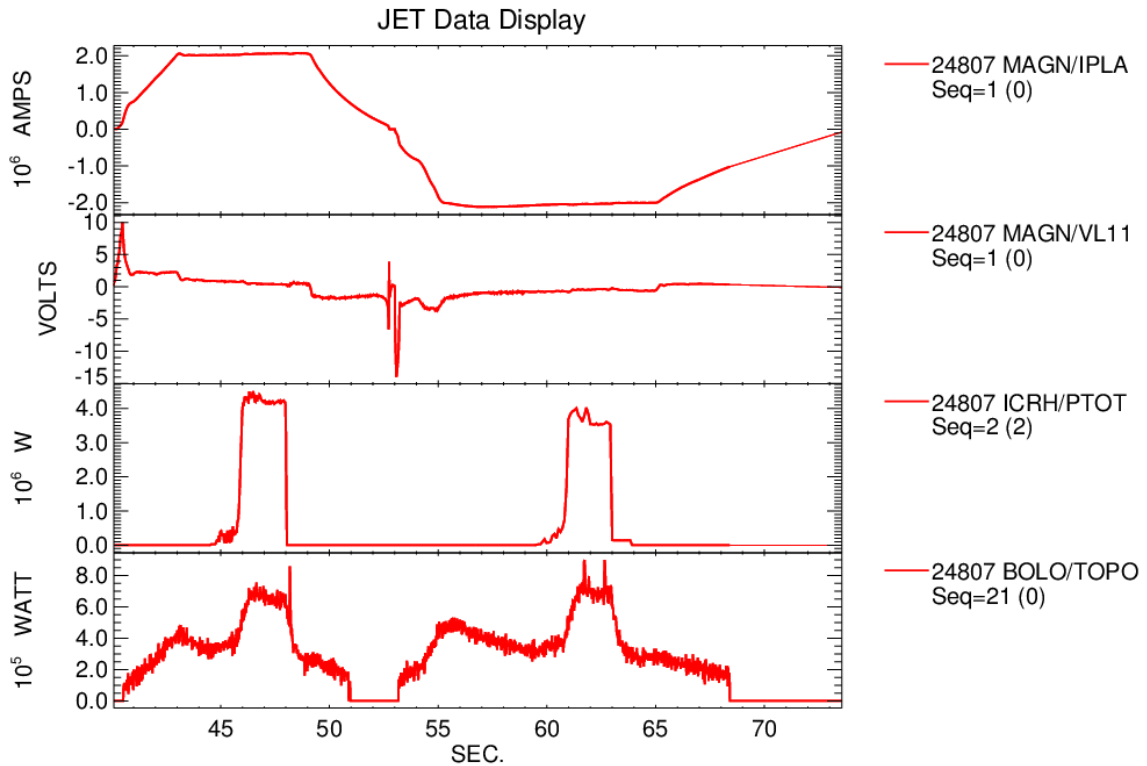


Figure 24 – JET AC pulse #24807. Two semi-cycles with 2 MA each and low dwell time between semi-cycles.

AC operation results of HT-7:

The HT-7 tokamak is a superconducting tokamak. This tokamak achieved a quasi-steady-state AC operation [30] assisted by a lower hybrid wave injection, with a plasma current of 125 kA, line-averaged density of $1.5 \times 10^{19} \text{ m}^{-3}$, electron temperature of $T_e = 500 \text{ eV}$ and 30–50 s plasma

duration. The HT-7 AC discharges are assisted by lower hybrid power during the plasma current reversal process to assist the transition. The lower hybrid power also helps to maintain the ionization during this critical process. With this configuration HT-7 was able to produce a quasi-steady state operation with many semi-cycles and without loss of ionization during the current reversals.

The work carried at HT-7 also suggests that when the overall plasma current is zero, it can be described as the sum of two opposite currents at the midplane [30].

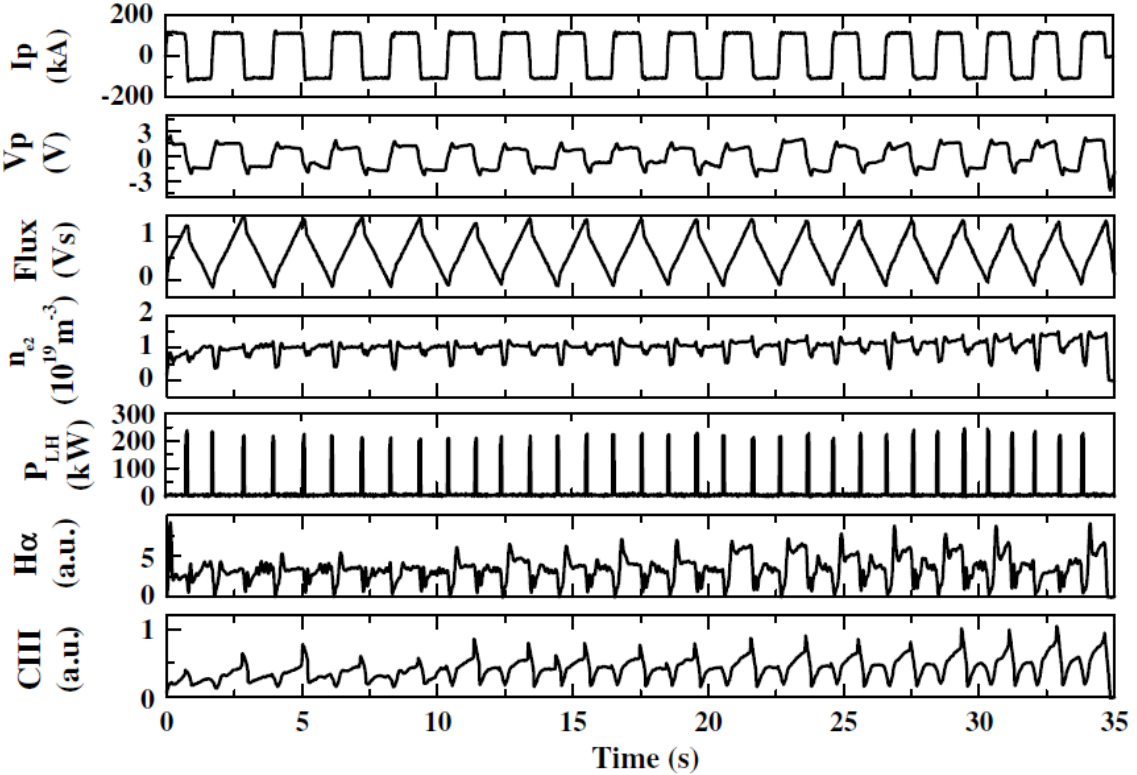


Figure 25 – AC operation at HT-7 tokamak, pulse # 83352. Lower hybrid power is used to assist the plasma current reversal process achieving operation without dwell time.

AC operation at ISTTOK:

As a result of this thesis work, the ISTTOK tokamak extended the discharge duration up to 40 semi-cycles without any loss of ionization. Unlike HT-7, the ISTTOK tokamak does not have auxiliary heating, consequently there is no lower hybrid to assist the current inversion process, to avoid the loss of ionization the poloidal field inside the vacuum vessel during the inversion needs to be as low as possible (same conditions as the breakdown) to decrease the magnetic lines connection length and avoid loss of electrons and consequently plasma cooling and loss of ionization. The AC operation of ISTTOK for more than 1 second is the main theme of this thesis and further information can be found on chapter 7 (results).

1.5. ISTTOK description

ISTTOK [32] (represented in Figure 26) is a large aspect ratio tokamak defined by the main parameters shown in Table 2. The ISTTOK maximum flux limits ISTTOK operation to about 30ms for a standard discharge. In order to increase the discharge duration ISTTOK regularly uses AC discharges. This enables ISTTOK to be used as a material testing facility.

Parameter	Value
Plasma current	7 kA
Major radius	0.46 m
Minor radius	0.085 m
Magnetic field	0.5 T
Electron temperature	<120 eV
Transformer flux	0.25 V.s
standard discharge duration	30 ms

Table 2 - ISTTOK tokamak parameters.

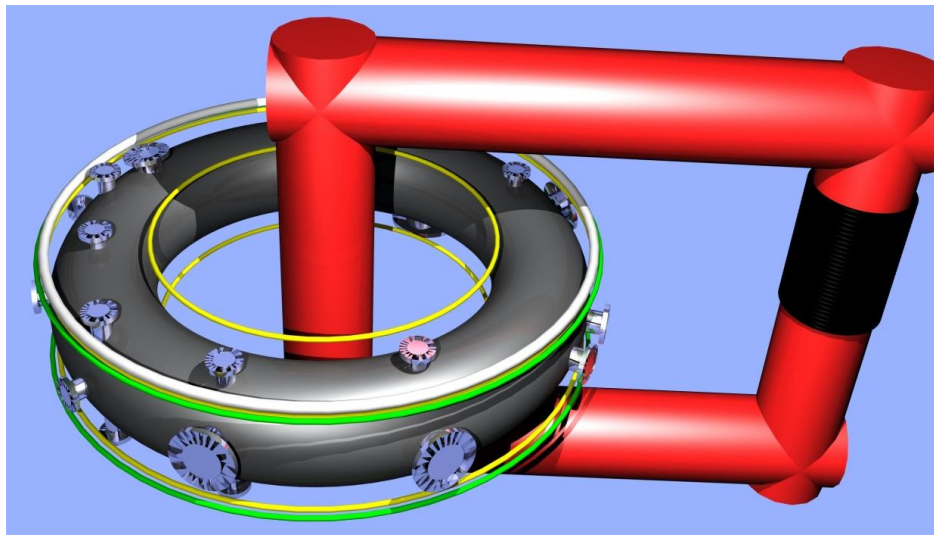


Figure 26 – ISTTOK tokamak geometry including all coils and port plugs. The old primary field coils are represented in black (40 turns), the new primary field coils are in white (2 x 14 turns), the vertical field coils are in yellow (4 x 5 turns), the horizontal filed coils (2 x 4 turns) are in green and the iron core is represented in red.

The ISTTOK tokamak has a continuous vacuum vessel surrounded by a relatively thick stabilizing copper shell (15 mm) with a toroidal and a poloidal cut which avoids the circulation of direct current in the toroidal and poloidal directions. The vessel is made from a set of resistive Inconel bellows with very thin walls joined by thick rings holding the vacuum pump system and several diagnostic ports. The effective resistivity of the vessel in the toroidal direction is $4.95 \times 10^5 \text{ S.m}^{-1}$. Although driven by the ohmic heating transformer, the continuous vessel carries a moderate parasitic current. This current has a small effect compared to the strong shielding effect of parasitic currents induced by the equilibrium field coils in the highly conductive copper shell $5.8 \times 10^7 \text{ S.m}^{-1}$. Nevertheless, the current eddies in the shell effectively retard the equilibrium field penetration during the plasma start-up and formation processes in ISTTOK. This effect contributes to degradation of the ISTTOK controllability. In fact to

overcome this effect the ISTTOK power supplies used for radial control of the plasma column are over dimensioned.

The poloidal field coils system in ISTTOK is formed by the ohmic heating solenoid, the vertical field coils and the horizontal field coils. The ohmic heating coils are composed by two sets of 14 coils in the low-field side. Since ISTTOK has an iron core the majority of the ohmic field passes through the iron core creating the flux necessary for driving the plasma current. The vertical field power supply is composed by four sets of coils each with 5 wires as represented in Figure 27, the outer coils are arranged in opposition to the inner coils, so the resulting field is near vertical in relation to a poloidal cut of the vessel. Since the currents flow in different directions, the vertical field is almost decoupled from the ohmic field. The horizontal field is composed by two sets of coils with 4 wires each and the current flows in different direction for each set, producing a field approximately horizontal. This field is not as uniform as the vertical field because contains less coils positions.

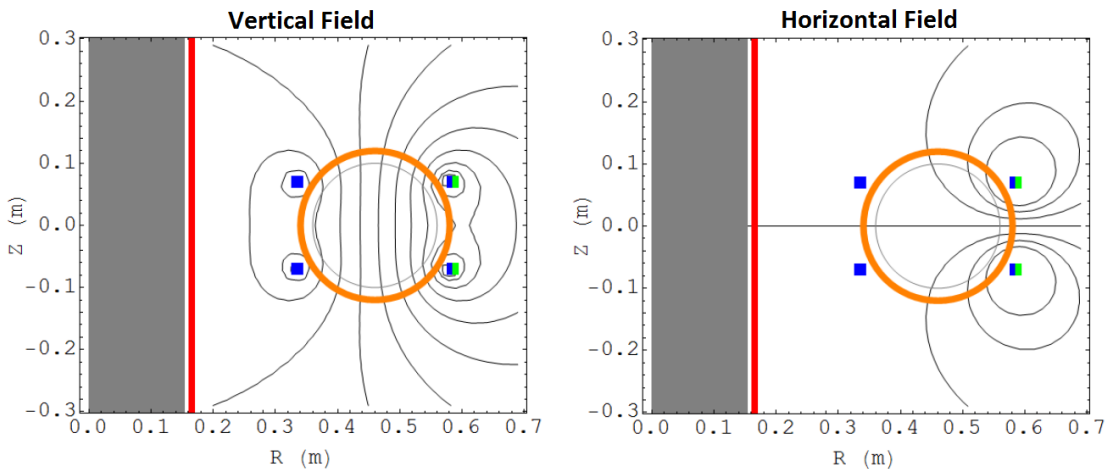


Figure 27 – Poloidal cut evidencing the ISTTOK vertical field and horizontal field mapping. The vertical field is a quadropole and the horizontal field is a duopole of coils.

It was recently upgraded with a new control system based on the Advanced Telecommunications Computing Architecture (ATCA) standard and with a new set of power supplies. This upgrade was aimed to improve the control of plasma parameters during the discharge and to allow new control strategies. The ISTTOK tokamak has a regular Alternate Current (AC) discharge program [33][34], one natural application of this control system is to improve the reliability of the discharge and extend the discharge duration. This led to a development of a more complex real-time controller that, among other features, allows configuring and executing several synchronization strategies between the main discharge parameters and the system feedback actuators. Since the controller is more complex and takes into account a larger number of variables and events, a user-friendly visual interface for programming the plasma discharge was also developed.

The hardware for the fast control [25][35] was developed in-house and is used in several experiments such as the JET vertical stabilization [23] and the COMPASS tokamak control [36][37]. Also, in the ITER fast plant system controller prototype an enhanced version of this hardware was used [38].

Chapter 2 - Diagnostics

The tokamak diagnostics (Figure 28) are used to infer some of the plasma properties. The most important plasma parameters are: plasma current, plasma position (or boundary reconstruction), plasma vertical velocity (in case of elongated plasmas), plasma density, plasma radiation, stored energy, pressure profile, plasma inductance, MHD stability, transport, ELM characteristics, turbulence, q profile, ion temperature, electron temperature and neutron production. Each of these properties can be calculated by several diagnostics and often one diagnostic can be used to determine several plasma parameters. As an example the Thomson scattering at JET [39] is used in the calculation of electron temperature and density. The density can be deduced by the total intensity of the scattered light and the electron temperature is obtained by measuring the width of this scattered spectrum. These and other parameters are used as an input for several equilibrium codes developed throughout the years by the fusion community and provide further insight on the plasma properties [40].

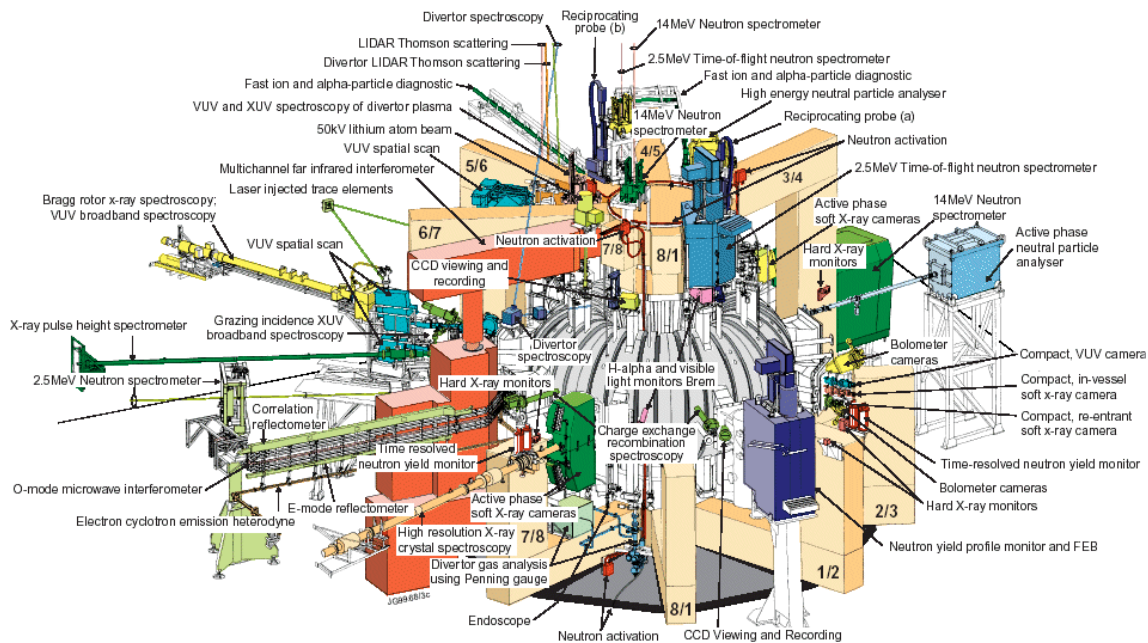


Figure 28 – JET tokamak diagnostics and their location.

In order to improve the plasma performance during a discharge, plasma properties must be available in real-time, but due to technologic limitations some of the most complex calculations are only performed after the pulse, making them unavailable for real-time operation. Since optimized plasma actuation is a key factor for high performance discharges and plasma parameters evolve during the discharge, it is essential to have accurate measurements of the plasma parameters in real-time in order to act on the plasma correctly. The plasma control is a complex system since acting in one individual plasma parameter normally influences other plasma parameters, to address this issue, the plasma control systems throughout the years evolved to allow more integration between all diagnostics and

actuators and nowadays plasma control systems are designed as multiple-input multiple-output (MIMO) systems.

Diagnostics can be qualified by their precision and accuracy of the measurements, in addition to these qualifications, in real-time systems the diagnostics are also benchmarked by their reliability, availability, delay of the measurement and the acquisition rate. The real-time diagnostics can also be qualified by their importance to the machine protection. Some real-time diagnostics are so important for the machine safety operation that their failure leads the plasma controller to perform exception handling routines to safely terminate the plasma discharge.

The ISTTOK tokamak has a smaller size compared with tokamaks such as JET and ASDEX, so, there is not enough physical space to fit some diagnostics that are present in the referred machines. Nevertheless, ISTTOK has several diagnostics namely: main Rogowski coil, Mirnov probes, electric probes, tomography, sine probe, cosine probe, H-alpha bolometer, interferometer, loop voltage, heavy ion beam, spectrometer, retarding field analyser and other electric probes to study plasma fluctuations. These diagnostics are detailed in the next subsection.

2.1. ISTTOK diagnostics

As mentioned in the previous sub-chapter, ISTTOK has several diagnostics. A list of these diagnostics is presented below.

Magnetic coils:

ISTTOK has a set of 12 Mirnov coils for real-time control. The magnetic probes are positioned inside the vacuum chamber as depicted in Figure 29 and they are oriented in order to measure the poloidal field created by the plasma current, so the coil wiring is in the poloidal direction (each coil has 50 turns with an area of 25 mm²). Since the magnetic probes output voltage is proportional to the derivative of the magnetic field, it is necessary to integrate this signal to obtain the magnetic field value. Analogue integrators (Figure 30) are used to integrate the signal from the probes. To avoid saturation these analogue integrators have a discharge time constant of about 100 ms.

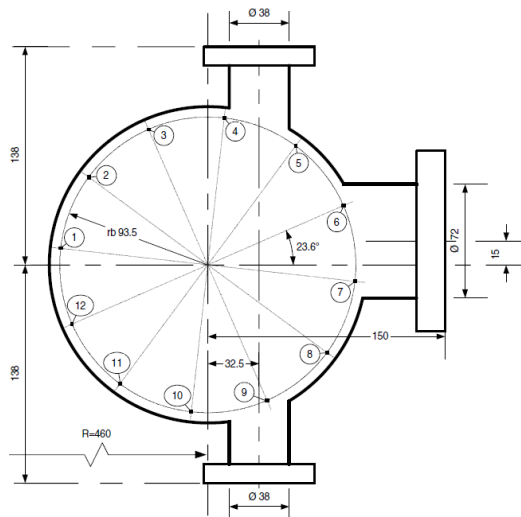


Figure 29 – Position of the 12 magnetic probes inside the vacuum chamber. The magnetic probes are oriented to measure partially the poloidal created by the plasma current. Probes are located at a 0.095 m radius.

The simplified algorithm used for plasma position calculation is based in the centroid algorithm for a circular plasma described by equation 18 and equation 19.

$$R_p = \frac{\sum_{i=1}^N R_{\text{probe}}^i \times H_p^i}{\sum_{i=1}^N H_p^i} \quad (18)$$

$$V_p = \frac{\sum_{i=1}^N V_{\text{probe}}^i \times H_p^i}{\sum_{i=1}^N H_p^i} \quad (19)$$

Where R_p is the radial position, V_p is the vertical position, H_p^i is the value of the magnetic field in probe i and N is the number of magnetic probes. Since the Mirnov coils are integrated and the analogue integrators have a characteristic discharge time it is necessary to correct this effect on the measurements.

$$ADC_{corr}^{ij} = ADC^{ij} + \frac{RC}{f_{acq}} \times Acc^{ij} \quad (20)$$

$$H_p^{ij} = C^i \times ADC_{corr}^{ij} \quad (21)$$

Where the ADC_{corr}^{ij} is the corrected ADC value, ACC^{ij} is the accumulator and H_p^{ij} is the magnetic field on each probe. The plasma current can also be obtained from the Mirnov coils data (equation 22).

$$I_p = \frac{2\pi r_{probes}}{N} \sum_{i=1}^N H_p^{ij} \quad (22)$$

Where the I_p is the plasma current and r_{probes} is the probes location radius which is 0.095 m.

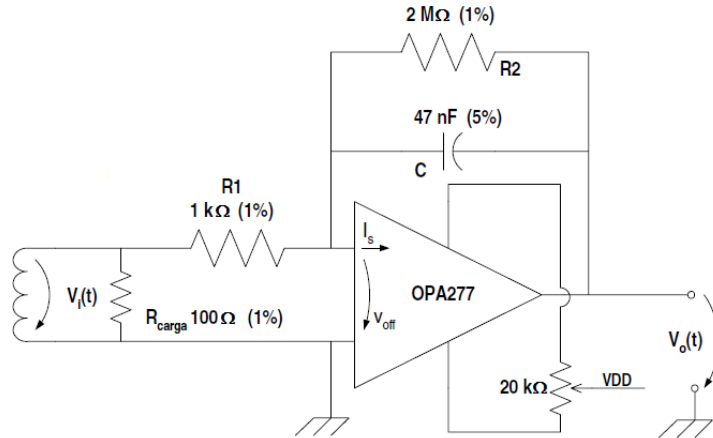


Figure 30 – ISTTOK analogue integrators schematic for integrating the magnetic probes output.

Another method (although not implemented) that could provide more precise results at the cost of real-time performance is the finite current filaments [41]. Since the ISTTOK real-time control software is modular, the block of code for each diagnostic can be easily replaced.

Moreover, ISTTOK does not have high plasma current and also cannot reach h-mode, the Shafranov shift can be ignored from plasma position calculation.

Main Rogowski coil:

The main Rogowski coil is used to measure the total plasma current. It consists on a helical wire coil with a near circular shape as depicted in Figure 31. The voltage at the terminals of the Rogowski coil is given by equation 23, where A is the area of the small loops, N is the number of turns, R is the major radius of the Rogowski coil and dI/dt is the rate of change of the current flowing inside the Rogowski coil.

$$V = -\frac{A \cdot N \cdot \mu_0}{2\pi R} \frac{dI}{dt} \quad (23)$$

To obtain the absolute value of the current flowing inside the Rogowski coil the coil's output should be integrated. In ISTTOK the Rogowski coil is located between the copper shell and the vessel wrapping the torus in a poloidal section to measure the plasma current in the torus. The

Rogowski coil output is integrated using an analogue integrator developed on site and then is acquired by the control system and the central ISTTOK data acquisition.

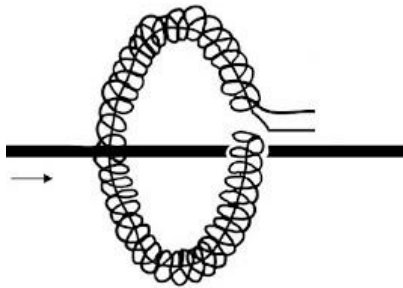


Figure 31 – Rogowski coil to measure (after integration) the current flowing in the area delimited by the Rogowski coil arrangement.

Loop voltage:

Since ISTTOK has an iron core, most of the flux passes through the iron core. To measure the loop voltage for the real-time control system, a loop was inserted around the iron core to measure the voltage according to equation 24.

$$\text{EMF} = -N \frac{\partial \Phi}{\partial t} \quad (24)$$

The loop voltage is measured by the control system to oversee the iron core flux saturation. To predict the flux saturation a combination of three variables is used (plasma current, primary field PS current and loop voltage). When the primary field power supply current is unusually high for a certain loop voltage, the flux is likely saturated.

Sine and cosine probes:

The sine and cosine probes are similar to rogowsky coils apart from the variable wiring density in the coil. The main objective of having a variable wiring density in the poloidal direction is to “linearize” the integrated signal from the probe in respect to the plasma vertical position. To calculate the wiring density it is necessary to calculate the magnetic field in a poloidal section as described in paper [42]. Observed from the outer midplane the sine coil turn density is proportional to a sine function according to the poloidal angle when the sine function is negative the coils are wired in the opposite direction. With this layout, if the plasma moves in the radial direction it will not affect the coil output signal and when the plasma moves in the vertical position the output signal (after integration) is proportional to the movement. The cosine probe (similar to the sine probe but rotated 90° in the poloidal direction) is based on the same principle and is used to measure the plasma radial position. The cosine probe output is also integrated using an analogue integrator developed on site.

Tomography:

The ISTTOK tomography diagnostic is composed by three arrays of optical sensors. These optic sensors sensibility is depicted in Figure 33. Each array has 10 photodiodes in line, but only the 8 central photodiodes are used for real-time control. The silicon photodiodes are manufactured by Hamamatsu and measure 1.5x2.5 mm² (poloidal x toroidal) with a separation of 0.55 mm between each sensor. Each camera has a circular pinhole with 1 mm drilled on a 0.1 mm copper sheet at a distance of 10 mm from the photodiode array. This arrangement

allows a full plasma coverage on a vessel cross section while maintaining a relatively low overlap of adjacent viewing cones (see Figure 32).

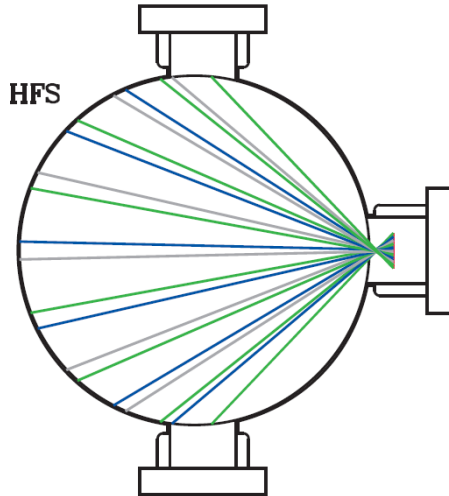


Figure 32 - ISTTOK cross-section displaying the equatorial tomography camera's viewing cones. Each two lines of the same colour represent the viewing area of one photodiode, as they are overlapped.

There is no filter in front of the cameras, so the photodiodes detect from soft x-rays to high infrared with different sensibility as depicted in Figure 33. The silicon photodiodes were doped to increase the sensibility to the UV and soft X-rays, but their sensitivity to these wavelengths is still below about 20% that of the visible electromagnetic range.

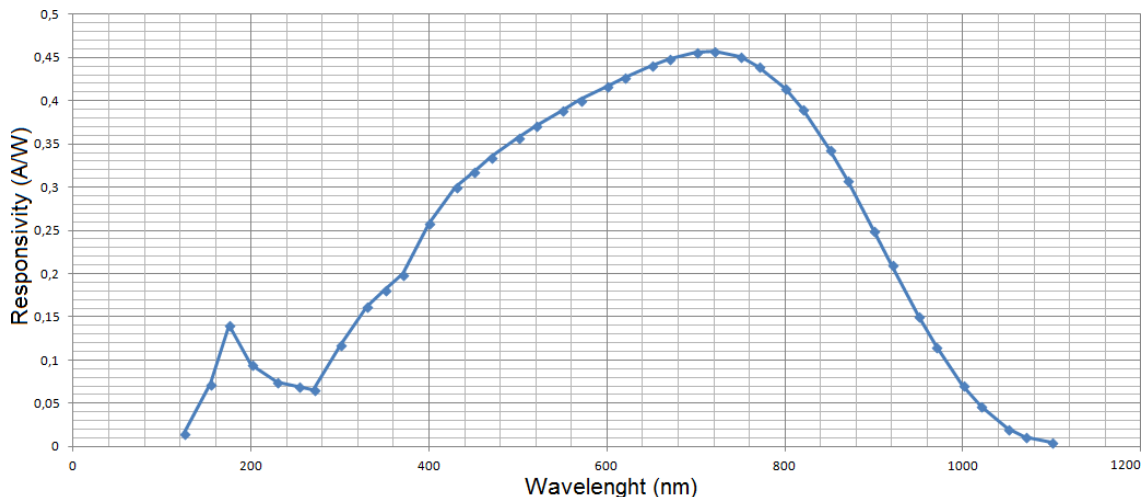


Figure 33 – Responsivity of the sensor versus radiation wavelength, as it can be observed the responsivity peak is near 700nm (red colour), the H_α radiation has a 656 nm wavelength.

The cameras were installed on three different positions (top, bottom and outer) in a tokamak cross section (see Figure 34) and there signals are carried directly through the vacuum port to amplifiers to avoid electromagnetic noise.

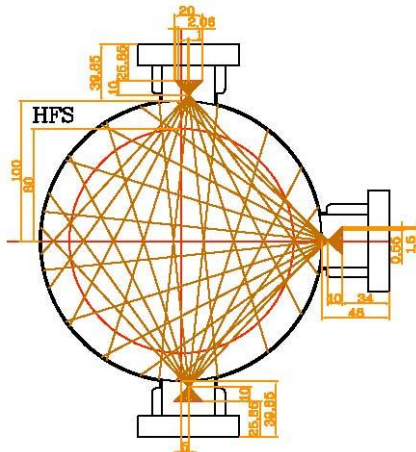


Figure 34 – Tomography diagnostic schematic. The ISTTOK tomography diagnostic has three sets of optic sensors each containing 8 lines of sight with pinhole. The sensors are located on the top, the bottom and on the low field side of ISTTOK.

Each photodiode is connected to a transimpedance amplifier according to the schematic on Figure 35. This transimpedance amplifier amplifies the photo diode current by 1.8×10^6 Volts per Ampere. Each PCB board (near the vacuum port) contains 8 amplifiers and the resulting signals are then carried to the acquisition board via twisted pair cables to minimize the induced electromagnetic noise.

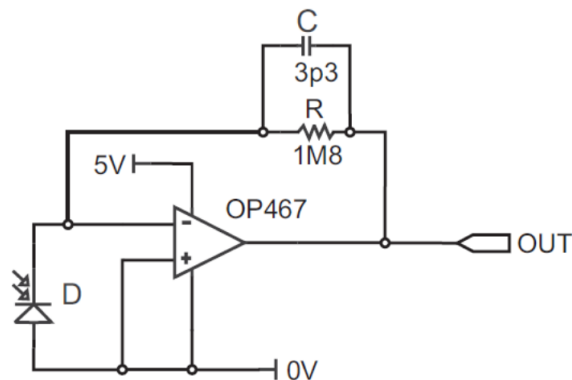


Figure 35 – schematic of the photodiode's amplifier

The tomography signals are acquired at the control cycle frequency. During each control cycle the reconstruction algorithm calculates the plasma position based on the Fourier-generic algorithm (with Bessel functions as base functions).

The Tomography objective is to find the emissivity function $g(r,\theta)$ as a function of the several line integrated measurements $f_L(p,\phi)$ obtained from the cameras (equation 25).

$$f_L(p,\phi) = \int_L g(r,\theta) dL \quad (25)$$

If $g(r,\theta)$ is assumed as a combination of basis functions [43][44][45][46], then equation 25 can be inverted. The algorithm for real-time calculation of the plasma position based on the Fourier generic method with decomposition in Bessel functions is described in detail on paper [47].

Electric probes:

The ISTTOK electric probes are used to characterise the plasma poloidal asymmetries [48] and are also used for measuring the plasma position indirectly by measuring the floating potential in four poloidal angles. There are four sets of electric probes installed in ISTTOK similar to the probe depicted in Figure 36. These probes are located at each 90° (top, bottom, inner and outer positions). The distance from the pins to the vacuum vessel centre is 75 mm while the plasma limiter is located at 85 mm from the vacuum vessel centre and the control system acquires the data from each probe pin 1 (floating potential).

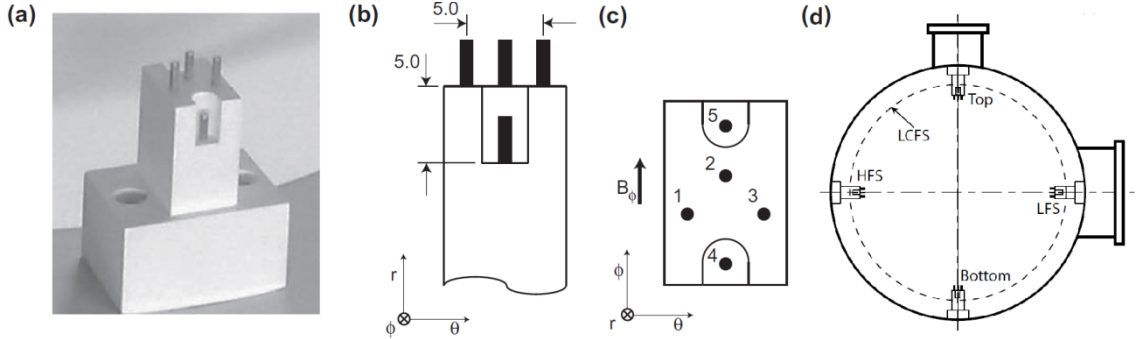


Figure 36 – ISTTOK electric probes used for real-time control. A total of four probes are installed in ISTTOK at each 90° , subfigure (d).

In circular plasma with standard plasma distribution and apart from natural plasma fluctuations and instabilities, the electric probes floating potential inside the plasma last closed flux surface (LCFS) is similar to the plasma potential. The behaviour of the ISTTOK plasma potential [49] is depicted in Figure 37. As it can be observed the floating potential is monotonic inside LCFS and if correctly modelled the plasma position can be hinted from the difference between the floating potential of two opposed electric probes. For example the vertical position can be hinted from the floating potential of the top and bottom electric probes.

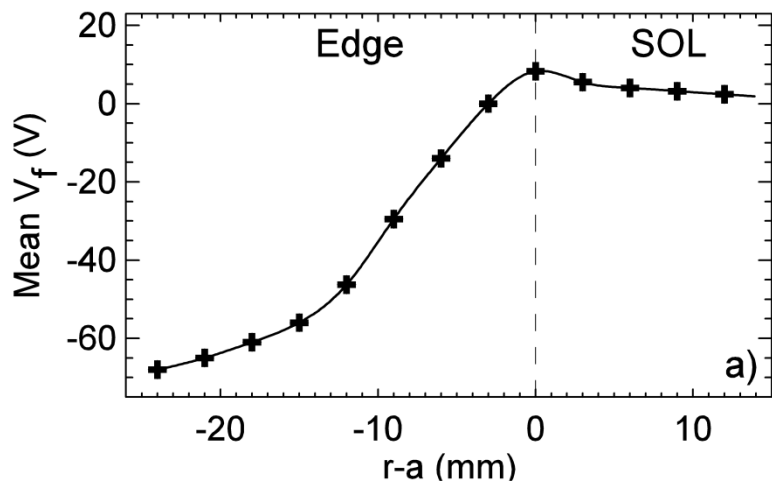


Figure 37 – Floating potential measurement at the ISTTOK tokamak obtained from several discharges with different probe positions. Since ISTTOK does not have heating sources other than ohmic heating the pressure profile is monotonic and consequently the floating potential is also monotonic apart from the scrape-off layer (SOL).

Interferometer:

The ISTTOK interferometer [50] is based on the heterodyne detection principle with quadrature detection for an absolute phase determination and has only one vertical line of sight that crosses the plasma in the radial centre. The interferometer uses a frequency of 100 GHz to cross the plasma as depicted in Figure 38, with this frequency and according with the plasma cut-off frequency (equation 26) can be used to measure the line integrated density up to $1.24 \times 10^{20} \text{ m}^{-3}$. The signal from the RF oscillator and the same signal after crossing the plasma are then mixed with the local oscillator frequency (99.15 GHz), resulting in an interference frequency of 850 MHz. Although more complex, this method has the advantage of reducing the frequency to be acquired by the data acquisition system and improves the sensibility of the system.

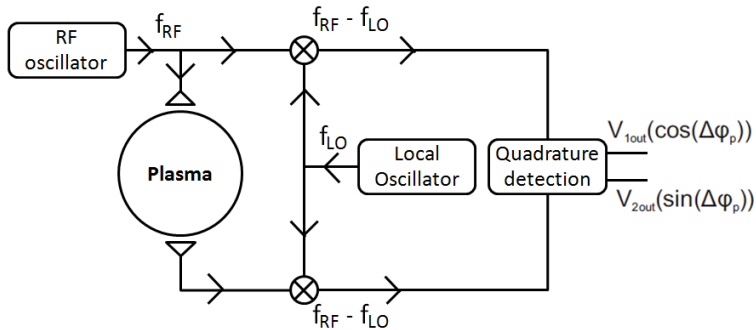


Figure 38 – ISTTOK interferometer based on the heterodyne detection principle.

$$n_c = \frac{\epsilon_0 m_e (2\pi f)^2}{e^2} \quad (26)$$

The interferometer output can be described by equation 27 and 28, when the cosine derivative is near 0 the sensibility of the measurement is greatly reduced. To avoid the ambiguity near the cosine derivative equals 0 operational zone a quadrature detection system is used.

$$V_{1\text{out}} = V_{1\text{DC}} + K_1 \cos(\Delta\varphi_p(t)) \quad (27)$$

$$V_{2\text{out}} = V_{2\text{DC}} + K_2 \sin(\Delta\varphi_p(t)) \quad (28)$$

The quadrature detection system produces an extra output signal (equation 28) by introducing an extra reference signal dephased by 90° from the original reference signal, resulting in an extra output signal proportional to the sine of the phase difference. After obtaining these two signals and subtracting the offsets it is possible to measure the phase $\Delta\varphi_p$ absolutely using the arctan function (equation 29). The ISTTOK line integrated density is only measured in one vertical cord and is obtained by multiplying the phase difference in radians by 6.964×10^{17} . Since the ISTTOK interferometer only has one vertical cord, plasma radial movements can affect the interpretation of the measurement.

$$\Delta\varphi_p(t) = \arctan_{4Q} \left(\frac{\sin(\Delta\varphi_p(t))}{\cos(\Delta\varphi_p(t))} \right) = \arctan_{4Q} \left(\frac{K_2(V_{2\text{out}} - V_{2\text{DC}})}{K_1(V_{1\text{out}} - V_{1\text{DC}})} \right) \quad (29)$$

The sine and cosine are acquired by the acquisition system and a list of the ISTTOK interferometer characteristics can be found in Table 3.

Parameter	Value
Radio frequency	100 GHz
Critical density	$1.24 \times 10^{20} \text{ m}^{-3}$
Position	Vertical and centred
Fringe value	$4.38 \times 10^{18} \text{ m}^{-3}$
Local oscillator frequency	99.15 GHz
Interference frequency	850 MHz
Propagation mode	TE ₁₀

Table 3 – ISTTOK interferometer parameters.

H-Alpha:

The H_α radiation is a part of the Balmer series (visible) for the hydrogen and is produced when an electron transits from the hydrogen n=3 level to n =2 (see Figure 39) corresponding to a 656 nm wavelength.

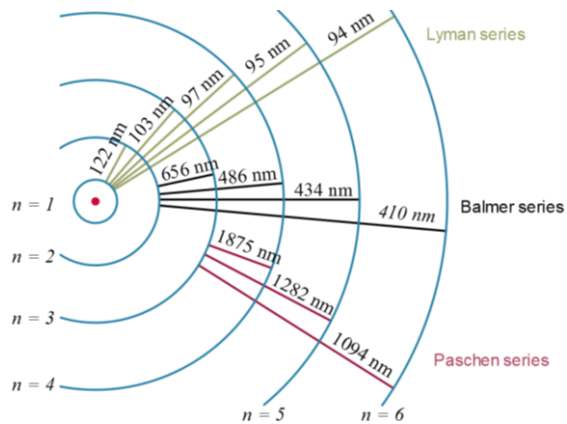


Figure 39 – Hydrogen excitation levels and radiation wavelength produced by transitions from different excitation levels. H_α radiation corresponds to the transition from the n=3 level to the n=2 level producing a radiation with 656 nm wavelength.

The ISTTOK H_α diagnostic is composed by a photodiode and a band filter centred in the H_α wavelength with 10 nm width. This diagnostic is located just outside an equatorial port and measures the H_α radiation coming from the inside of the vessel. The signal from the photodiode is then amplified and acquired by the acquisition system.

Heavy ion beam:

The heavy ion beam [51] (HIB) is one of the most versatile plasma diagnostics allowing to measure plasma density, electron temperature, poloidal magnetic field and plasma potential profiles with high spatial resolutions. The temporal resolution of this diagnostic is also high enough to study fluctuations associated to the previously mentioned parameters. Unfortunately in large tokamak experiments [52] the toroidal field is so strong that the required beam energy to travel along the plasma would be extremely high and for that reason these ion beams are limited to diagnose the plasma edge. Since ISTTOK vacuum vessel only has 20 cm of diameter and relative low plasma density and toroidal field, it is possible to diagnose the plasma using this diagnostic since the ion beam is able to travel across the ISTTOK plasma, although it has some natural curvature mainly due to the toroidal field.

The ISTTOK HIB (Figure 40) is able to operate either with caesium ions (Cs⁺) or with xenon ions (Xe⁺), but the ion beam current is higher in the case of Xe⁺ operation. In this mode of operation

the HIB has the following characteristics: 22 keV of the energy, 15 μ A of the intensity and 3 mm of the beam full width at half maximum (FWHM).

After passing through the plasma, the ions that suffer additional ionizations (by electron collisions) are additionally deflected by the toroidal field since they have an additional positive charge (Xe^{2+}).

The detection system consists of two multi-cell detectors, one that collects secondary ions and the other that collects the primary ions that travel through the plasma without further ionisations and are only deflected by the magnetic field. The secondary detector consists in a column of 12 ($6 \times 12 \text{ mm}^2$) flat copper cells separated by 0.3 mm for insulation. It is installed inside the tokamak vacuum vessel at the position calculated taking into account the primary Xe^+ trajectory and the normal collisions pattern that produce the secondary Xe^{2+} ion trajectories in the ISTTOK magnetic field. The secondary ions enter the cells in the detector plane at about a 60° pitch angle. For the primary beam detection there is a matrix of 3x5 detectors to measure the beam deflection by the toroidal and poloidal fields inside the vacuum vessel.

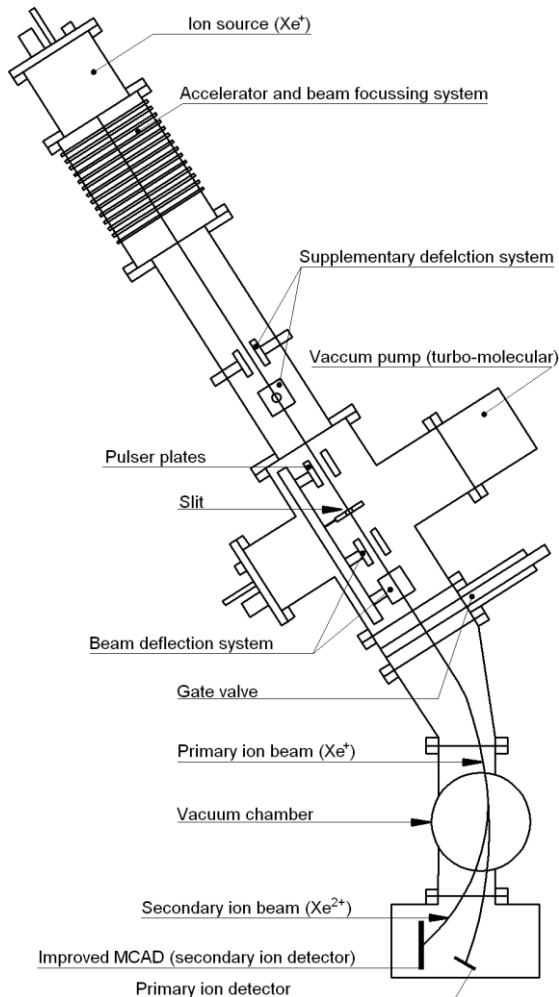


Figure 40 – ISTTOK Heavy Ion Beam schematic. The ion beam travels through the plasma where is deflected by the magnetic field. The ions are further ionized according to the plasma density and ions more ionized curve more in the presence of the ISTTOK magnetic field, these ions are collected by the secondary ion detector allowing plasma density and temperature measurements.

Retarding field analyser:

The retarding field energy analyser (RFEA) [53] is one of the most reliable diagnostic to measure the ion temperature in the boundary of the plasma. ISTTOK has a compact and simple RFEA design. The system consists on a stainless steel pinhole (with 0.6 mm diameter), three fine nickel grids separated by 1 mm, and a collector, all with mica insulation. All the components are placed inside a boron nitride housing that measures $14 \times 14 \times 23$ mm³. The RFEA system can measure either electron temperature or ion temperature. The RFEA consists of a collector electrode with two or more separately biased fine grids placed in front of it. The ions enter the RFEA through a small aperture as depicted in Figure 41.

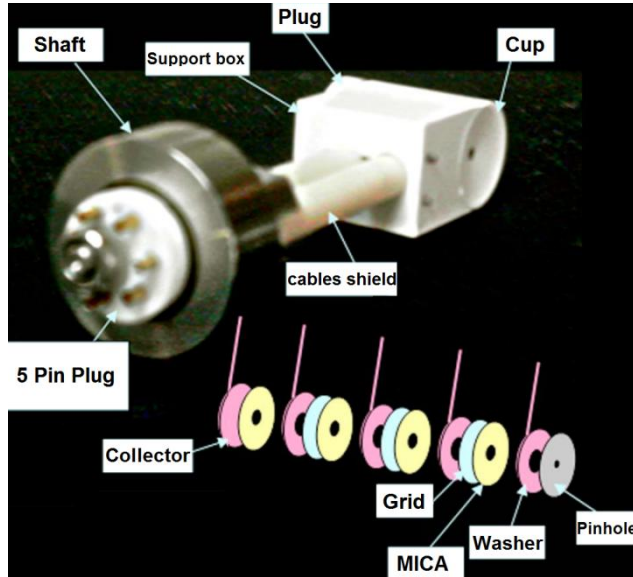


Figure 41 – ISTTOK Retarding field energy analyser.

The ion temperature is obtained by measuring the collected current as a function of the retarding potential. After collecting the data it is necessary to iteratively determine the plasma potential in relation to the probe ground and least square fit the collected signals taking into account the Maxwellian distribution of the collected ions.

Since this diagnostic requires iterative calculations and does not measure relevant plasma parameters for real-time operation, it was not included in the real-time control system.

Spectrometer:

There are two spectrometers in the ISTTOK tokamak. These spectrometers are used to perform impurity studies. One of the spectrometers is based on a "Mcpherson, model 2501" spectrograph with 1 m focal length, f/8.7 aperture mounted in the Czerny-Turner configuration and 0.1 Å best resolution when equipped with a 1200 l/mm (100 x 100 mm² size) grating. This spectrometer can be used to monitor the time evolution of several impurity lines in monochromator mode or the ions temperature (Doppler broadening) in spectrometer mode, when equipped with a "Princeton Applied Research, model 1205 OMA" (512 channels, 12.5 x 5 mm² sensor) camera or a "Alton Instruments Inc., LS2000 Optical Multichannel Analyzer", (2048 pixels, 14x200 μm^2 size) with 5 ms minimum integration time which allows ion temperature measurements with a good time resolution [54]. The other spectrometer is a more recent "CVI Laser DK480I" imaging spectrograph. This spectrometer is equipped with a triple-grating turret system, blazed at 300, 500 and 750 nm and 1200 gr/mm each. The 68x68

mm^2 gratings provide a maximum resolution of 0.06 nm and a reciprocal dispersion of approximately 1.60 nm/mm. The image spectrographs are able to resolve spatially separated points focused at the input slit due to their special optical design and this feature enables a more versatile usage of this spectrometer compared to the previous one.

This diagnostic requires manual operation and due to this fact it was not integrated in the real-time control system.

Other Langmuir probes:

During some experimental campaigns, ISTTOK has several configurations of electric probes [49]. Two of the most used electric probes (poloidal array and rake probe) are depicted in Figure 42. These probes are used to measure geodesic acoustic modes, zonal flows, plasma Mach number, Reynolds stress and plasma fluctuations.

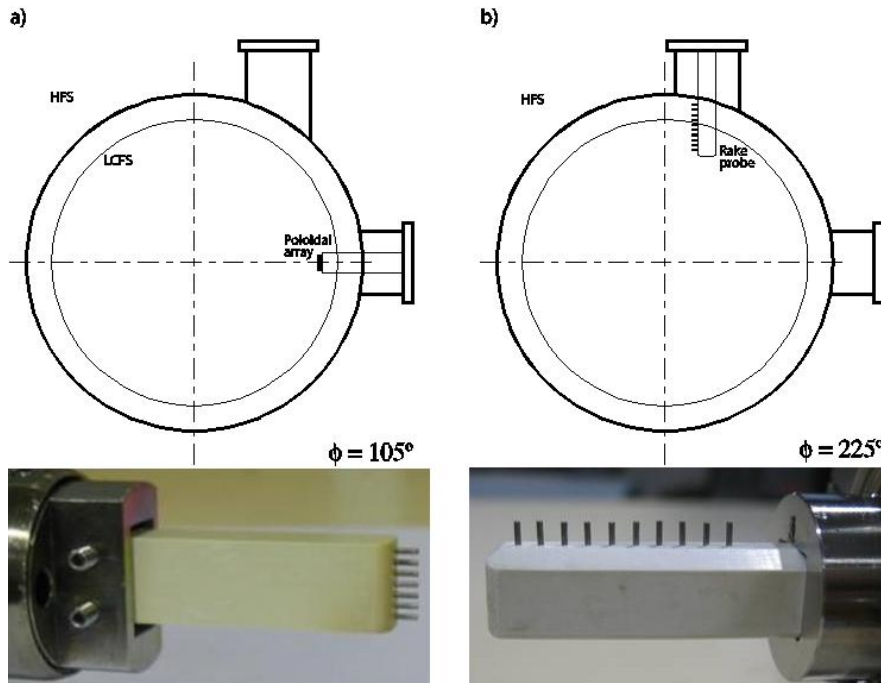


Figure 42 – Schematic and pictures of: a) Poloidal array of electric probes and b) rake probe (vertical array of electric probes). The radial array has a 3 mm spacing between pins and the poloidal array has a 2 mm spacing between pins.

Since these diagnostics are not always inside the tokamak and do not produce additional data relevant for real-time operation, they are not included in the real-time control system.

The ISTTOK tokamak is a very flexible machine and because of that, some of these diagnostics are not present for all the discharges, as they are used only for specific experimental campaigns being replaced by others due to the low number of access ports. Figure 43 depicts the position of the ISTTOK diagnostics around the torus.

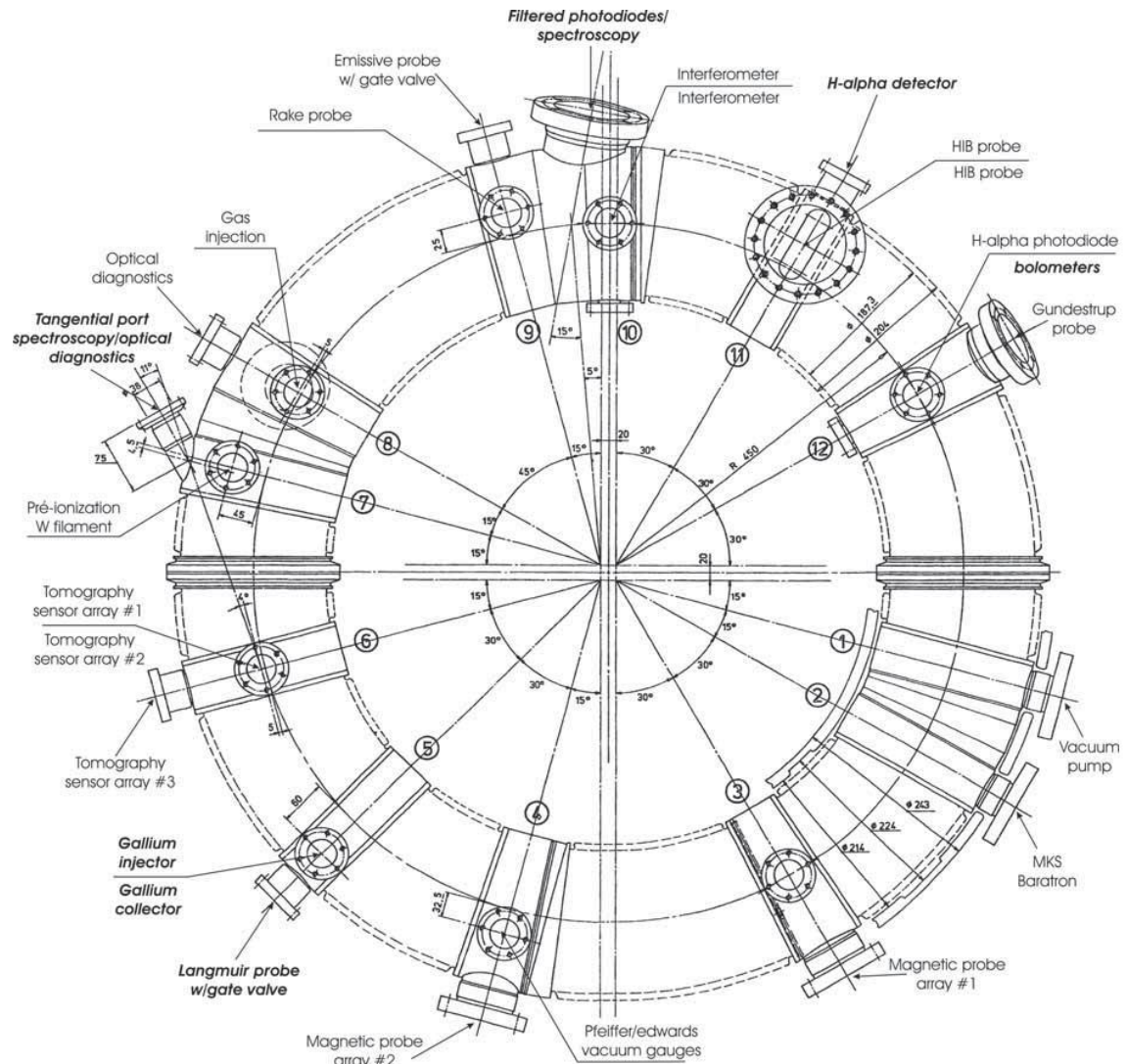


Figure 43 – Location of the ISTTOK diagnostics around the torus.

2.2. Diagnostics integration on the real-time platform

Only a subset of the ISTTOK diagnostics were integrated in ISTTOK, this subset was determined by the following factors:

- Automatic operation (not dependent on human intervention).
- Production of real-time relevant plasma parameters.
- Diagnostic automatic data processing is possible.
- The acquired data is analysable within the real-time constraints.
- Permanent diagnostic.

Based on these criteria, the selected Diagnostics for real-time control were: main Rogowski coil, Mirnov probes, electric probes, tomography, sine probe, cosine probe, H-alpha bolometer, interferometer, loop voltage.

The heavy ion beam (HIB) was not selected because at the time of the commissioning of the control system, the HIB acquisition was being updated with new transimpedance amplifiers, for that reason and also because it is still manually operated it was not viable to include the HIB in the real-time control. Nevertheless it can be easily added to the control system due to the modularity of the control system and this issue might be addressed in a future update.

The diagnostics that met the referred requirements were integrated into the plasma control system in order to produce a Multiple Input Multiple Output (MIMO) system. The developed control system has the redundancy advantage and also allows the machine operator to select each diagnostic contribution when establishing an observer measurement. In Figure 44 is represented each integrated diagnostic connection to the measured plasma parameters.

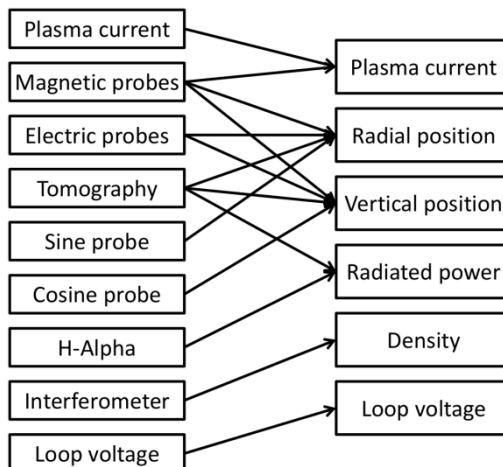


Figure 44 - ISTTOK Diagnostics contribution to the measured quantities.

Some diagnostics produce better results in low plasma current than others, for example the tomography [55][56] produces a more reliable output than the magnetic probes in low plasma current condition. The machine operator can select different diagnostics weight combination

for low and higher plasma currents for both the radial and vertical position in the visual configuration environment.

An exception handling mechanism is used for the iron core flux saturation using the loop voltage together with the ohmic PS current. When the iron core saturates the discharge must either invert the plasma current or terminate the discharge (both options can be selected by the machine operator).

To acquire the real-time diagnostics, ISTTOK has a set of two acquisition boards based on the ATCA standard, this system is described on chapter 4 and the software is described in chapter 5. Each board has a 18-bit ADC that acquires data at 2 MSamples/s. Since the control system runs at 100 μ s it is possible and useful to filter the acquired data. The full data flow path of the acquired data from the diagnostics is presented in Figure 45. The control system hardware is further described in chapter 4.2.

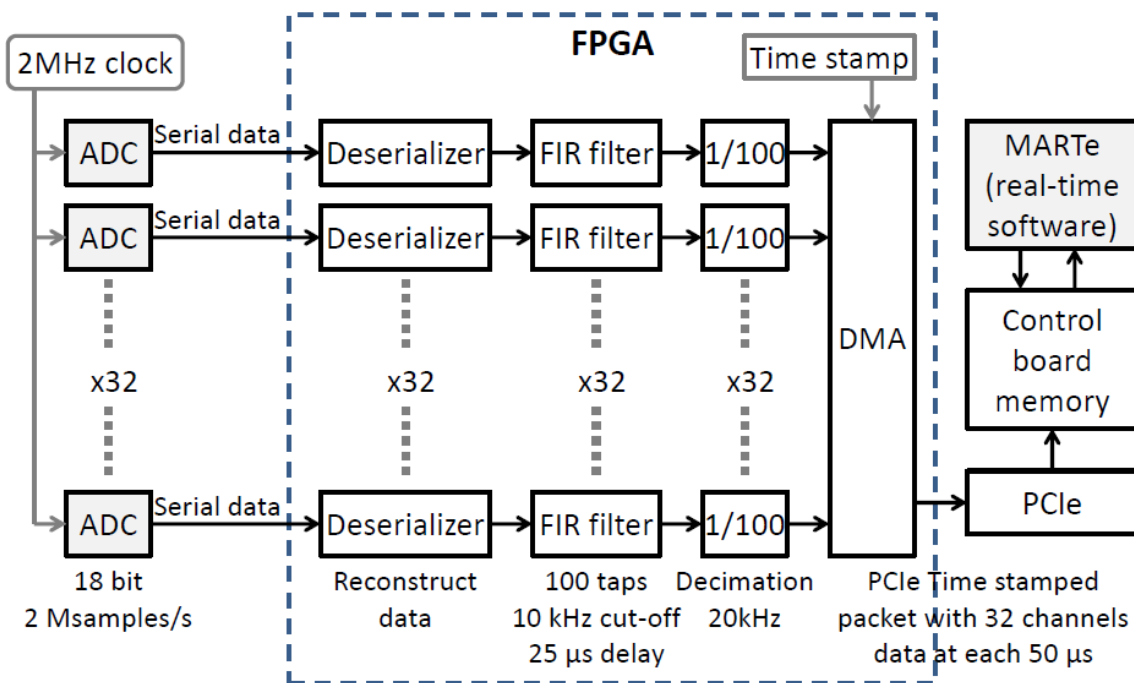


Figure 45 – Full data path schematic from the acquisition up to the controller board memory. Data is acquired at 2 MSamples/s and decimated to 20 kSamples/s after filtering with a 100 tabs finite impulse response filter (FIR).

Chapter 3 - ISTTOK actuators

In order to improve the tokamak operational space, a new magnetising field power supply was developed and the vertical and horizontal field power supplies [27] were upgraded in order to be integrated with the new control system. The power supplies have their own independent current feedback control and communicate by means of an optical link with the main control system at a rate of 921.6 kbit/s. The power supplies current controller has a 34.6 μ s control cycle running on a DSPIC30F2020TM microcontroller.

The ISTTOK actuators [57] are now composed by three power supplies and one piezoelectric gas insertion module. The power supplies control the magnetizing field, the vertical field and the horizontal field and the piezoelectric valve is used to control the gas injection.

The main difference between the old and the new systems is the primary field power supply. The previous ISTTOK primary field power supply was based on a capacitor bank discharging over a resistor in series with the ISTTOK primary field coils. This system was triggered from the central ISTTOK triggering system 1 ms after a fast discharge of another high voltage capacitor bank (named PRECO) that was responsible for the plasma breakdown. The previous magnetising field power supply operated only on a pre-programmed basis without feedback on the plasma current and was not integrated with the rest of control system.

To improve the plasma current control a new power supply was developed. This new power supply is based on IGBT PWM H-bridge capable of four quadrants operation and is connected to the main control system to receive current references. The primary field PS has a microcontroller to feedback control of the primary PS current. Since the new power supply is also connected to a different set of coils, the discharge from the high voltage capacitor bank was also removed. This new power supply has also a higher current specification.

3.1. ISTTOK configuration

The ISTTOK primary field configuration was changed together with the deployment of the new primary field PS. Due to the lack of control the old system used a high voltage capacitor bank to force the plasma breakdown. After firing this system, the old primary field PS was triggered to discharge the capacitor bank to the coils wired around the ISTTOK iron core. To produce the old AC discharges the old primary field power supply had an IGBT H-bridge that inverted the capacitor bank current at a fixed time interval.

The new primary field power supply has a similar schematic of the horizontal and vertical field power supply and is described further in the next sub-chapter. The new PS uses the same capacitor bank and the high voltage capacitor bank was removed from the system. The main difference is that the new PS is fully controllable and has feedback control on current. Figure 46 depicts the difference between the old and the new configurations of the primary power supply.

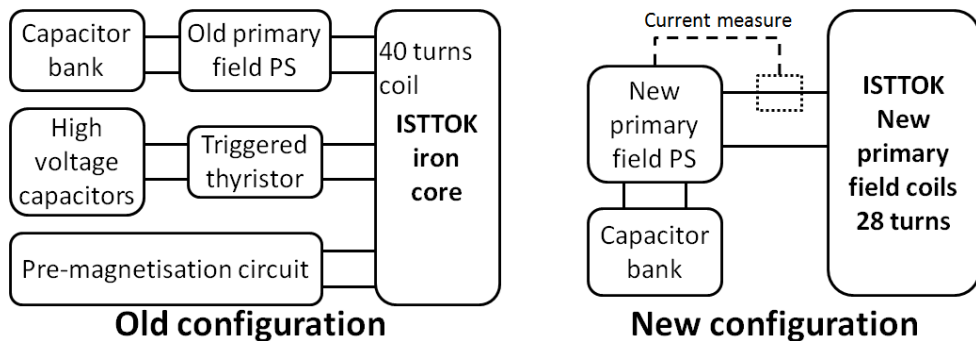


Figure 46 – Old and new configuration of the primary field circuit.

The ISTTOK tokamak has also a system to clean the vacuum vessel based on the glow discharge principle. Basically an AC current from the grid is connected to a coil around the iron core, producing an AC loop voltage and low temperature plasma to clean the vacuum chamber. Since the primary field power supply and the glow discharge circuit would be strongly coupled if both were connected at the same time, a mode of operation selector was developed to avoid simultaneous connection. This system is depicted in Figure 47.

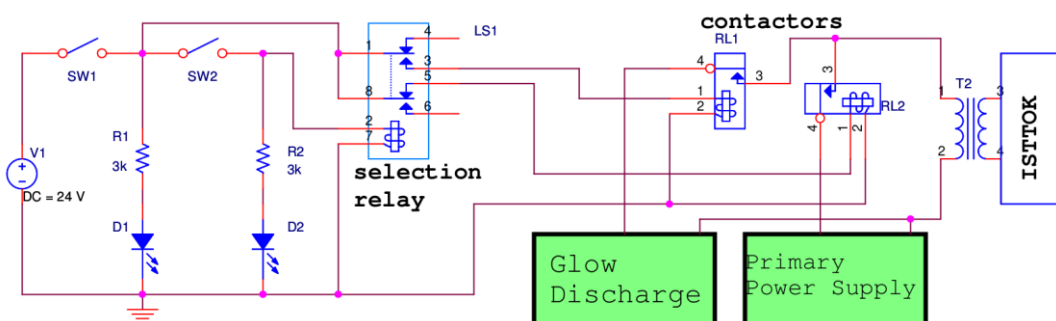


Figure 47 – Mode selection circuit schematic. This circuit was designed to prevent the simultaneous usage of the glow discharge circuit and the primary field power supply, also preventing the power supply from back electromagnetic force caused by the glow discharge operation (the two circuits would be strongly coupled if both were connected at the same time). SW1 and SW2 define the operation mode.

3.2. ISTTOK power supplies

The ISTTOK toroidal field power supply is based on a 12-phase rectification with control on the thyristors fire angle. This PS is directly powered from the three-phase grid and the 12 phases are produced by a delta-star transformer connection. This PS is able to produce from 4 kA up to 8 kA during 5 seconds and this current can be externally controlled. Normally, in tokamak operation, the toroidal field has a fixed value during the discharge unless the scientific programme has special requirements regarding the toroidal field. Although the new control system was also designed to control the toroidal field by reproducing a pre-programmed waveform, this feature was not tested since it was not required scientifically and because of that, this PS will not be discussed in this thesis.

The other ISTTOK power supplies are based on H-bridges with individual control of each branch of the bridge in real-time [57] (see Figure 48). In the case of the Horizontal field power supply, two MOSFET in parallel were used for each branch of the H-bridge, the selected MOSFET was IRFP3703. Each of these MOSFET is rated for 30V and 210A with a resistance of 2.8 mΩ ($R_{DS(on)}$) between the drain and source when conducting current. The vertical field has seven parallel IRFP4568 MOSFETs for each H-bridge branch. These MOSFETs are rated for 150V and 171 A with a resistance of 4.8 mΩ each. Although the referred MOSFET have their own freewheeling diodes, it was chosen to include additional 150EBU02 diodes in parallel to increase the freewheeling characteristics of the H-bridge circuit.

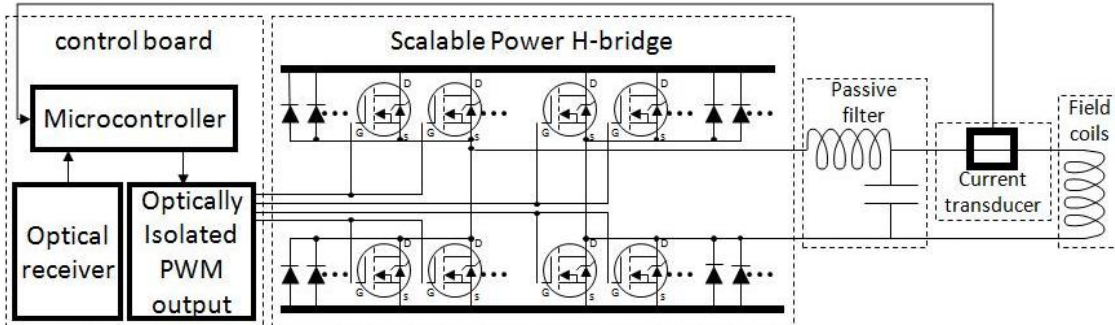


Figure 48 – Horizontal and Vertical field power supplies schematic. The horizontal field power supply H-bridge uses two parallel IRFP3703 and 150EBU02 freewheeling diodes. The vertical field power supply H-bridge uses seven parallel IRFP4568 MOSFETs and 150EBU02 freewheeling diodes.

Since the primary field PS has a higher voltage input, it relies on an H-bridge with IGBTs (Figure 49) instead of the MOSFETs in parallel found in the other two PS. The IGBT selected for the primary field PS is the BSM400GA120DN2, rated for 1200 V and 550 A. To filter the output, the power supplies have high voltage polypropylene non-polar capacitors.

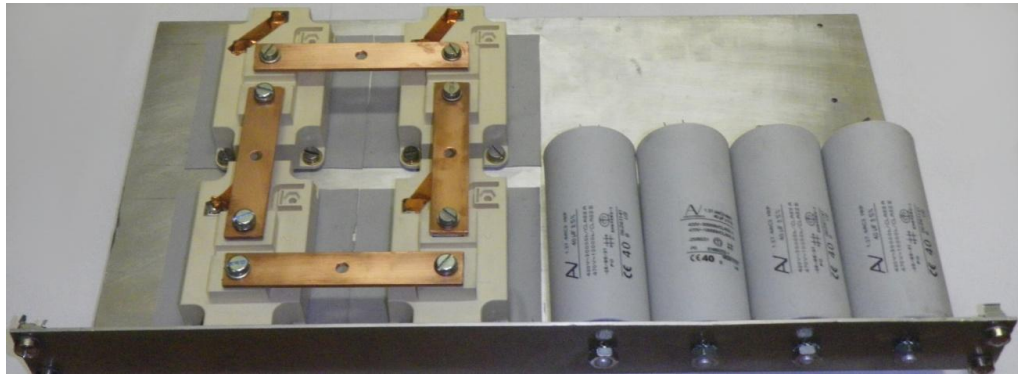


Figure 49 – Primary field power supply without the connecting wires. This power supply is based on a switching mode H-bridge using BSM400GA120DN2 IGBTs and fast polypropylene capacitors for filtering. This power supply was build to fit a 19" rack.

All these power supplies have a similar control module (Figure 50). All modules were installed in a 3U 19" rack. This rack contains the auxiliary voltage power supplies (for the control modules) and one controller and driver board for each PS (all schematics are on the annexes section). The controller and driver modules for each PS are connected via the backplane (Figure 51). To avoid output bouncing when the power supplies are connected a safety relay was installed. The power to the driver circuit is only connected once the microcontroller from the control board is properly initiated because the outputs of the microcontroller are not guaranteed in the initialization sequence and this could potentially short circuit the power H-bridge for a brief initialization period.

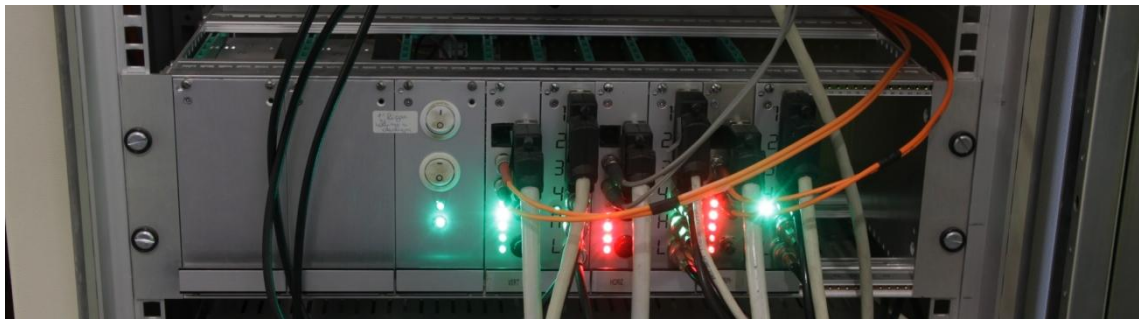


Figure 50 - Power supplies control module. Inside the 19" rack there are the following modules (from left to right): 24 V DC power supply, 24 V DC power supply, 5 V DC power supply and on/off switches, vertical field power supply control module, insulation module to drive the vertical field power supply, horizontal field power supply control module, insulation module to drive the horizontal field power supply, primary field power supply control module and the insulation module to drive the primary field power supply.

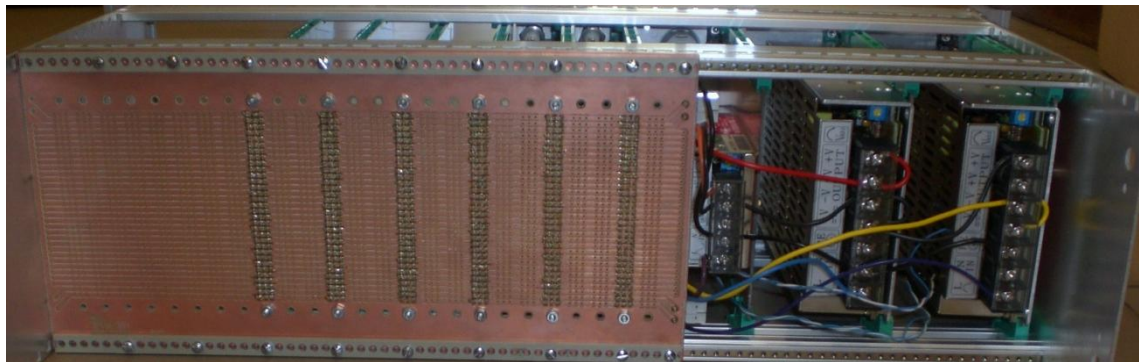


Figure 51 – Backplane of the power supplies control module.

The controller board (Figure 52) includes a DSPIC30f2020 microcontroller based on a modified Harvard architecture that runs one instruction per main clock cycle and the clock was set to 29.49 MHz (multiple of the communication speed). For this application the microcontroller was directly programmed in assembly to increase the control on the real-time characteristics of the system since it was designed as a hard real-time system. The control cycle for the power supplies is about 34 μ s. Although the code execution time is by far smaller this time was chosen to avoid over switching the H-bridge. At each control cycle an interrupt is generated to run the feedback code. First the microcontroller reads the ADC value corresponding to the actual power supply current and then compares with the last current request. According to both values the controller decides the outputs to the H-bridge. The PS current measurement is obtained from a Hall effect current transducer (LF-1005-S) which translates current from -1750 A to 1750 A with an accuracy of 0.5% and a response time lower than 1 μ s. The output from the current transducer is connected (after signal conditioning) to the microcontroller's ADC which acquires data at 2 MSamples/s with 10-bit resolution.

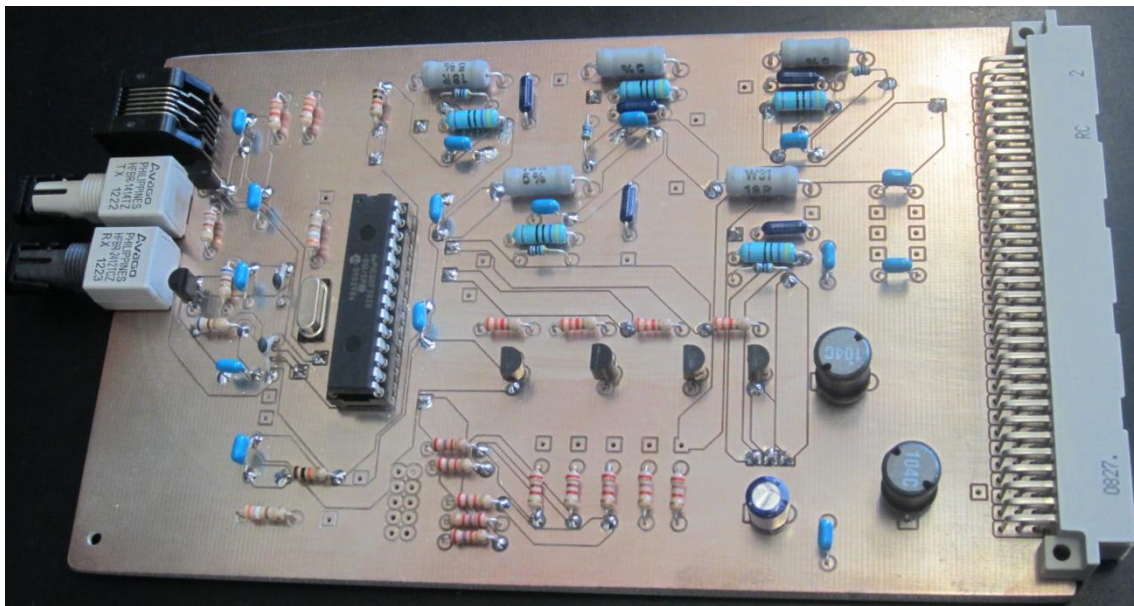


Figure 52 – Power supplies controller board. This board includes a DSPIC30F2020 microcontroller, HCPL-1414 and HCPL-2412 optic communicators and signal conditioning to acquire the current transducer data.

The driver board (Figure 53) makes the interface between the control board and the H-bridge gates. To avoid damaging the controller board electronics it is necessary to have galvanic isolation between the two. The driver board has HCPL-3120 optocouplers with a minimum of 630 V of galvanic isolation. The driver board also includes DC-DC converters to power the optocouplers.



Figure 53 – Driver board (without front panel). This board provides the interface and galvanic isolation between the control board and the power H-bridge.

The communication with the main control system is made through the rs-232 protocol with the digital signals converted to optic to avoid the harsh electromagnetic environment characteristic of the tokamak operation. The communication is made at 921.6 kbit/s and the communication protocol can be found in the annexes section.

Two similar power supplies control modules are installed in the COMPASS tokamak and they are used to drive the radial and the vertical field fast amplifiers. These modules are replicas from ISTTOK power supplies modules but have an additional control board with a different version of the driver board to control up to 6 thyristors. These modules are depicted in Figure 54 and demonstrate how ISTTOK can serve as a test-bed for bigger machines.

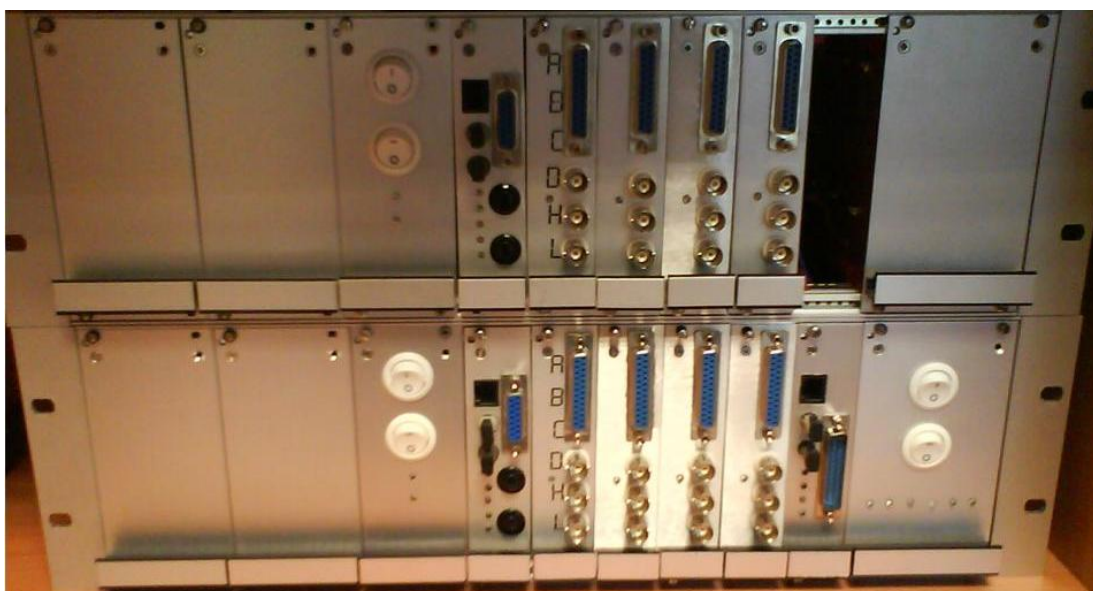


Figure 54 – COMPASS tokamak fast amplifiers control module. This module controls the radial and vertical fast amplifiers and it also includes a module to control the thyristors that connect the transformer to the H-bridge voltage.

ISTTOK power supplies specifications:

The ISTTOK tokamak has 4 power supplies that are used in operation: (i) toroidal field power supply, (ii) magnetising field power supply, (iii) vertical field power supply and (iv) horizontal field power supply.

Toroidal field power supply characteristics:

- Voltage input: three-phase from grid.
- Power supply technology: 12-phase delta-star rectification with open-loop thyristor fire angle control.
- Power supply control hardware: 8-bit open-loop loop thyristor fire angle control (non-linear).
- Current range: 4kA to 8kA, normally operated at about 6kA for 0.5T
- Magnetic field generated: normally 0.5T (centre of the vacuum chamber)
- Maximum operation time: 3s

Primary field power supply characteristics:

- Voltage input: 3.4 F capacitor bank up to 350V.
- Power supply technology: switching mode H-bridge with IGBTs.
- Power supply control hardware: based on a DSPIC30f2020 microcontroller.
- Maximum range : from -300A to 300A in 2.5A steps (plasma coupled)
- Power supply internal control cycle: 34.6 μ s (conservative value for longer lifecycle, can be lowered in microcontroller software if needed).
- Control loop: feedback with current transducer, then on/off controller after receiving optically current set-point from ATCA/MARTE at each 50 μ s or 100 μ s (depending on the ISTTOK real-time control code, normally it runs at each 100 μ s).
- Coupling with plasma through ISTTOK iron core (1:28 ratio).
- Maximum operation: 1s (software protection programmed in the microcontroller).

Vertical field power supply:

- Voltage input: 60V DC (five 12V 90Ah batteries in series).
- Power supply technology: switching mode H-bridge with parallel MOSFET.
- Power supply control hardware: based on a DSPIC30f2020 microcontroller.
- Maximum range : from -450A to 450A in 2.5A steps (plasma coupled)
- Power supply internal control cycle: 34.6 μ s.
- Control loop: feedback with current transducer, then on/off controller after receiving optically current set-point from ATCA/MARTE at each 100 μ s.
- Negligible plasma coupling.
- Maximum operation: 1s (software protection programmed in the microcontroller).
- Power supply ripple: 12.5A.

Horizontal field power supply:

- Voltage input: 12V DC provided by one 12V 90Ah battery.
- Power supply technology: switching mode H-bridge with parallel MOSFET.

- Power supply control hardware: based on a DSPIC30f2020 microcontroller.
- Maximum range : from -120A to 120A in 2.5A steps (plasma coupled)
- Power supply internal control cycle: 34.6 μ s.
- Control loop: feedback with current transducer, then on/off controller after receiving optically current set-point from ATCA/MARTE at each 100 μ s.
- Negligible plasma coupling.
- Maximum operation: 1s (software protection programmed in the microcontroller).
- Power supply ripple: 5A.

Summary of the power supplies characteristics:

	Min. current	Max. current	Voltage input	Technology	Control Cycle	Max. duration	Rise time to 85% of max current
Toroidal	4 kA	8 kA	3-phase	12-phase rect.	-	5s	850 ms
Primary	Plasma coupled, ± 250 A		250V	IGBT	34.6 μ s	1s (in SW)	Plasma coupled
Vertical	-450A	450A	60V	Parallel mosfet	34.6 μ s	1s (in SW)	2ms
Horizontal	-120A	120A	12V	Parallel mosfet	34.6 μ s	1s (in SW)	2ms

Table 4 – ISTTOK power supplies characteristics.

3.3. Power supplies control

Since the system is time independent, the ISTTOK power supplies (see Figure 48) can be modelled using state space equations. The horizontal and vertical field power supplies can be viewed as the circuit depicted in Figure 55 since the plasma coupling can be neglected for these two circuits.

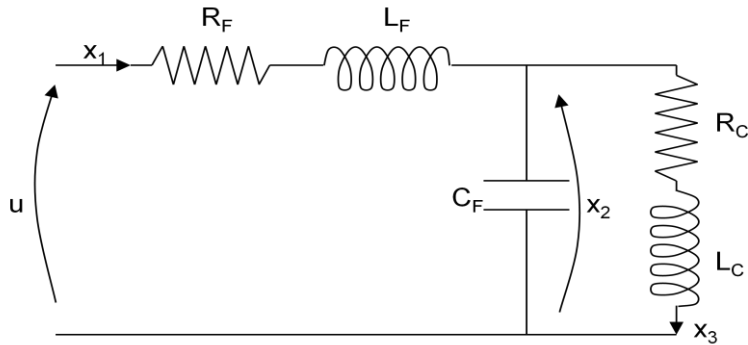


Figure 55 – Equivalent power supplies circuit used for simulating the power supply behaviour.

Where X_1 is the circuit current, X_2 is the capacitor voltage, L_F is the filter inductance, C_F is the filter capacitance, X_3 is the current flowing in the tokamak coils, L_C is the inductance of the tokamak field coils, R_C is the tokamak coils resistance, R_F is the circuit resistance and finally, u is the output from the power H-bridge.

The state-space equations of this circuit can be obtained from the fundamental electric circuit equations described by equation 30 (resistor equation), equation 31 (capacitor equation) and equation 32 (inductor equation).

$$V = R \cdot I \quad (30)$$

$$I = C \frac{dV}{dt} \quad (31)$$

$$V = L \frac{dI}{dt} \quad (32)$$

The Kirchhoff laws are:

$$\sum_{k=1}^N i_k = 0 \quad (33)$$

$$\sum_{k=1}^N V_k = 0 \quad (34)$$

Equation 33 is valid for each junction and equation 34 is valid for each circuit loop.

With these equations it is possible to write the circuit equations in the space-state format:

$$\begin{cases} \dot{x}_1 = -\frac{R_E}{L_F}x_1 - \frac{1}{L_F}x_2 + \frac{1}{L_F}u \\ \dot{x}_2 = \frac{1}{C_F}x_1 - \frac{1}{C_F}x_3 \\ \dot{x}_3 = \frac{1}{L_C}x_2 - \frac{1}{L_C}x_3 \end{cases} \quad (35)$$

Rewriting on the state-space format, we obtain:

$$\begin{cases} \dot{\mathbf{x}} = \mathbf{Ax} + \mathbf{Bu} \\ \mathbf{y} = \mathbf{Cx} \end{cases} \quad (36)$$

With:

$$\mathbf{A} = \begin{bmatrix} -\frac{R_E}{L_F} & -\frac{1}{L_F} & 0 \\ \frac{1}{C_F} & 0 & -\frac{1}{C_F} \\ 0 & \frac{1}{L_C} & -\frac{R_C}{L_C} \end{bmatrix} \quad (37)$$

$$\mathbf{B} = \begin{bmatrix} \frac{1}{L_F} \\ 0 \\ 0 \end{bmatrix} \quad (38)$$

$$\mathbf{C} = [0 \ 0 \ 1] \quad (39)$$

After obtaining the state-space equations for the circuit it is possible to simulate the power supply behaviour. The power supplies were modelled in Simulink™ according to the circuit on Figure 56.

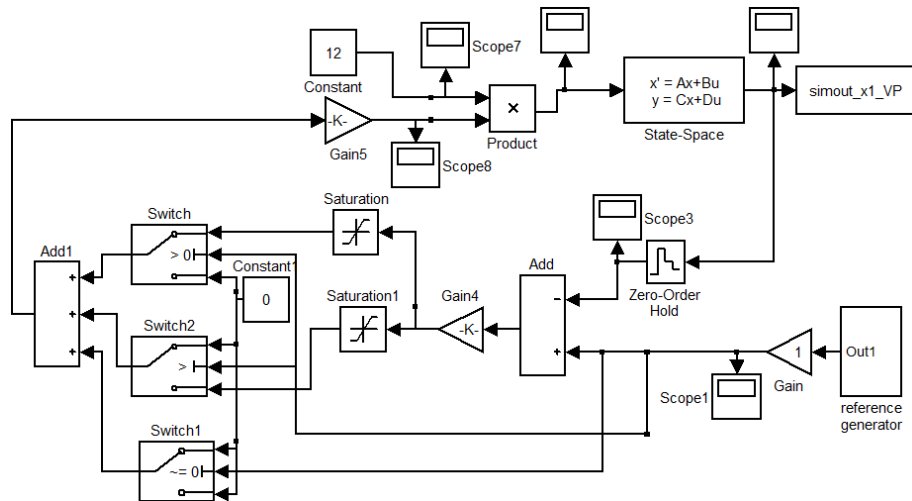


Figure 56 – Simulink model for the Horizontal field power supply control including the horizontal field PS state-space equations.

Since ISTTOK has a thick copper shell that filters the effect of the power supply on the magnetic field inside the vacuum vessel, the type of controller was selected on the speed of

action criteria relegating noise to a less important factor. With this issue in consideration the selected control algorithm for the PS current control was a modified on/off controller. Depending on the reference and the PS current it selects the following three states: (i) no voltage; (ii) full voltage in the positive direction; and (iii) full voltage in the opposite direction. A comparison of the simulation with the actual Horizontal field current and the reference can be found in Figure 57.

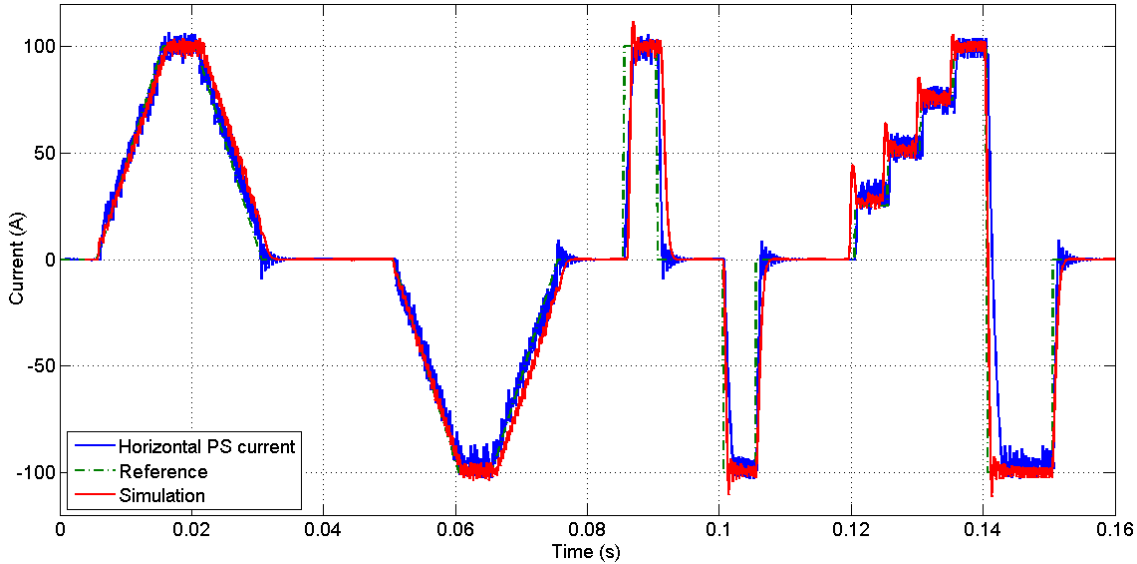


Figure 57 – Horizontal field power supply reference tracking. This figure also compares the simulation with the actual horizontal field power supply operation.

A detailed view of the simulation versus the actual operation is depicted in Figure 58. As it can be observed the commutation noise is fairly similar to the experimental result.

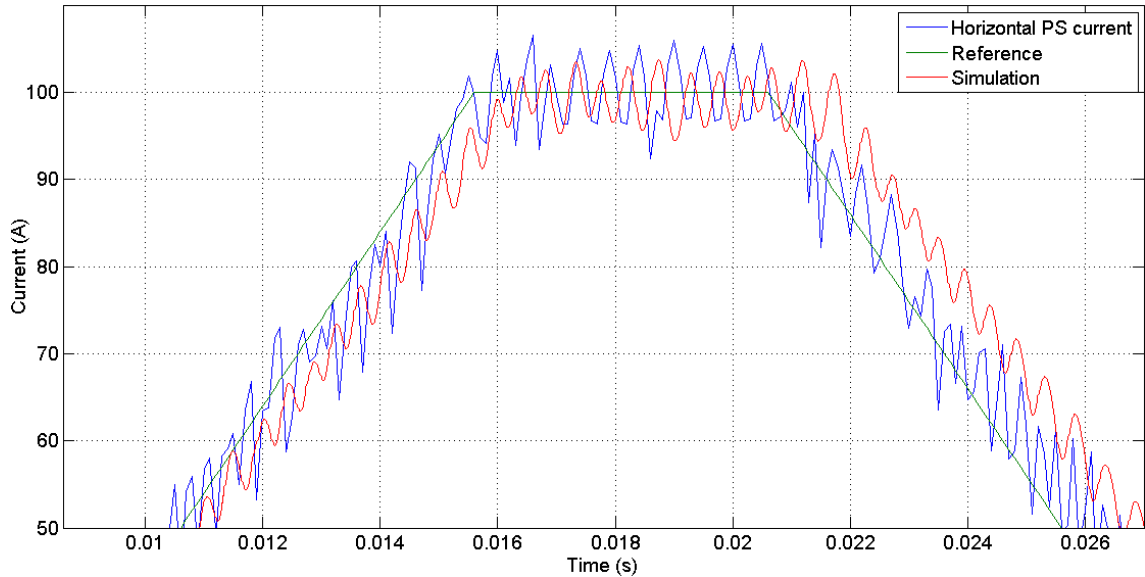


Figure 58 – Detail of the Horizontal field power supply reference tracking and comparison with the simulated power supply response.

The vertical field power supply operation versus the reference is depicted in Figure 59.

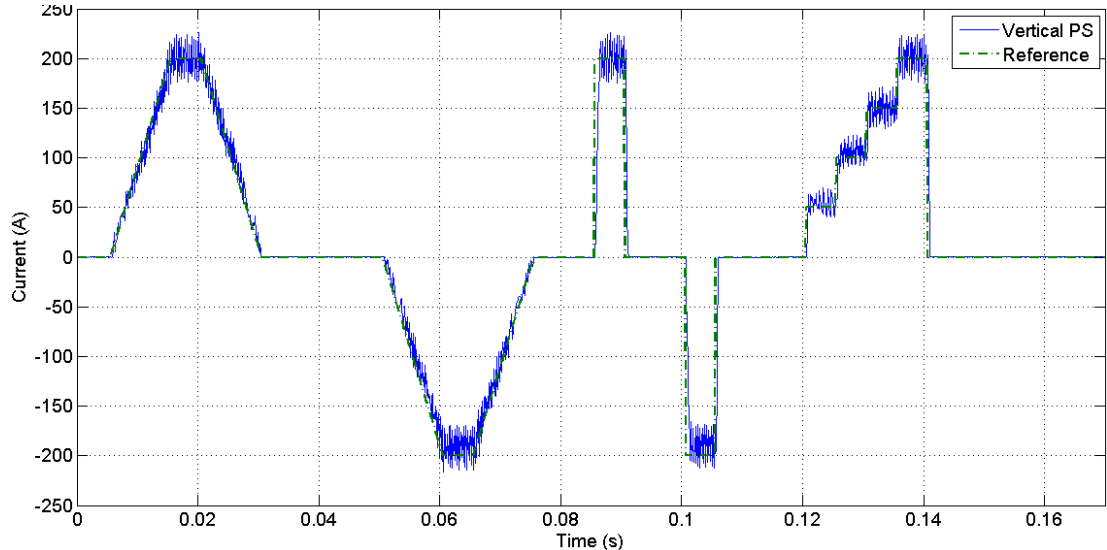


Figure 59 – vertical field power supply reference tracking.

The primary field reference tracking was also tested. However, the primary field PS is strongly coupled with the plasma current or vacuum vessel and therefore it was first necessary to saturate the iron core. Once the iron core was saturated it was possible to perform the reference tracking test of the primary field PS. This test is depicted in Figure 60.

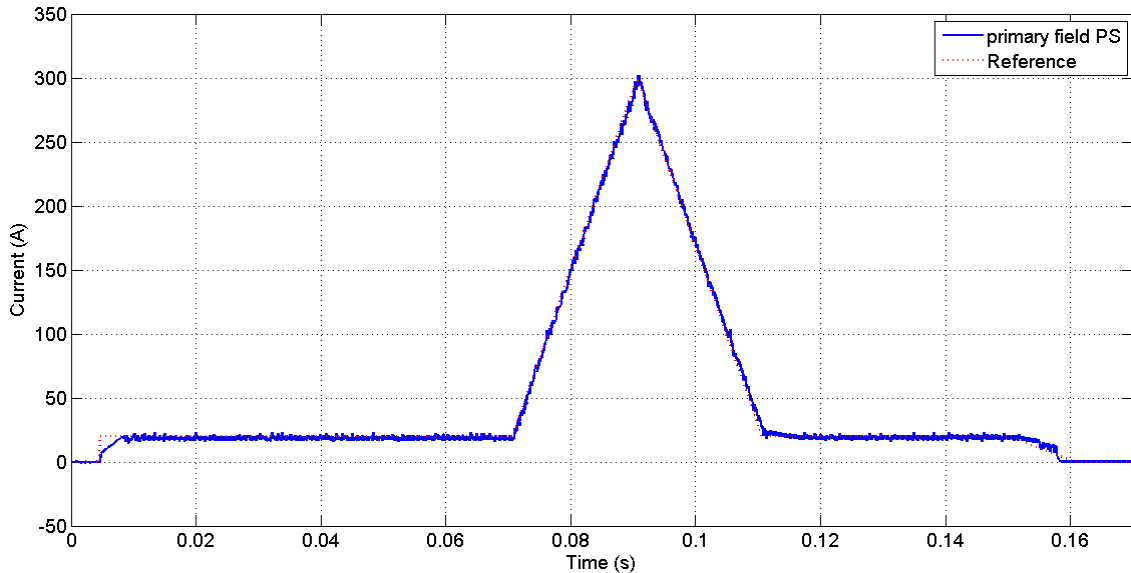


Figure 60 – Primary field power supply reference tracking. Since ISTTOK has an iron core, this power supply is strongly coupled to the transformer secondary (vacuum vessel + plasma), since this test was produced without plasma, it was necessary to saturate the iron core to be able to drive this amount of current in the primary field circuit.

Under the new control system, the ISTTOK power supplies have two modes of operation; (i) current control and (ii) scenario control. In the first type of control the power supplies receive the current set-point (SP) and their internal controller regulates the current output to match the requested SP. In the latter form of control each power supply is used to control the respective scenario. The primary field power supply is used to control the plasma current, the horizontal and vertical field power supply control the vertical and the radial position respectively.

The ISTTOK power supplies always receive their set-points in current values. The plasma parameters are controlled using PID algorithms for feedback. The process variable is the plasma parameter to be controlled, the plasma parameter waveform is programmed in the main control system prior to the discharge and the result of this PID algorithm is the current reference that is sent to the respective actuator.

For scenario control the operator can program the k_p , k_i , k_d for a standard proportional-integral-derivative (PID) controller defined by equation 40. The PID controller can be implemented in differential form that is obtained from differentiating equation 40, but in ISTTOK the implemented PID corresponds to equation 43. This format of PID controller was selected because it is more robust and anti-windup. It is obtained by simply limiting the output with the operational value of the corresponding output. For example the output of the PID controller for the primary field PS is bounded between -300 A and + 300A corresponding to the PS operational limits.

$$Out = K_p \cdot e(t) + K_i \cdot \int_0^t e(\tau) \cdot d\tau + K_d \cdot \frac{d}{dt} e(t) \quad (40)$$

$$e = SP - PV \quad (41)$$

$$Out_k = Out_{k-1} - K_p \cdot (e_k - e_{k-1}) + K_i \cdot T \cdot e_k - \frac{K_d}{T} (e_k - 2e_{k-1} + e_{k-2}) \quad (42)$$

$$Out_k = Out_{k-1} - K_p \cdot (PV_k - PV_{k-1}) + K_i \cdot T \cdot e_k - \frac{K_d}{T} (PV_k - 2PV_{k-1} + PV_{k-2}) \quad (43)$$

In equation 43 the term error (e), defined by equation 41, was replaced by the process variable (PV) in some parts of the equation, this prevents a jump in the output request when the reference changes dramatically from one control cycle to the next one.

When there is a transition from current control to scenario control with a PID controller the ControllerGAM (see chapters 4.4 and 4.5) uses the last current measurement of the respective power supply and loads this value on the variable $Out_{(k-1)}$ of equation 43. This prevents a jump in the current request to the power supply and consequently “smoothes” the convergence to the required set-point. The typical behaviour on the scenario control is depicted in Figure 61. In this figure it is possible to observe the effect of the PID control on the plasma current, radial position and the vertical position controlled by the primary field PS, the vertical field PS and the horizontal field PS respectively. These circuits have a very low coupling between them, but since ISTTOK produces circular plasmas, the last flux surface is defined by the limiter. This means that the plasma position strongly affects the plasma current circuit when the plasma is pushed to the limiters since the plasma is reduced in size undermining the plasma capacity to conduct a large portion of current. Also it should be noticed that the greater the plasma current the greater the request on the vertical field PS to balance the plasma radial position. This means that the reaction of the vertical field PS is slightly changed since this power supply will be in a different operation zone (the current rise takes more time at high current than when it is at lower current).

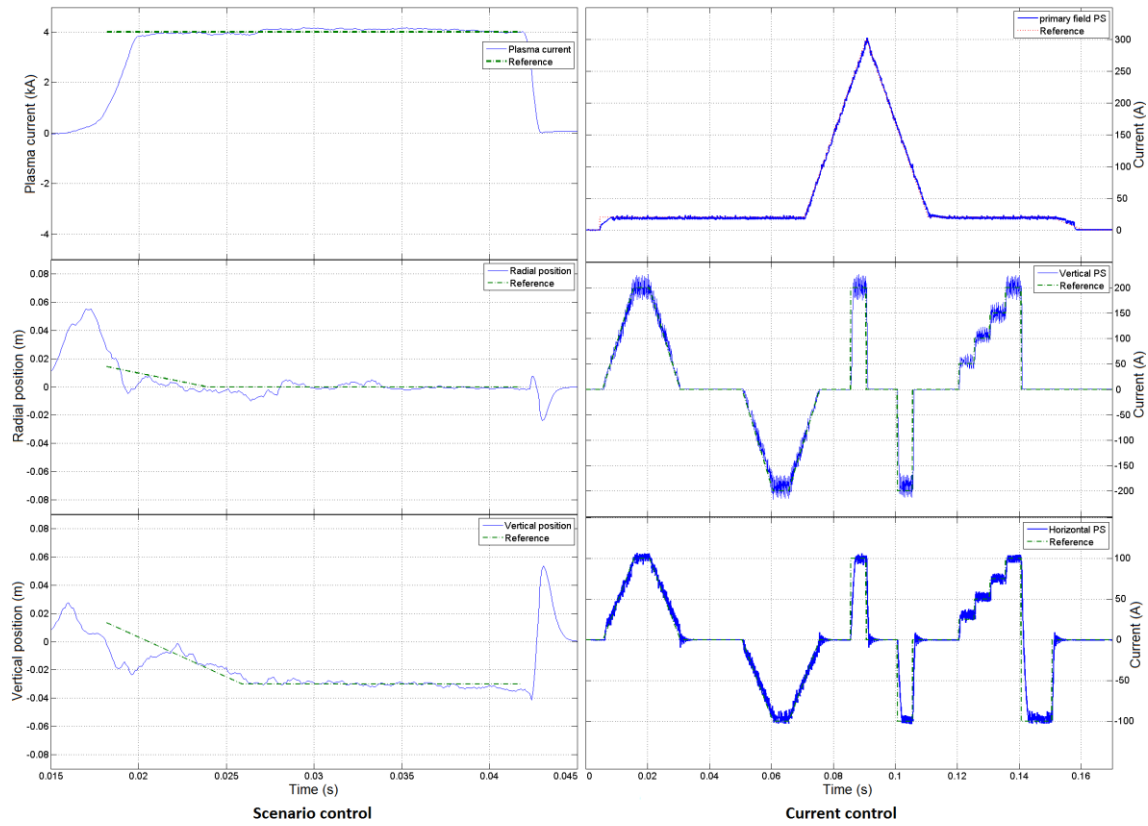


Figure 61 – Differences in reference following between scenario control and current control. In the left and from top to bottom are: plasma position, radial position and the vertical position. In the right and from top to bottom are: magnetizing field PS current, vertical field current and horizontal field current.

3.4. Other actuators

The ISTTOK tokamak has two gas insertion modules; one slow module used for setting the background pressure before the discharge and another based on a piezoelectric valve used for real-time control. Since the gas flow on the piezoelectric valve (MaxTeK MV-112) is highly non-linear in the applied voltage, it was decided to use only two states: fully open and fully closed. The “gas puff” injector can be used in feedback control in either plasma density or radiated power. The feedback algorithm uses a programmable period of gas puffing (normally around 1 ms) and the time between gas puffs depends on the reference and process variable. The action of this feedback algorithm can be observed in Figure 62. In order to maintain the programmed H_α radiation reference (2.3 a.u.) the control system has a high puffing rate in the beginning of the discharge and decreases the rate towards the end of the discharge. This can be explained by the gas recycle process (natural in the tokamak) that is contributing to refuel the plasma.

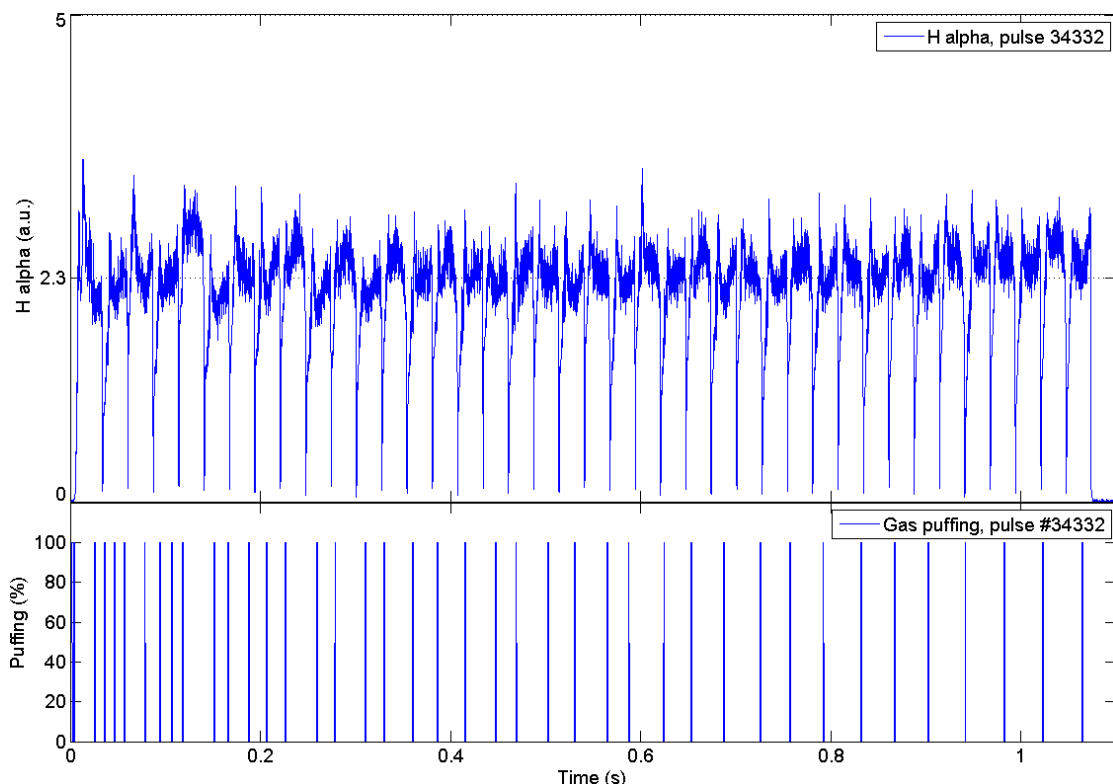


Figure 62 – Puffing feedback on H_α radiation in a long AC discharge (pulse 34332). The reference waveform was set to the value 2.3 throughout all the discharge. The rate of the puffing is much superior on the first part of the pulse, after this initial phase, the recycling process provides almost the sufficient fuelling so the gas puffing period is increased.

The gas puffing reservoir is normally adjusted to 800mbar and to study the effect of the gas puffing in the plasma density and radiation several discharges with different puffing profiles were made. Figure 63 depicts this study and as it can be observed the gas puff is highly non-linear in the first small puffs. Since before the first puff the tube that connects the puffing to the tokamak has almost no gas, the first puff will mainly fill this gap, and consequently has a modest effect on the plasma. No significant difference between the reference (no puff) and the pulse 34483 (only one small gas puff). After this pipe is filled, the reaction time of the puffing circuit is about 2 ms that can be obtained by comparing pulse 34489 with pulse 34492.

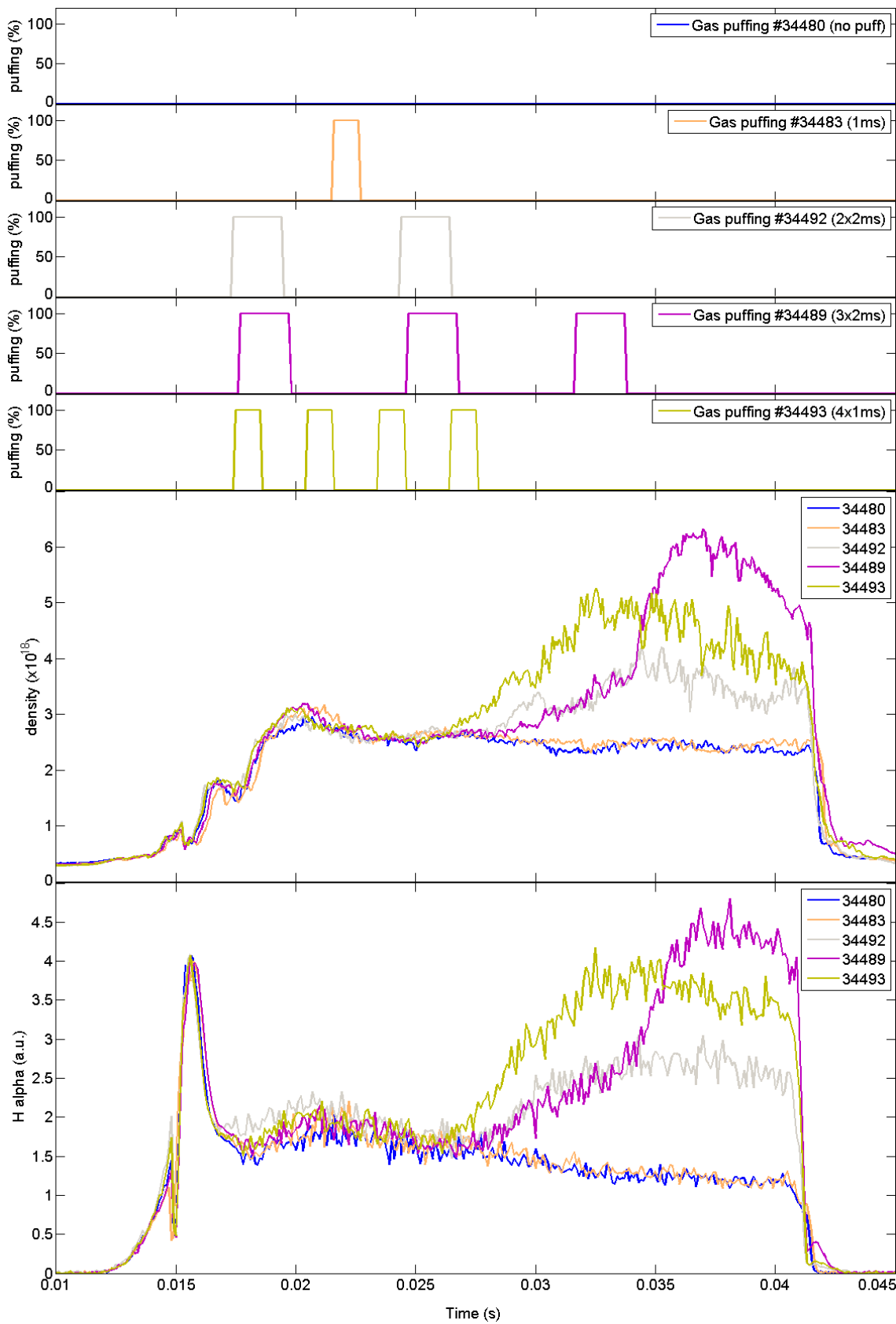


Figure 63 – Puffing tests with 800 mbar on the gas puffing reservoir. This graph evidences the behaviour of density and radiation versus the gas puffing. All other parameters were constant.

Chapter 4 - Design of the ATCA control and data acquisition system.

In order to produce systematic alternate discharges a real-time control system was developed based on the Advanced Telecommunications Computing Architecture (ATCA) standard. The real-time control system was programmed on top of the MARTe framework with a 100 μ s control cycle, this issue will be described in the sub-chapters 4.3, 4.4 and 4.5.

Furthermore, the ISTTOK tokamak actuators (vertical field power supply, horizontal field power supply, primary field power supply and gas puffing) were upgraded to be able to communicate with the ATCA control system. Several diagnostics were also connected to ATCA digitizers to provide real-time information for the control system including: tomography, Mirnov coils, interferometer, electric probes, current in the primary power supply, loop voltage and plasma current.

An overview of the ISTTOK control system is depicted in Figure 64 and this system is further described in the next sub-chapters.

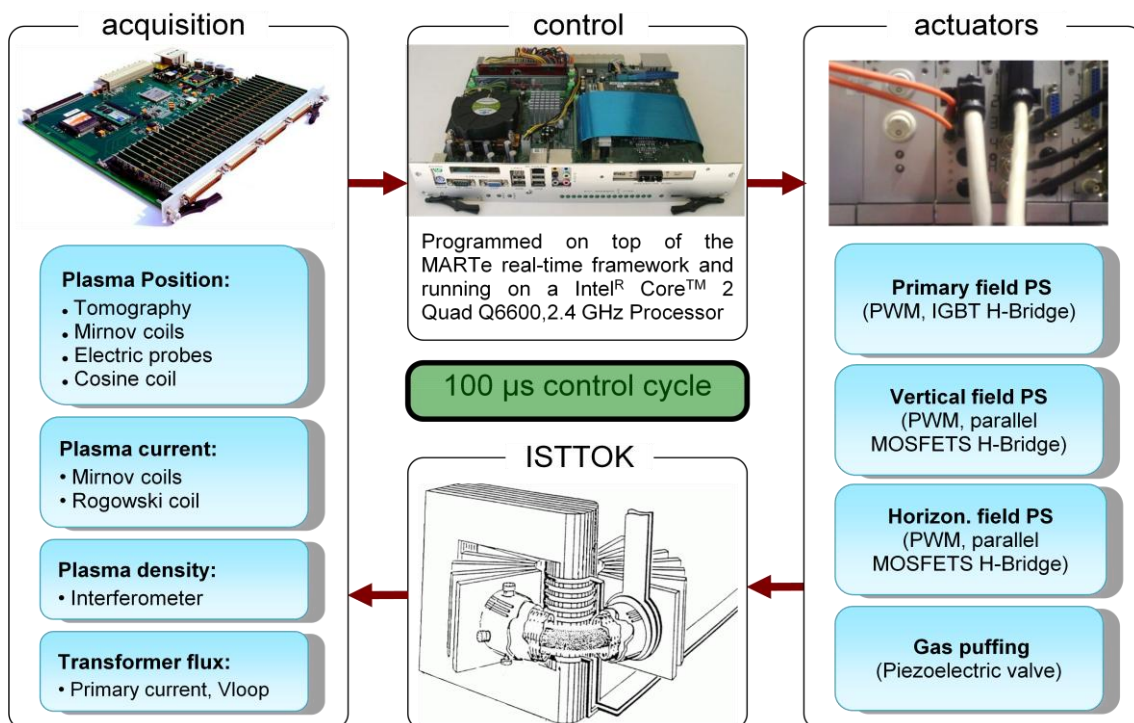


Figure 64 – Overview of the new ISTTOK control system.

4.1. System layout

The old ISTTOK real-time control system was based on a customised in-house PCI board (named PCI-TR-512) connected to a host PC for communication with the slow control system [58][59]. This control board has 512 MB of RAM, a spartan-3 FPGA and a TMS320C6415T DSP, this board acquired data from 8 ADCs at 2 MSamples/s with 14 bit. This system controlled only the horizontal and vertical field power supplies to correct the plasma position inside the vacuum vessel. This system schematic is depicted in Figure 65.

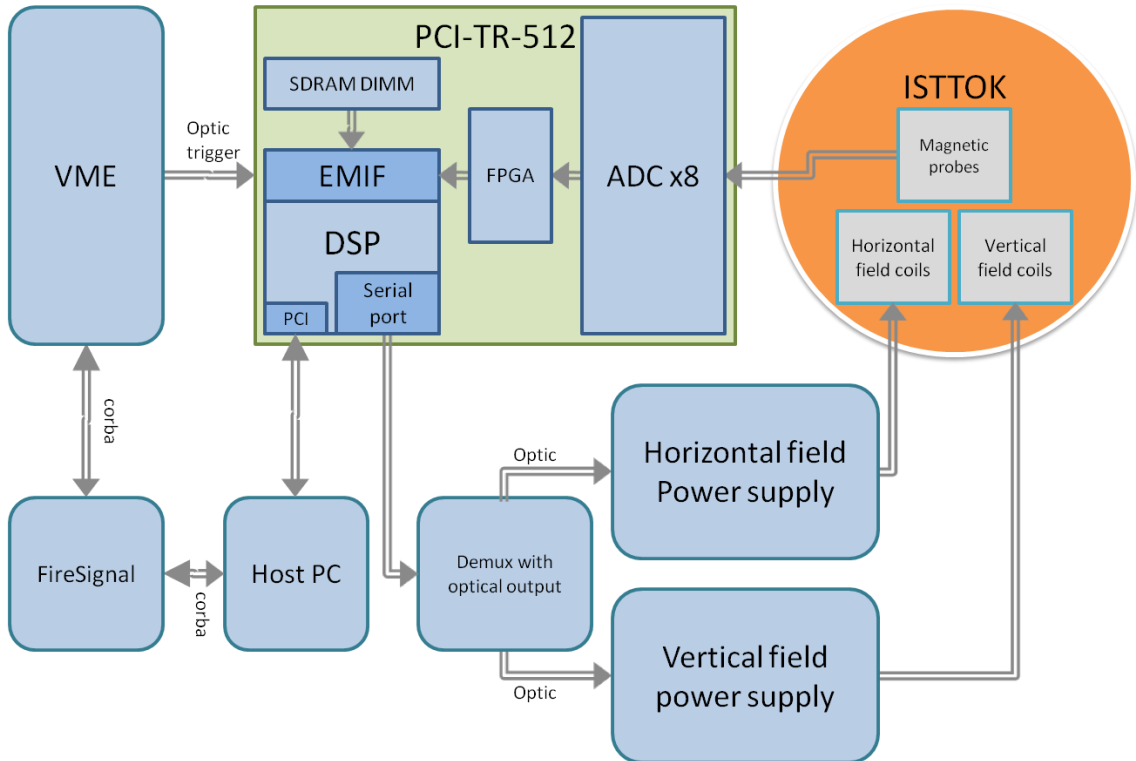


Figure 65 – Old ISTTOK real-time control system schematic. In the PCI-TR-512 the data is acquired by 8 ADCs and stored via the FPGA and the external memory interface (EMIF) in the RAM module (SDRAM DIMM), after the discharge is finished the data stored in the RAM module is retrieved to the ISTTOK database. During the real-time the magnetic probes data is used for plasma position feedback control. The actuator commands are sent via a serial port.

As described before, the old primary field power supply had no feedback control and was triggered by the VME triggering system that is configured by the FireSignal [60] middleware which was maintained with the control system update. This middleware controls the system configuration and connection to the database. The FireSignal software is modular and distributed, where each hardware client connects to the central server in a plug-and-play philosophy. The FireSignal central server (programmed in Java) is the core of this system and is responsible for managing all the commands and data broadcast. The nodes are responsible for integrating the hardware devices. Several users can connect (via the security manager) to FireSignal in a cooperative environment using a graphical user interface. The FireSignal schematic with the internal connections is depicted in Figure 66.

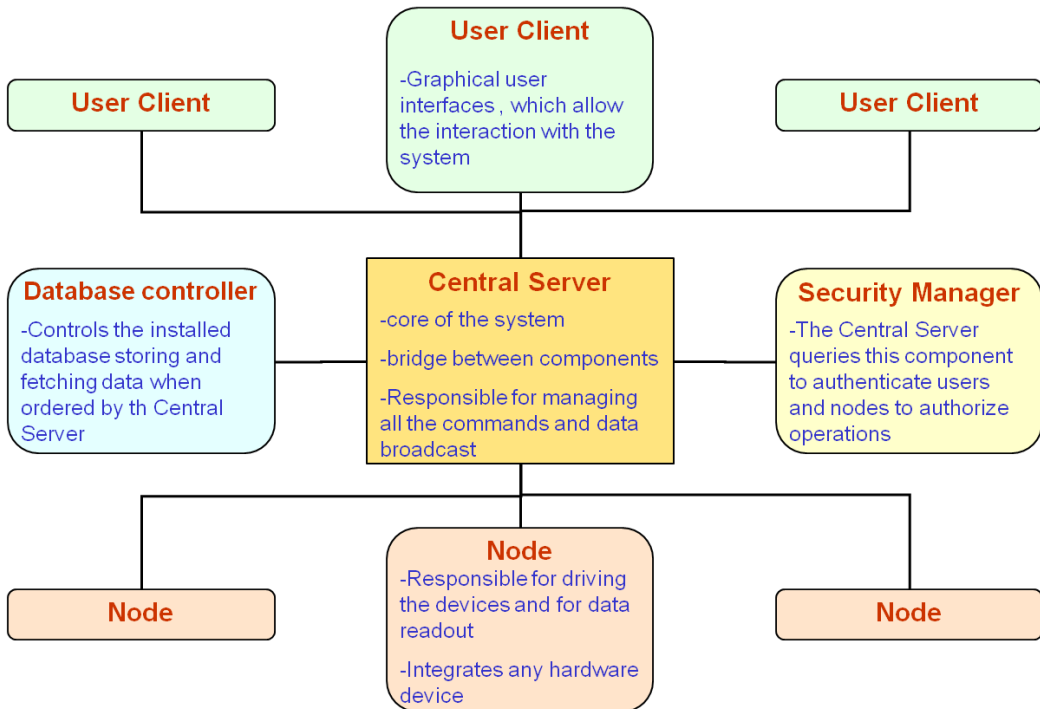


Figure 66 – FireSignal schematic highlighting the system modularity.

The old PCI control system was very limiting because it only had 8 ADC channels without possibility to integrate any more in a unique control system. Furthermore, the amount of program data was also insufficient for a more complex control system. The main aim for the new control system was to gather the information from all real-time diagnostics and use this data to control all real-time actuators, aiming at improving the real-time control of the plasma parameters and extend the duration of the AC discharges. Since the objective was to improve the fast real-time control, the ISTTOK slow control, database, VME trigger system and FireSignal middleware were maintained apart from small changes required to connect all the systems. The new control system integration schematic is depicted in Figure 67.

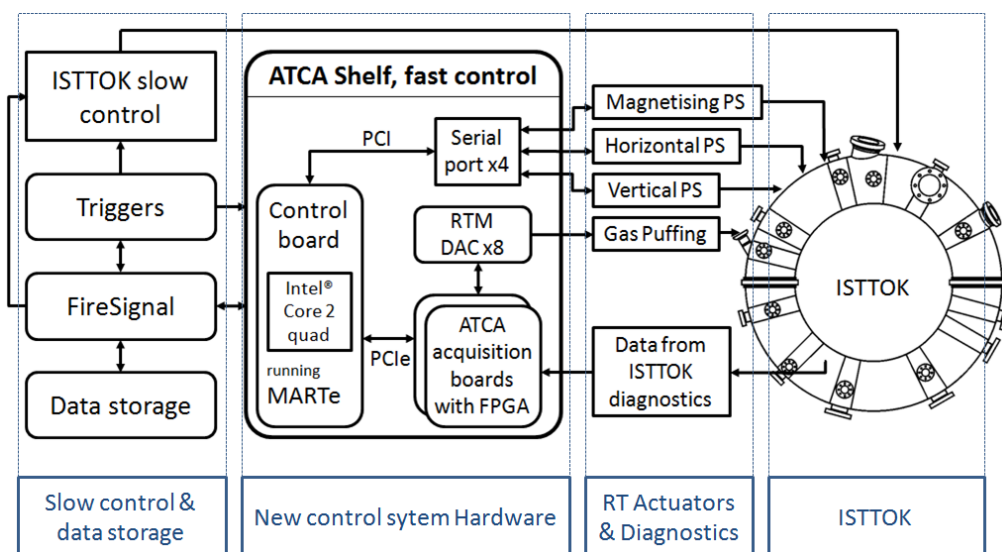


Figure 67 - ISTTOK overall control schematic. Data are acquired by the ATCA data acquisition boards, decimated and transferred to the host at a fixed 100 μ s period. Based on the MIMO configuration the controller outputs the relevant references to the ISTTOK actuators.

Compared to the old system, the ATCA hardware replaced the PCI-TR-512 board and the host PC, while the power supplies communication protocol and communication speed were updated in order to be a multiple of the new quad serial port. The VME trigger system now triggers the new control system through the ATCA rear transition board (RTM). This board also receives a 2 MHz optic signal to distribute and synchronize the clock for all acquisition boards. This enables all the channels of the acquisition boards to acquire data with the same timing.

Regarding the database interaction with the new control system, there is a driver pooling one control system variable that is set at the end of each discharge, when the discharge is complete, the database accesses the data stored on the real-time system. The real-time data stored in the ATCA system includes the raw data from diagnostics, the observed plasma parameters, the values sent to the actuators and some auxiliary data, mainly internal control variables used for debugging the system. The ISTTOK ATCA crate also includes two additional boards that are used only for fast data acquisition and not for real-time. For this reason, these fast acquisition boards have their own driver and are directly configured through FireSignal. The data storage from these boards is also coordinated directly to the ISTTOK database by FireSignal.

4.2. ATCA crate hardware

The ATCA standard is specified by the PICMG (PCI Industrial Computer Manufacturers Group) and the current version (at the time of this thesis) of the specification is 3.x. This PICMG standard [61] aims to define the architecture for building high end, “carrier grade” equipment. The PICMG 3 specifications are oriented around switch fabric technology instead of a conventional parallel bus. The specifications provide guidelines to allow board, backplane, and chassis vendors to independently develop products that will be interoperable when integrated together. It includes also details about the board dimensions, equipment practice, connectors, power distribution and robust system management architecture.

The PICMG 3.x is a term used to describe the family of specifications which include:

- PICMG 3.0 is the overall general specification that defines mechanics, board dimensions, power and data connectors, power distribution, and system management.
- PICMG 3.1 defines an Ethernet switch fabric over the generic backplane fabric interconnect up to 10 Gbit/s per link.
- PICMG 3.2 defines how InfiniBandtm systems are built within the architecture and will specify link physical layers, protocols, and protocol mappings.
- PICMG 3.3 defines a StarFabric implementation over the backplane providing TDM, cell, control, and packet connectivity over the same fabric.

The board dimension specified by PICMG 3 is 8U (322.25 mm) high and 280 mm deep and the boards are spaced at a 1.2 inches (30.48 mm / 6HP) pitch. This board dimensions are higher than other hardware specifications and result in an area of about 140 square inches (about 900 cm²), compared with about 120 square inches (about 790 cm²) for 6U VME and CompactPCI. This additional real estate allows developing high performance computing blades or a system with a high number of inputs or outputs. The standard PICMG 3 backplane is a “full mesh”, wherein every slot has a dedicated link to every other slot. Another advantage of this architecture is the high power dissipation specification. In the PICMG 3.x specification the ATCA crate can dissipate up to 3kW of heat and up to 200W per board compared with the limit of 50W in the case of a CompactPCI with forced air cooling.

The main advantage of the ATCA crate for the next generation of fusion devices is the improved Reliability, Availability and Serviceability (RAS) characteristics inherent from the PICMG 3.x specification correct application.

The PICMG 3.x also specifies two important system managers, the Intelligent Platform Management Controller (IPMC) and the Shelf Manager. When a board is inserted into the shelf, the onboard IPMC is powered from the redundant -48V on the backplane (low power).

The shelf manager queries the node board to determine what links it uses. The shelf manager keeps track of every board links and sends a message to enable connections between compatible links/fabrics of all boards and manages the power up of the inserted modules. The

shelf manager has to keep track of all the node boards and the advanced mezzanine cards (AMCs) if available. The shelf manager is responsible for managing the connections between nodes, the power distribution and the fan speeds according to the temperature sensors.

The ISTTOK ATCA crate hardware includes a control board, two acquisition boards for real-time control and another two similar acquisition boards but with a different firmware for 2 MSamples/s acquisition (not for real-time control). All of these boards are connected via the PCIe bus in the backplane of the ATCA crate. To receive the 2 MHz clock and the trigger there is also one rear transition module (RTM) connected to the back of one acquisition board. Although not specifically designed for the ATCA crate the control hardware also includes a quad-serial port communicator connected to the ATCA control board motherboard via PCI bus. The ISTTOK ATCA is depicted in Figure 68.

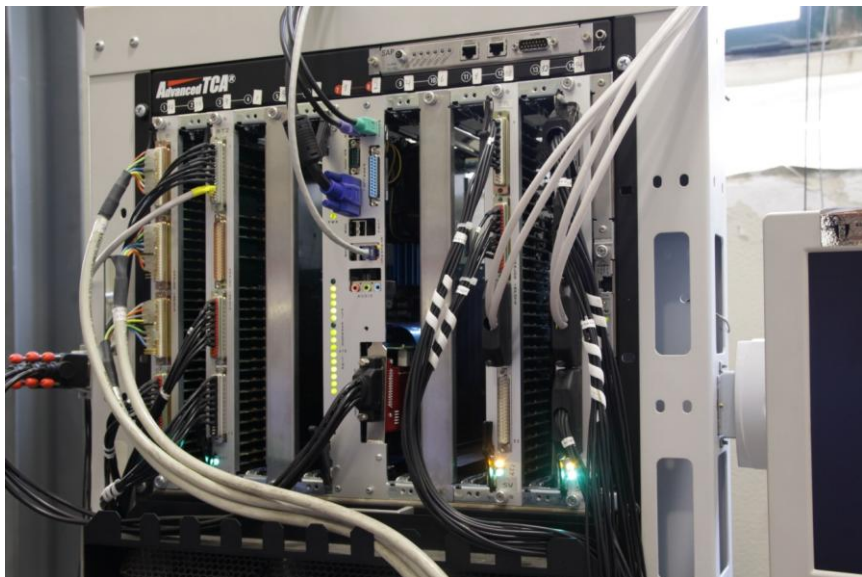


Figure 68 – ATCA crate image. The ISTTOK ATCA crate includes a control board, two acquisition boards for real-time control and another two acquisition boards with a different firmware for 2 MSamples/s acquisition (not for real-time control).

A list of the several ISTTOK ATCA control system components is detailed below.

ATCA acquisition board and rear transition module:

To acquire the ISTTOK real-time diagnostics it was used an in-house developed acquisition board (Figure 69). This board is a full size ATCA board (322.25 mm x 280 mm) and it includes 32 differential ADC channels with galvanic isolation up to 1 kV. The acquisition board has a Virtex 4 XC4VFX60 FPGA (or alternatively the XC4VFX100 model) to (i) control the data acquisition, (ii) data processing, (iii) data transfer, (iv) interaction with the ATCA controllers, (v) connection with the RTM module, (vi) component configuration and (vii) synchronization. The selected FPGA is able to process 80 GMACS (Giga Multiply ACCumulates per Second) and includes two PowerPC (not used in this implementation) running at 450 MHz that add more 1400 DHRYSTONE MIPS (Mega Instructions Per Second) of processing power to this board.

Up to date, there are two firmware developed for the acquisition board, one of them is the real-time firmware where the data from the ADCs (after decimation) is streamed to the control

board. The other firmware is used for the 2 MSamples/s acquisition with local storage. After the pulse the data is retrieved to the main database.

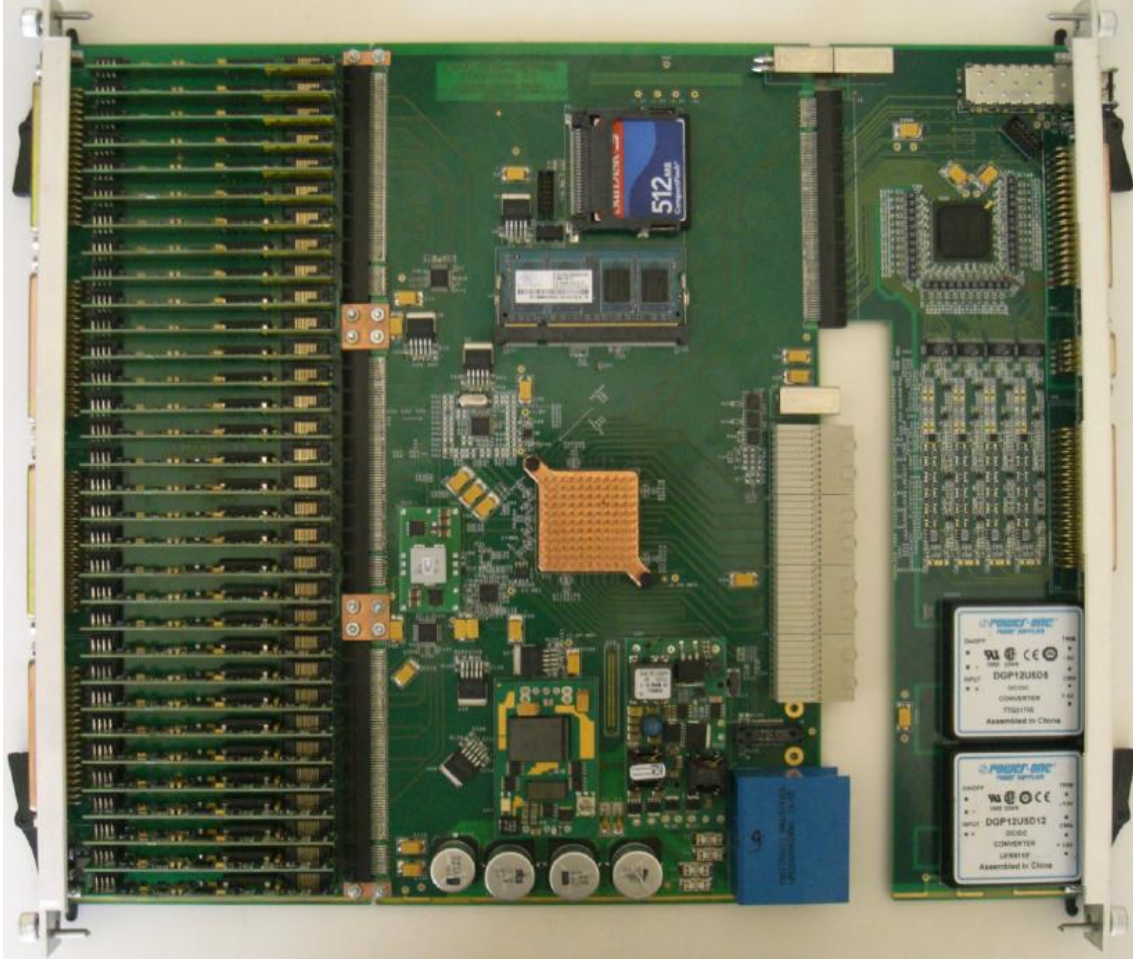


Figure 69 – ATCA acquisition board on the left and the RTM module connected in the right. The acquisition board contains an FPGA, 32 ADC modules, RAM memory and compact flash memory to store the FPGA firmware. The RTM board connects with the acquisition board through the rear of the ATCA crate and contains eight DAC, eight digital I/O, one RS-232 serial port and two optic inputs for clock and trigger.

Every module of all the acquisition boards is synchronized to the clock from the M-LVDS (Multipoint Low-voltage differential signalling) lines of the ATCA. The clock signal is generated by the master acquisition board and according to the firmware written for the acquisition boards, the master is decided by the slot number inside the ATCA crate (board inserted in slot 3 is the master board). All the boards (used for control) have the same firmware installed (written in Verilog with the ISE software from Xilinx). The master acquisition board receives the external clock signal through a RTM board input and distributes a clock signal to all the other boards through the M-LVDS lines. The master board module also detects the existence or not of an input clock signal, if there is no input clock system the clock is generated locally and also distributed to all the other boards.

When the acquisition board is programmed with the real-time firmware, the acquisition board has to transmit the data from all the ADCs to the ATCA controller board for each control cycle. Since the ADCs have 18-bit resolution, the transmitted data from each channel uses 4 bytes of data. In total for transmitting the data for all the 32 ADC modules 128 bytes are used plus a

few bytes used for time stamping the data. Considering the data transmission speed, the acquisition board transmits the data in about 600 ns. The acquisition board schematic is depicted in Figure 70.

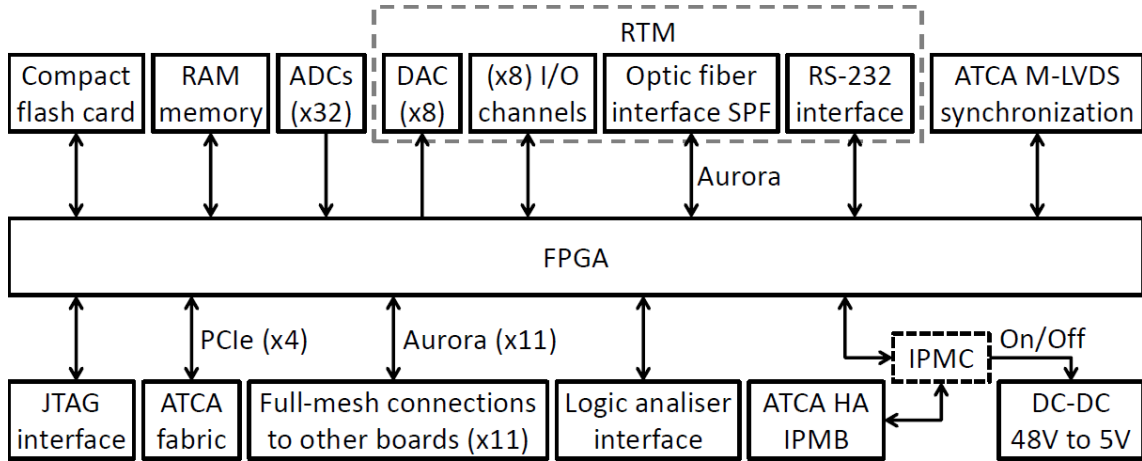


Figure 70 – Connections to the FPGA in the acquisition board. The FPGA controls the data flow of the acquisition board.

As referred before, the acquisition board has 32 ADC modules similar to the module presented in Figure 71. These modules acquire a differential signal with 1 kV of galvanic isolation provided by the DCV010505DP DC-DC converter that powers the analogue part of the circuit.

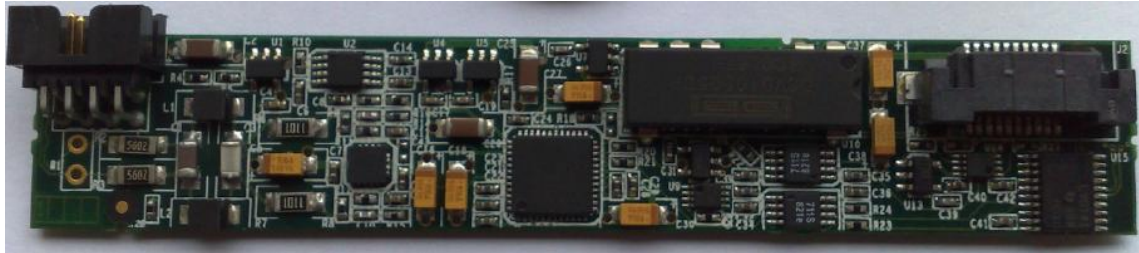


Figure 71 – Acquisition modules. The ADC (AD7641BCPZ) acquires data at 2MSamples/s with 18-bit resolution. Data is acquired in differential mode and the ADC channels have 1 kV of galvanic isolation.

The module front-end includes an anti-aliasing passive filter with a cut-off frequency of 500 kHz. After this filter the signal passes through an amplifier/attenuator (THS4520RGTT) to select the input voltage range. This range can be selected by changing the resistors used by the amplifier/attenuator allowing input voltages from -2/+2 V up to -32/+32 V which are then digitized at 2 MSamples/s. The samples are sent at a 100 MHz bit rate using a digital isolator (IL711S-1E) that isolates galvanically the FPGA digital layer from the acquisition modules digital voltage up to 2.5 kV. The ADC samples are processed by the FPGA at 2 MSamples/s and pass through a digital FIR (finite impulse response) filter inside the FPGA (Figure 72). This filter with 100 symmetric tabs is a low-pass filter with a cut-off frequency of 10 kHz. The decimation by a factor of 100 lowers the data frequency to 20 kHz. In fact, since a new data package is produced at each 50 µs, the control cycle must be a multiple of this time. For each cycle the data is sent to an FPGA output FIFO after being processed.

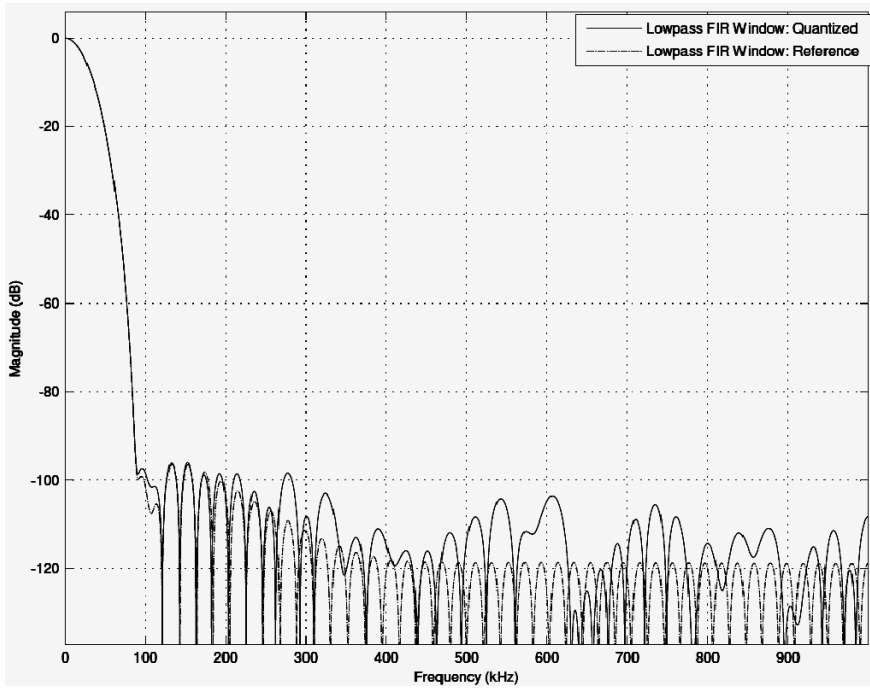


Figure 72 – FPGA digital 100 tabs FIR filter response in frequency.

At each cycle the FPGA generates data packages in the PCIe format that are sent through direct memory access (DMA) to the ATCA control board. The data sent includes (i) the processed ADC data, (ii) the sample time-stamp, (iii) some status bits, (iv) the slot identification and (v) the RTM I/O status.

The RTM board also depicted in Figure 69, contains a small form-factor pluggable (SFP) which is a compact, hot-pluggable transceiver used for both telecommunication and data communications applications. This flexible plug can host either optic or copper network cable transceivers. The RTM board also includes an eight digital input/output plug and eight DACs able to update their output at 5 MHz. Each DAC has 2 differential outputs and each one of these can output a voltage from -5 V up to 5 V, if used together the total output ranges from -10 V to 10 V. One of these DAC outputs is used to drive the ISTTOK gas puffing system.

ATCA controller board:

The ATCA controller board includes a full-size standard ATX PC motherboard (305 mm × 244 mm) in a mezzanine configuration. The ATX motherboard is mounted on top of a support board that connects to the ATCA crate. The support board provides all the interfaces needed for (i) the PCIe switch, (ii) the support for the PC hard disk drive (HDD), (iii) the IPMC for communication with the ATCA shelf manager, (iv) the DC-DC converters for supplying the adequate voltages to the PC motherboard and HDD, (v) the on/off for the ATX motherboard, (vi) the front panel LEDs and (vii) everything else related with the PICMG 3.x protocol implementation. With this configuration, the controller board actually occupies 2 slots of the ATCA crate which is a small price to pay for the flexibility of the system. The Controller board is depicted in Figure 73.

The present ISTTOK ATCA controller board contains a standard Asustek motherboard with an Intel™ Q8200 chip with 4 cores running at 2.33 GHz, but this motherboard and processor can

be easily replaced by another more sophisticated set if required in a future control system update, this highlights the versatility of this design.

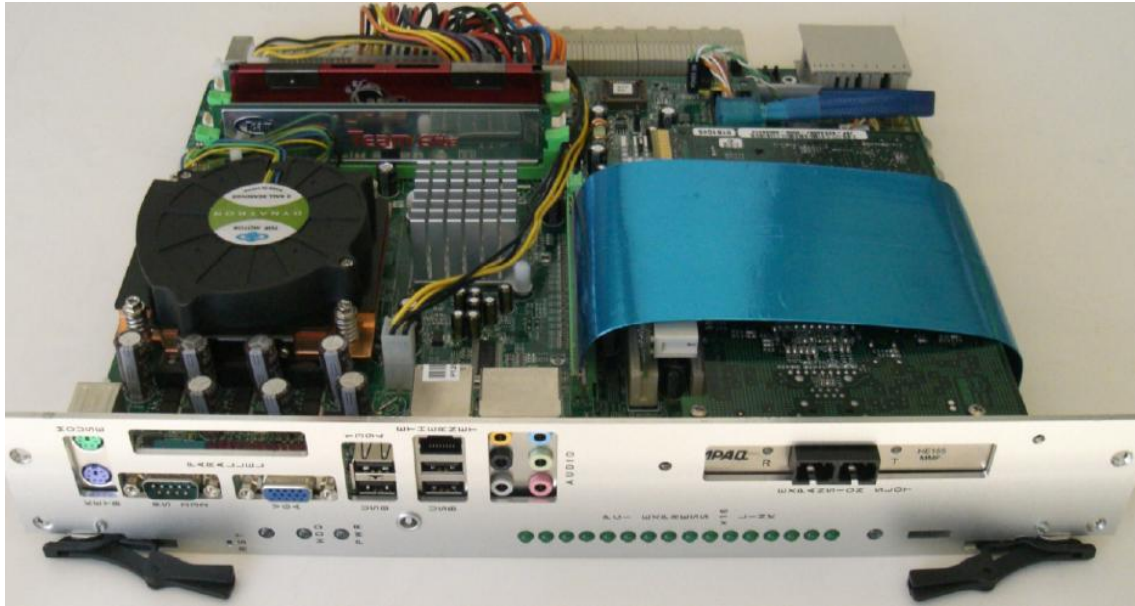


Figure 73 – ATCA controller board. This ATCA board is composed by a standard mother board with an Intel Q8200 4-core processor running at 2.33 GHz. In this boar is also included a PCI module with a quad serial port transceiver.

Although not depicted in Figure 73, the ISTTOK controller board contains a Lindy™ Quad-serial port RS-232, 16C950, 128 Byte FIFO, PCI Card (Figure 74) for power supply communication connected to the motherboard PCI slot. To avoid occupying many slots, the quad serial port is connected to a PCI “L” connector that is also connected to the motherboard PCI slot. This allows the board to be parallel to the motherboard thus occupying much less space. In fact, Figure 73 is the controller board for the JET tokamak vertical stabilization system. The main difference (besides the motherboard and processor module) between this controller board and the ISTTOK version is that in the case of the JET tokamak the PCI board installed is for ATM network communication and in the case of ISTTOK is a PCI module to control the ISTTOK power supplies. In each serial port there is a RS-232 to optic converter for galvanic isolated communication with the ISTTOK PS control module.



Figure 74 – Lindy™ Quad-serial port RS-232, 16C950, 128 Byte FIFO, PCI Card for power supply communication. This quad-serial port is connected directly to a PCI port in the motherboard of the ATCA controller board.

For further clarification on the controller board connections, a simplified schematic is depicted in Figure 75.

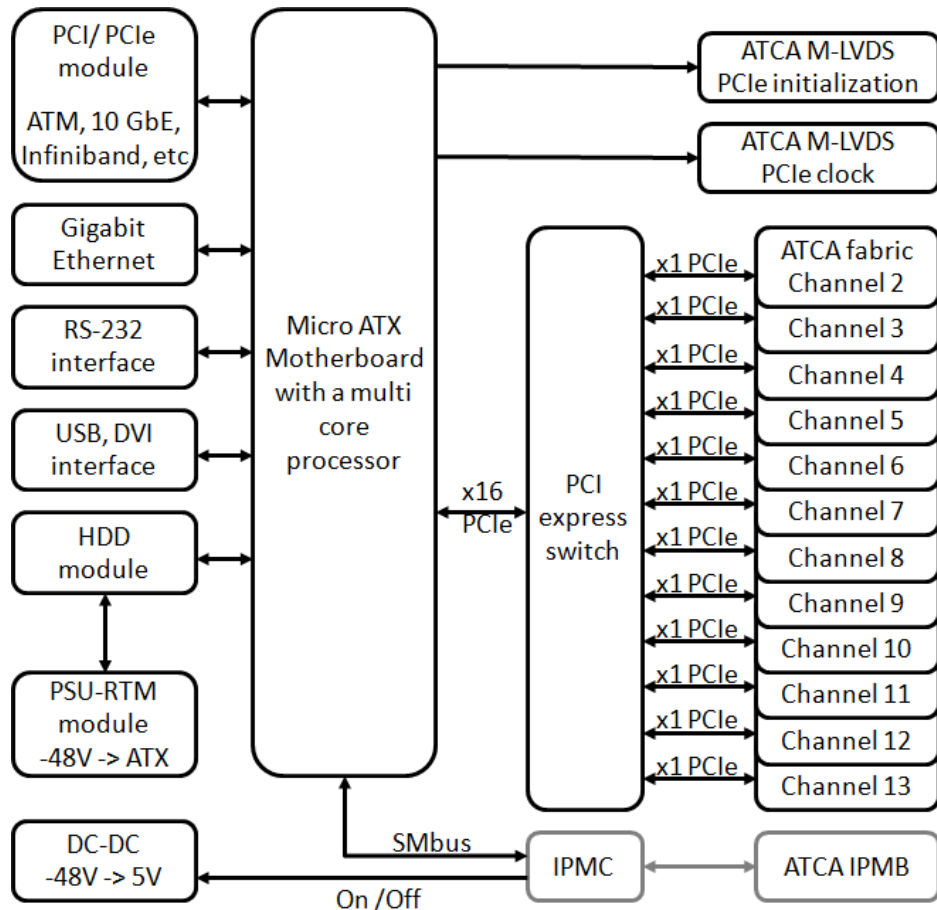


Figure 75 – ATCA controller board simplified schematic including all connections to an ATX motherboard.

The ISTTOK real-time control system algorithms run on the PC contained in the controller board. The control system is based on the MARTe framework that will be described in the next sub-chapter.

4.3. MARTe framework

The Multi-threaded Application Real-Time executor (MARTe) development history is tied with the JET tokamak [62]. In the past, the JET only had dedicated hardware/software solutions for the magnetic control. The shape controller (SC) was operating on VxWorks Power-PC and the vertical stabilization (VS) system was deployed on 4 DSP. This system was very limiting in terms of flexibility, testing/debugging and it took a long time to commission every upgrade. To tackle these issues the JETRT was developed which included the first version of the cross-platform library named BaseLib that provided a clear separation between application and infrastructure software. Although it was a step in the right direction it still had some limitations since it did not provide a real separation between the user application from the plant-interface software and the code needed to be recompiled entirely in case of changes in interface side and/or application side. This framework evolved to the Multi-threaded Application Real-Time executor (MARTe) which will be discussed in this sub-chapter. This framework was selected for implementing the ISTTOK real-time control system over the ATCA hardware described in the previous sub-chapter.

At the date of this thesis, several machines have implemented real-time control systems using the MARTe framework. Each real-time system has different cycle time characteristics and is implemented on different operating systems and architectures. These implementations are summarized in Table 5. This table evidences the flexibility of the MARTe real-time framework with control cycles as low as 50 µs up to control cycles of 10 ms.

Working Systems				
Device	Cycle time	System/sub-system	Operating system	Architecture
JET	50 µs -10ms	Several sub-systems	Linux/RTAI/VxWorks	ATCA/VME/PC
COMPASS	50 µs/500 µs	Fast and slow PS	Linux	ATCA
FTU	250 µs	Lower Hybrid power	RTAI	VME
RFX	200-250 µs	Magnetic control system	Linux(PreemptRT)	PXI
ISTTOK	100 µs	Tokamak RT control	Linux	ATCA

Tests				
Device	Cycle time	System/sub-system	Operating system	Architecture
ITER FPSC	50 µs	Signal broadcast	Linux	ATCA
ASDEX	synchronized	Interface with DCS	Linux	PC
KSTAR	Several tests	Evaluation for ITER	Several Linux	ATCA/PC
FTU	50 µs/1 ms	Electron cyclotron	RTAI	PC

Table 5 – MARTe worldwide footprint. List of working systems using MARTe framework and list of test with the MARTe framework.

The MARTe framework is based on the C++ programming language and is aimed at providing a standard development base for programming real-time systems across several architectures. The main driving concept for developing the MARTe framework was to standardise the development of real-time control systems by creating a clear separation between the applications, the hardware and the operating system. The underlining BaseLib2 (an evolution of the previously described BaseLib) is responsible for providing the abstraction layer that enables MARTe to be deployed in several architectures and operating systems without changing the application code.

BaseLib2

A real-time control system is composed by several layers, the hardware, the operating system and the real-time application. The hardware is responsible for the physical interaction with the machine to be controlled and the operating system is a collection of machine-readable instructions that manages the computer resources and provides common services for computer programs. Modern and complex hardware structures, namely on PCs, require an operating system to work; otherwise the machine code is far too complex for a single human to program on it since PCs use a CISC (Complex Instruction Set Computing) architecture where one single instruction can perform a complex operation. By opposition, the ISTTOK power supplies controller relies on a RISC (Reduced Instruction Set Computing) microcontroller programmed in assembly, without any operating system. To interface between the hardware and the operating system is necessary to have a low level device driver and to interface with MARTE framework is necessary to implement a high level driver. In the ISTTOK control system, the ATCA hardware communicates with the controller board operating system via a device driver provided by the MARTE framework.

The PC processors evolved from single core to several processing units (cores) in the same processor. Because of this evolution, the operating systems are now responsible to schedule tasks for efficient use of the system which may also include accounting for cost allocation of processor time, mass storage and other resources and usually the operating system distributes tasks between all the CPUs cores. For real-time applications with CPUs is useful to isolate one core for each real-time thread avoiding at maximum the interference of operating system tasks with the real-time application. The Linux operating system was the operating system selected for the ISTTOK control system because it is relatively easy to isolate CPU cores for usage by the MARTE real-time threads.

A control system can be viewed as an interconnection of computational blocks, devices that read signals from the environment and then write them out of the digital system and the main advantage of the MARTE/BaseLib2 combination is the clear separation of the computational blocks. The MARTE framework enables the usage of a large preset of blocks and the development of only the real-time application specific code blocks.

The underlying BaseLib2 is the supporting collection of libraries that make MARTE possible and was designed to provide an abstraction layer between the real-time code developed in C++ and the operating system. In fact the BaseLib2 allows MARTE to run in the following operating systems: OS/2tm, VxWorkstm, Linuxtm, Linux/RTAItm, Solaristm, MS Windowstm and Mac OStm.

The BaseLib2 is organized as a set of consecutive layers from level 0 up to level 6. The lowest level (level 0) has the interaction with the operating system and the highest level (level 6) is the highest abstraction level and builds on all the features of the lower levels. In fact, each level builds on the predecessors, for example the “level 1” features are build upon the level 0 and the “level 2” builds upon “level 1” and “level 0” and so on. When compiling the BaseLib2 directory using the standard “makefile” the compiler first compiles the base directory then the several levels directories in sequence and finally some MARTE framework add-ons. This organization is described in Figure 76 and Figure 78.

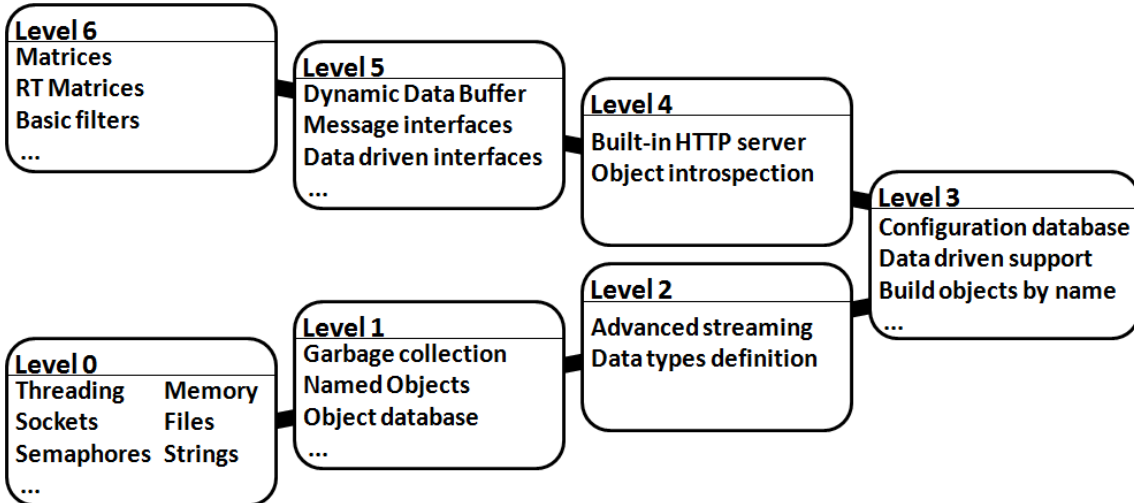


Figure 76 – BaseLib2 abstraction levels. BaseLib2 is divided by several layers, the lower the level number the nearer to the operating system interaction and the higher the level the higher the abstraction from the operating system. Only level 0 interacts directly with the operating system and each level builds on top of the previous ones using their functions.

MARTE	Real-time code
B a s e L i b 2	level 6 Memory Mapped CDB (MMCDB) maths objects
	Dynamic Data Bufer (DDB) Generic Acquisition Module (GAM)
	level 5 Messages State Machine Menu
	level 4 HTTP, HTML protocol libraries
	ConfigurationDataBase (CDB)
	level 3 ConfigurationDataBase OutputStream (CDBOS) parser
	level 2 streams ConfigurationDataBase (CDB)
	Garbage Collection
	level 1 ObjectRegistryDataBase (ORDB) GlobalObjectDataBase (GODB) ConfigurationDataBase (CDB)
	level 0 OS Abstraction Core Primitives
	Operating system
	Hardware

Table 6 – BaseLib2 levels and relative position on the abstraction

The BaseLib2 level 0 is a mixture of different classes that provides to the developer a complete system abstraction. The levels subsequent to level 0 are completely free from operation system specific elements. In fact, the level 0 classes are the “glue” between the operating system and the rest of the BaseLib2 and MARTE. To port the MARTE framework to another operating system it would be necessary only to adapt some of the level 0 classes. The level 0 abstraction ends at the operating system level without offering the device drivers API (application programming interface).

The BaseLib2 level 0 lays the foundations to access the (i) system processor, (ii) CPU core where the threads are deployed, (iii) write and access to memory, (iv) provide memory access abstraction, (v) access the high resolution timer, (vi) stack holder, (vii) file access, (viii) semaphores, (ix) mutex, (x) spinlocks, (xi) network access with IPv4.0 support, (xii) sockets, (xiii) streams, (xiv) error management, (xv) variables type definitions, (xvi) process and thread management, (xvii) priority management, (xviii) mathematical operations and (xix) basic string management.

With operating system specific operations provided by level 0, the level 1 operation does not rely on any hardware or operating system specific arguments. For interfacing with the operating system is relies on the level 0 classes that are compiled before level 1 is compiled. The level 1 offers another layer of abstraction by providing the libraries needed to implement the (i) object registry database, (ii) global object database, (iii) error system Instruction, (iv) configuration database and the (v) stream attributes. Some of these features are better implemented in other high level programming languages such as Java, however C++ was selected for the MARTE framework because it provides a good balance between the real-time performance and the complexity abstraction for simple code programming. The level 1 implements some of the Java features such as an improved run time type identification and persistency making possible to declare properties for accessing the objects similar to a garbage collector. With this implementation it is possible to achieve the same common ancestor letting, where all the objects inherit common methods and common functionalities like being a part of the object registry database. The object registry database can be easily browsed by any other object providing debugging functionalities and runtime linking and loading.

The level 2 is dedicated to strings and data streaming. This collection of libraries implements a series of advanced operations with character sequences and performs input/output operations without requiring the concept of beginning and end of transmission. The advanced streaming features are built on top of the level 0 streaming definitions.

The level 3 is responsible for reading and writing configuration files from a stream (including files). The configuration files are analysed by a parser that reads the parameters and (if requested) instantiates the objects in a tree structure that reflects the stream content. The fundamental component of this level is the configuration database (CDB) and the CDB parser. The CDB is used to start-up the real-time code in MARTE as it contains the definitions of which objects will be loaded and their parameters, to load these objects it uses the previously built level 1 definitions which are also based in level 0 definitions. The CBD tree data structure is composed by two components, the nodes and the objects. The former is a container that once created needs to have at least one object or node with other objects. These objects can be accessed since each object is listed in the objects registry database.

Built upon the previous levels, the level 4 implements a Hypertext Transfer Protocol (HTTP) server (and client) that has the fundamental role of providing communication with every object that implements a HTTP interface. The tree structure mentioned in the previous paragraph is also *browsable* since it is rendered with recursive links. This allows interaction with objects via HTTP. The server can manage more than one client at a time and the stream is

usually coded in HTML (version 1.0). The ISTTOK code uses this HTTP server feature to configure the discharge control and this issue is further described in the next chapter.

Level 5 has a major role in the data communication between GAMs (generic application modules) by implementing the dynamic data buffer (DDB) which will be described further on this chapter. This BaseLib2 level implements the object messaging definitions, the state machine definitions, the signals (and signal interfaces), the data driven interfaces and the DDB. The messages can be either remote via UDP/IP or to the local objects. Any object that is the destination of these messages has to extend a message handle in order to be able to interpret the message.

Built upon all the previous levels, the level 6 implements the last layer of the BaseLib2 which is characterized by having the advanced mathematical implementation such as matrixes, advanced mathematical operations with matrixes, basic filters and waveforms.

The main focus of the BaseLib2 is to provide the base libraries to abstract the user from memory managing features (such as pointers and memory allocation) by incentivising the usage of the reference concept. The BaseLib2 includes methods to create automatically objects and to destroy them via a garbage collector. These objects are stored in a list with a tree reference and can be easily searched and addressed. This type of implementation has two main advantages: first it is much less prone to coding errors (which are frequent when using pointers and memory allocation) and secondly it provides a simplified structure to program a real-time system.

MARTE, dynamic data buffer (DDB) and generic application module (GAM)

Built upon the BaseLib2 foundations, MARTE is the main application of the MARTE framework. MARTE uses the BaseLib2 libraries to implement a modular control system. The main idea is to provide real-time code execution layout and abstraction tools for the users to implement their real-time control algorithms with as little effort as possible. As described in the BaseLib2 section, the memory management, communication interface, operating system connection and hardware interfacing are greatly simplified by using the MARTE framework.

MARTE can be described as a collection of real-time threads scheduled by an internal state machine (capable of sending messages upon state change). In fact MARTE is responsible for creating one or more real-time threads (according with the configuration database file provided by the user), each of these threads runs a sequence of code blocks, named generic application module (GAM), each control cycle. The MARTE real-time threads (RTTh) are lunched in the operating system in the selected CPU core (if a multi-core processor is available) preferably in an isolated CPU core (for better real-time performance) and these threads can run in parallel, synchronously or asynchronously. Each real-time thread is totally configurable in cycle-time and in the code they execute. MARTE also keeps accurate information about execution times of each GAM and the overall execution time of each thread.

MARTE requires an external time and triggering mechanism to function as a micro-scheduler. This requirement increases the system flexibility since depending on the project, the time is either provided by an (IOGAM) input output generic application module (GAM used for hardware interface) or by the local CPU time (a high precision emulator is provided by the

MARTE framework) which is used normally for debug and development or by non-critical synchronization processes. Regarding the real-time thread synchronization, a new control cycle starts only when the time is a multiple of the programmed control cycle period (Figure 77). This will unlock the real-time thread and execute all the GAMs in sequence. In case of the time source times-out waiting for the external signal an error will be produced and the user can configure the action that the system executes in the event of a timeout.

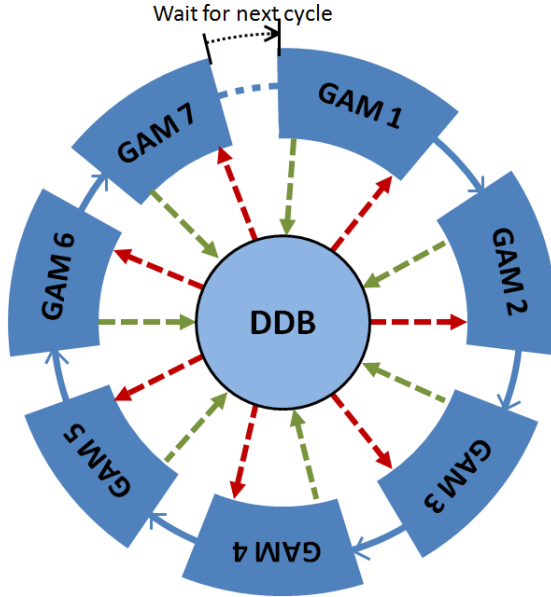


Figure 77 - MARTE control cycle. MARTE acts as a scheduler synchronizing the GAM execution. In each thread a set of GAMs run in sequence and at the end of the execution of the last GAM, MARTE waits until the next cycle time to start again the GAMs sequence execution. GAMs communicate via DDB.

A control system can be divided in sub-blocks where each block performs a specific task for the control system. In a real-time system there are several tasks to be performed, the most common are the interface with hardware (read and output), algorithm execution, decision taking, debug, providing information about the system and store data for future analysis. In MARTE these well compartmented blocks of code are named generic acquisition modules (GAMs) and these GAMs are the atomic element of a MARTE real-time system. Each real-time thread runs a user defined set of GAMs in sequence as depicted in Figure 77. A GAM also implements a specific interface specified in the BaseLib2 library. According to this specification, each GAM has three communication points, one for configuration and two for data input and output.

During the initialization process, the GAMs declare what data they expect to receive and what information is going to be written as output. The GAM class defines an `init()` method which is automatically called when the GAM objects are loaded (MARTE start-up), this enables the GAM instance to receive the initialization parameters and construct the signal interfaces that implement the data input and data output features for each GAM. The GAMs also have an `execute()` method that is called at every control cycle, where input data and output data references buffers can be accessed by the signal interfaces handler. These modules also keep track of their internal history and the input signal interface and output signal interface. These interfaces are a reference to where the signals are stored in memory and these are provided by the BaseLib2 abstraction layer.

Since each GAM is not aware of the other GAMs, the only means of communication is the input and output interfaces which are constituted by a set of atomic signals such as integer or float. These GAMs share data through an optimised memory bus named Dynamic Data Buffer (DDB). During the initialization each GAM defines their input and output signal interfaces (set of variables), so each GAM knows exactly which type of data will receive and which type of data it will write on the DDB. The data written in the DDB is accessible to all the other GAMs by a reference name and the data that each GAM accesses is defined in the initialization process by the CDB file that is processed by MARTE in this initialization process. During the initialization process, MARTE checks if there is a signal being produced for the signal to be consumed and also check if there are two GAMs writing on the same signal name. This is only possible if the user specifically configures this type of overwriting, otherwise it will give an initialization error. This assures coherency across all the DDB data.

Each real-time thread implements their own DDB, meaning that, by standard, the DDB data of a real-time thread can only be accessed by the GAM instances that are running on that real-time thread. If there is more than one real-time thread and it is necessary to access other real-time thread data (which is not the usual case), it has to be developed an IOGAM to transfer data between the two DDBs. The MARTE framework also provides GAMs to send signals across the network to other MARTE systems, but in this case the real-time can only be assured in the producer side. In the consumer side timeout strategies can be implemented to produce an error in case of the data is not received on the expected time.

Figure 78 depicts the components of a MARTE real-time system.

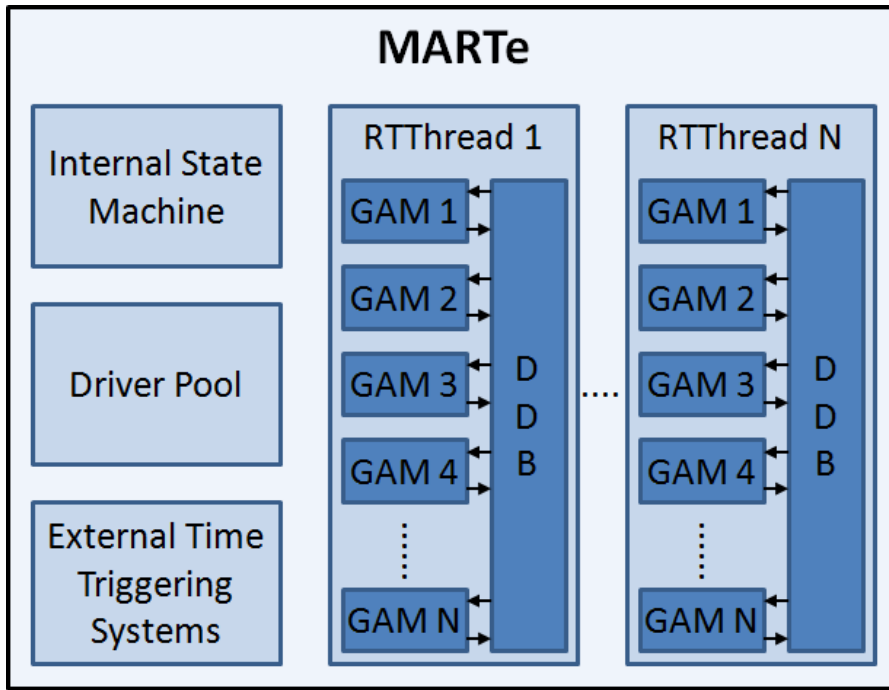


Figure 78 – MARTE objects. The MARTE application can launch several real-time threads, each running several GAMs at their own control cycle time. Each real-time thread has one dedicated DDB.

The major part of the effort for developing a real-time control system under the MARTE framework is the design of the application specific GAMs, although some of the general GAMs are already distributed alongside with MARTE framework. The application specific algorithms

modules have to be developed as all the real-time system organization. This type of implementation is very flexible and the clear boundaries on the code enable a GAM to be replaced by a signal producer or a plant model in order to simulate the behaviour of the control system. This can be done even before being deployed in the target machine since a MARTe real-time system can run in a standard PC without the same real-time performance) by replacing the hardware interface GAMs (IOGAMs) with either a model or a signal producer simulation GAM. This simulation environment allows an efficient debug and tuning strategy and a reduced commissioning time to a real-time system. After the system fine-tuning in a simulation environment the final implementation specific GAMs can be inserted back (replacing the simulation GAMs) and deployed to the final real-time system. The code reusability and portability is also enhanced by this strategy since some GAMs can be used in different real-time systems.

A special type of GAM is used to interface with the hardware. This input or output GAM is called an IOGAM. The IOGAM provides a unique high-level interface to any kind of hardware by enforcing the methods to read and write. The number of inputs and outputs has also to be specified. As depicted in Figure 79, the connection between the IOGAM with the operating system low-level driver that controls the hardware is provided by one high-level driver. This is designed for each type of hardware. The acquisition hardware is usually configured to retrieve the last acquired values or to reply with the most recent values (at the expense of the real-time performance). The output hardware is normally configured with the values to output.

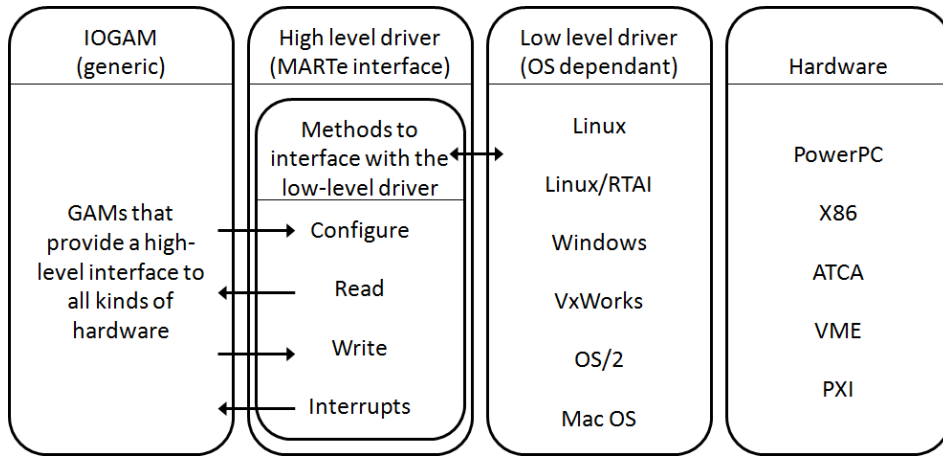


Figure 79 – IOGAM interface with the hardware.

Since MARTe is interface agnostic, it has neither a predefined GUI nor a predefined high level protocol. This requires the development of a module to translate a GUI into the language used in the MARTe framework. Nevertheless, MARTe provides a message server that can be used to interface with the MARTe objects. This can be used to interface with external tools such as EPICS and MDSPlus, being these interfaces provided by the MARTe community.

Logger

The ability to debug a real-time system efficiently without compromising on the real-time features is of major importance for maintaining the system healthy. The ability to log the system resources during code execution enables the user to efficiently understand how the system is behaving and compare it against the desired behaviour.

In order to have a minimal impact in the system real-time performance, the real-time GAMs are the producers of data and a process with very low priority process (preferably running on a different CPU core than the real-time thread) processes the messages to be sent in a FIFO (first-in first-out) queue. Then the messages are dispatched via User Datagram Protocol (UDP) protocol to one or more addresses (IP). This decouples the real-time performance from the logging system.

The JTLogger application is provided in the MARTe framework package. This is a Java based program that normally is running on a remote PC or segregated from the real-time code that organizes the received messages for visualization according to several parameters such as (i) the producer address, (ii) the importance and (iii) the producing object name. With these message properties it is possible to filter the incoming messages. The MARTe framework also provides a plug-in for storing the incoming messages into a file.

4.4. Real-time control

Taking into consideration the MARTe framework description in the previous sub-chapter, the main characteristics leading to the choice of MARTe for the ISTTOK real-time control system where:

- **Multi-platform** - MARTe runs on all major OS: Linux, RTAI, Windows, MacOSX, VxWorks and Solaris.
- **Modular** - Clear boundary between algorithms, hardware interaction and system configuration.
- **Facilitates simulation and commissioning** - Replace actuators and plants with models and keep all the other modules untouched.
- **Code reusability** - GAMs can be instantiated several times and can be reused in different control systems and many GAMs are already written and are distributed with the MARTe framework, example: data collection GAM, reference generator, plot, etc...
- **Live introspection tools** - Logger service separated from real-time threads.
- **Built-in HTTP server** - Each object/GAM can have a HTTP interface.
- **Interface agnostic** – An application developed in the MARTe framework can be interfaced by different platforms, example: EPICS, MDSPLUS, etc...
- **Precise control on the cycle time** – MARTe acts as a micro-scheduler and synchronizes the control system execution with a fixed cycle time.

The ATCA control board runs a custom configured version of Gentoo. This Linux distribution was preferred due to its highly configurable interface which (as other Linux distributions) allows the user to enable and disable several kernel features. The MARTe framework was installed on top of that Linux distribution. Since ISTTOK control system included a quad core CPU, it was possible to select the CPU core for running each individual process. The Linux operating system services were constrained to the first CPU core by using the kernel boot option “isolcpus=1,2,3”, which prevented Linux services from running in the remaining cores. After Linux operating system boot, each ISTTOK specific process is distributed to a specific CPU core using the “taskset” command with the corresponding CPU core. The result of the process distribution is on Table 7. To further optimize the real-time code execution, all the ISTTOK real-time code was compiled with the option “-O3” in the C++ compiler (gcc).

CPU	Process
Core 0	Linux services
Core 1	Drivers for acquisition boards
Core 2	MARTe services
Core 3	ISTTOK real-time thread

Table 7 – CPU load distribution per CPU core in a quad core CPU.

For configuration purposes, two objects that interact with MARTe were produced (see Figure 80). These objects implement a HTTP server in C++ using the BaseLib2 libraries. The “Discharge configurator” handles the most used configuration parameters such as plasma current/position waveforms and the “Advanced configuration” is used to configure the less changeable parameters such as the serial port address of the UART that communicates with a

specific power supply. These objects are a part of the human-machine interface (HMI) and are further described in the chapter 5.

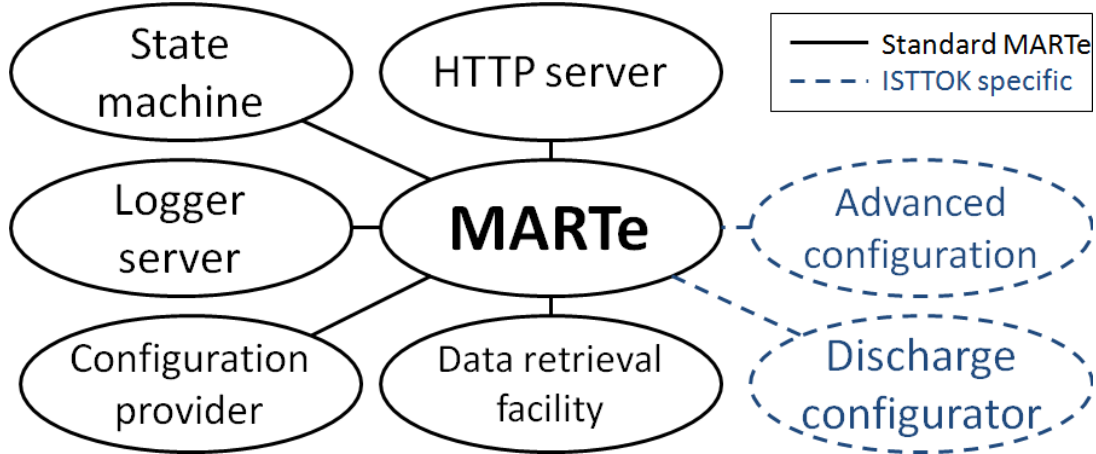


Figure 80 – MARTe connections including the following services: HTTP server, logger server, configuration provider, data retrieval facility, state machine. In addition two more objects were created to configure the system, these two objects are the “discharge configurator” and the “advanced configurator”, which are used to change the control configuration via two HTML WebPages.

After commissioning the control system, the control cycle was measured using a control cycle variable produced automatically by the MARTe framework. This introspection ability is very useful for debugging the real-time performance of the control system code. MARTe stores the execution time for each individual GAM and stores the overall control cycle as well. The frequency of occurrence of a certain control cycle is depicted in Figure 81. As it can be observed, the control cycle is clearly centred in 100 µs and has a jitter generally inferior to 0.4 µs.

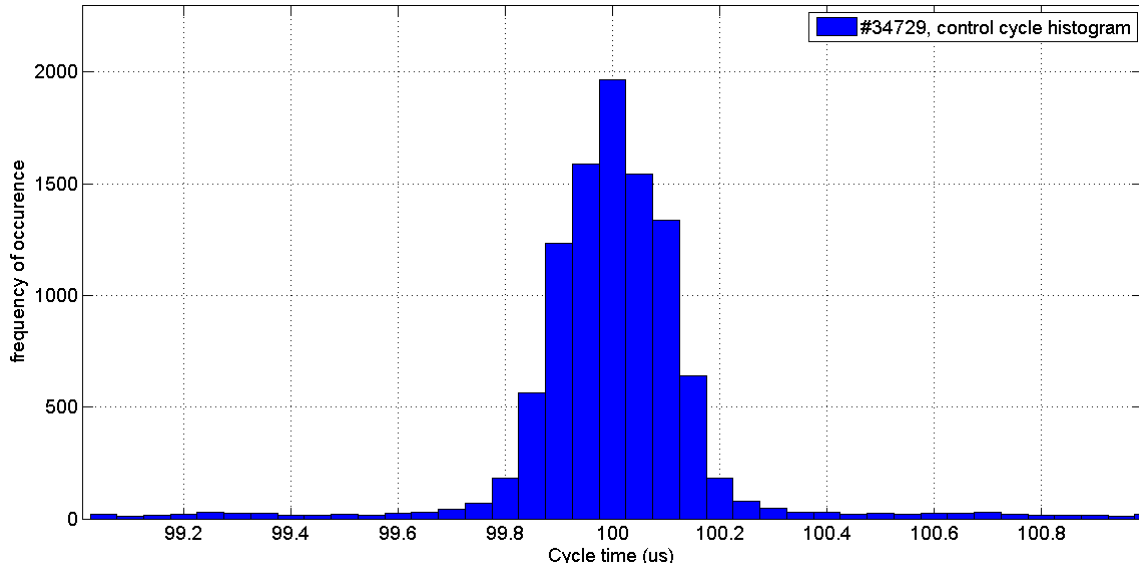


Figure 81 – Control cycle histogram for pulse #34729. The control cycle is centred in 100 µs and the jitter is generally lower than 0.4 µs.

The ISTTOK control flow chart is depicted in Figure 82, with each block representing a set of GAMs, as an example, the “diagnostics pre-processing” represents individual GAMs for pre-

processing each diagnostic, such as automatic offset removal and diagnostic sub-parameters calculation. The ISTTOK GAMs are further described in the next sub-chapter.

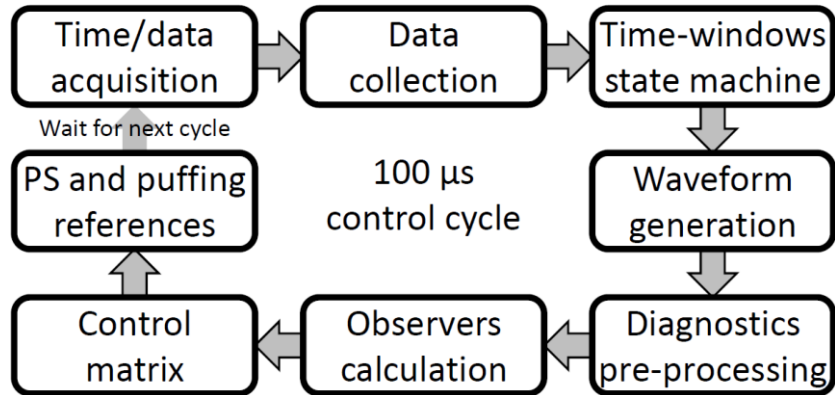


Figure 82 - The full controller scheme is conceptually represented by a set of macro blocks, starting from data acquisition and data collection, followed by waveforms and parameter calculation and finalised by the diagnostic and controller execution, which lead to the reference generation for the actuators.

ISTTOK control

The ISTTOK control software was completely redesigned to accommodate all the real-time diagnostics and all the real-time actuators in a Multiple Input Multiple Output (MIMO) fashion. In addition, the control concept was updated, featuring a new event-driven approach.

The controller configuration is based on time-windows, so that the user can specify different control strategies to be executed during different phases of the experiment. The machine operator selects before the discharge which diagnostics are to be used in feedback control as well as their contribution to the measurement. In each time-window, the machine operator can select between three modes of operation for the power supplies, (i) pre-programmed current waveform, (ii) proportional–integral–derivative (PID) controller on plasma position or plasma current and (iii) auto-PID. The auto-PID control feature changes between three sets of user defined PID constants based on the distance of the observed quantity in respect to the reference waveform (error definition) aiming to be more responsive when distant from the objective and softer when near the set-point. In the ISTTOK control system there are two different sets of time-windows, the positive and the negative plasma current time-window sets. Depending on the plasma current direction one of these sets is executed.

The gas puffing can be programmed in four different modes, (i) absolute time pre-programmed voltage output, (ii) feedback waveform in time-windows, (iii) voltage output synchronized with time-windows and (iv) pre-puffing during breakdown and feedback waveform during the time-windows. The ISTTOK gas injection system is based on a piezoelectric valve that can be either open or closed and is directly controlled by a RTM DAC. According to the programmed algorithm, the valve is only opened for a short programmable period (normally about 1 ms), with the time between each puff depending on the feedback reference waveform and the process variable value, puffing more frequently if the process variable is under the requested value. Feedback used in modes (ii) and (iv) can be assigned to either density or H_α radiation.

When there are many potential changes in the control type during a discharge it is useful to implement a goal oriented strategy. This type of strategy was particularly useful for implementing the plasma sensitive transitions such as the breakdown and the plasma current inversions. In the goal oriented transitions a set of programmable waveforms are run until the goal is achieved, for example, during a plasma current inversion the inversion waveforms are executed until there is substantial plasma current in the opposite direction. After that the controller jumps in time to the execution of the first opposite plasma current time-window.

The time-window change can be triggered either by elapsed time or by an external synchronization event. The latter can be illustrated with two examples. The “auto-breakdown” feature uses the power supplies with pre-programmed current in the beginning of the discharge and when the plasma current is greater than a certain value it jumps to the control type defined in the first time-window. In addition to the goal oriented references, there is also an exception-handling event which is the iron core flux saturation. The second example is the feature that automatically inverts the plasma current when the ISTTOK iron core is saturated. After the saturation has been reached, it is not anymore possible to continue to drive efficiently the plasma current in the same direction, so there are only two options left: (i) invert the plasma current or (ii) end the discharge. In this mode the system time and the control sequence jumps to the beginning of the first time-window of the inverse cycle, allowing the AC discharge to continue in the opposite plasma current direction with all the actuators synchronized with that event.

Figure 83 shows the standard method for programming a long AC discharge: First the breakdown waveforms are executed until the breakdown goal is achieved and then the control is handled to the programmed positive current time windows. After executing all the positive time windows in sequence, the inversion to negative current set of waveforms are executed until there is plasma current in the opposite direction (goal achieved). Subsequently, the controller jumps to the execution of the negative current time windows in sequence and then the control is handled to the inversion to positive current waveforms that are executed until there is a significant (threshold defined by the operator) positive plasma current (goal achieved). After this successful inversion the same positive time windows are executed as well as the rest of sequence. The discharge will repeat the two sets of programmed time windows (for positive and negative cycle) over and over again until the number of programmed AC cycles is reached.

The machine operator is still able to program the discharges using other methods (such as fully pre-programmed discharge or time windows without goal oriented waveforms) but the described method has the advantage of being much simpler to implement since the operator only needs to program two sets of time windows and the breakdown and inversion waveforms. The inversion and breakdown waveforms are normally kept constant from discharge to discharge basis and the user also has the ability to load previous pulses configuration from the control graphical interface.

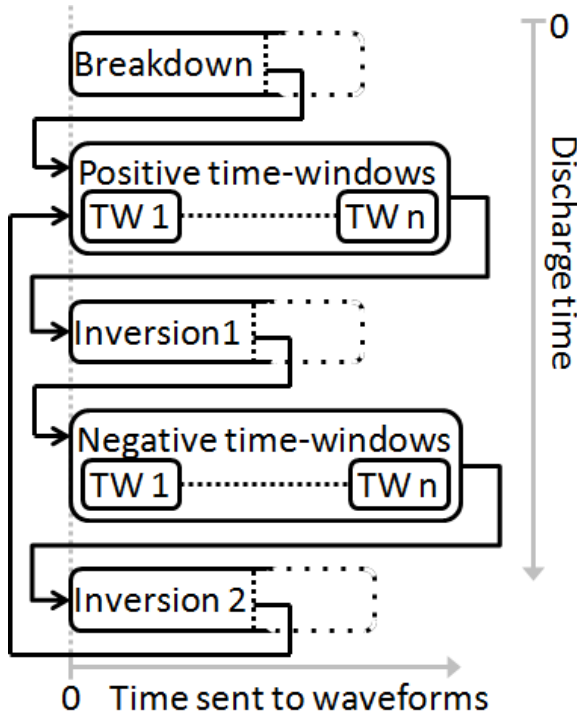


Figure 83 – AC discharge sequence schematic. If programmed accordingly, the discharge will repeat the two sets of programmed time windows (for positive and negative cycle). Breakdown and inversion (positive to negative and vice-versa) are pre-programmed waveforms that are executed until their objective is concluded, after which the controller jumps in time to execute the corresponding time windows.

An example of a combination between pre-programmed and feedback control is shown in Figure 84. Although it is not possible to observe in the figure, the breakdown and inversion periods end when their objective is accomplished and then the controller jumps to the next time windows set.

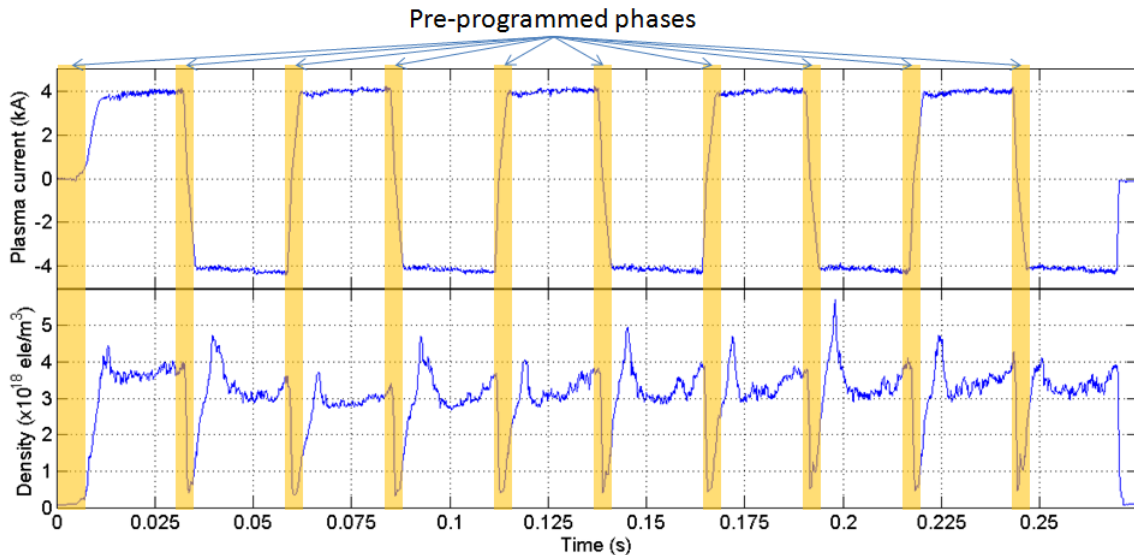


Figure 84 – Pulse #34135. This figure evidences the pre-programmed parts of on AC discharge.

4.5. ISTTOK Generic Application Modules (GAMs)

The Generic Application Modules (GAMs) are compact pieces of code that normally address a well defined set of tasks. Once the GAM code is written it can be instantiated several times, thus the GAMs must be written in such a way to promote code reusability. Each instance runs sequentially under the MARTE framework and the complete set of instances constitutes the control system.

To promote code reusability, it is a good programming practice to program a GAM to perform a specific task and not program many tasks inside a single GAM. This task should be clearly defined in order for the GAM to be easily replaceable by a different algorithm for the same task. There are several categories of GAMs such as:

- **Hardware input/output** – For interfacing with the hardware input and outputs, an IOGAM should be produced for each type of hardware.
- **Algorithms** - Data processing and data construction.
- **Decision taking** – State machine GAM or controller GAM.
- **Persistence** – Data storage GAM, actually there is one GAM supplied with the MARTE framework for this purpose named DataCollectionGAM.
- **Debug** – Some GAMs used for the real-time can be replaced (for debug purposes) by models and synthetic data producers GAMs.
- **Information** – Information about the system status.

A useful exercise to find the number of GAMs and their content for a certain real-time system is to draw the control system flow chart with as many components as possible, while maintaining the logic and not over detailing the processes.

The input and output variables of each instance of a GAM are defined in the configuration file loaded in the real-time control system start-up. Once these variables are defined the GAM instances can interchange variables using the Dynamic Data Buffer (DDB). Each variable in the DDB can be written and read by any GAM instance. In this way all variables in the same real-time thread are accessible to all the GAM instances, for example, the system time is written by the ATCAadcDrv GAM and is read by many GAM instances.

The ISTTOK GAMs were designed with clear task boundaries to maximize the code reusability, this allows a GAM to be replaced by another without changing the remaining GAMs, for example, if a new algorithm for the plasma position is developed using the magnetic probes the MagneticsGAM can be replaced by the new GAM with the new algorithm without intervening in the remaining code which is very useful with large projects. The ISTTOK control system has a set of 19 GAMs and a total of 25 instances as described in Table 8.

The execution time histograms for all the GAMs can be observed in Figure 85, Figure 86 and Figure 87 and the values for the average execution time and standard deviation are presented in Table 9.

GAM name	Instance name	Short Description
TimeInputGAM	ATCAAdc	Board signals acquisition
TimeWindowsGAM	time_windows	Discharge state machine
TomographyGAM	Tomography	Tomography processing
ElectricProbesGAM	electric_probes	Electric probes processing
MagneticsGAM	magnetic_probes	Mirnov coils processing
SineProbeGAM	sine_probe	Sine probe processing
CosineProbeGAM	cosine_probe	Cosine probe processing
MainRogowskiGAM	main_rogowski	Main rogowski processing
InterferometryGAM	Interferometry	Interferometry processing
HAlphaGAM	H_alpha	H-alpha processing
TechnicalSignalsGAM	technical_signals	Machine signals processing
PlasmaStatusGAM	plasma_parameters	Plasma variables processing
MachineProtectionGAM	machine_protection	Machine health processing
WaveformGAM	waveform_primary	Primary PS waveforms
	waveform_vertical	Vertical PS waveforms
	waveform_horizontal	Horizontal PS waveforms
	waveform_toroidal	Toroidal PS waveforms
	waveform_puffing	Gas puffing waveforms
ControllerGAM	Controller	Integrated controller
PowerSupplyCommunicatorGAM	PSCommunicator_horizontal	Horizontal PS communications
	PSCommunicator_vertical	Vertical PS communications
	PSCommunicator_primary	Primary PS communications
OutputGAM	ATCADac	Output to RTM DACs
DataCollectionGAM	DataCollection	Data storage
FireSignalDischargeStatusGAM	Codac	Discharge status to FireSignal

Table 8 – Association between GAMs and instances running on the ISTTOK control system. The table is ordered by the sequence in the control cycle, from “ATCAAdc” (first instance to run) to “Codac” (last before end of cycle). WaveformGAM is instantiated five times and PowerSupplyCommunicatorGAM is instantiated tree times.

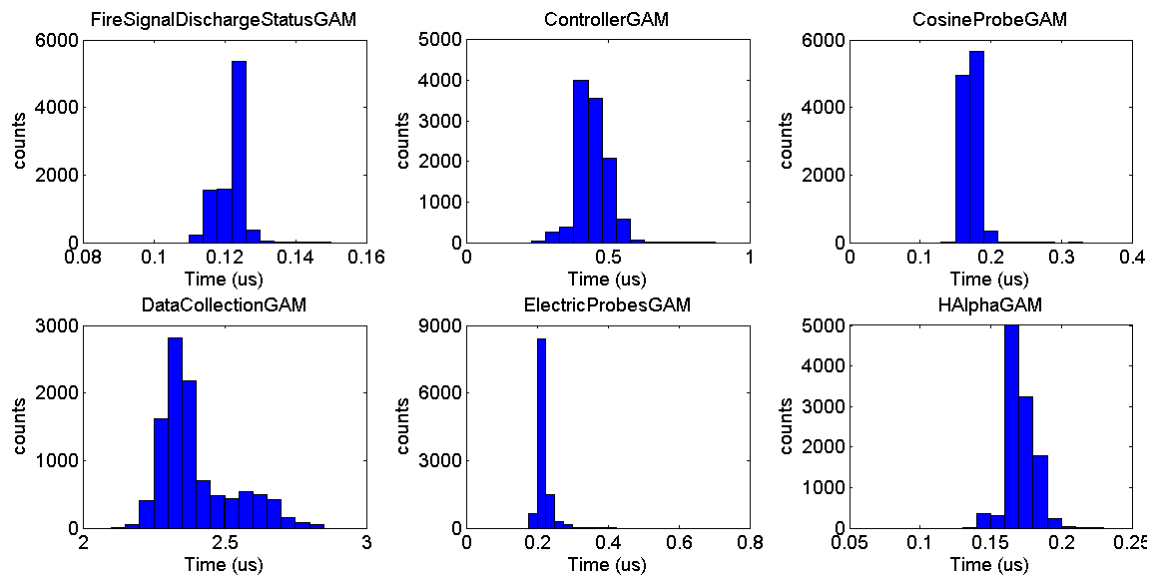


Figure 85 – Execution time histograms for the FireSignalDischargeStatusGAM, ControllerGAM, CosineProbeGAM, DataCollectionGAM, ElectricProbesGAM and HAlphaGAM.

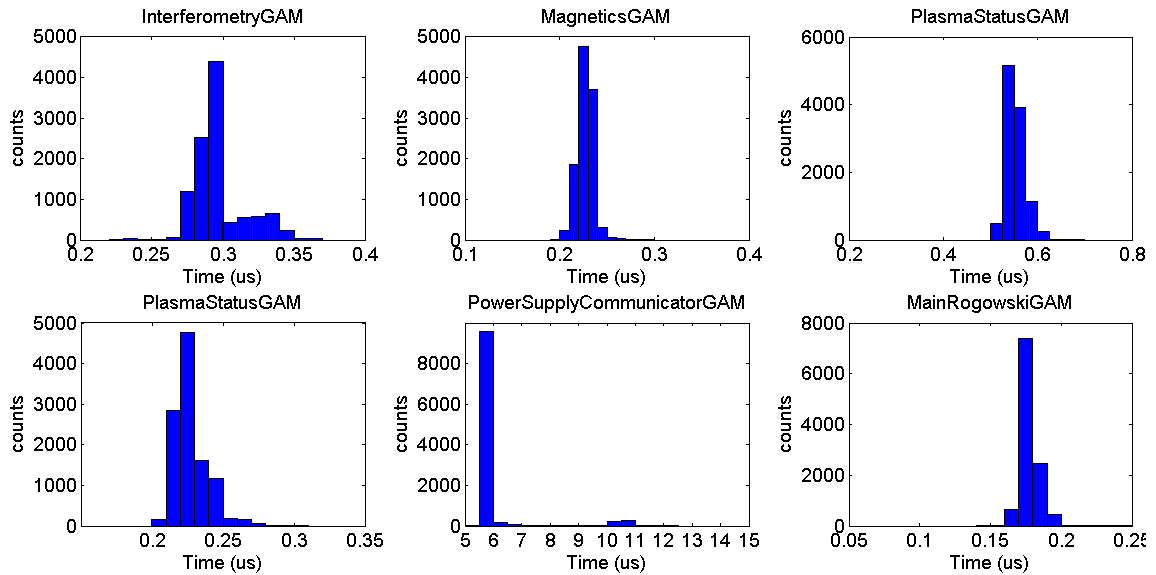


Figure 86 - Execution time histograms for the InterferometryGAM, MachineProtectionGAM, MagneticsGAM, PlasmaStatusGAM, PowerSupplyCommunicatorGAM and MainRogowskiGAM.

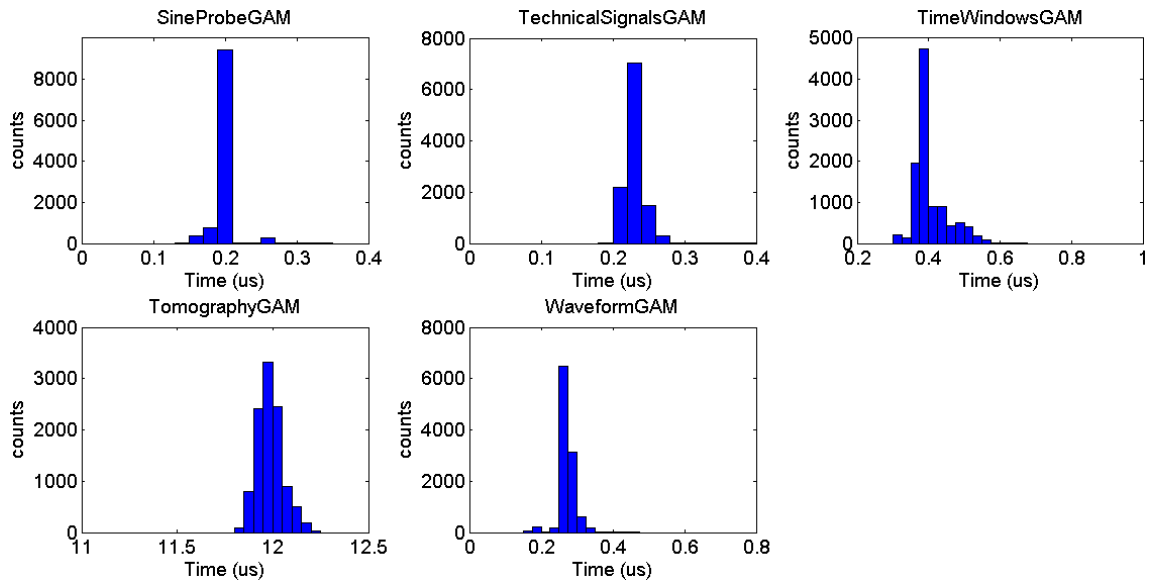


Figure 87 – Execution time histograms for the SineProbeGAM, TechnicalSignalsGAM, TimeWindowsGAM, TomographyGAM and WaveformGAM.

The mean execution time and standard deviation for all the ISTTOK GAMs is detailed in Table 9

GAM name	Mean value (μ s)	standard deviation (μ s)	GAM name	Mean value (μ s)	standard deviation (μ s)
FireSignalDischargeStatusGAM	0,13059	0,096404	PlasmaStatusGAM	0,22785	0,027322
ControllerGAM	0,44842	0,081863	PowerSupplyCommunicatorGAM	5,8763	1,7281
CosineProbeGAM	0,17179	0,08286	MainRogowskiGAM	0,17899	0,056341
DataCollectionGAM	2,5124	0,62975	SineProbeGAM	0,20063	0,068408
ElectricProbesGAM	0,21695	0,091276	TechnicalSignalsGAM	0,22989	0,080091
HAlphaGAM	0,17275	0,07926	TimeWindowsGAM	0,40379	0,20813
InterferometryGAM	0,29477	0,058056	TomographyGAM	12,024	1,2475
MachineProtectionGAM	0,22723	0,026203	WaveformGAM	0,27398	0,070779
MagneticsGAM	0,563	0,60653			

Table 9 – ISTTOK GAMs mean execution times and standard deviation.

The PowerSupplyCommunicatorGAM which is intended for communication with the power supplies is the main source of jitter. In fact this GAM is responsible for the control cycle ISTTOK real-time code being 100 μ s instead of 50 μ s. The ISTTOK real-time code generally runs in about 40 μ s but since the PowerSupplyCommunicatorGAM has about 5 μ s of jitter and this GAM is instantiated 3 times (one for each PS) about 0,1% of the control cycles are not met in 50 μ s. In this case MARTe uses the multiple of the control cycle to resynchronize the GAM sequence execution. In the case of failure to meet the 50 μ s control cycle, the control cycle would be moved to 100 μ s in that particular cycle, so the control cycle would be 50 μ s and occasionally 100 μ s. Normally this would not represent a problem since the code is synchronized by absolute time but it was decided to keep the control at a constant 100 μ s cycle. This issue could be solved by designing a high level driver for the power supplies interface, but a control cycle of 50 μ s instead of 100 μ s does not increase the overall performance of the ISTTOK real-time control.

A short description of each individual GAM can be found below.

TimeInputGAM



Table 10 – TimeInputGAM inputs and outputs.

This IOGAM is used to gather data from the ADCs of the ATCA acquisition boards. The GAM interfaces with the ATCA acquisition boards' driver and obtains the system time and the data for all the ADC's of the ATCA system. Then, the GAM writes to the DDB all of this data every control cycle in order to be available for all the other GAMs during the control cycle. This GAM is included in the MARTe framework package of standard GAMs. The driver for interfacing with the ATCA hardware is also included.

TimeWindowsGAM

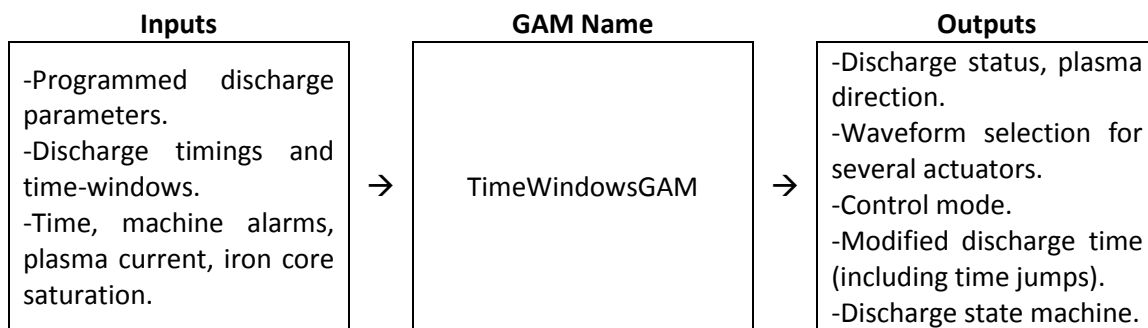


Table 11 – TimeWindowsGAM inputs and outputs.

The TimeWindowsGAM is the main real-time state machine for the discharge. This GAM changes the control type based on external events such iron core saturation, current ramped up after auto break-down or inversion or machine protection events. This GAM also changes the control sequentially according to the programmed time-windows. There are several discharge modes that can be programmed by the user corresponding to user-defined

waveforms (a set of waveforms for each plasma direction) such as breakdown, inversion, current control, scenario control (calculated plasma properties such as plasma position, plasma current, etc...), synchronized and unsynchronized gas puffing and density feedback.

The TimeWindowsGAM controls which waveforms are in use and the waveforms timing, for example, if the auto-breakdown is selected by the user, the TimeWindowsGAM starts applying the programmed breakdown waveforms from time = 0 and when the plasma current is above a certain threshold the TimeWindowsGAM changes the waveform mode to the one defined for the first time-window (starting again by the time = 0 for those waveforms). This has the advantage of executing a certain set of tasks without pre-programming exactly their timing (event driven format). This means that with exactly the same discharge pre-programming the discharge timing can be different for distinct machine conditions. This behaviour is depicted on Figure 88.

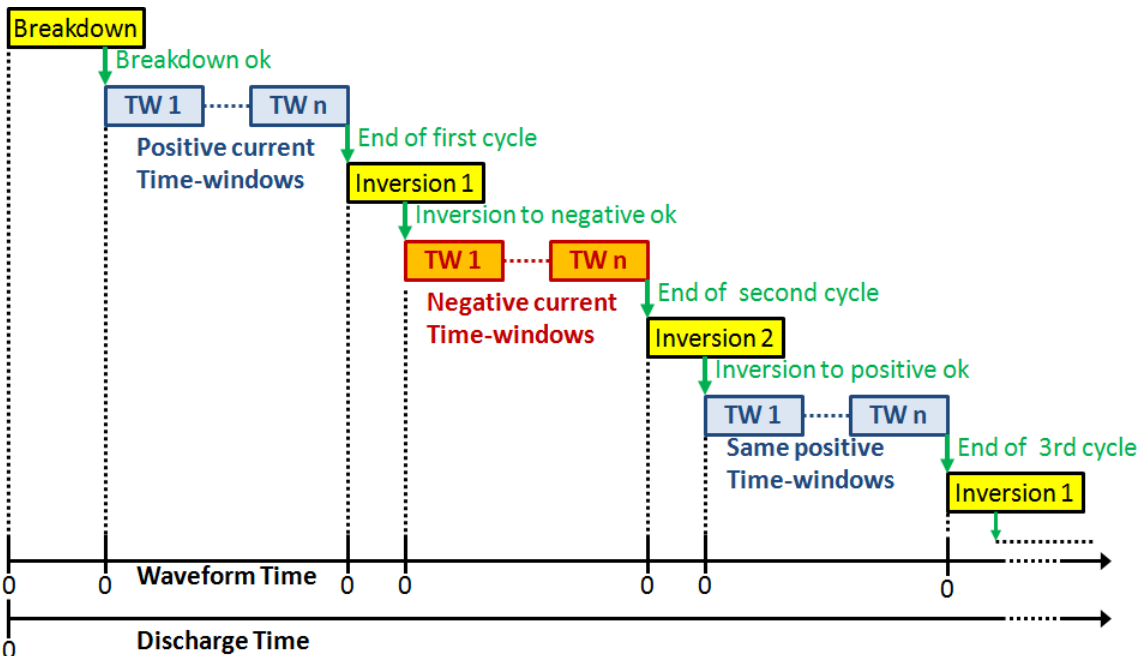


Figure 88 – Discharge time and waveform time of a discharge with auto-breakdown and pre-programmed inversion waveforms. This figure shows the effect of the TimeWindowsGAM on the time that is sent to the user defined waveforms. This feature allows the repetition of the alternate current semi-cycles without programming more than two semi-cycles.

Another type of waveform switching occurs when a time-window ends and another time-window starts. This transition is also assured by the TimeWindowsGAM. In this case the TimeWindowsGAM continues to increase the discharge time at the normal pace and changes the waveform mode (current control or scenario control depending on the discharge configuration), so that the waveform has the correct timing and the output from the selected waveform (direct PS current or scenario waveforms). The transition in control is done afterwards by the ControllerGAM.

When there is a time-window named “inversion” (meaning that the plasma current is to be inverted at a certain time) or there is an event of iron core saturation (when flux driven through the iron core approaches the maximum value the plasma current starts to decay even if the primary current is largely increased) the TimeWindowsGAM ends the current plasma cycle (referred to either positive or negative current cycles) and if additional cycles were

programmed, the GAM switches the actuators control mode to the programmed in the first time-window of the opposite plasma current direction (the modified discharge time is set to time = 0). If the user selects many cycles the odd semi-cycles have similar programming than the first and the even semi-cycles have similar programming than the second semi-cycles and this is repeated until the end of the discharge alternating between the positive time-windows set and the negative time-windows set.

Figure 89 depicts the modified discharge time that is sent to the waveforms while the schematic representing this type of operation is depicted in Figure 88.

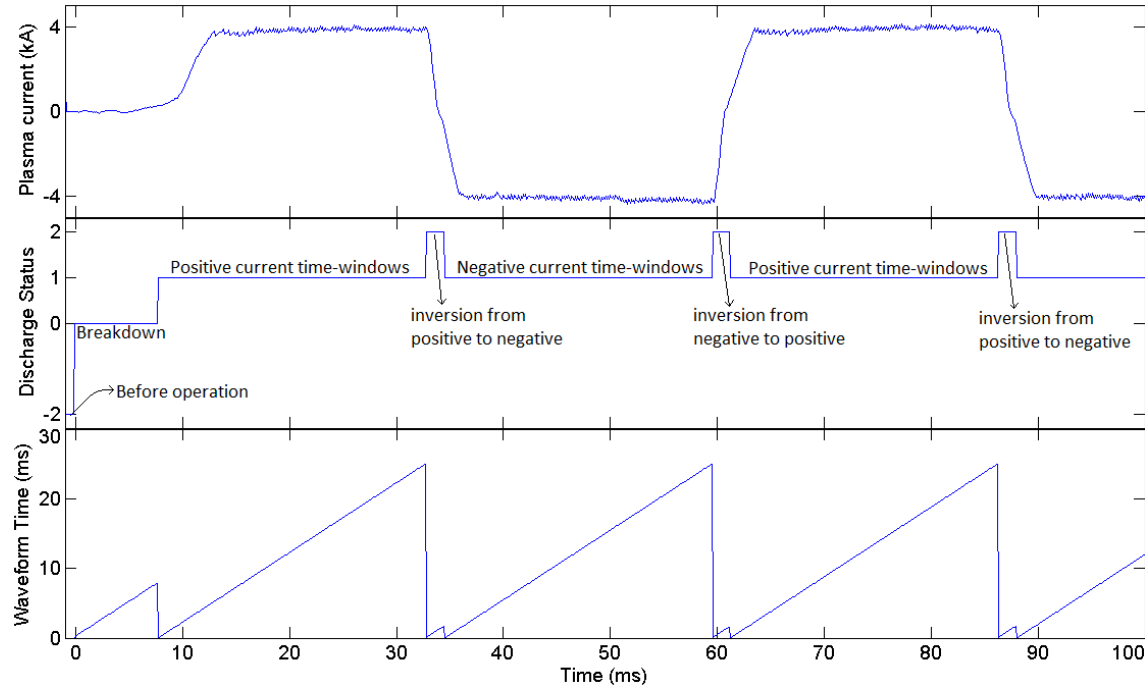


Figure 89 - Plasma current, discharge status and waveform time. At each event completion/interruption, the time sent to the waveforms is reset to 0, flowing normally afterwards. Using this scheme it is possible to repeat control sub-sequences for many cycles.

This GAM also controls the end of the discharge, ending the discharge if the discharge time has passed the limit defined by the user. This GAM also stops the discharge if the number of alternate discharge cycles have reach the limit value programmed by the user. There are event driven interrupts that can also stop the discharge. If a soft or hard stop alarm is received from the MachineProtectionGAM it can decide how to better shutdown the pulse.

TomographyGAM

Inputs	GAM Name	Outputs
- ADC data stored on DDB (tomography channels). - Time.	TomographyGAM	Tomography plasma position and the total intensity.

Table 12 – TomographyGAM inputs and outputs.

The TomographyGAM contains the code used to reconstruct the plasma position in real-time by using three sets of optic sensors (Figure 34), each set contains 8 optic sensors. This GAM is well compartmented so that it can be replaced by another tomography GAM running a different reconstruction mechanism, improving the overall code flexibility.

Between the discharge trigger and the user configurable variable “wait for starting operation” this GAM acquires the background noise of each individual channel. After this period the GAM subtracts each channel background signal average from the corresponding signal data, automatically removing the offset. The channel data is acquired by the TimeInputGAM which stores all the data on the DDB.

Currently, this GAM runs the Fourier-generic algorithm (with Bessel functions as base functions) to calculate the plasma position (this issue is further described in section 2.1). The matrixes that support the calculations are stored in a file apart from the GAM. When the GAM is initialized it reads this file (that is configured in the advanced configuration object described in chapter 6) and retrieves the matrixes constants. This enables to replace those matrixes just by reloading the GAM with a different file.

After processing the tomography code, the GAM produces three variables to the DDB; the vertical and horizontal positions and the sum of all channels. The sum of all channels intensity is compared in Figure 90. As illustrated, the tomography total intensity is comparable to the H_α radiation, which is an expected result since the absorption peak of the tomography sensors (Figure 33) is near the H_α wavelength (656 nm) and the H_α is the main component of the ISTTOK plasma radiation.

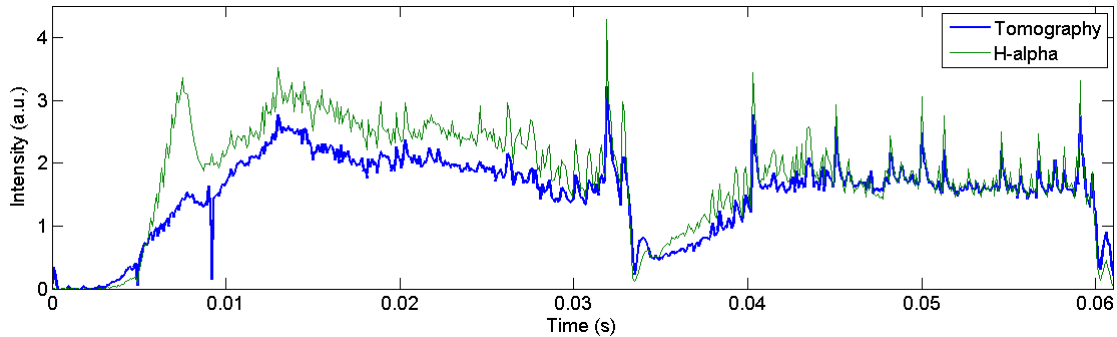


Figure 90 – Comparison between the total tomography intensity and the H_α radiation for pulse #34854. This pulse was a 6kA AC discharge with 2 semi-cycles. The H_α diagnostic is more sensible in the initial discharge phase where the radiation from carbon impurities is still not high. For this reason the H_α diagnostic detects better the first plasma ionization.

ElectricProbesGAM

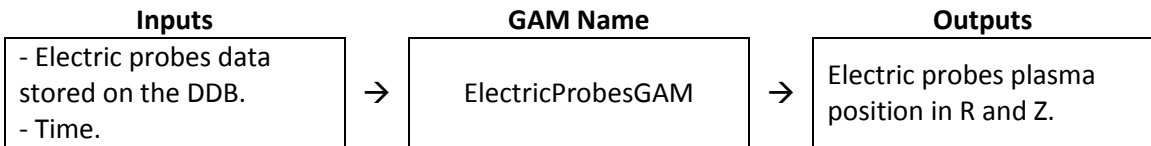


Table 13 – ElectricProbesGAM inputs and outputs.

The ElectricProbesGAM, as the name indicates, is a GAM that receives the signals of the electric probes. This GAM algorithm uses the floating potential signals measured at r = 75 mm to estimate the plasma position inside the vacuum chamber as described in the section 2.1. The main advantage of electric probes diagnostic is that no integration of the diagnostic output is required contrary to the magnetic probes.

MagneticsGAM

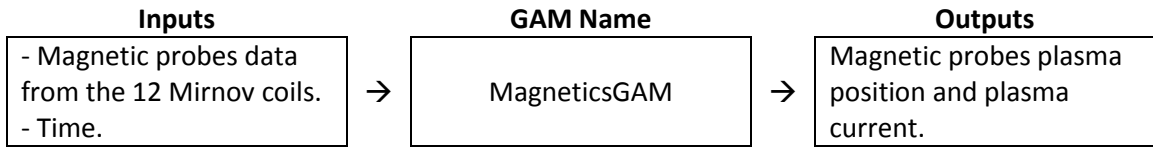


Table 14 – MagneticsGAM inputs and outputs.

The MagneticsGAM contains the code for reconstructing the plasma position from the 12 Mirnov probes. The underlying algorithm for this reconstruction is the centre of mass described in section 2.1. This GAM also produces an output with the estimated plasma current based on the value of all the coils.

Unfortunately, the analogue integrators for the ISTTOK magnetic coils were designed for single pulse or low duration AC discharge. The discharge constant of these integrators was set at 30 ms which is very low for the actual duration of an ISTTOK AC discharge (> 1 s). Consequently, long AC discharges on ISTTOK do not use this diagnostic. To solve this issue a new design of acquisition module is being tested for the same ATCA acquisition board. This new acquisition module features a chopper circuit to cancel most of the acquisition offset, being therefore suitable for numeric integration at 2 MSamples/s inside the FPGA. At the time of this thesis, the integration was performed offline with very encouraging results and a new firmware for the FPGA in the ATCA acquisition board is being developed to support the real-time operation with these modules. This will enable ISTTOK to operate with magnetic probes real-time diagnostic for very long AC discharges operation envisaged in the future update of the ISTTOK power supplies.

SineProbeGAM

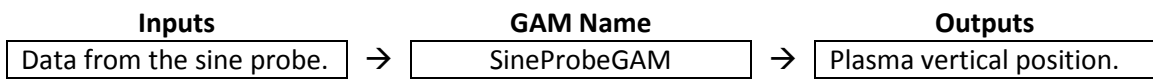


Table 15 – SineProbeGAM inputs and outputs.

As described on the ISTTOK diagnostics subchapter (2.1) the sine probe after integration produces a signal proportional to the plasma vertical position. This GAM first removes the offset before operation and then uses the sine probe signal to output the plasma vertical position.

CosineProbeGAM

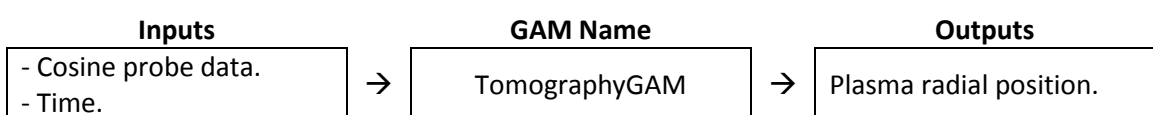


Table 16 – CosineProbeGAM inputs and outputs.

The CosineProbeGAM implements the same type of algorithms as the SineProbeGAM but for the plasma radial position.

MainRogowskiGAM

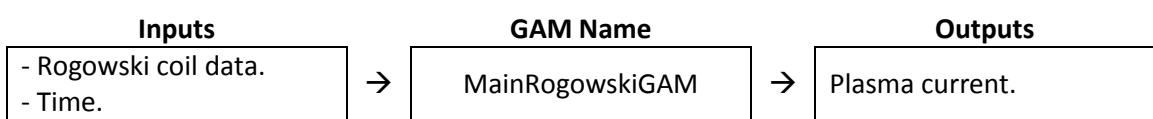


Table 17 – MainRogowskyGAM inputs and outputs.

The MainRogowskiGAM is a block of code that is used to retrieve the information provided by one Rogowski coil inside the copper shell but outside the vacuum vessel. The output of this Rogowski coil is then integrated by an analogue circuit to provide a signal proportional to the plasma current. This GAM also removes the offset induced by the toroidal field in this circuit just before the discharge and then outputs the plasma current to the DDB. Since the MagneticsGAM also provides the plasma current, a combination of these two overlapped measurements can be combined for the plasma current value or used in an interruption if these values diverge.

InterferometryGAM

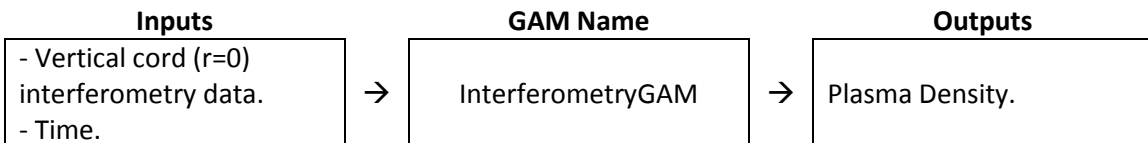


Table 18 – InterferometryGAM inputs and outputs.

As described in the ISTTOK diagnostics section (2.1) the ISTTOK interferometer measurement cord in the vertical direction and at the centre of the vacuum vessel ($r=0$). The algorithm used in this GAM to retrieve the plasma density is also described in the sub-chapter previously mentioned. This GAM corrects automatically the fringe jumps when the difference between samples in phase is lower than π . The output of this GAM can be used for plasma density feedback if the machine operator selects that option. The output value of this GAM is the line average density in m^{-3} divided by 10^{18} . This division aims at reconciling the output of the interferometry diagnostic with that of the H_α radiation. This enables the control system to offer an option to feedback the gas injection according to the density or the H_α radiation using the same reference waveform location.

HAlphaGAM

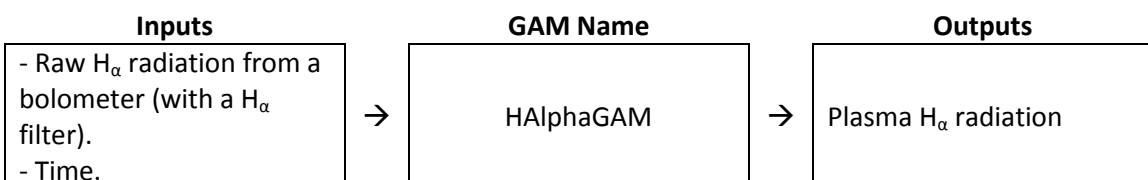


Table 19 – HAlphaGAM inputs and outputs.

The HAlphaGAM uses the data from one bolometer with a H_α band-pass filter. Since diagnostic is not absolutely calibrated, the output value was calibrated to be near the value obtained for the plasma density since the plasma radiation is related also (but not entirely) with the plasma density. For the long AC discharge operation the selected feedback mode on the gas injection is related with the H_α output because it is more stable than the plasma density output due to sporadic fringe jumps in the density measurement.

TechnicalSignalsGAM

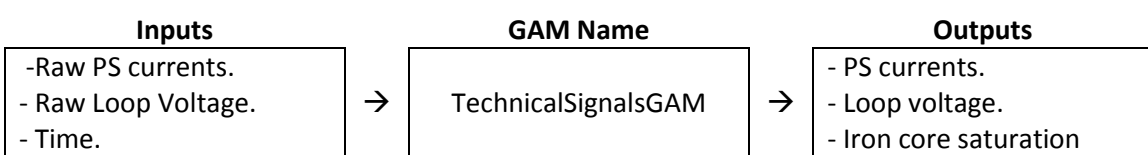


Table 20 – TechnicalSignalsGAM inputs and outputs.

The TechnicalSignalsGAM was designed to gather all information related to the auxiliary ISTTOK measurements such as the power supplies currents and loop voltage. This GAM processes the gathered data and outputs the PS currents and the loop voltage without offsets. This GAM also outputs a predictor value for the iron core saturation.

PlasmaStatusGAM

Inputs	GAM Name	Outputs
<ul style="list-style-type: none"> - Plasma parameters from all diagnostics. - Diagnostics weight. 	→ PlasmaStatusGAM	<ul style="list-style-type: none"> - Plasma current. - Radial position. - Vertical position. - Plasma density.

Table 21 – PlasmaStatusGAM inputs and outputs.

The PlasmaStatusGAM gathers all the information about the diagnostics output. With this information and with the diagnostics contribution to the final measurement, this GAM calculates the plasma parameters that will be used by the control system. The machine operator has the option to select different weights to the diagnostics for two different plasma conditions: the low plasma current scenario and the higher plasma current scenario. For example the tomography diagnostic is more accurate than the magnetic probe in low plasma conditions so the operator can place a higher weight in the tomography measurements in low current than the magnetic probes. When in higher current (value selected by the operator) the operator might select a higher weight to the magnetic probes compared to the tomography. The user can also give all the weight to a determined diagnostic and this will work as a diagnostic selector for a determined plasma parameter. The operator can select these weights for the plasma radial and vertical positions and these weights are not necessarily correlated.

MachineProtectionGAM

Inputs	GAM Name	Outputs
<ul style="list-style-type: none"> - Iron core limits. - All PS slow stops. - H_α radiation. - Density. - Loop voltage. - PS currents. - Plasma current 	→ MachineProtectionGAM	<ul style="list-style-type: none"> - Iron core saturation Boolean. - Soft stop Boolean. - Hard stop Boolean.

Table 22 – MachineProtectionGAM inputs and outputs.

The MachineProtectionGAM was designed to gather all information related with the machine safe operation. In machines with higher degree of complexity than ISTTOK there is an interlock system to protect the machine. In the case of ISTTOK this system is manual. To prepare for future operation with very long discharges it is necessary to gather information about the machine overall health, this GAM is used as a first protection layer for the ISTTOK real-time control. In future updates that will extend further the ISTTOK AC discharges duration temperature sensors for diverse components should be inserted in this GAM. With all machine health measurements combined this GAM produces the warning/alarms necessary for the real-time state machine GAM (TimeWindowsGAM) to interpret and act accordingly either by inverting the plasma current or to react to a soft or hard stop and terminate the discharge safely.

WaveformGAM

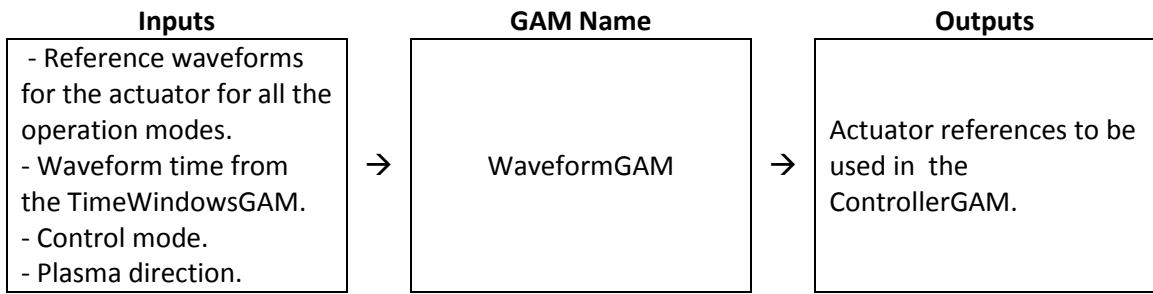


Table 23 – WaveformGAM inputs and outputs.

The WaveformGAM is used to store all the real-time references waveforms and to retrieve the output of the selected waveform at the time provided by the TimeWindowsGAM. For example, the “waveform_vertical” (vertical PS waveforms) instance of the WaveformGAM stores the current reference waveforms sets for (i) the vertical PS current for the auto-breakdown feature, (ii) current waveforms for normal operation, (iii) radial position reference and (iv) inversion vertical current references. For each operation mode two waveforms are stored, one for positive plasma current and another for negative plasma current. According with the plasma state machine (TimeWindowsGAM) one of these stored waveforms is selected. In fact a waveform container object was developed to be instantiated for each waveform. This object (“IWaveform.cpp” and “IWaveform.h”) has all the functions to retrieve all the information of the waveform such as the function that is called with the time as an argument and the function retrieves the interpolated waveform value by using a SAR (successive approximation register) algorithm and then interpolating the two nearest point according to equation 44, where “j” is the index of the point immediately before the query point, (Y, t) is the pair data and time vector of the waveform and “out” is the output of the equation and “ t_{in} ” is the time to be interpolated. The query of this function with “ t_{in} ” returns the “out” variable.

$$out = Y_j + (Y_{j+1} - Y_j) \frac{t_{in} - t_j}{t_{j+1} - t_j} \quad (44)$$

The “IWaveform” object implements several other functions such as add a point, delete a point, save a waveform, retrieve the first element of the waveform, retrieve the last element, remove repeated points, sort the waveform in order and define the waveform boundaries.

ControllerGAM

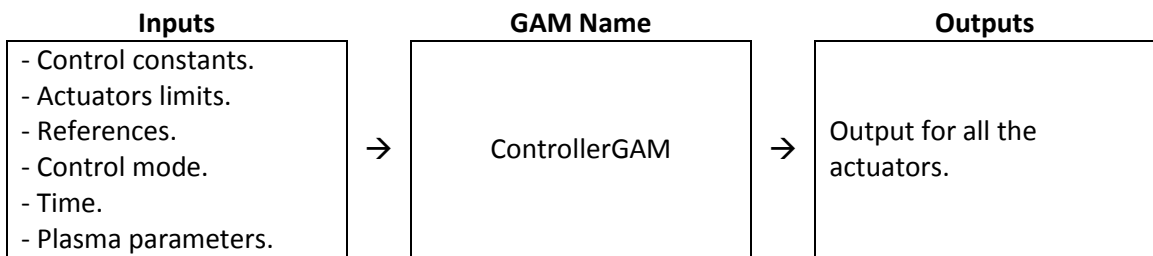


Table 24 – ControllerGAM inputs and outputs.

The ControllerGAM is the GAM responsible for the ISTTOK real-time feedback. This GAM receives every parameter related with the real-time control (as described in Table 24) and retrieves the outputs for every actuator according to the selected control mode that it receives from the state machine (TimewindowsGAM) and in some control modes it implements a

multiple-input multiple-output (MIMO) strategy for the ISTTOK control. When changing the control mode this GAM uses the stored actuators parameters and process variables to ensure a “smooth” transition between control modes, avoiding abrupt transitions. Just like the TomographyGAM, the ControllerGAM also obtains the control matrix (used in the MIMO control) from an external file that is loaded when the GAM is initiated and does not interfere with the real-time performance.

PowerSupplyCommunicatorGAM

Inputs	GAM Name	Outputs
- Current to send to the power supply. - PS serial port address. - Communication protocol settings.	→ PowerSupplyCommunicatorGAM	- Send current reference for the PS. - Current measured in the PS. - PS slow stop.

Table 25 – PowerSupplyCommunicatorGAM inputs and outputs.

The PowerSupplyCommunicatorGAM is used to interface the communication with the power supplies control module. This communication is provided by a quad-serial port inserted in the PCI port of the ATCA controller board which has a proprietary linux driver. The code for this GAM was based on the code made for the COMPASS tokamak which currently features the same serial board and the same controller for the fast amplifiers.

OutputGAM

Inputs	GAM Name	Outputs
Value to set in the DACs.	→ OutputGAM	→ Set values to the DACs.

Table 26 – TomographyGAM inputs and outputs.

This IOGAM interfaces with the acquisition board that has the RTM module which contains the DACs. The GAM receives the value to set in the DACs from the DDB variables and sets the respective DACs output value according with these variables. Like the TimeInputGAM it also interfaces through a driver with the ATCA hardware and is also distributed with the standard MARTe framework package.

DataCollectionGAM

Inputs	GAM Name	Outputs
The inputs for this GAM are a number of selected DDB variables.	→ DataCollectionGAM	→ This GAM records the data of selected DDB variables with a time-stamp.

Table 27 - DataCollectionGAM inputs and outputs.

This GAM is used to store the selected DDB variables into the ATCA controller board RAM memory. The selected variables that are in the DDB at the end of each control cycle are saved and time-stamped for later analysis/debugging. The stored data is fetched by FireSignal and SDAS after the ISTTOK pulse is ended and stored on the ISTTOK main database. The user can also access this data after the discharge via the MARTe framework HTTP server services. This GAM is distributed with the MARTe framework package.

FireSignalDischargeStatusGAM

Inputs	GAM Name	Outputs
- Discharge Status. - System Time.	→ FireSignalDischargeStatusGAM	→ Discharge ended Boolean variable.

Table 28 - FireSignalDischargeStatusGAM inputs and outputs.

A pooling driver for the ISTTOK main database is constantly checking (every 1 second) if the ISTTOK operation has already finished via the MARTe HTTP server. This GAM simply implements a HTTP webpage with a variable that provides the information for the pooling driver. When the discharge is finished and the database gets that information, the data is fetched and stored by the DataCollectionGAM in the ISTTOK main database.

Summary

All the GAMs detailed in this sub-chapter are a part of the ISTTOK real-time control. This layout was designed to provide a flexible control system, where each GAM is associated either with a specific diagnostic or with a specific function. If a diagnostic is updated, it is possible just to rewrite the specific diagnostic GAM without rewriting all the real-time control system and this code compartment is very useful on a flexible machine such as ISTTOK.

Chapter 5 - System configuration

The MARTE framework provides a HTML server that can be used to interface with the real-time configuration. By default this server contains all objects currently running on MARTE and also includes a configuration file uploader that allows new configuration files to be read and used. This feature opens the possibility to reconfigure the parameters that all GAMs use for their own configuration. There is also the possibility to interact with GAMs using their own customised HTML page although this is not recommended as it can affect the real-time performance of the system. The GAMs only have a HTML page to display their internal configuration parameters to cross-check their current state.

In order to produce a user friendly interface to configure the ISTTOK discharges, two objects (in C++) were developed. These objects are named “discharge configurator” and “advanced configurator”. As the name suggests, these objects are used to configure the experiments parameters. In the case of the “discharge configurator” (see Figure 91) all the parameters related with the discharge can be edited in a user-friendly HTML interface. The parameters that are not often changed between discharges are editable in the “advanced configurator” HTML interface. This interface also includes some parameters to configure the control system hardware. The user programs the discharge using a standard web browser such as Google chrometm, Microsoft internet explorertm or Mozilla firefoxtm.

Summarizing, the main characteristics of this interface are:

- HTML and Javascript based interface provided by the BaseLib2.
- Visual configuration file save and load.
- Auto-save configuration file save at the end of each discharge.
- Password-protected.
- Automatic graphical waveform representation.
- Time-windows with different control strategies.
- Ability to program breakdown and inversion recipes.
- Synchronization against external sources of events (e.g. Puffing and current inversion).
- Programming of several diagnostics contribution for the real-time control parameters.
- Discharge configurator and an advanced configuration for expert settings edition.
- User-friendly interface.

5.1. Remote configuration layout

The machine configuration for the real-time control is provided by two objects named “Discharge Configuration” and “Advanced Configuration” that interact with MARTE and use the BaseLib2 libraries as depicted in Figure 80. These objects are not GAMs and therefore they are isolated from the real-time thread. Since both have a HTTP server the natural way to interact with these objects is to use an internet browser. The web pages are available through the ISTTOK internal network.

These two objects are written in C++ code and implement a web page with HyperText Markup Language (HTML) and Javascript™ code. These configuration objects also include an automatic graphical waveform representation that scales the waveform graph automatically after inserting or deleting a waveform point generating the correspondent scalable vector graphics (SVG) extensible markup language (XML) type code which automatically updates the waveform representation.

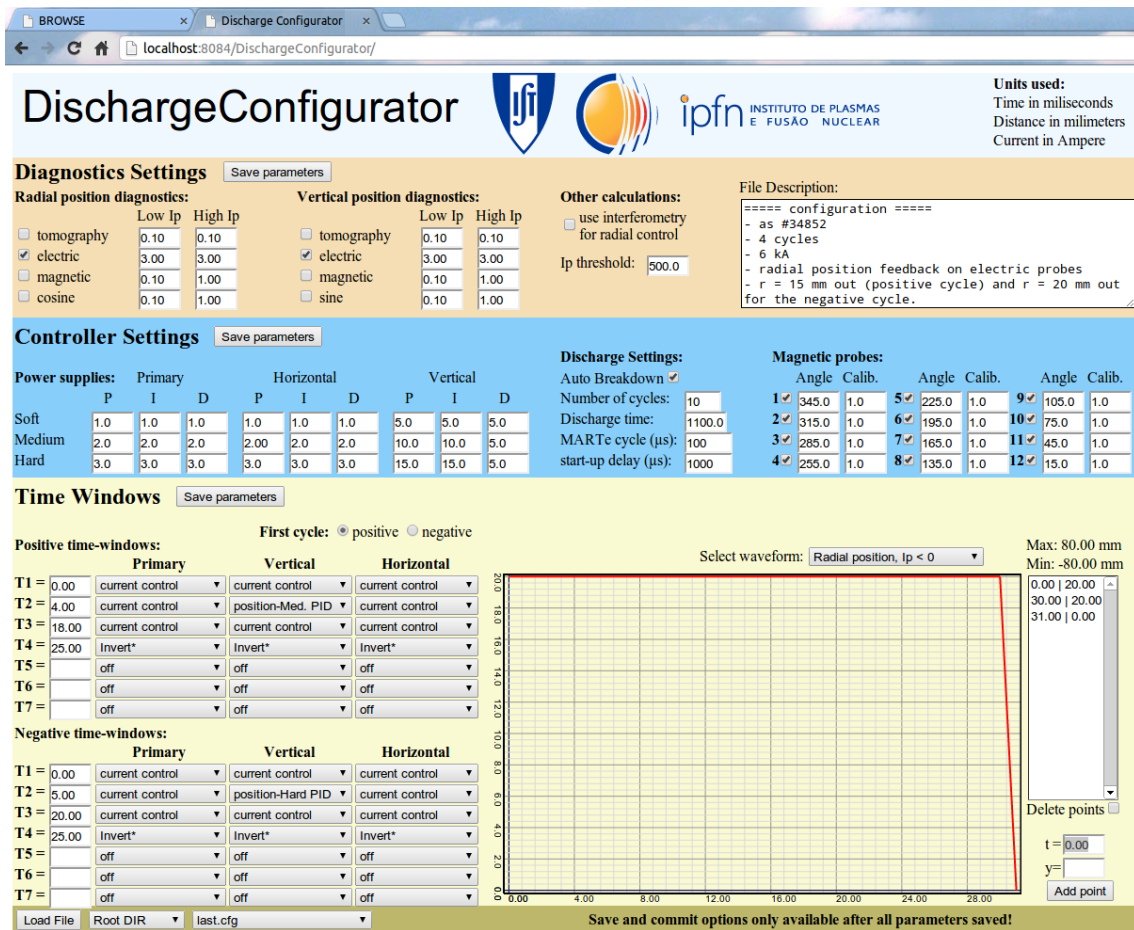


Figure 91 – “discharge configuration” webpage. This HTML page is used to configure the basic discharge parameters such as the type of control per time-window, the actuators reference waveform, the discharge timing and the real-time diagnostics used to measure the plasma position.

The “discharge configurator” (Figure 91) is divided in 3 sections; (i) Diagnostics settings, (ii) controller settings and (iii) time-windows configuration.

In the diagnostic settings, the operator can specify each diagnostic contribution for the calculated quantity since plasma parameters can be obtained from several diagnostics.

In the control settings, the operator configures the discharge duration, number AC cycles and selects the auto-breakdown feature. The user also configures the control constants for scenario control (see section 3.4).

In the “time windows” section, the user can select the type of control for each PS during a specific time interval; the user can add up to seven different time windows per AC semi-cycle time (one for positive plasma current and another for negative plasma current). This subject is further discussed in section 3.3. After saving all these sections in the “discharge configuration” it is possible to commit the changes to the real-time system by pressing the “save on default filename and commit” button (this button is not present until all parameters are saved and validated) depicted in Figure 92. The webpage will display the validated configuration (in non-edit mode) than can be submitted to the real-time control system.

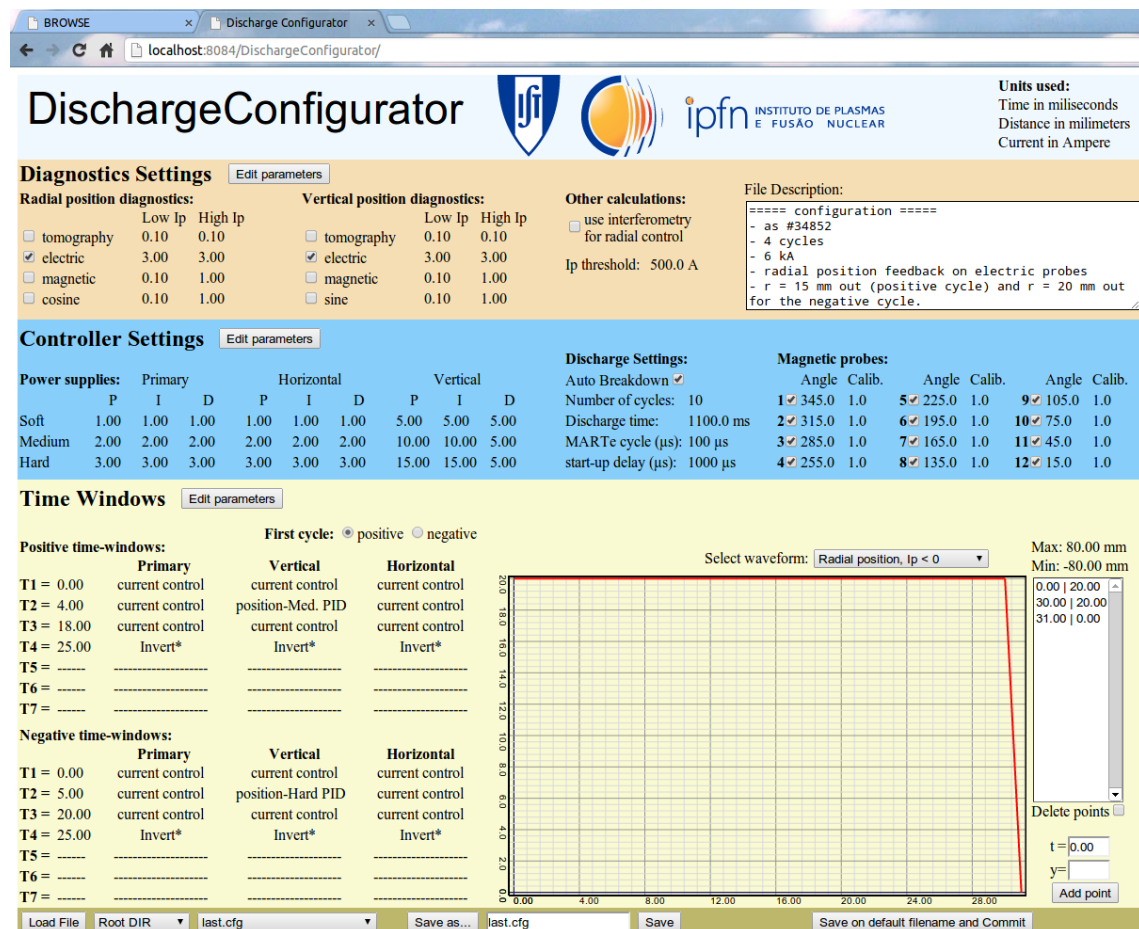


Figure 92 - Discharge configurator webpage after submitting all the changes. Once all changes are validated, the configuration is displayed and can be committed to the MARTe framework. After committing, all GAMs are “destroyed” and restarted with the new configuration file containing the committed changes.

The “Advanced configuration” (Figure 93) is similar to the “discharge configurator” but contains the less likely to be changed parameters of a discharge. It contains (i) the power supplies limits, (ii) the plasma position limits, (iii) the serial port address for communication

with the PS, (iv) the real-time thread priority, (v) the CPU core were the real-time thread is running and (vi) the predictor constants for the iron core saturation.

This configuration editor contains also the waveforms for breakdown, current inversion and gas feedback.

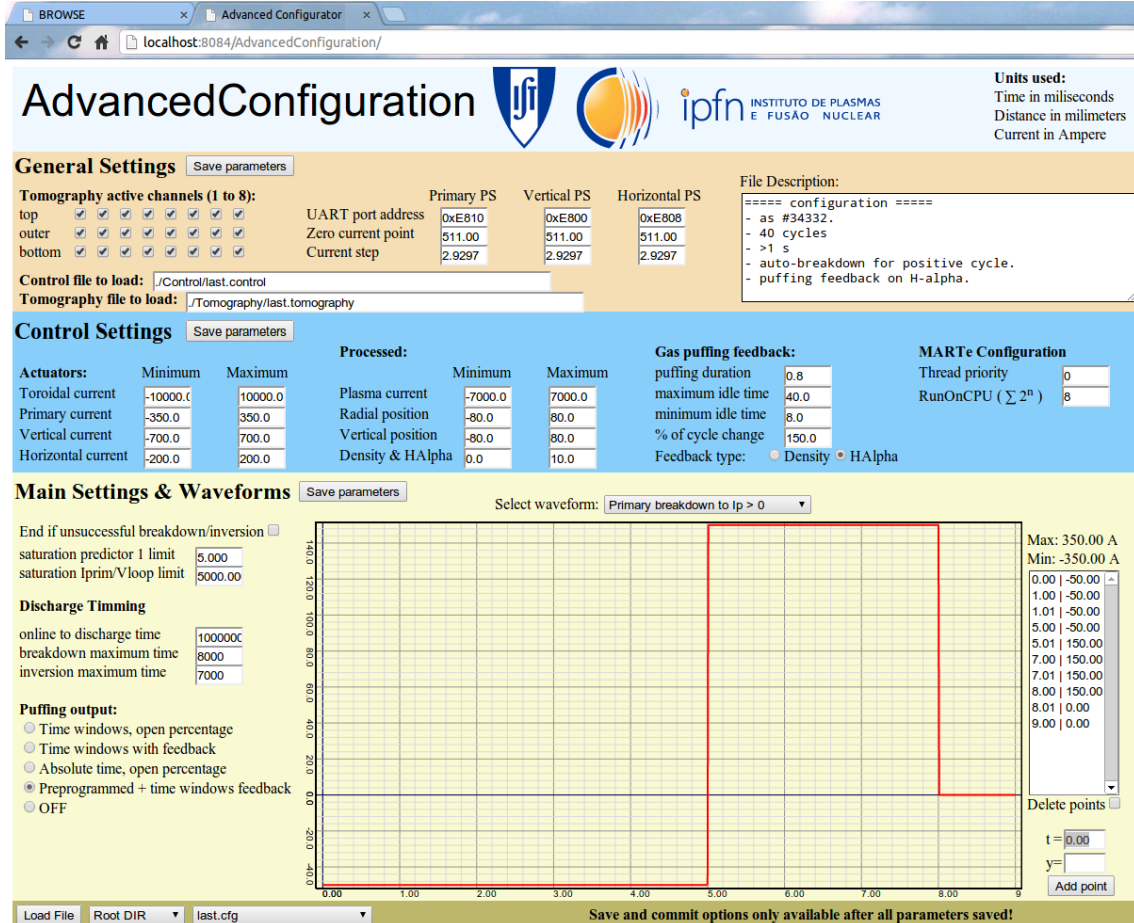


Figure 93 – “Advanced configuration” webpage. This HTML page is used to configure the advanced discharge parameters that normally don’t change between discharges. This configuration also includes the breakdown and inversions pre-programming. The gas puffing can also be edited in this HTML page.

As the “discharge configurator” object, when saving each section of the webpage (save parameters button), a validation routine is triggered to check if all inserted parameters are valid in order to ensure a proper machine configuration. The “advanced configuration” webpage, after saving all the sections, displays the validated data in non-edit mode (Figure 94). This enables the user to cross check the information that can be submitted to the control system or simply save the configuration with a user defined file name. When all sections are in display mode the “save on default filename and commit” button appears to the user on the bottom right of the configuration webpage. After the user presses this button, it overwrites the parameters on the default MARTe configuration database file (last.cfg) used for system initialization and triggers the new configuration file reading, thus reconfiguring the control system.

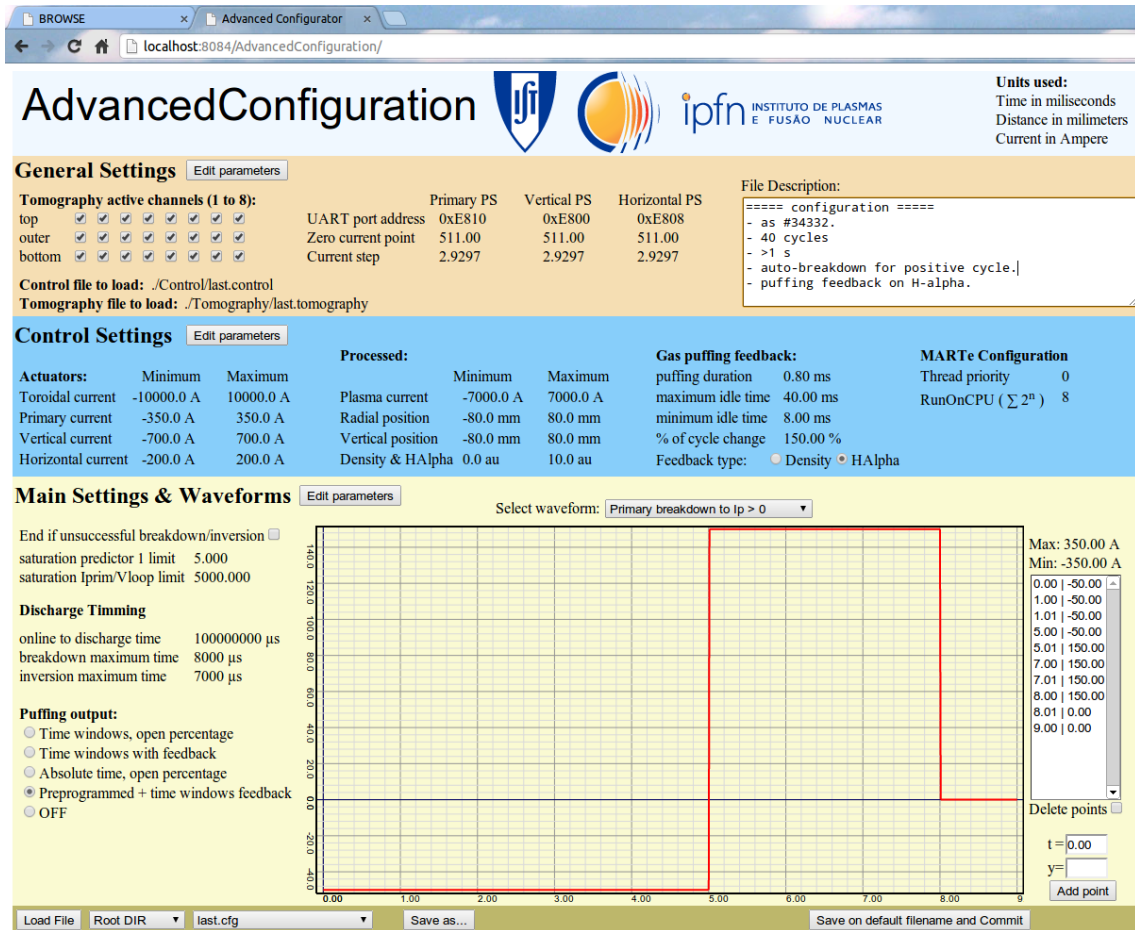


Figure 94 - Advanced configuration webpage in display mode. Once all changes are validated, the machine advanced configuration can be committed to the MARTE framework. After committing, all GAMs are “destroyed” and restarted with the new configuration file containing the committed changes.

As a matter of fact, these two objects are a frontend for editing the MARTE configuration file (long text file with human readable information similar to XML). This file is where MARTE and all the GAMs get the configuration from. When the user clicks on the save button, the configuration file is overwritten with all the parameters stored on these objects. After all changes are made to the real-time configuration, the user can save and commit it. This action will trigger MARTE to destroy all the objects (including the real-time thread and GAMs) and reload the new configuration file. Using this strategy, MARTE restarts hereafter with the new configuration parameters. After each pulse this configuration file is stored with the corresponding pulse number so that it can be retrieved when the user wants to repeat a pulse or needs only small changes to a known pulse. These two objects also have a specific load button for this operation.

5.2. User-level configuration

The human machine interface provides the tools necessary to configure several discharge parameters. The vast majority of the MARTe initialization parameters are editable in the “advanced configuration” and “discharge configurator” objects. As stated before, these objects use the MARTe framework HTTP server and implement a HTML webpage as a frontend to edit the configuration database file that contains the initialization parameters for all the GAMs that are executed in the real-time system. Following these lines, all the “discharge configurator” and “advanced configuration” parameters will be described in detail in this section. The “discharge configurator” parameters are depicted in Figure 95 and the “advanced configuration” is detailed in Figure 98.

Discharge configurator detailed parameters

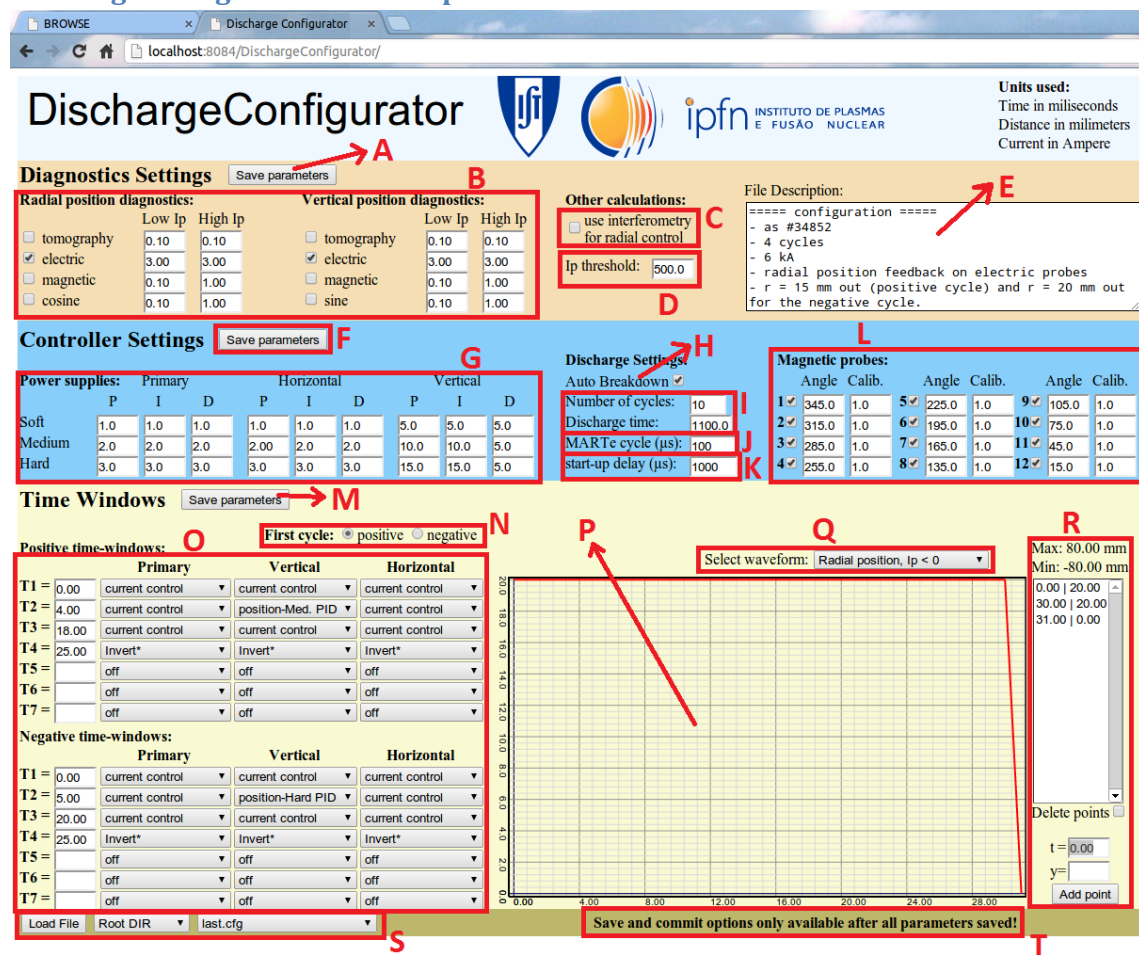


Figure 95 – Discharge configurator HTML webpage with labels.

Label A - Save/edit the diagnostics settings

This button toggles the edit and display mode of the “diagnostics settings” area. When in edit mode the parameters on the diagnostics settings can be edited and pressing this button after editing will trigger the validation procedure for the parameters within this area.

Label B – Diagnostic weights for measurement elaboration

The parameters represented by this label are used to determine each diagnostic contribution for the radial and vertical plasma positions. The user can select the contribution of the diagnostics for low and high plasma current (defined by label D) for each plasma parameter. For example, the tomography diagnostic is more trustworthy in low plasma current than the magnetic probes and the weights should reflect this.

Label C – Use interferometer for radial position control

Since the interferometer is positioned in a vertical cord that passes through the radial centre of the vacuum vessel, abrupt changes in the density (especially when the radiation is not greatly affected) are mainly caused by a plasma movement in the radial direction. This can be used as an additional diagnostic for validating the radial position. The parameter on this label enables or disables this contribution.

Label D – Plasma current threshold for diagnostic contribution

Low and high plasma current definition: this parameter is useful for switching the diagnostics weight contribution (defined in label B) constants when the plasma current passes through this threshold parameter.

Label E – Comments

This text box is used to insert the comments for the overall configuration. When loading other configuration files it is useful to have quick information about their content and this text box provides the machine operator a simple annotation tool for each configuration file.

Label F - Save/edit the controller settings

As label A, this button is used to toggle between edit and display mode of the controller settings. Once this button is pressed in edit mode it will validate the inserted parameters and display their validated content (within the machine limits).

Label G – Power supplies PID constants

These parameters set the response type of the power supplies PID controllers. There are three PID constants for each actuator. The PID mode is defined in the label O (each time-window can have a different control mode for each actuator).

Label H – Auto-breakdown mode

This tick box is used to enable or disable the auto-breakdown feature. As described in the sub-chapter 4.4, the ISTTOK real-time control implements a goal oriented strategy. If the auto-breakdown feature is enabled the controller will run the breakdown waveforms until there is sufficient plasma current and after this goal is achieved the control executes what the user defines in the time-windows (label O). If this option is not selected the control starts directly with the execution of the control type that is defined in the time-windows.

Label I – Discharge duration parameters

These parameters define the discharge duration. The “discharge duration” parameter sets a hard limit for the discharge duration time whereas the “number of cycles” defines the number of AC discharge semi-cycles. Between these two parameters the first to be surpassed defines the end of the discharge, either by time or by AC discharge semi-cycles completion.

Label J – MARTe control cycle

This parameter basically defines the MARTe control cycle time. Since the ATCA acquisition board firmware was set to send a new package of data at each 50 µs and these sent packages are used to trigger MARTe control cycle, the MARTe control cycle is limited to a multiple of the 50 µs defined by the acquisition sequence. In normal operation the ISTTOK control cycle is set to 100 µs.

Label K – Start-up delay

This parameter defines the idle time since the MARTe system is first triggered for a discharge and is usually set to 1 ms. The start-up delay is used by the diagnostic GAMs to acquire data and then subtract their offset just before the discharge.

Label L – Magnetic probes constants

These values are used for providing the magnetic probes position and their calibration to the magnetic probes diagnostic GAM. More information concerning this issue can be found on section 2.1 and section 4.5.

Label M - Save/edit the time-windows settings

As the previous save/edit buttons, this button is used to toggle between edit and display mode of the time-windows settings. If this button is pressed in edit mode it will toggle to display mode just after parameter validation and the displayed values become validated. If this button is pressed in display mode it will open the variables for edition.

Label N – First cycle direction

This parameter defines which set of time windows will be the first to be run by the control system. If the selection is “first cycle: positive” the positive time-windows will be executed first and by opposition if the selection is “first cycle: negative” the negative time-windows will be the first to run. If the auto-breakdown feature (label H) is asserted, the positive breakdown will run if the first cycle is positive and the negative breakdown waveform will be run if the first cycle is negative.

Label O – Time-windows edit panel

This panel defines the control mode at each given time. For each time slice, the controller GAM acts according with this panel selection (Figure 96). As it can be observed in the mentioned figure there are many options available to the user. The user can select several control modes since the power supplies can either be controlled on current or in scenario mode. The scenario mode is when the power supplies are used to control plasma parameters, the primary PS controls the plasma current, the vertical field PS controls the radial position and the horizontal field PS controls the vertical position. A list of these modes can be observed in the figure and is described below:

- **Off** – The respective power supply is turned off during the respective time-window.
- **Current control** – The respective power supply receives the respective current waveform reference for the selected time-window. This means that the power supply is controlled in current during the time-window.
- **Position/plasma current soft PID** – The respective power supply is on scenario control using the corresponding scenario waveform as reference and using the “soft” PID

constants set in label G for feedback control in that corresponding scenario. Depending on the power supply, it will adjust the plasma current, the radial position or vertical position according with the respective scenario waveform.

- **Position/plasma current Med. PID** – the same as the previous mode but the user defined intermediate PID constants.
- **Position/plasma current hard PID** – The same with “hard” PID constants.
- **Position/plasma current auto PID** – Using the soft, medium and hard user defined PID constants the system switches between these constants according with the difference from the process variable to the reference waveform.
- **Integrated control** – Although the power supplies are almost decoupled in their action on the plasma parameters, this mode provides an action in scenario control taking into account their small interdependences. When one PS is set into integrated control, the validation tool places all the others also on this mode, because it would make no sense to have just one PS in integrated control.
- **Invert** – This special instruction tells the control system that the respective time-windows set is finished and the plasma current is to be inverted. If the number of AC semi-cycles is finished then the control system will end the discharge. When this command is not inserted, the same action will be taken only when the iron core is saturated. Obviously, when this mode is set to a specific power supply the validation tool will extend to all the others.

Positive time-windows:			
	Primary	Vertical	Horizontal
T1 =	0.00	current control	current control
T2 =	4.00	current control	current control
T3 =	18.00	current control	current control
T4 =	25.00	Invert*	current control
T5 =		off	off
T6 =		off	current control
T7 =		off	position-Soft PID

Negative time-windows:			
	Primary	Vertical	Horizontal
T1 =	0.00	current control	current control
T2 =	5.00	current control	position-Hard PID
T3 =	20.00	current control	current control
T4 =	25.00	Invert*	Invert*
T5 =		off	off
T6 =		off	off
T7 =		off	off

Figure 96 – Detail of the discharge configurator time-windows editor. For each actuator and for each time window it is possible to edit the control mode as can be observed in the figure.

The corresponding waveforms are selected in label Q drop-down box and can be edited using label R waveform points editor and are automatically displayed in label P waveform display panel.

For example if the T1 time is set to 4 ms and T2 time is set to 18 ms for the positive time-windows and in the vertical power supply at T1 is selected “position Med. PID”, it means that from the 4 ms up to the 18 ms of the positive plasma current cycles (in AC discharges eventually more than 1 semi-cycle), the vertical field power supply is controlling the radial position according to the radial waveform (defined using labels P, Q and R) using the medium PID constants defined in the label G.

Label P – Waveform display panel

This panel is used to display the selected waveform. The object is produced by a SVG code specially designed to be used in standard HTML. The displayed waveform is automatically updated when a point is inserted or deleted by interacting with label R. This waveform display has the ability to zoom automatically the waveform and no user intervention is needed. The axis scale is also automatically updated with all ticks displayed in an intelligible format.

Label Q – Waveform selection

This drop-down menu is used for selecting the waveform to be edited by label R and displayed by label P. Since the power supplies can be programmed to work on scenario or current control, the user can edit several waveforms as it can be observed in Figure 97. A short description of each waveform is presented below:

- **Current control, primary current for $I_p > 0$** – Primary field power supply current output reference waveform when the plasma current is positive (available to the positive time-windows).
- **Current control, vertical current for $I_p > 0$** – Vertical field PS current output reference waveform to be used in the positive time-windows.
- **Current control, horizontal current for $I_p > 0$** – Horizontal field PS current output reference waveform to be used in the positive time-windows.
- **Scenario control, plasma current for $I_p > 0$** – Plasma current reference waveform to be used in the positive current time-windows.
- **Scenario control, radial position for $I_p > 0$** – Radial plasma position reference waveform to be used in the positive current time-windows.
- **Scenario control, vertical position for $I_p > 0$** – Vertical plasma position reference waveform to be used in the positive current time-windows.
- **Current control, primary current for $I_p < 0$** – Primary field PS current output reference waveform to be used in the negative current time-windows.
- **Current control, vertical current for $I_p < 0$** – Vertical field PS current output reference waveform to be used in the negative current time-windows.
- **Current control, horizontal current for $I_p < 0$** – Horizontal field PS current output reference waveform to be used in the negative current time-windows.
- **Scenario control, plasma current for $I_p < 0$** – Plasma current reference waveform to be used when plasma current control is required in the negative current time-windows.
- **Scenario control, radial position for $I_p < 0$** – Radial position reference waveform for negative current time-windows.
- **Scenario control, vertical position for $I_p < 0$** – vertical position reference waveform for negative current time-windows.

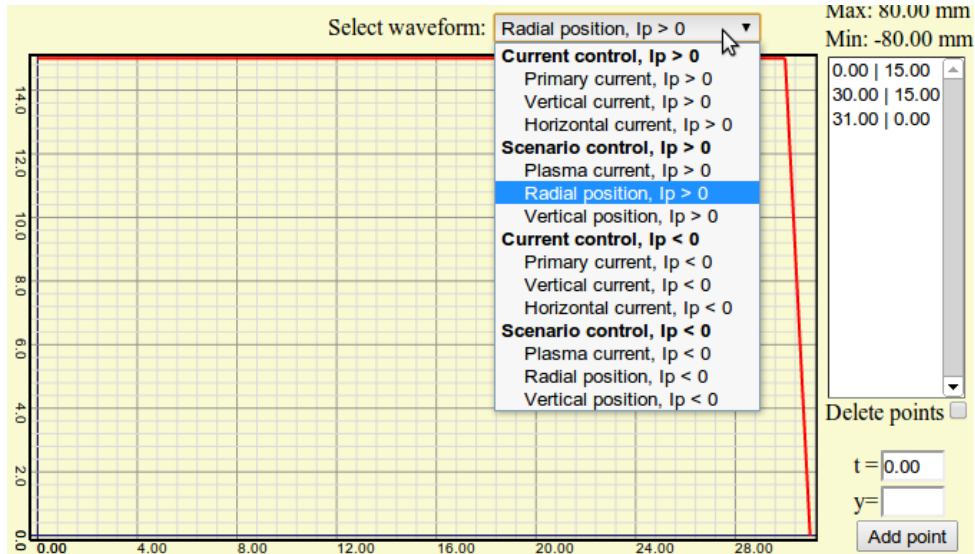


Figure 97 – detail of the waveform selection for the discharge configurator. The selected option will be displayed in the waveform panel for editing that waveform.

Label R – waveform edit

This interface is used for adding or removing points from the selected waveform in label Q. When the user asserts the “delete points” check-box, each time the user clicks over a point the interface removes that point until there only remaining two points (the minimum for a waveform). The user can add points to the waveform by filling the “t=” and “y=” forms and the click the “add point” button. The waveform results from the linear interpolation of all points and if not specified, the values before the first point and after the last one are set to zero.

Label S – Load other configuration file

The drop-down menus on this label are used to select the configuration file loading. After each discharge the system automatically saves the configuration file and labels it with the pulse number so that they can be easily retrieved. The user has the ability to load all discharge parameters for the configurations files saved after each discharge. The user is also able to load the user saved configuration files (this option is available in label T). After selecting the desired configuration database file, the parameters are loaded to the webpage after the user clicks the “load” button.

Label T – Save and commit options

These options are only available after the user placed every edit/save section (label A, F and M) on display mode, i.e., the inserted data is validated. When every section is in display mode, two options appear in the bottom right side of the webpage, the option to save the configuration database file with a user defined name or the option “save on default file and commit”. The latter option overwrites the ISTTOK MARTe default configuration file (last.cfg) and forces the system to reload with the new initialization file effectively committing the changes on the webpage to the control system.

Advanced configuration detailed parameters

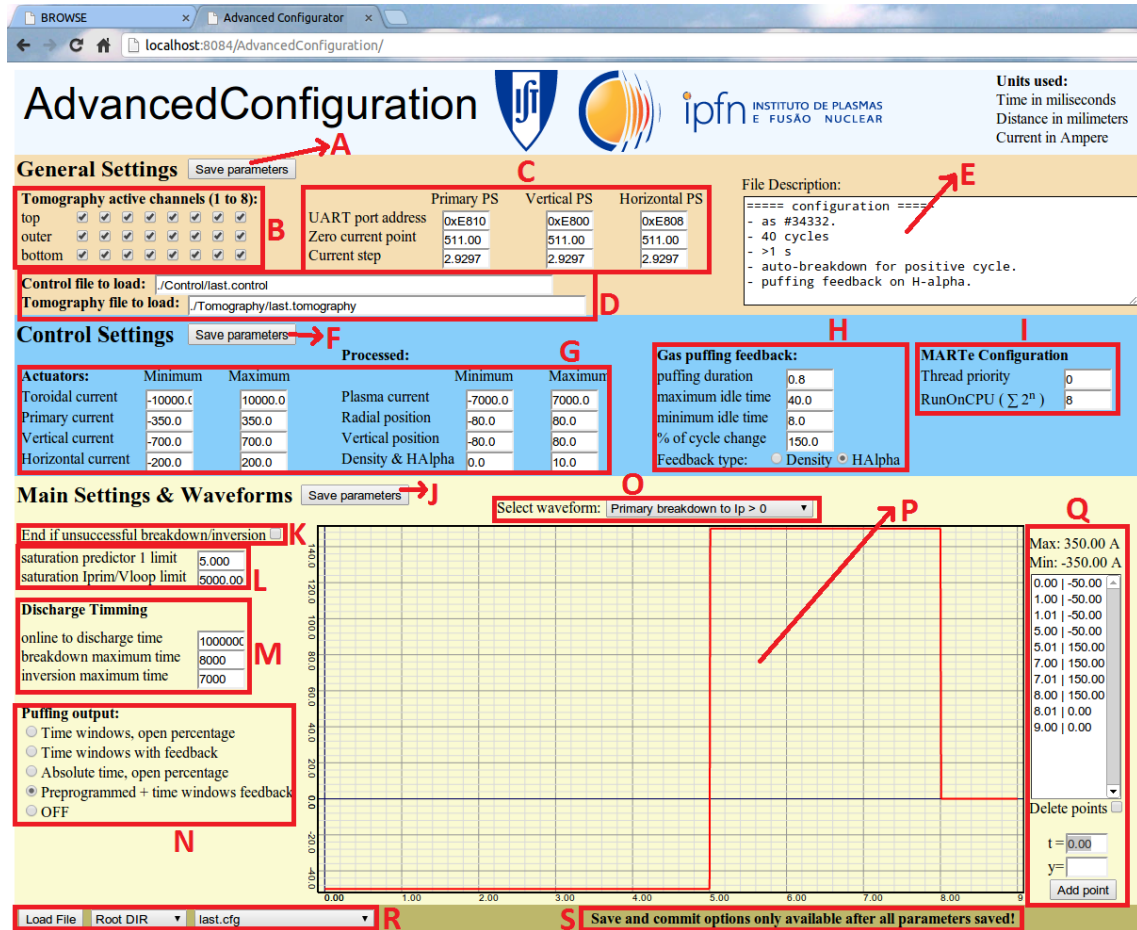


Figure 98 - Advanced configuration webpage with labels.

Label A - save/edit the general settings

As the previous save/edit buttons described in the “discharge configurator” section, this button is used to toggle between edit and display mode of the general settings of the “advanced configuration”. If this button is pressed in edit mode it will toggle to display mode just after parameter validation and the displayed values will be already validated. If this button is pressed in display mode it will open the variables for edition.

Label B – Tomography active channels selection

This series of check boxes allows the user to select the used tomography detectors. If one of the channels is not functioning properly, the user has the ability to disable that channel at the cost of the tomography reconstruction accuracy.

Label C- Power supplies constants

These parameters are used to calibrate each power supply and to define the communication port in the quad-serial port that is connected through PCI bus to the main controller board. These parameters are not expected to be changed unless something is changed in the hardware.

Label D- Tomography and Controller matrixes file locations

These two strings define the file location of the auxiliary files for the ControllerGAM and for the TomographyGAM. If the user simply wants to change the control matrix without touching

the ControllerGAM code it just need to provide another file containing the desired control matrixes and the same is valid for the tomography reconstruction.

Label E – Comments

This text box is used to insert the comments for the overall advanced configuration. When loading other configuration files it is useful to have quick information about their content and this text box provides the machine operator a simple annotation tool for each configuration file.

Label F - Save/edit the control settings

As the previous save/edit buttons, this button will also toggle between edit and display mode and in this case for the control settings. If this button is pressed in edit mode it will toggle to display mode just after parameter validation and the displayed values will be already validated. If this button is pressed in display mode it will open the variables for edition.

Label G – Actuators and parameters limits

These parameters define the limits for the actuators and their scenario control parameters. These limits are then enforced when editing the actuators waveforms in the “discharge configurator”.

Label H – Gas injection control settings

These parameters define the actuation of the control system for the gas injection feedback. As mentioned in the sub-chapter 3.4, the gas puffing feedback consists in small gas puffs (about 1ms) with a varying period between gas puffs to provide more or less gas according to the needs. The “puffing duration” parameter defines each gas puff duration, the “minimum idle time” and “maximum idle time” parameters define the minimum and the maximum time between gas puffs, the “% of cycle change” parameter acts like the gain of a PID system and the “feedback type” parameter defines which process variable is to be used in the system feedback (H_{α} radiation or density). The feedback algorithm compares the process variable with the feedback reference waveform and acts on the period between puffs variable. The reference waveform can be defined using the O, P and Q labels.

Label I – MARTe configuration parameters

These parameters are used for MARTe real-time control configuration. The “thread priority” parameter defines the MARTe real-time thread priority and the “RunOnCpu” parameter defines in which CPU core is the real-time thread going to be deployed. It is recommended not to change these values unless the user has a vast knowledge of the MARTe framework and the underlying operating system.

Label J - Save/edit the main settings

As the previous save/edit buttons, this button will also toggle between edit and display mode and in this case for the main settings of the “advanced configuration”. If this button is pressed in edit mode it will toggle to display mode just after parameter validation and the displayed values will be already validated. If this button is pressed in display mode it will open the variables for edition.

Label K – End if unsuccessful breakdown/inversion setting

In the implemented goal strategy control, the goal may timeout, for instance the breakdown might not be successful within the time configured in label M. When this happens the system can either end the discharge or continue and skip the goal oriented waveforms into the next control sequence as the objective had been reached. For example, if the user programs a discharge that it is not critical to have all AC discharge cycles this option should be disabled, because even if a cycle fails the remaining might still be able to work.

Label L – Iron core saturation predictor settings

These parameters are inputs for the iron core saturation predictor. Changing these numbers might remove a safety barrier. The plant is still further protected but is not advisable to change these parameters without in-depth knowledge of the iron core saturation predictor algorithms.

Label M – Discharge timing constants

This section contains the timeout definition for the goal oriented waveforms. When in breakdown mode the system will execute the breakdown set of waveforms until it reaches the goal (sufficient plasma current) or until the time defined on the “breakdown maximum time” parameter. If the time is elapsed before reaching the goal, an error will be asserted and depending on the label K definition the system will either end the discharge or skip the breakdown phase and execute the next time-windows set. The same principle is applied to the plasma current inversion process and correspondently with the value defined on the “inversion maximum time parameter”. The “online to discharge time” parameter is used for acting on the system before the pulse like the toroidal field (which was not yet fully integrated).

Label N – Gas injection synchronization strategy

This set of radio buttons is used to select the gas injection synchronization strategy. The gas injection waveforms among others are selected in label O, displayed on label P and edited on label Q. The gas injection can be synchronized with the control system by the following types:

- **Time-windows, open percentage** – This option is used to synchronize the gas puffing with the time-windows control. In this mode the user is free to program the voltage waveform applied to the piezoelectric valve. In fact the user programs the “puffing output %, $Ip > 0$ ” waveform that is synchronized with the positive time-windows and the “Puffing output %, $Ip < 0$ ” waveform is synchronized every time with the beginning the negative plasma current cycles (negative time-windows).
- **Time-windows with feedback** – In this mode the gas injection is also synchronized with the time-windows as the previous mode, but instead of specifying the voltage applied to the piezoelectric valve, the user specifies the feedback waveform and the control system will try to match this reference (by controlling the gas injection) based on the parameters specified in label H.
- **Absolute time, open percentage** – in this mode the user specifies the voltage applied to the piezoelectric valve waveform in absolute time, i.e., without any synchronization with the discharge other than the discharge time.

- **Pre-programmed + time-windows feedback** – This hybrid mode uses the absolute time waveform to specify the applied voltage waveform until the breakdown phase is finished and afterwards, when in time-windows control mode, it behaves like the “time-windows with feedback” mode, i.e., until the end of breakdown it works as a pre-programmed waveform (like “absolute time, open percentage” mode) and afterwards it has a feedback control synchronized with the time-windows (as “time-windows with feedback” mode). This mode is useful for having a discharge with feedback control but at the same time control the gas pre-fill during the breakdown phase.
- **Off** – Simply turn off the gas puffing.

Label 0 – Select waveform for display/edit

Several waveforms can be selected in a drop-down box as depicted in Figure 99.

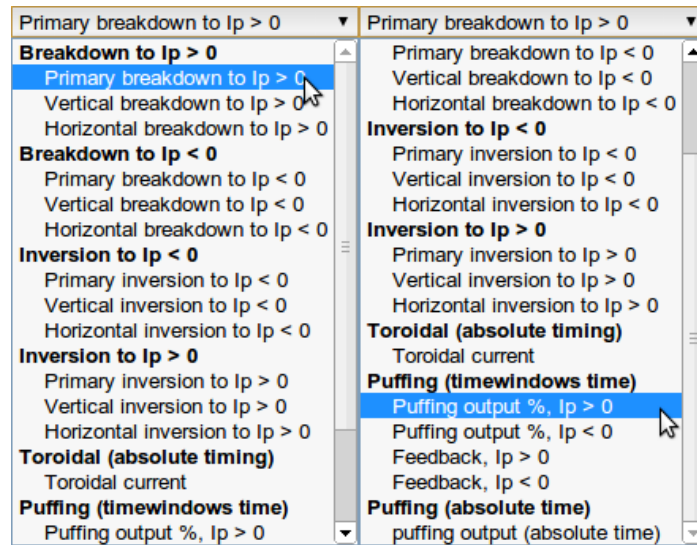


Figure 99 – Advanced configuration waveform selection drop-down menu. The right drop-down menu is the same menu after the scroll down in order to display all the waveform names in this figure.

A list of these waveforms and a short explanation is provided below:

- **Primary breakdown to $Ip > 0$** – Primary field PS current waveform for creating plasma current in the positive direction (plasma breakdown). This waveform and the remaining PS waveforms for breakdown to $Ip > 0$ are goal oriented, meaning that when there is sufficient plasma current the controller switches to other control mode to the positive time-windows.
- **Vertical breakdown to $Ip > 0$** – Vertical field PS current waveform for creating plasma current in the positive direction (plasma breakdown). This waveform is synchronized with the remaining breakdown waveforms for $Ip > 0$.
- **Horizontal breakdown to $Ip > 0$** – Horizontal field PS current waveform for creating plasma current in the positive direction (plasma breakdown). As the previous waveforms, this waveform is also goal oriented and synchronized with the previous waveforms.
- **Primary breakdown to $Ip < 0$** – Primary field PS current waveform for creating plasma current in the negative direction (plasma breakdown). This waveform and the

remaining PS waveforms for breakdown to $I_p < 0$ are goal oriented, meaning that when there is sufficient plasma current in the negative direction, the controller switches to other control mode to the negative time-windows. This waveform is synchronized with the remaining breakdown waveforms for $I_p < 0$ and together they are responsible for the plasma breakdown to the negative direction.

- **Vertical breakdown to $I_p < 0$** – Vertical field PS current waveform for creating plasma current in the negative direction (plasma breakdown). Works as the “Primary breakdown to $I_p < 0$ ” mode and is also synchronized with this waveform.
- **Horizontal breakdown to $I_p < 0$** – Horizontal field PS current waveform for creating plasma current in the negative direction (plasma breakdown). Works as the “Primary breakdown to $I_p < 0$ ” mode and is also synchronized with this waveform.
- **Primary inversion to $I_p < 0$** – Primary field PS current waveform for inverting the plasma current from the positive direction to the negative direction. These inversion to $I_p < 0$ waveforms are responsible for the transition between the positive time-windows control mode and the negative time-windows control mode by inverting the plasma current, when this goal is achieved the control is handled to the control defined in the negative time-windows.
- **Vertical inversion to $I_p < 0$** – Vertical field PS current waveform for inverting the plasma current from the positive direction to the negative direction. Works as the “Primary inversion to $I_p < 0$ ” mode and is also synchronized with this waveform.
- **Horizontal inversion to $I_p < 0$** – Horizontal field PS current waveform for inverting the plasma current from the positive direction to the negative direction. Works as the “Primary inversion to $I_p < 0$ ” mode and is also synchronized with this waveform.
- **Primary inversion to $I_p > 0$** – Primary field PS current waveform for inverting the plasma current from the negative direction to the positive direction. These inversion to $I_p > 0$ waveforms are responsible for the transition between the negative time-windows control mode and the positive time-windows control mode by inverting the plasma current, when this goal is achieved the control is handled to the control defined in the positive time-windows.
- **Vertical inversion to $I_p > 0$** – Vertical field PS current waveform for inverting the plasma current from the negative direction to the positive direction. Works as the “Primary inversion to $I_p > 0$ ” mode and is also synchronized with this waveform.
- **Horizontal inversion to $I_p > 0$** – Horizontal field PS current waveform for inverting the plasma current from the negative direction to the positive direction. Works as the “Primary inversion to $I_p > 0$ ” mode and is also synchronized with this waveform.
- **Toroidal current** – toroidal current waveform only synchronized with the system time. The toroidal field current control was not tested yet since it was never required in the experimental campaigns up to date because most of the experiments use a fixed toroidal field.
- **Puffing output %, $I_p > 0$** – Voltage waveform sent to the piezoelectric valve synchronized with the positive time-windows (positive plasma current). This waveform is used in the “Time-windows, open percentage” mode defined in label N.
- **Puffing output %, $I_p < 0$** – Works as the previous waveform but is synchronized with the negative time-windows (negative plasma current).

- **Puffing feedback, $Ip > 0$** – The gas puffing feedback waveform is synchronized with the positive time-windows (positive plasma current). This waveform is used in “Pre-programmed + time-windows feedback” and “Time-windows with feedback” modes defined in label N.
- **Puffing feedback, $Ip < 0$** – Works as the previous waveform but is synchronized with the negative time-windows (negative plasma current).
- **Puffing output (absolute time)** – Voltage waveform sent to the piezoelectric valve only synchronized with the discharge time (not time-windows). This waveform is used in “Pre-programmed + time-windows feedback” and “Absolute time, open percentage” modes defined in label N.

Label P – Waveform display panel

This panel is used to display the selected waveform. The displayed waveform is automatically updated when a point is inserted or deleted by interacting with label Q. This waveform display has the ability to zoom automatically the waveform in the display. The axis display is also automatically updated with all ticks displayed in an intelligible format.

Label Q - waveform edit

This interface is used for adding or removing points from the selected waveform in label O. When the user asserts the “delete points” check-box, each time the user clicks over a point the interface removes that point until there only remaining two points (the minimum for a waveform). The user can add points to the waveform by filling the “t=” and “y=” forms and the click the “add point” button. The waveform results from the linear interpolation of all points and if not specified, the values before the first point and after the last one are set to zero.

Label R – Load other configuration file

The drop-down menus on this label are used to select the configuration file to load. After each discharge the system automatically saves the configuration file and labels it with the pulse number so that they can be easily retrieved. The user has the ability to load all discharge parameters for the configurations files saved after each discharge and also the user saved configuration files (this option is available in label S). After selecting the desired configuration database file, the parameters are loaded to the webpage interface after the user clicks the “load” button.

Label S – Save and commit options

These options are only available after the user placed every edit/save section (label A, F and J) on display mode, i.e., the inserted data is validated. When every section is in display mode, two options appear in the bottom right side of the webpage, the option to save the configuration database file with a user defined name or the option “save on default file and commit”. The latter option overwrites the ISTTOK MARTe default configuration file (last.cfg) and forces the system to reload with the new initialization file effectively committing the changes on the webpage to the control system.

5.3. System operation

This sub-chapter includes several discharge programming strategies using the human machine interface provided by the “discharge configurator” and “advanced configuration” objects. The following discharge types are described in this section: (i) software shot for tests (ii) pre-programmed discharge, (iii) Single cycle feedback discharge, (iv) time predictable AC discharge and (iv) AC discharge with gas injection feedback and goal oriented waveforms.

Although not mentioned in this section, the control system is flexible enough for providing alternative methods to program a discharge as long as they are coherent. This tutorial is intended to provide the base knowledge about the control system.

Software shot for tests

This discharge type is intended only for testing specific control system or hardware elements. Therefore no plasma is produced by using this functionality. This type of discharge can be achieved with the ISTTOK real-time control system by the following procedure (all standard options are omitted from this description):

(In the “discharge configurator” webpage)

1. Disable auto-breakdown feature.
2. Number of AC cycles = 1.
3. Select the desired “discharge time” that will control the duration of the software shot.
4. Select first cycle positive (negative can also be selected but it will use other waveforms not described in this procedure).
5. Edit the first positive time-window control mode to either “off (corresponding PS will not work) or current control (corresponding PS will work in current control).
6. Edit each PS waveform for $I_p > 0$ (corresponding to the positive time-windows). Remember that due to strong coupling, without plasma the primary field PS will only follow the current reference waveform after the iron core is saturated.
7. Edit the comments section to reflect this configuration.
8. Place every section into display mode and the “save on default file and commit” button will appear.
9. Click on the save and commit button.

(In the “advanced configuration” webpage)

1. If gas puffing output is to be tested select on the “absolute time, open percentage” in the puffing options, if there is no need of gas injection select the option “off”.
2. If gas puffing is required, edit the “Puffing output (absolute time)” waveform.
3. Edit the comments section to reflect this configuration.
4. Place every section into display mode and the “save on default file and commit” button will appear.
5. Click on the save and commit button.

Pre-programmed discharge

The fully pre-programmed discharge was the only option when there was no real-time control system. This control mode has many disadvantages because it lacks the real-time control during the plasma discharge and requires a person will a vast knowledge on the machine configuration in order to work acceptably. Nevertheless this mode can be used to test new operation regimes by forcing the actuators to follow a reference waveform. For example it can be used for density limit experiments with the plasma being pushed against the limiter.

This type of discharge can be achieved with the ISTTOK real-time control system by the following procedure:

(In the “discharge configurator” webpage)

1. Disable auto-breakdown feature.
2. Number of AC cycles = 1.
3. Select the desired “discharge time” that will control the duration of the software shot.
4. Select first cycle positive (negative can also be selected but it will use other waveforms not described in this procedure).
5. Edit the first positive time-window control mode to current control (corresponding PS will work in current control).
6. Edit each PS waveform for $I_p > 0$ (corresponding to the positive time-windows). Include in the beginning of the current waveforms a correct magnetic field configuration in order to provide the adequate conditions for breakdown and then edit the rest of the waveform in order to reflect the desired experiment. The user can also program waveforms for an AC discharge but the probability of failure is greater than using the proper method to programme this type of discharge.
7. Edit the comments section to reflect the configuration.
8. Place every section into display mode and the “save on default file and commit” button will appear.
9. Click on the save and commit button.

(In the “advanced configuration” webpage)

1. Select an adequate gas puffing injection mode in the puffing options. Each mode has different characteristics that are described in the previous sub-chapter.
2. Edit the necessary gas puffing waveforms for the selected gas puffing option.
3. If the gas puffing injection is in feedback mode the user should check the gas puffing feedback parameters.
4. Edit the comments section to reflect the configuration.
5. Place every section into display mode and the “save on default file and commit” button will appear.
6. Click on the save and commit button.

Single cycle feedback discharge

This type of discharge is the most used in the tokamak machine. It consists in a single cycle discharge with feedback along the discharge. This type of discharge can be achieved with the ISTTOK real-time control system by the following procedure:

(In the “discharge configurator” webpage)

1. Enable or disable the auto-breakdown feature according to the user preference, with auto-breakdown feature active it is easier to program the discharge but it is more difficult to synchronize the discharge with events outside the real-time control system.
2. Number of AC cycles = 1.
3. Select the desired “discharge time” that will control the duration of the software shot or use the “invert” option in the last used time-window.
4. Select first cycle positive (negative can also be selected but it will use other waveforms not described in this procedure).
5. Edit the time-windows section with the desired mode of control for each actuator for every time-window to be used.
6. Edit each PS waveform and scenario control waveform for $I_p > 0$ (corresponding to the positive time-windows). If the option to auto-breakdown is not selected then include in the beginning of the current waveforms a correct magnetic field configuration in order to provide the adequate conditions for breakdown and then edit the rest of the waveform in order to reflect the desired experiment.
7. Check the values of the PID constants if this type of control is to be used in the discharge.
8. Diagnostic parameters should also be checked because the feedback system will rely on the selected diagnostics.
9. Edit the comments section to reflect the configuration.
10. Place every section into display mode and the “save on default file and commit” button will appear.
11. Click on the save and commit button.

(In the “advanced configuration” webpage)

1. Select an adequate gas puffing injection mode in the puffing options. Each mode has different characteristics that are described in the previous sub-chapter.
2. Edit the corresponding gas puffing waveforms for the selected gas puffing option.
3. If the gas puffing injection is in feedback mode the user should check the gas puffing feedback parameters.
4. If auto-breakdown is selected, the breakdown waveforms should be checked.
5. Edit the comments section to reflect the configuration.
6. Place every section into display mode and the “save on default file and commit” button will appear.
7. Click on the save and commit button.

Time predictable AC discharge

Before the introduction of the control system described in this thesis, the standard ISTTOK AC discharges were produced as described in this section. The main advantage of this type of discharge is the ability to synchronize the discharge with a diagnostic/actuator that is not measured or controlled by the ATCA real-time system. The drawback of this type of discharge is that it does not use the full potential of the control system.

This type of discharge can be achieved with the ISTTOK real-time control system by the following procedure:

(In the “discharge configurator” webpage)

1. Enable auto-breakdown feature.
2. Selected the desired number of AC semi-cycles.
3. Check the maximum duration of the discharge and check if the number of AC cycles times the time-windows durations plus breakdown duration is inferior to this duration.
4. Select the first AC cycle plasma direction.
5. Edit the positive and negative time-windows section with the desired mode of control for each actuator for every time-window to be used and for both plasma current directions. The invert option should be inserted in the last active time-window and the time (of this special time-window) should be set to a value before the previewed iron core saturation.
6. Edit each PS current waveform and scenario control waveform for both plasma current directions; basically all the waveforms except the ones that will not be requested by the time-windows control mode selection.
7. Check the values of the PID constants if this type of control is to be applied throughout the discharge.
8. Diagnostic parameters should also be checked because the feedback system will rely on the selected diagnostics.
9. Edit the comments section to reflect the configuration.
10. Place every section into display mode and the “save on default file and commit” button will appear.
11. Click on the save and commit button.

(In the “advanced configuration” webpage)

1. Select an adequate gas puffing injection mode in the puffing options. Each mode has different characteristics that are described in the previous sub-chapter.
2. Edit the corresponding gas puffing waveforms for the selected gas puffing option.
3. If the gas puffing injection is in feedback mode the user should check the gas puffing feedback parameters.
4. Disable the “End if unsuccessful breakdown/inversion” setting.
5. Check the breakdown waveforms for either positive plasma current or negative plasma current according with the first cycle plasma direction selected in the previous webpage. Normally the ISTTOK breakdown waveforms include some milliseconds of iron core pre-magnetization. To transform this goal oriented waveforms into time predictable waveforms the user should program the entire pre-magnetisation phase and then the beginning of the actual breakdown with no more than 1 ms for the remaining “breakdown time”. This specific configuration will just start the breakdown sequence that will be completed after the control is handed to the time-windows sequence.
6. Set the maximum breakdown time to reflect the previous point. The objective is to perform all the pre-magnetization and just after the breakdown sequence starts the

time for breakdown ends and the control is handled to the selected time-window. By programming this sequence, the breakdown time remains fixed instead of the goal oriented strategy (where the time is depends on the successful completion of the breakdown goal).

7. Set the maximum inversion time to 0. The time-windows will be responsible for the inversion within a fixed time.
8. Edit the comments section to reflect the configuration.
9. Place every section into display mode and the “save on default file and commit” button will appear.
10. Click on the save and commit button.

AC discharge with gas injection feedback and goal oriented waveforms

With the introduction of the control system described in this thesis it is now possible to implement a goal oriented strategy where the time for each phase is not known a priori. This type of control enables the user to explore the full potential of the ISTTOK tokamak by providing the tools to extend the AC discharge duration limited only due to the power supplies duration. This type of discharge is further described at the end of the sub-chapter 4.4.

This type of discharge can be achieved with the ISTTOK real-time control system by the following procedure:

(In the “discharge configurator” webpage)

1. Enable the auto-breakdown feature.
2. Selected the desired number of AC semi-cycles.
3. Check the maximum duration of the discharge and check if the number of AC cycles times the time-windows durations plus breakdown duration is inferior to this duration.
4. Select the first AC cycle plasma direction.
5. Edit the positive and negative time-windows section with the desired mode of control for each actuator for every time-window to be used and for both plasma current directions. Preferably insert the inversion time in the last edited time-window for both directions. If this value is not inserted the plasma current will invert when the iron core saturates.
6. Edit each PS waveform and scenario control waveform both plasma current directions, basically all the waveforms except the ones that will not be requested by the time-windows control mode selection.
7. Check the values of the PID constants if this type of control is to be applied throughout discharge.
8. Diagnostic parameters should also be checked because the feedback system will rely on the selected diagnostics.
9. Edit the comments section to reflect the configuration.
10. Place every section into display mode and the “save on default file and commit” button will appear.
11. Click on the save and commit button.

(In the “advanced configuration” webpage)

1. Select an adequate gas puffing injection mode in the puffing options. Each mode has different characteristics that are described in the previous sub-chapter. For long AC discharges the most indicated control mode “Pre-programmed + time-windows feedback”.
2. Edit the corresponding gas puffing waveforms for the selected gas puffing option.
3. If the gas puffing injection is in feedback mode the user should check the gas puffing feedback parameters. For long AC discharges it is recommended to use gas injection feedback in H_α radiation and to have a maximum “idle time” of not less than 40 ms due to recycling in the last part of the long AC discharge.
4. Check the breakdown waveforms for either positive plasma current or negative plasma current according with the first cycle plasma direction selected in the previous webpage. Leave sufficient time after the pre-magnetization phase for the plasma to breakdown.
5. Verify all the plasma current inversion waveforms.
6. Set the maximum breakdown time to have sufficient time for the plasma to breakdown. When there is enough plasma current the control will automatically be handled to the programmed time-windows.
7. Set the maximum inversion time to a value that allows the plasma current to invert normally. If the inversion is successfully the control will jump to the execution of the next time-windows set.
8. Edit the comments section to reflect the configuration.
9. Place every section into display mode and the “save on default file and commit” button will appear.
10. Click on the save and commit button.

Chapter 6 – Results

This chapter is intended to demonstrate the improvement in the ISTTOK operation as a result of the developed real-time control system while some particular results were already discussed in the previous chapters. To demonstrate the improvements in the control system, a pulse similar to one of the best old control system pulses was developed. Figure 100 shows a comparison between two AC discharges, one with the old control system (pulse #16711) and another with the new control system (pulse #34135). For the recent pulse, the system was programmed to invert the plasma current each 25ms. The current inversion was predefined in the “advanced configuration” whereas the main part of the experiment had feedback on the plasma position. The ISTTOK interferometer has just one vertical cord and the relatively high density measured at the beginning of the AC cycles is most probably an effect of the plasma position. In this experiment the plasma current inversions use goal oriented pre-programmed current waveforms without position feedback, while during the flattop the plasma is controlled in position and is pushed to the low field side, hence the lower density measurement.

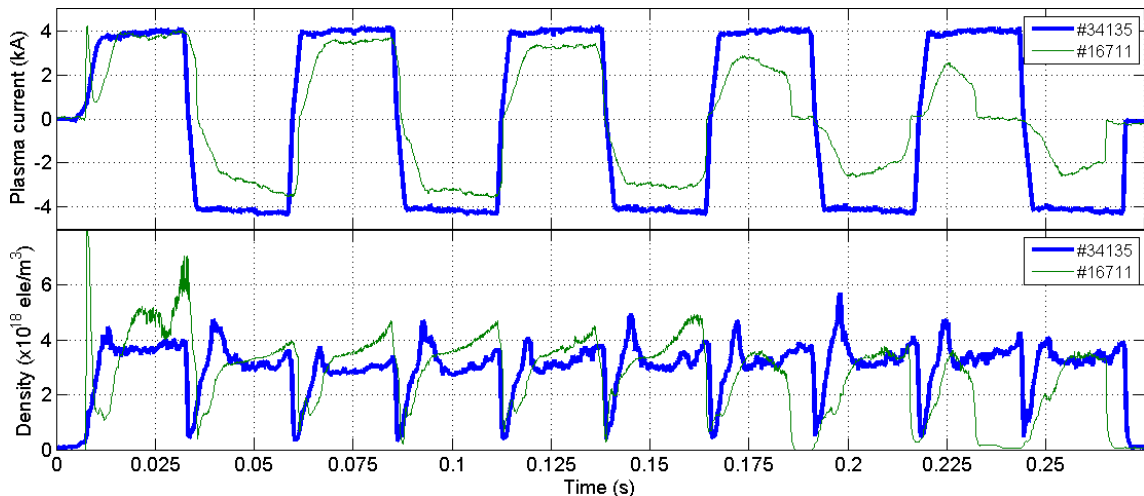


Figure 100 - 10 semi-cycles AC discharge with the old (pulse #16711) and the new control system (pulse #34135). On top the plasma current and below the corresponding density measured by a central vertical cord interferometer. The magnetising field power supply was not controllable in the old control system.

The improvement in the plasma current control is evident and the main reason for this improvement was the development of a new primary field power supply that is also a part of this thesis. With this new power supply there was no need to have an additional capacitor bank discharge for providing breakdown as it existed in the old control system (this was the main reason for the spike in the plasma current at the beginning of the old AC discharge). The transition between AC semi-cycles is now as smooth as possible and the plasma stays ionized during the plasma current reversal process. The plasma density feedback was also introduced by this real-time control system and further results of the new control system will be presented along the rest of this chapter.

6.1. Alternate current results

The ISTTOK tokamak is now able to produce long AC discharges with a high level of reliability. One of the first successful AC discharge was pulse number 33001 depicted in Figure 101. This pulse was obtained in an intermediate evolution step in the ISTTOK control system presented by this thesis. At the time of this pulse there was still no real-time feedback control on the gas puffing, but it provided interesting results proving the advantages of the new control system at an earlier stage.

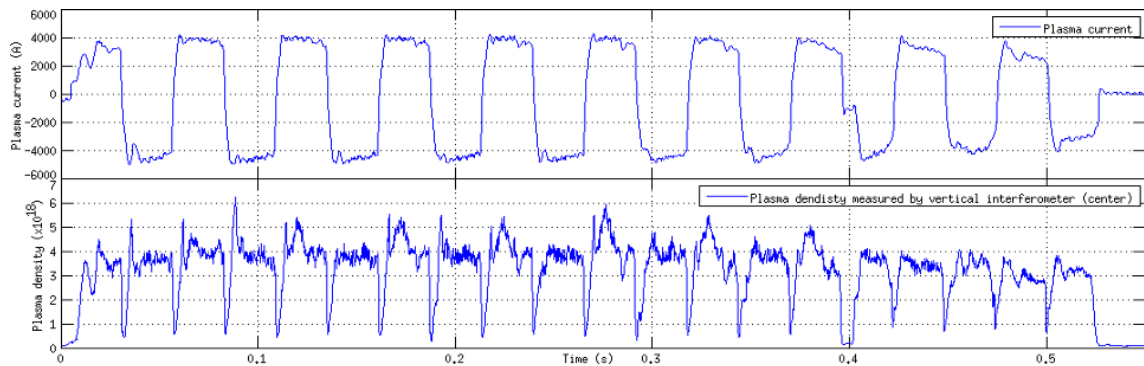


Figure 101 – ISTTOK pulse #33001, 20 semi-cycle AC discharge without feedback control on gas puffing. Degradation on plasma parameters can be observed in the last semi-cycles do to wall recycling.

In this discharge (pulse number 33001), there were still discharge degradation problems. Not all current reversal process were fully accomplished since in the transition near 0.4 s there was a full loss of ionization and the plasma had another breakdown with a few milliseconds of dwell time. The degradation in the plasma current and density of the last semi-cycles of the AC discharge is also noticeable. Aiming at enhancing the discharge performance a gas puffing feedback mechanism (described in chapter 3.4) was integrated in the ISTTOK control system. Right after the introduction of the gas puffing feedback the reliability of the alternate discharges and control was improved as illustrated in Figure 102.

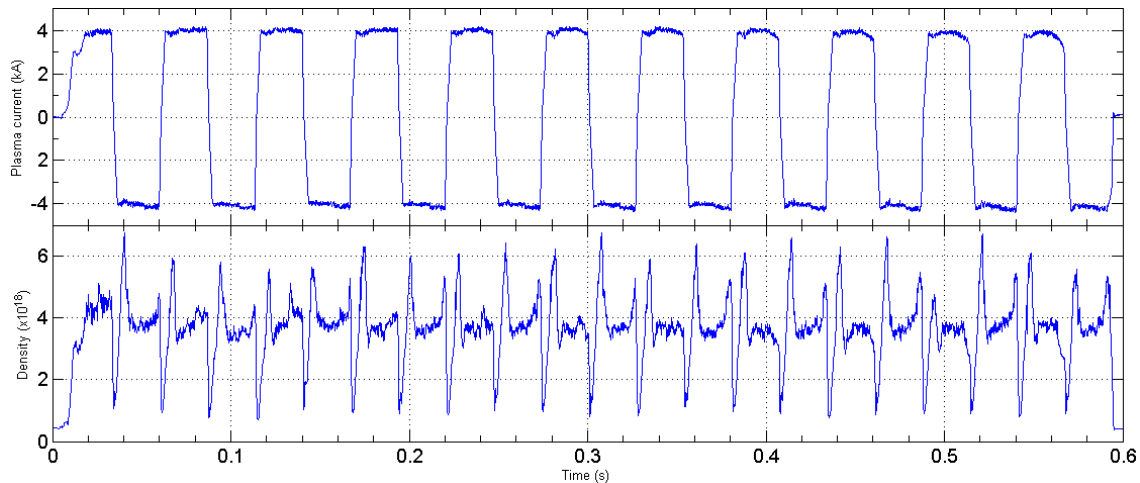


Figure 102 - ISTTOK pulse #34261, 22 semi-cycles AC discharge with real-time control on gas puffing using an $H\alpha$ waveform as a reference. Unlike discharge #33001, the puffing control assured no plasma parameters degradation on the final semi-cycles.

This discharge (pulse number 34261) showed a great improvement in the last cycles of the AC discharge as compared to the system without gas puffing feedback (pulse number 33001) previously described. This result suggests that the flux from the wall due to recycling is not enough to keep the discharge. After this encouraging result a further extension of the plasma duration was attempted. This was achieved in a latter ISTTOK campaign where the discharge duration was extended to over one second of operation with 40 AC semi-cycles. A typical discharge (pulse #34332) is depicted in Figure 103. The unique limiting factor was the ISTTOK power supplies that were not designed for longer operation. This problem shall be addressed in a future upgrade by extending the power supplies maximum operation time.

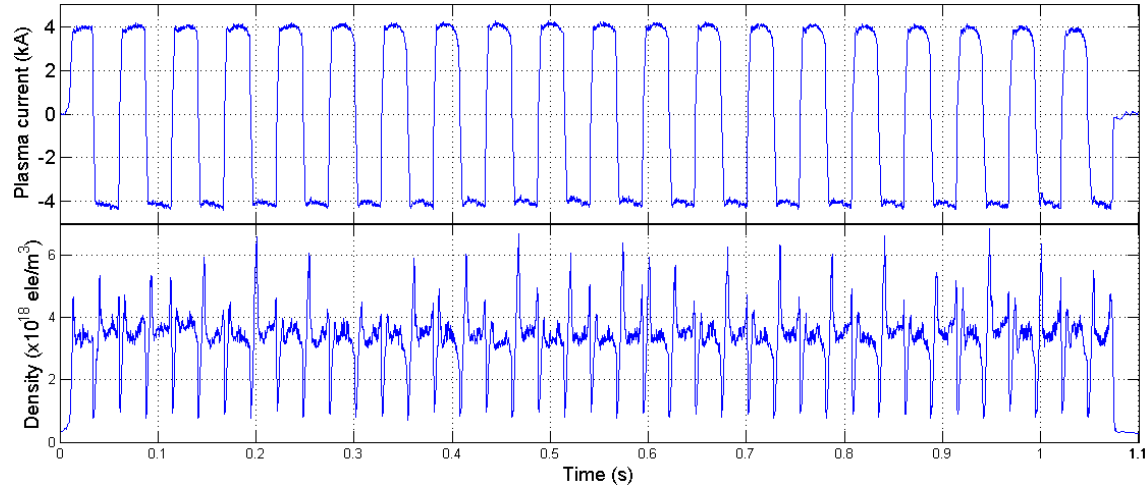


Figure 103 – Pulse #34332 – 40 semi-cycles AC discharge at $\pm 4\text{kA}$. Feedback control on the $\text{H}\alpha$ radiation and as a consequence the density is stable around $3.8 \times 10^{18} (\text{e}/\text{m}^3)$. More than one second of operation was achieved without loss of ionization during the current reversal process.

Since the new control system has the ability to save configuration files for all the pulses it is possible and easy to load the configurations of one of these long AC discharges and repeat a pulse with the same characteristics as can be observed in Figure 104. This system has high reproducibility and in fact this was tested by repeating 14 times the same long AC discharge programming. The duration of each discharge was greater than 1s with 40 AC semi-cycles.

In the referred figure it is also possible to observe the behaviour of the plasma density and H_α radiation when there is real-time feed-back control of the gas injection by the H_α radiation value. The density and H_α radiation are quite stable throughout the discharge with reproductive behaviour from discharge to discharge.

Since the most effective method of programming ISTTOK AC discharges is using the goal oriented waveforms (described in the timewindowsGAM section of sub-chapter 4.5) for breakdown and current reversal process, the discharge timings are slightly different from discharge to discharge although the main characteristics are maintained. The phenomenon can be observed in Figure 105 (zoomed version of Figure 104).

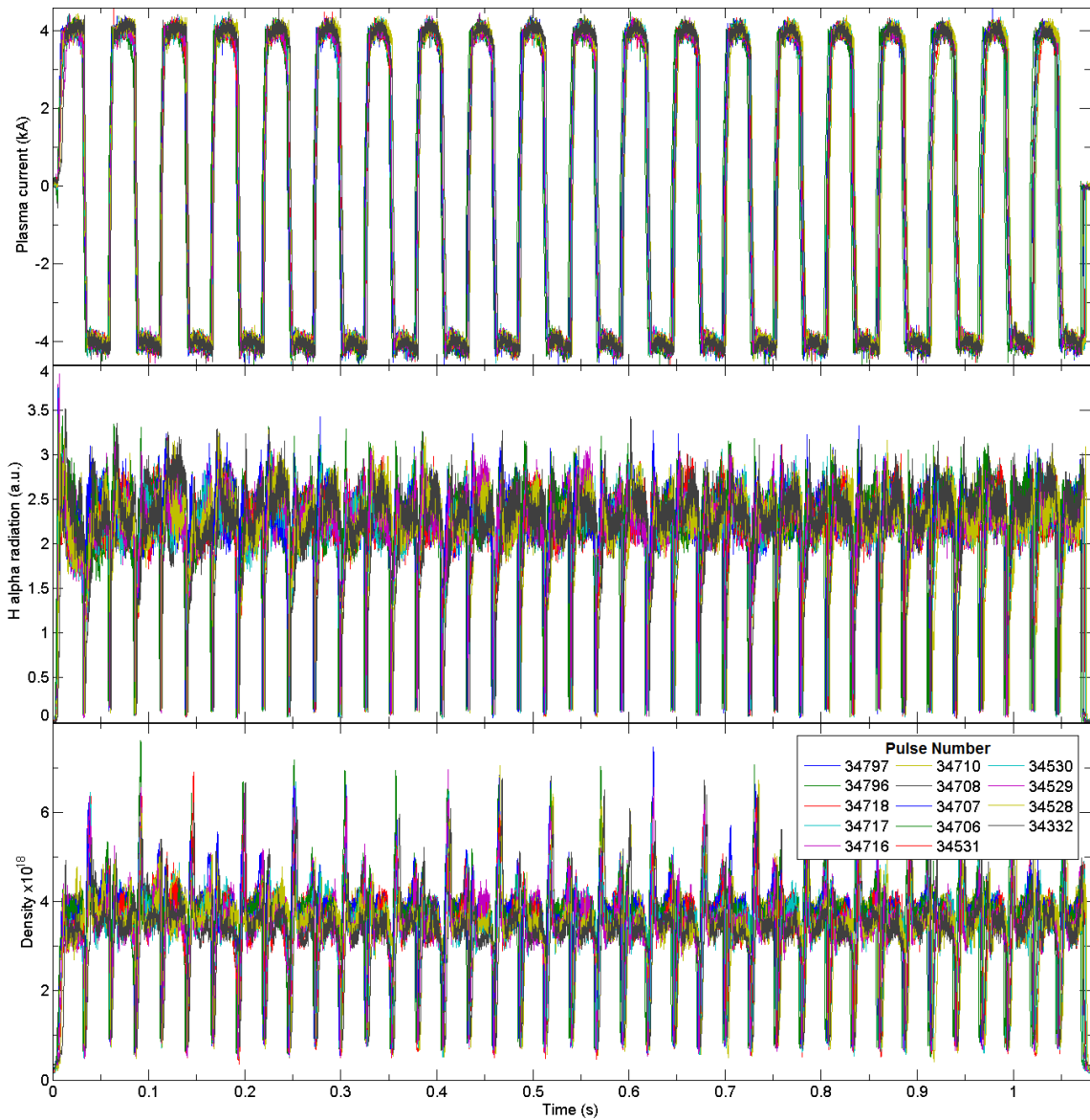


Figure 104 – Overplot of 14 AC discharges, highlighting the control system discharge reproducibility.

Nevertheless, the success of these pulses depends on the plasma conditions and problems might arise in the first pulses after a machine opening due to the subsequent high impurity content. However, by performing long AC discharges the machine recovers much faster than in the past since one of these pulses is equivalent of 40 single side plasma discharges. The machine can recover from an opening in a couple of days whereas in the past the recovery process took more than one week.

Figure 106 details the breakdown of the same 14 AC discharges mentioned previously. As it can be observed, the breakdown depends on the pre-magnetisation of the iron core since when there is some small plasma current build-up in the opposite direction, the breakdown is faster and the plasma current build-up is also faster. By observing Figure 105 and Figure 106 it is also noticeable that the current reversal process is faster than the breakdown phase.

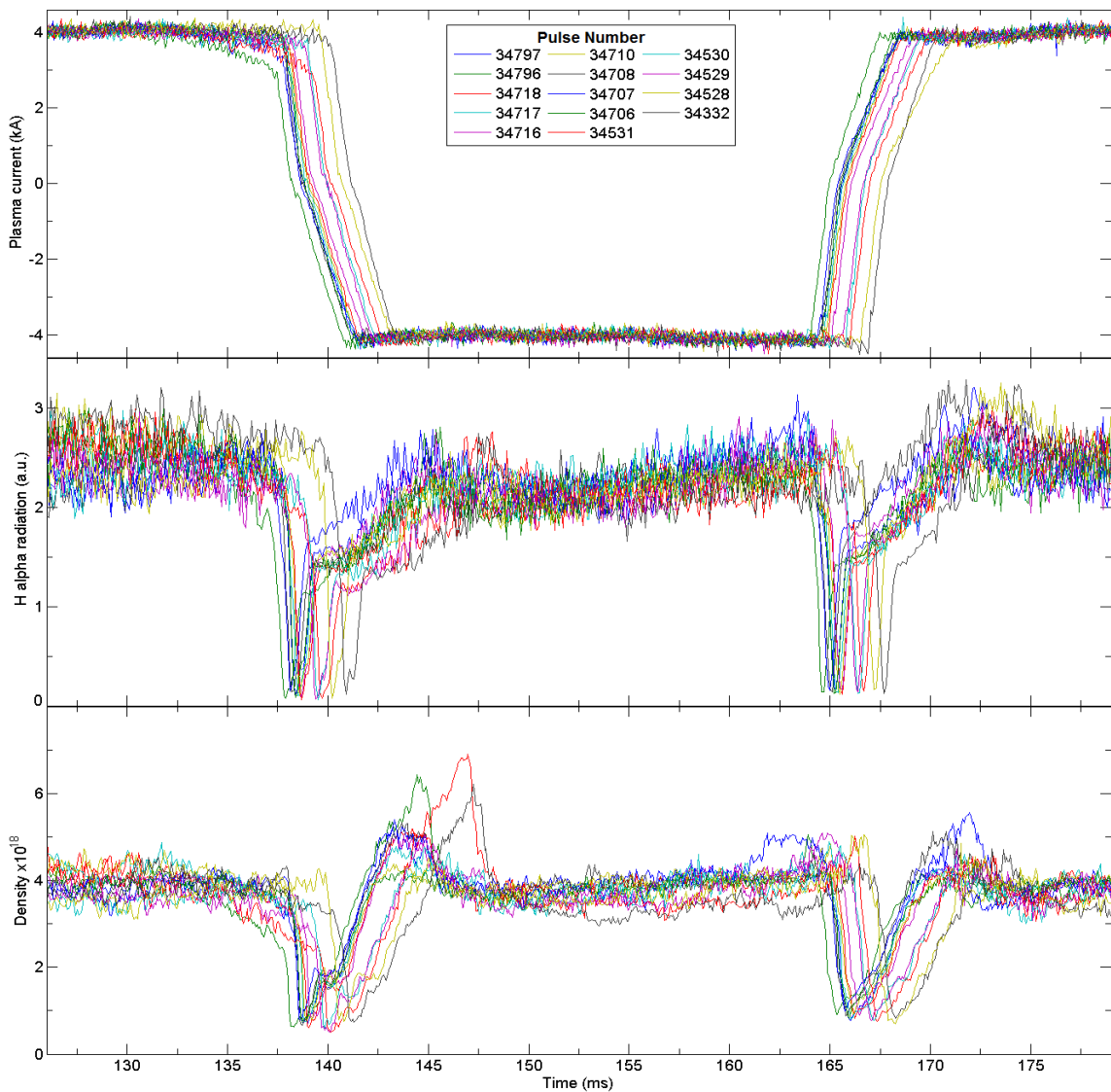


Figure 105 – Zoomed version of the previous figure. This figure contains the overplot of 14 AC discharges with similar control system programming. This figure highlights the similarity between all discharges as well as the difference in the discharge timing originated by the goal oriented control philosophy.

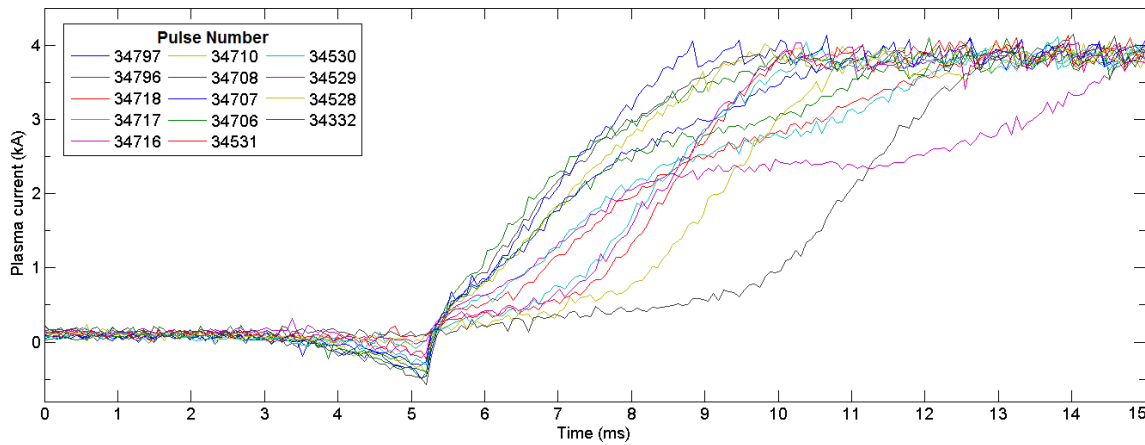


Figure 106 - Detail of 14 different breakdowns (same pulse numbers as the two previous figures).

6.2. Machine operation results

Besides allowing for longer and more stable AC discharges, the present control system enabled ISTTOK to perform new experiments that were not possible under the former control system. Since ISTTOK is now able to perform reliable and long AC discharges it can now be used for material testing, recycling studies and impurity accumulation experiments. Three different experiments will be presented in this section: (i) scenario control results; (ii) impurity accumulation in long AC discharges experiments; and (iii) tungsten samples exposure to the plasma.

Plasma control results

A reference discharge with plasma current at 4 kA was used to test the new control in simultaneous scenario control (plasma current, radial position and vertical position). The result of this control experiment is exemplified in Figure 107.

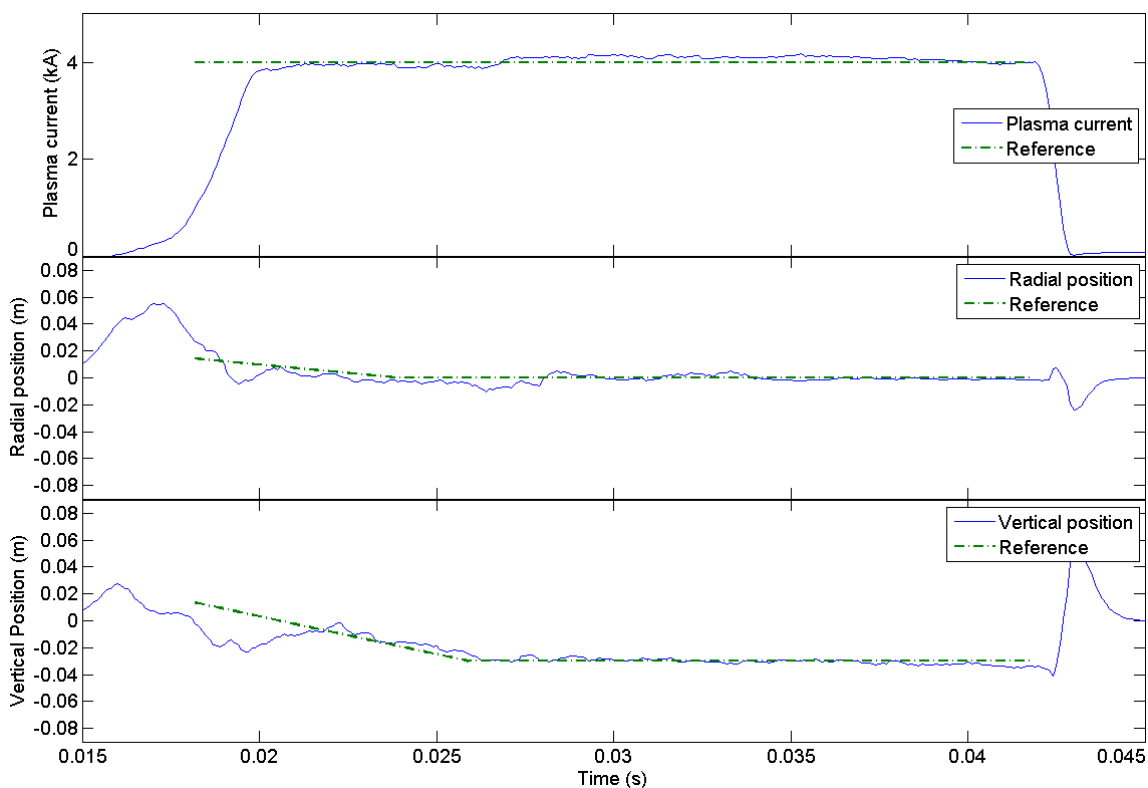


Figure 107 – Pulse #34104. Simultaneous feedback control on the plasma current, radial position and horizontal position.

As illustrated in the figure above, the new ISTTOK real-time control is able to simultaneously control the horizontal and vertical plasma position. As detailed in chapter 3.3 the PS can be programmed in two regimes: (i) current control or (ii) scenario control, where the former is detailed in chapter 3.3.

Another example of the real-time control is depicted in Figure 108. This figure (from pulse number 34434) details the actual currents on the Horizontal and Vertical field PS when the real-time system was controlling the plasma position.

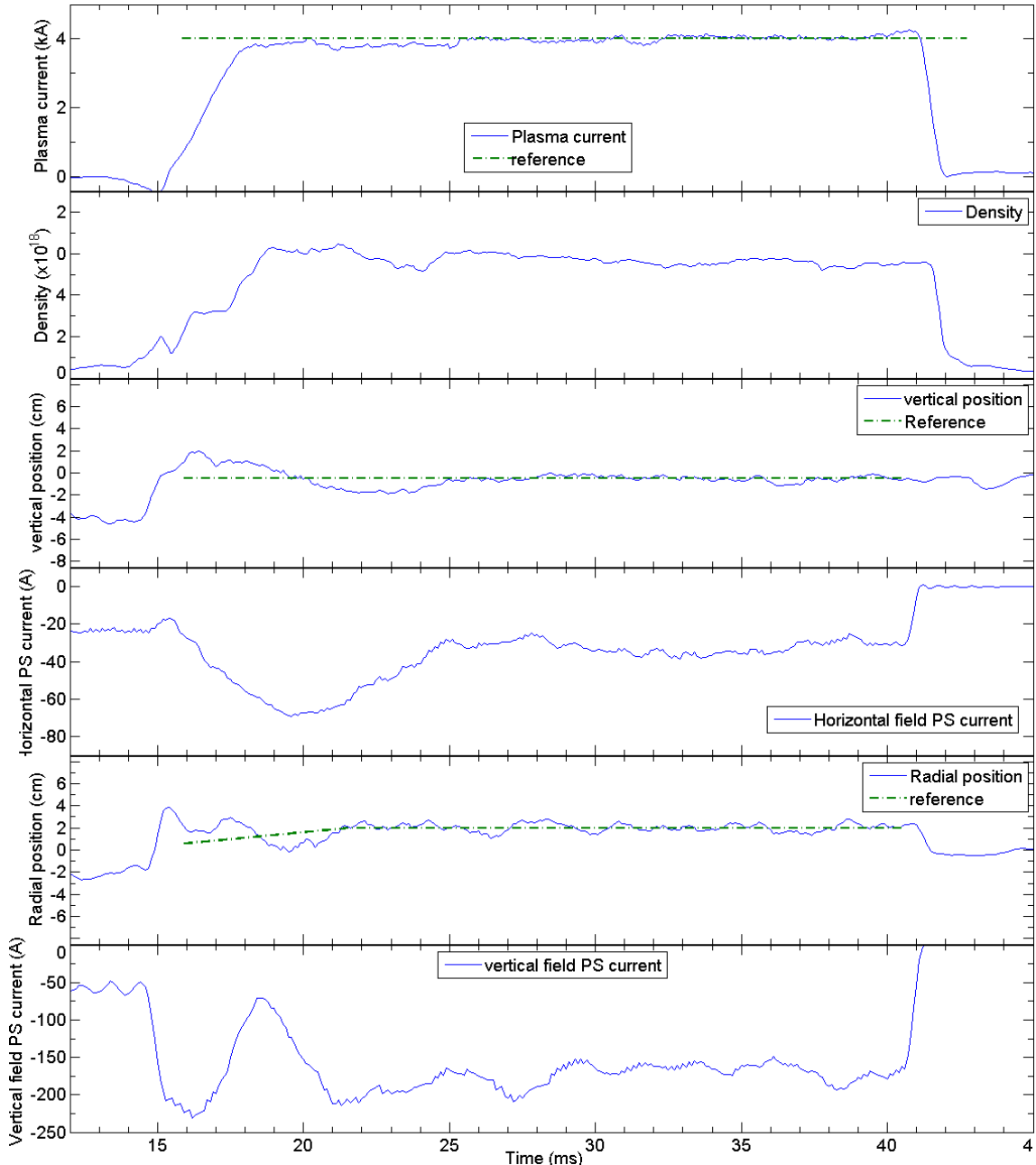


Figure 108 – Horizontal and Vertical field power supplies currents in plasma position control. The real-time control sends each control cycle a reference to each PS in order to match the required plasma position reference.

The maximum plasma current achieved up to date with the new control system was 6 kA exemplified by Figure 109. There are several limiting factors for the plasma current. The first obvious limiting factor is related with the ISTTOK vacuum vessel dimensions (85 mm radius). Nevertheless, it is anticipated that the plasma current can be increased 6 kA by increasing the voltage on the primary field power supply capacitor bank over the present 210 V (safe operation point). The primary field PS main components were projected for up to 1000V and 400A. Based on these numbers and in the fact that ISTTOK has a very strong coupling between the primary field PS and the ohmic circuit due to the iron core and the fact that the primary field coils consist in 28 turns parallel to the torus it can be extrapolated that the maximum plasma current for the installed primary field PS would be around 10 kA in case the voltage in the capacitor banks is increased to the limit. Since the ISTTOK capacitor bank is more than 30

years old for safety reasons it is advisable that the present capacitor bank voltage should not exceed 250V effectively limiting the voltage of the primary field PS and consequently the plasma current maximum value.

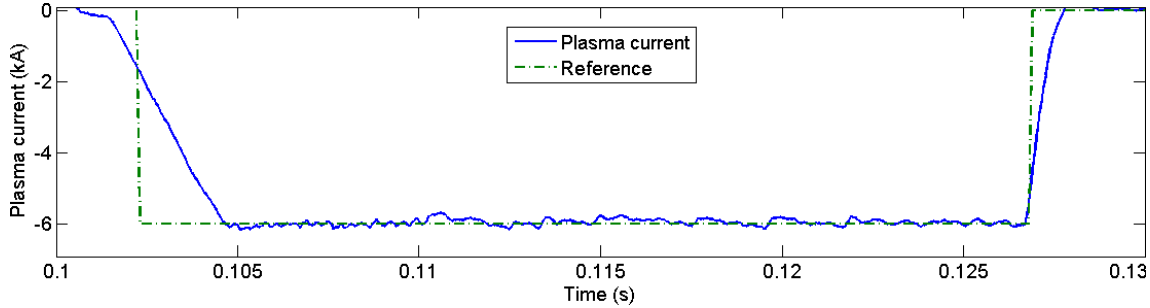


Figure 109 – Pulse #34037. Plasma current control at 6 kA.

Impurity accumulation in long AC discharges experiments.

For long AC discharges operation it is necessary to have feedback on the gas injection system in order to maintain a fairly constant density. The typical puffing rate of hydrogen under these conditions can be derived from the gas puffing rate depicted in Figure 62 of chapter 3.4. As illustrated, the gas puffing ratio is much higher in the beginning of the discharge and roughly after one hundred milliseconds the gas puffing rate begins to decrease most probably because plasma fuelling to the gas recycling process from the vessel and limiter becomes important [63].

To assess the impurity accumulation during a long AC discharge a spectrometer (see location on Figure 43) was set to measure the evolution of the C_{III} radiation ($\lambda = 464.74$ nm) during the AC discharge. Pulse number #34531 (depicted in Figure 110) contains the evolution of the carbon impurities in the plasma to determine impurity accumulation during the long AC discharges experiments.

The C_{III} ($\lambda = 464.74$ nm) to H _{α} ($\lambda = 656.28$ nm) normalized radiation ratio depicted in Figure 110 also shows a relative stable carbon content without a clear evidence of degradation throughout the AC discharge. This data strongly suggests that the discharge would continue with more AC cycles if not limited by the power supplies duration. This provides an additional argument to upgrade the power supplies operation as a future work.

Figure 111 details the C_{III} and H _{α} radiation during a small portion of the discharge. This figure shows that there are carbon radiation spikes in the beginning and end of the negative plasma current semi-cycles (the density measurement also has spikes in the same phase). This can be explained by the fact that in this type of discharges the radial control is disabled for the beginning and end of the discharge (active in the main part of the semi-cycle) since it easier to create the proper magnetic configuration (null poloidal field in the centre of the vacuum vessel) for current reversal process using this artefact. In fact, during the beginning and end of the negative plasma current semi-cycles the plasma is pushed to the outer wall which contains the carbon limiter. Since more power is deposited in the carbon limiter during the described periods it is natural that the carbon radiation is increased in those stages, with the C_{III} radiation decreasing during the steady state part of the discharge.

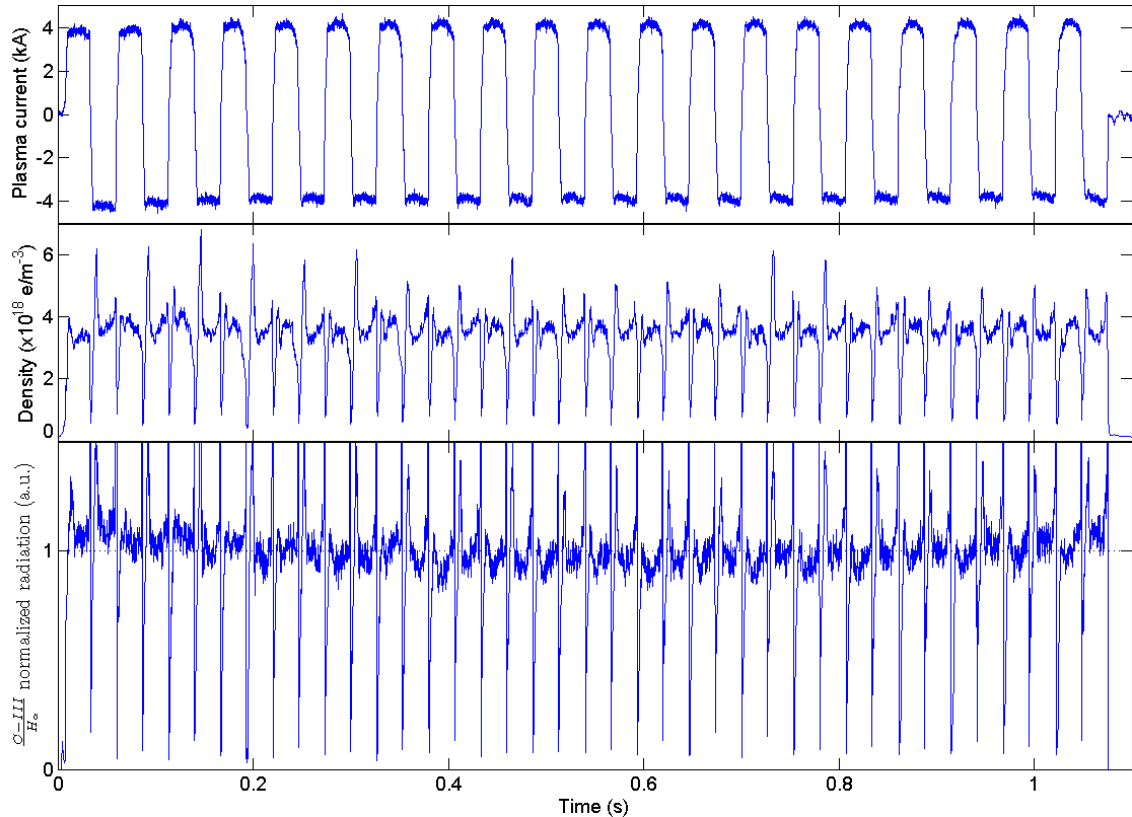


Figure 110 – ISTTOK pulse #34531, 40 semi-cycles AC discharge. From top to the bottom: (i) plasma current, (ii) plasma density and (iii) C_{III} ($\lambda = 464.74 \text{ nm}$) to H_{α} ($\lambda = 656.28 \text{ nm}$) normalized radiation. This ratio shows a clear non-degradation of the impurity content during the entire AC discharge.

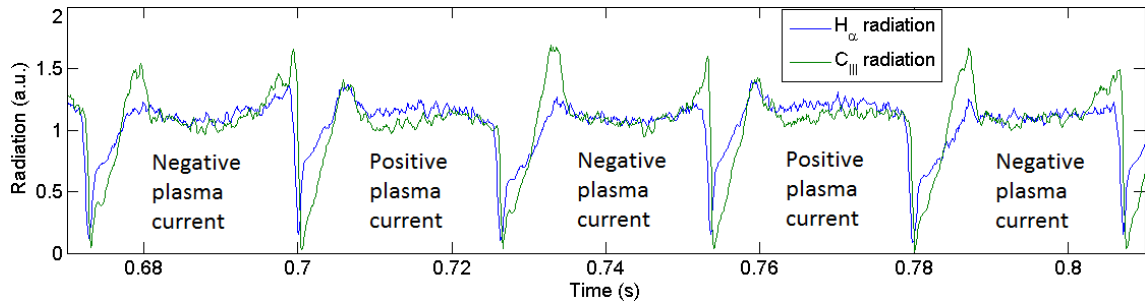


Figure 111 – Pulse #34531. Detail of the C_{III} ($\lambda = 464.74 \text{ nm}$) and H_{α} radiation ($\lambda = 656.28 \text{ nm}$).

Tungsten probe experiments.

To study the power deposition during the AC operation, a tungsten foil was inserted 20 mm inside the plasma in the low field side. Since the probe has small dimensions (7 mm x 25 mm x 0.3 mm) it has low temperature inertia.

The tungsten foil was exposed to a plasma without position control during the current inversion as the set of inversion waveforms were only designed to create the adequate conditions for a successful current reversal which means a near zero poloidal field in the centre of the vessel during the inversion. Figure 112 shows the time evolution of the tungsten foil temperature measured by an infrared camera and reveals that during the plasma inversions from positive to negative current there was a higher energy deposition on the outer wall mainly because in this inversion recipe the plasma was “pushed” to the outer wall. During the

inversions from negative plasma current to positive current the energy deposition becomes insignificant because the plasma was kept away from the probe during the inversion.

As illustrated, the temperature measurement saturated (infrared camera saturates at 1600°) after just 13 semi-cycles (0.36 s) of the AC discharge, far from the normal AC ISTTOK discharge duration of more than one second.

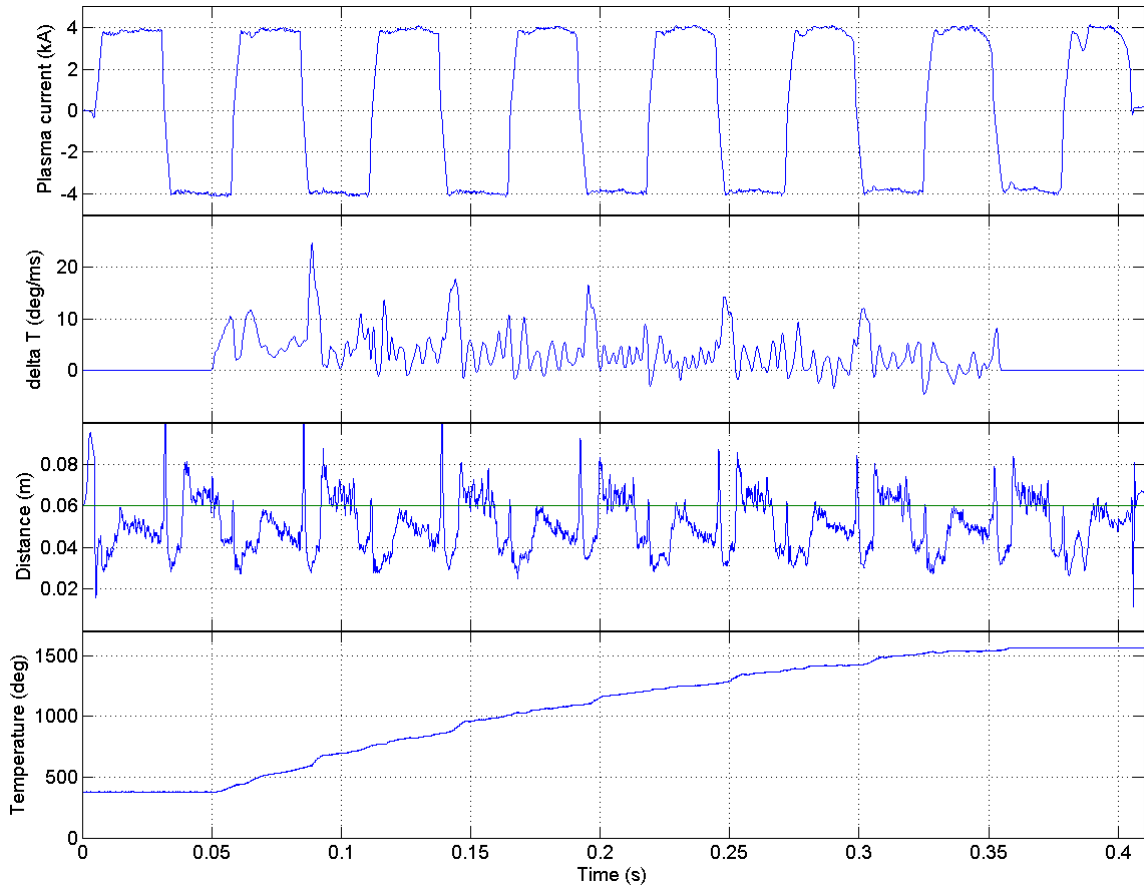


Figure 112 - Pulse #35044, 20 cycles AC discharge with a tungsten probe at $r = 65$ mm (20 mm inside plasma from limiter). From top to bottom: (i) plasma current, (ii) temperature at the probe variation (smooth), (iii) distance from plasma centre to probe and (iv) tungsten probe temperature saturating at the temperature sensor maximum value (1600 degrees).

To avoid saturating the temperature sensor so quickly and to provide extra data for the scientific programme, the probe was moved further outside to $r = 70$ mm (15 mm inside the limiter position). The results from this discharge are presented in Figure 113.

The side result of these experiments was the unexpected partial meltdown of the tungsten probe as depicted in Figure 114 of Chapter 7, proving that the ISTTOK tokamak can now be used for plasma-wall interaction studies. In particular allows the test of fusion relevant materials taking advantage of the ISTTOK flexible environment. The result of this work will enable new studies on this area of great interest for the fusion community.

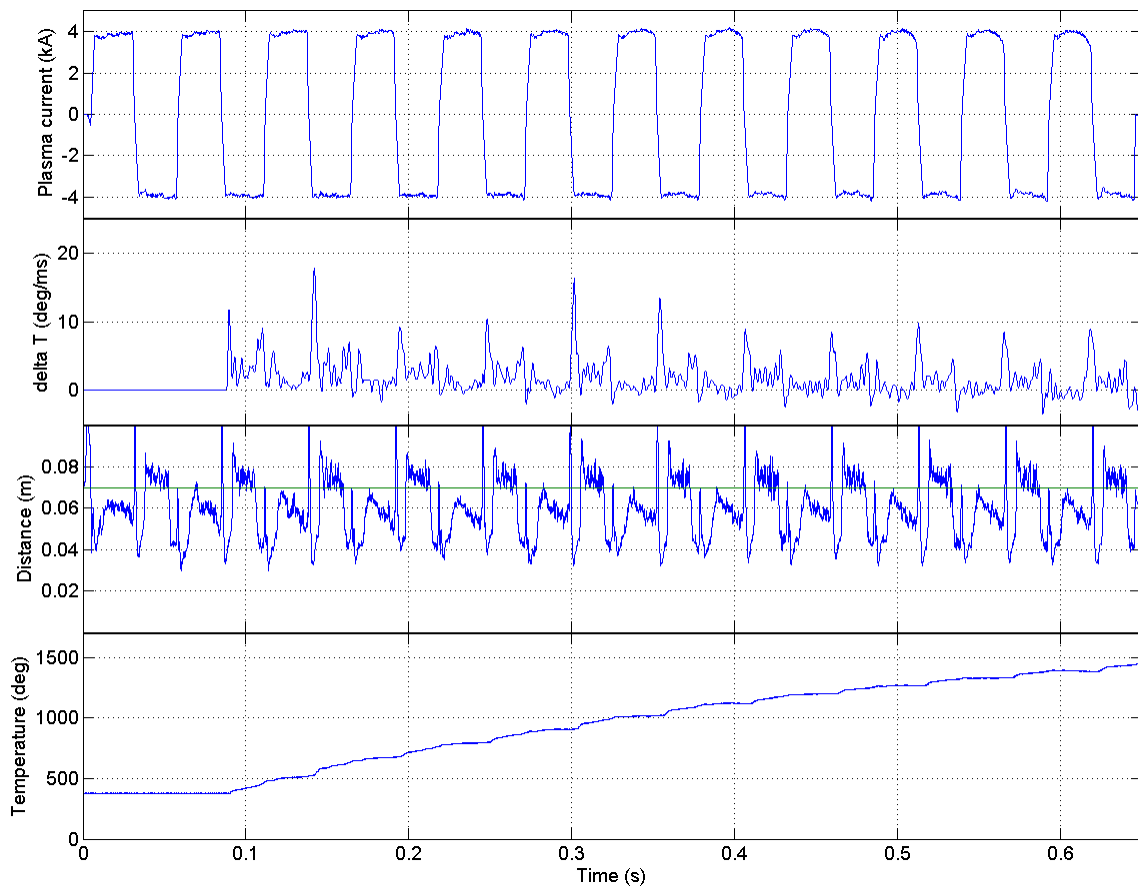


Figure 113 – Pulse #35047, 24 semi-cycles AC discharge with a tungsten probe at $r=70$ mm (15 mm inside plasma, limiter at $r=85$ mm). From top to bottom, (i) plasma current, (ii) temperature variation at the probe, (iii) distance from plasma centre to probe and (iv) probe temperature.

Chapter 7 – Conclusions

The ISTTOK control system demonstrated a reliable operation for more than 3000 discharges up to date and enabled ISTTOK to extend the discharge duration per AC pulse opening new opportunities mainly in the area of plasma-wall interaction studies. In the last ISTTOK campaign the discharge duration was extended beyond one second of operation with 40 AC semi-cycles without ionization loss during the plasma current inversions and was only limited by the power supplies operational time interval. A future update shall address this issue.

All real-time diagnostics and actuators were successfully integrated in the ATCA CODAC hardware and a MIMO control strategy was implemented. This enables feedback control with several different strategies depending on the machine operator selection.

The new control system was successfully deployed and together with the new magnetising field power supply allows new operational space to be explored namely for the alternate current discharge operation.

The MARTe framework provided the adequate tools for developing the ISTTOK tokamak real-time control and a 100 µs control cycle was achieved with a jitter generally lower than 0.4 µs.

Two software objects were produced to interact and configure the control system. These two configuration objects are isolated from the real-time thread that runs the ISTTOK control code. When the pulse ends, the real-time configuration file is stored and the machine operator can now load previous configurations and repeat the pulse including event-driven configurations.

Time windows operation with different control strategies was successfully implemented and together with the graphical HMI software allows an easy path to program a discharge capable of handling complex events. Several synchronization strategies can be implemented using the event driven paradigm largely improving the number of stable AC cycles.

Several synchronization strategies have been produced and tested and are now available for the operator. This is a very useful instrument when designing alternate discharges or when automatic breakdown or automatic inversions on the iron core saturation features are used.

Although the system can still be configured for time deterministic operation, the even-driven discharge programming is now the standard discharge operation. The event-driven paradigm can be very useful when programming long discharges with several objectives per discharge such as the envisaged for ITER [64].

The carbon content during a long AC discharge is apparently stable during the 40 AC semi-cycles and all other measured plasma parameters also appear to be stable during the discharges.

The power deposition on the walls and limiters during the AC discharges is mainly dependant on the plasma position during the current reversal process.

One of the future applications of this work is the plasma surface interaction studies. The ability to produce stable discharges lasting more than one second enables ISTTOK to produce plasma surface interaction studies similar (at smaller scale) to linear plasma machines such as pilot-PSI [65] and magnum-PSI [66]. Figure 114 depicts the result of a test with a tungsten piece exposed to ISTTOK plasma at $r = 65$ mm.

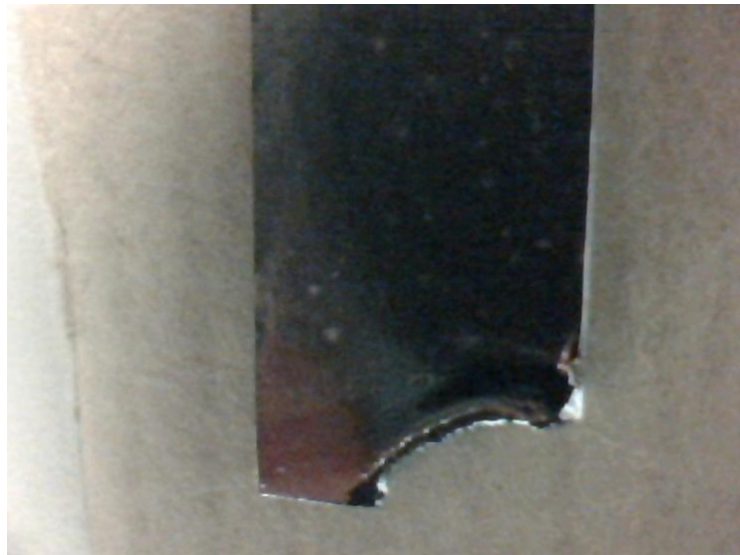


Figure 114 – Partial meltdown of a tungsten piece after exposure to the ISTTOK AC discharges. The dimensions of this tungsten piece are 7 mm x 25 mm x 0.3 mm.

After this work, the natural evolution of the ISTTOK tokamak is the envisaged power supplies upgrade in order to further extend the AC discharges duration. A substantial improvement in the discharge time duration will present serious challenges regarding the magnetic field coils temperature, where high temperature super-conducting coils is being evaluated as a possible solution [67]. With this upgrade, other issues become more and more important such; (i) the impurity content evolution during long AC operation, (ii) wall recycling and saturation (described in the TRIAM-1M tokamak team paper [68]) and (iii) plasma facing components thermal behaviour. Regarding the plasma facing components, the ISTTOK tokamak has performed several tests with a liquid metal limiter. This liquid limiter based on a gallium jet has provided an efficient method to handle the limiter heat load without perturbing the experiment [69][70][71].

Acknowledgements

This work has been sponsored by the Contract of Association between European Atomic Energy Community and Instituto Superior Técnico (IST) and by the Contract of Associated Laboratory between Fundação para a Ciência e Tecnologia (FCT) and IST. Some of the work developed was within the technical contract granted by IAEA (CRP F1.30.14) on “Utilization of the Network of Small Magnetic Confinement Fusion Devices for Mainstream Fusion Research”.

The content of publication is the sole responsibility of the author and it does not necessarily represent the views of the European Union or FCT.

Bibliography

- [1] “JET tokamak,” [Online]. Available: <http://www.efda.org/jet/>. [Acedido em 2013].
- [2] “National Ignition Facility,” [Online]. Available: <https://lasers.llnl.gov/>. [Acedido em 2013].
- [3] E. I. Moses, “The National Ignition Facility: Ushering in a new age for high energy density science,” *Phys. Plasmas*, vol. 16, 2009.
- [4] HiPER, “<http://www.hiper-laser.org/>,” [Online]. [Acedido em 2013].
- [5] D. Batani, “The HiPER project for inertial confinement fusion and some experimental results on advanced ignition schemes,” *Plasma Phys. Control. Fusion*, vol. 53, 2011.
- [6] A. W. Morris, “MAST: Results and Upgrade Activities,” *IEEE Transactions on Plasma Science*, vol. 40, pp. 682-691, 2012.
- [7] J. Harris, “A flexible heliac configuration,” *Nucl. Fusion*, vol. 25, 1985.
- [8] T. Klinger, “Towards assembly completion and preparation of experimental campaigns of Wendelstein 7-X in the perspective of a path to a stellarator fusion power plant,” *Fusion Engineering and Design*, 2013.
- [9] K. Ikeda, “Progress in the ITER Physics Basis,” *Nuclear Fusion*, vol. 47, 2007.
- [10] International Atomic Energy Agency, ITER Technical Basis, 2002.
- [11] International Atomic Energy Agency, “ITER physics basis,” *Nuclear Fusion*, vol. 39, pp. 2137-2638, 1999.
- [12] International Atomic Energy Agency, “Progress in the ITER Physics basis,” *Nuclear Fusion*, vol. 47, 2007.
- [13] International Thermonuclear Experimental Reactor (ITER), “<http://www.iter.org>,” [Online]. [Acedido em 2013].
- [14] IFMIF, “<http://www.ifmif.org/>,” [Online]. [Acedido em 2013].
- [15] E. Bertolini, “The JET project: progress towards a Tokamak thermonuclear reactor,” *Power Engineering Journal*, vol. 7, 1993.
- [16] E. Volker, “The W7-X project: scientific basis and technical realization,” *Fusion Engineering*, 1997.

- [17] J. A. Wesson, Tokamaks, Clarendon Press, 2004.
- [18] R. Albanese, "Plasma response models for current, shape and position control in JET," *Fusion Engineering and Design*, 2003.
- [19] J. P. Goedbloed, Advanced Magnetohydrodynamics (With Applications to Laboratory and Astrophysical Plasmas), Cambridge university press, 2010.
- [20] R. Albanese, "Prediction of the growth rates of VDEs in JET," *Nucl. Fusion*, vol. 44, 2004.
- [21] Y. Nakamura, "Mechanism of vertical displacement events in JT-60U disruptive discharges," *Nuclear Fusion*, vol. 36, 1996.
- [22] E. Lazarus, "Control of the vertical instability in tokamaks," *Nucl. Fusion*, vol. 30, 1990.
- [23] F. G. Rimini, "First Plasma Operation of the Enhanced JET Vertical Stabilisation System," *Fusion Engineering and Design*, vol. 86, 2011.
- [24] F. Sartori, "The System Architecture of the New JET Shape Controller," *Fusion Engineering and Design*, vol. 74, 2005.
- [25] A. Batista, "Atca digital controller hardware for vertical stabilization of plasmas in tokamaks," *Review of Scientific Instruments*, 2006.
- [26] R. Albanese, "Experimental results with an optimized magnetic field configuration for JET breakdown," *Nuclear Fusion*, vol. 52, 2012.
- [27] I. S. Carvalho, "ISTTOK control system upgrade," *Fusion Engineering and Design*, 2013.
- [28] I. S. Carvalho, "ISTTOK real-time architecture," *Fusion engineering and design (submitted under review)*, 2013.
- [29] I. S. Carvalho, "Real-time control for long ohmic alternate current discharges," *Fusion engineering and design (submitted under review)*, 2013.
- [30] J. Li, "Quasi-steady-state ac plasma current operation in HT-7 tokamak," *Nuclear Fusion*, vol. 47, p. 1071, 2007.
- [31] B. J. D. Tubbing, "AC Plasma Current Operation in the JET Tokamak," *Nuclear Fusion*, 1992.
- [32] C. Varandas, "Engineering aspects of the tokamak ISTTOK," *Fusion Technology*, 1996.
- [33] J. Cabral, "Operation of the tokamak ISTTOK in a multicycle alternating flat-top plasma current regime," *Nuclear Fusion*, 1997.
- [34] H. Fernandes, "Engineering aspects of the ISTTOK operation in a multicycle alternating flat-top plasma current regime," *Fusion Engineering and Design*, 1998.

- [35] A. Batista, "ATCA control system hardware for the plasma vertical stabilization in the JET tokamak," *Real Time Conference, 16th IEEE-NPSS*, pp. 308-313, 2009.
- [36] D. Valcárcel, "An ATCA embedded data acquisition and control system for the compass tokamak," *Fusion Engineering and Design*, vol. 84, 2009.
- [37] D. Valcárcel, "Real-time software for the compass tokamak plasma control," *Fusion Engineering and Design*, vol. 85, 2010.
- [38] B. Gonçalves, "ITER fast plant system controller prototype based on ATCA platform," *Fusion Engineering and Design*, vol. 87, 2012.
- [39] L. Frassinetti, "Spatial resolution of the JET Thomson scattering system," *Rev. Sci. Instrum.*, vol. 83, 2012.
- [40] S. Wiesen, "Integrated modelling of a JET type-I ELMy H-mode pulse and predictions for ITER-like wall scenarios," *Plasma Physics and Controlled Fusion*, vol. 53, 2011.
- [41] S. Tsau, "Real-time plasma boundary reconstruction in the KSTAR," *Fusion Engineering and Design*, vol. 82, 2007.
- [42] M. Razavi, "Designing a Sine-Coil for Measurement of Plasma Displacements in IR-T1 Tokamak," *Rev. Sci. Instrum.*, vol. 81, 2010.
- [43] A. Cormack, "Representation of a function by its line integrals, with some radiological applications," *Journal of Applied Physics*, vol. 34, p. 2722, 1963.
- [44] A. Cormack, "Representation of a function by its line integrals, with some radiological applications II," *Journal of Applied Physics*, vol. 35, p. 2908, 1964.
- [45] L. Wang, "A simplified expression for the Radon transform of Bessel basis function in tomography," *Review of Scientific Instruments*, vol. 62, p. 842–843, 1991.
- [46] L. Wang, "An analytical expression for the Radon transform of Bessel basis function in tomography," *Review of Scientific Instruments*, vol. 62, p. 1115–1116, 1991.
- [47] P. Carvalho, "ISTTOK plasma control with the tomography diagnostic," *Fusion Engineering and Design*, vol. 85, pp. 266-271, 2010.
- [48] C. Silva, "Characterization of the poloidal asymmetries in the ISTTOK edge plasma," *Plasma Phys. Control. Fusion*, vol. 53, 2011.
- [49] C. Silva, "Interaction between mean and fluctuating $E \times B$ shear flows on the ISTTOK edge plasma," *Plasma Phys. Control. Fusion*, vol. 54, 2012.
- [50] S. Vergamota, Interferometria de micro-ondas no tokamak ISTTOK, vol. Master's thesis,

Instituto Superior Técnico, 1993.

- [51] R. B. Henriques, "New detection system and signal processing for the tokamak ISTTOK," *Rev. Sci. Instrum.*, vol. 83, 2012.
- [52] M. Brix, "Recent improvements of the JET lithium beam diagnostic," *Rev Sci Instrum.*, vol. 83, 2012.
- [53] I. S. Nedzelskiy, "Compact retarding field energy analyzer for the tokamak ISTTOK boundary plasma," *Rev. Sci. Instrum.*, vol. 76, 2006.
- [54] R. B. Gomes, "High dispersion spectrometer for time resolved Doppler measurements of impurity lines emitted during ISTTOK tokamak discharges," *Rev. Sci. Instrum.*, vol. 74, 2003.
- [55] P. Carvalho, "Fast tomographic methods for the tokamak isttok," em *Prooceedings of the 17th IAEA TM on RUSFD*, 2007.
- [56] P. Carvalho, "Tomographic visualization for plasma position control in isttok," *IEEE Transactions on Plasma Science*, 2008.
- [57] I. S. Carvalho, "Fast controlled digital link for a tokamak current source control," em *Proceedings of the IEEE 19th International Symposium on Power Electronics, Electrical Drives, Automation and Motion (Speedam)*, 2008.
- [58] D. Valcárcel, Controlo em tempo real da posição da coluna de plasma no tokamak ISTTOK, Master thesis, Instituto Superior Técnico, 2008.
- [59] D. Valcárcel, "Validation of isttok plasma position controller," em *Proceedings of the 17th IAEA Technical Meeting on Research Using Small Fusion Device*, 2007.
- [60] A. Neto, "Firesignal - data acquisition and control system software," *Fusion Engineering and Design*, 2007.
- [61] PICMG. [Online]. Available: <http://www.picmg.org/>.
- [62] A. Neto, "MARTE: a Multi-Platform Real-Time Framework," *16th IEEE NPSS Real Time Conference*, 2009.
- [63] H. Juan, "Wall recycling in long duration discharges on HT7-Tokamak," *Plasma Science and Technology*, vol. 7, 2005.
- [64] A. Winter, "Status of the ITER Plasma Control System Conceptual Design," *Proceedings of ICALEPS*, 2009.
- [65] K. Bystrov, "Erosion yields of carbon under various plasma conditions in Pilot-PSI," *Journal*

of Nuclear Materials, vol. 415, 2011.

- [66] A. Kleyn, "Plasma–surface interaction in ITER," *Vacuum*, vol. 80, 2006.
- [67] H. Fernandes, "Toroidal high temperature superconducting coils for ISTTOK," *Fusion Engineering and Design*, vol. 86, p. 1458–1461, 2011.
- [68] M. Sakamoto, "Global particle balance and wall recycling properties of long duration discharges on TRIAM-1M," *Nuclear Fusion*, vol. 44, 2004.
- [69] R. B. Gomes, "ISTTOK tokamak plasmas influence on a liquid gallium jet dynamic behavior," *Journal of Nuclear Materials*, 2011.
- [70] R. B. Gomes, "Interaction of a liquid gallium jet with the tokamak ISTTOK edge plasma," *Fusion Engineering and Design*, vol. 83, 2008.
- [71] R. B. Gomes, "Liquid gallium jet–plasma interaction studies in ISTTOK tokamak," *Journal of Nuclear Materials*, 2009.
- [72] J. Weiland, *Collective Modes in Inhomogeneous Plasmas*, IOP, 2000.
- [73] V. Shafranov, "Plasma equilibrium in a tokamak," *Nuclear Fusion*, vol. 11, 1971.
- [74] O. Mitarai, "Alternating current tokamak reactor with long pulses," *Fusion Technology*, 1989.
- [75] M. Huart, "AC operation of JET tokamak: modification of the JET poloidal field system," in *Proceedings of the 14th IEEE Symposium of Fusion Engineering*, 1991.
- [76] H. Fernandes, *Operação Indutiva do Tokamak ISTTOK*, Master thesis, IST, 1993.
- [77] B. Carvalho, *Real-Time Control of the ISTTOK Tokamak*, PhD thesis, Instituto Superior Técnico, 2003.
- [78] G. F. Franklin, *Feedback Control of Dynamic Systems*, Addison-Wesley Publishing Company.
- [79] Y. Peng, "Anti-windup, bumpless, and conditioned transfer techniques for pid controllers," *IEEE Control Systems Magazine*, 1996.
- [80] O. Mitarai, "Plasma density at the current reversal in the STOR-1M tokamak with AC operation," *Nuclear fusion*, 1992.
- [81] O. Mitarai, "Alternating current tokamak reactor with long pulses," *Fusion Technology*, vol. 15, p. 204, 1989.
- [82] W. Gao, "Study of impurity behaviour in ac plasma on the HT-7 tokamak," *Plasma Phys.*

Control. Fusion, vol. 50, 2008.

- [83] I. Hutchinson, *Principles of Plasma Diagnostics*, Cambridge University Press.
- [84] P. Stangeby, *The Plasma Boundary of Magnetic Fusion Devices*, Taylor & Francis.
- [85] C. Silva, “Control of the edge turbulent transport by emissive electrode biasing on the tokamak ISTTOK,” *Plasma Phys. Control. Fusion*, vol. 48, 2006.
- [86] C. Silva, “Improved confinement events triggered by emissive electrode biasing on the tokamak ISTTOK,” *Nuclear Fusion*, vol. 44, 2004.
- [87] J. tokamak, “<http://www.efda.org/jet/>,” [Online].
- [88] M. Miyamoto, “Material properties of co-deposition formed on plasma facing materials in all-metal machine TRIAM-1M,” *Journal of Nuclear Materials*, 2003.
- [89] E. Tsitrone, “Key plasma wall interaction issues towards steady state operation,” *Journal of Nuclear Materials*, 2007.
- [90] Mukhovatov V. S., “Plasma equilibrium in a Tokamak,” *Nucl. Fusion*, vol. 11, 1971.
- [91] W. Horton, “Drift waves and transport,” *Reviews of Modern Physics*, vol. 71, 1999.
- [92] M. L. Walker, *IEEE Control Systems Magazine*, vol. 26, 2006.
- [93] B. Carvalho, “A low cost, real-time dsp based diagnostic for the control of operation of a fusion experiment,” *Review of Scientific Instruments*, 2003.

Acronyms

AC – Alternate Current

ADC – Analogue to Digital Converter

AMC – Advanced Mezzanine Card

API – Application programming interface

ASDEX – Tokamak located in Germany

ATCA – Advanced Telecommunications Computing Architecture

ATM – Asynchronous Transfer Mode (telecommunications and computer network)

ATX - Advanced Technology eXtended (motherboard form factor)

CDB - Configuration DataBase (configuration file for MARTe)

CISC – Complex Instruction Set Computing

COMPASS – Tokamak located in Czech Republic

CPU - Central Processing Unit

D – Deuterium (hydrogen isotope)

DAC – Digital to Analogue Converter

DC – Direct Current

DDB – Dynamic Data Buffer (related to MARTe)

DMA – Direct Memory Access

ELM – Edge Localised Mode

EMF – ElectroMotive Force

EPICS - Experimental Physics and Industrial Control System (software)

FIFO – First In, First Out (data buffer manipulation)

GAM – Generic Application Module (related to MARTe)

GMACS - Giga Multiply-Accumulate Operations per Second

HDD – Hard Disk Drive

HIB – Heavy Ion Beam

HMI – Human-Machine Interface

HT-7 – Tokamak in China

HTML – HyperText Markup Language

HTTP – Hypertext Transfer Protocol

IGBT – Insulated-Gate Bipolar Transistor

IOGAM – Input Output Generic Application Module (related to MARTe)

IPMC – Intelligent Platform Management Controller (related to ATCA)

ISTTOK – Tokamak in Portugal

ITER – International Thermonuclear Experimental Reactor (tokamak under construction)

JET – Joint European Torus (Tokamak in the UK)

LCFS – Last Closed Flux Surface (related to tokamak physics)

LED – Light-Emitting Diode

MARTE - Multi-threaded Application Real-Time executor

MHD – Magneto-Hydro-Dynamics (related to tokamak physics)

MIMO – Multiple-Input Multiple-Output

MIPS - Peripheral Component Interconnect

M-LVDS - Multipoint Low-Voltage Differential Signalling

MOSFET - Metal–Oxide–Semiconductor Field-Effect Transistor
NBI – Neutral Beam Injection
PC – Personal Computer
PCB – Printed Circuit Board
PCI - Peripheral Component Interconnect
PCIe – Peripheral Component Interconnect Express
PICMG - PCI Industrial Computer Manufacturers Group
PID - Proportional-Integral-Derivative (controller)
PS – Power Supply
PWM - Pulse-Width Modulation
RF – Radio Frequency
RFEA – Retarding Field Energy Analyser
RISC – Reduced Instruction Set Computing
RTAI - Real-Time Application Interface (real-time extension for the Linux kernel)
RTM - Rear Transition Module
RTTh – Real Time Thread
SFP - Small Form-factor Pluggable
T – Tritium (hydrogen isotope)
UART - Universal Asynchronous Receiver/Transmitter
UDP - User Datagram Protocol
UV – Ultra Violet
VME – Versa Module Eurocard
VS – Vertical Stabilisation
XML - eXtensible Markup Language

Annexes

ISTTOK power supplies communication protocol:

This protocol is used for the communication between the power supplies controller and the ATCA crate. This bespoke protocol is aimed to ensure higher reliability on the most significant bits of each message. In case of ISTTOK, this protocol is used for controlling the primary, vertical and horizontal field power supplies and each of these power supplies has one individual controller.

Specifications:

1. The power supplies communication protocol (PSCP) uses two separate bytes to receive and transmit information.
2. Each byte has 8 bits plus one odd parity bit.
3. Each byte has a single start bit and a double stop bit.
4. The communication baud rate is set to 921600 Baud.
5. The first byte is identified with a “0” on the 8th bit and the second byte is identified with a “1” in the 8th bit.
6. There are special commands for “charge”, “start operation”, “stop operation” and “shutdown”.
7. After the “charge” command the power supplies controller (PSC) reply with the status of the initiative.
8. After the “shutdown” command the PSC also reply with the status of that initiative.
9. After the “start operation” command the PSC reply with “started ok” or with the specific impediment. If a start operation is sent during operation the reply will be a “started ok”
10. After the stop operation the PSC should reply with “stopped” message. If a repeated “stop operation” command is sent when the PSC is already on idle mode (stopped or shutdown) the answer will be also “stopped”.
11. If there is a problem during the operation the PSC will send twice the error found and will enter in the auto shutdown mode.
12. A shutdown command during operation will trigger the stop operation and shutdown modes but the PSC will only reply on the stop operation.
13. Normally the communication is started by the plasma shape control unit with the exception of an error report as seen in the point 11 of this specification.
14. If the PSC don’t receive a valid instruction they will reply with a “command error” instruction.
15. During operation mode the PSC receive the desired current set-point in a 10-bit linear format (-1500A -> 0 value, 0A -> 511 value, 1500A -> 1022 value).
16. If the power supplies don’t have a capacitor bank the charge and shutdown instructions are not available and the power supplies status is similar to always charged. (the charge and shutdown commands are not available and will be considered as communication error)

Instructions for the power supplies controller:

Start operation instruction:

8 th bit	7 th bit	6 th bit	5 th bit	4 th bit	3 rd bit	2 nd bit	1 st bit	HEX
1	1	1	1	1	1	1	0	FE
1	1	1	1	1	1	1	1	FF

Comments: enters operation mode

Stop operation instruction:

8 th bit	7 th bit	6 th bit	5 th bit	4 th bit	3 rd bit	2 nd bit	1 st bit	HEX
0	0	0	0	0	0	0	0	00
0	0	0	0	0	0	0	1	01

Comments: exits operation mode.

During operation instructions:

8 th bit	7 th bit	6 th bit	5 th bit	4 th bit	3 rd bit	2 nd bit	1 st bit	HEX
a ₂	a ₁	a ₀	-a ₉	-a ₈	-a ₇	-a ₆	0	----
a ₉	a ₈	a ₇	a ₆	a ₅	a ₄	a ₃	1	----

Comments:

- The “-“ signal denotes the complementary bit. Example a₉= 1 then “-a₉” is equal to “0”
- The ADC value has 10-bit format (from 0 to 1022). 1023 is reserved
- 0 value correspond to a set-point of -1500 Ampere.
- 511 value corresponds to a set-point of 0 A.
- 1023 value corresponds to a set-point of 1500 A.
- All other values are interpolated.

Replies from the power supplies:

During operation instructions:

8 th bit	7 th bit	6 th bit	5 th bit	4 th bit	3 rd bit	2 nd bit	1 st bit	HEX
a ₂	a ₁	a ₀	-a ₉	-a ₈	-a ₇	-a ₆	0	----
a ₉	a ₈	a ₇	a ₆	a ₅	a ₄	a ₃	1	----

Comments:

- Outputs the value read on the ADC of the power supplies.
- The ADC value has 10-bit format (from 0 to 1022). 1023 is reserved

- 0 value corresponds to a set-point of -1500 Ampere.
- 511 value corresponds to a set-point of 0 A.
- 1022 value corresponds to a set-point of 1500 A.
- All other values are interpolated.

Temperature fault instruction:

8 th bit	7 th bit	6 th bit	5 th bit	4 th bit	3 rd bit	2 nd bit	1 st bit	HEX
1	0	1	1	0	1	1	0	B6
1	0	1	1	0	1	1	1	B7

Comments: overheat of the H-bridge

24V failure (future implementation) instruction:

8 th bit	7 th bit	6 th bit	5 th bit	4 th bit	3 rd bit	2 nd bit	1 st bit	HEX
0	1	0	0	1	0	0	0	48
0	1	0	0	1	0	0	1	49

Comments: 24V SMPS are not active, not possible to start a shot.

Start ok instruction:

8 th bit	7 th bit	6 th bit	5 th bit	4 th bit	3 rd bit	2 nd bit	1 st bit	HEX
1	1	1	1	1	1	1	0	FE
1	1	1	1	1	1	1	1	FF

Comments: the power supply is ready to receive set-point commands

Stopped instruction:

8 th bit	7 th bit	6 th bit	5 th bit	4 th bit	3 rd bit	2 nd bit	1 st bit	HEX
0	0	0	0	0	0	0	0	00
0	0	0	0	0	0	0	1	01

Comments: power supply controller is on idle mode.

Stop error (not frequent and possibly not implemented) instruction:

8 th bit	7 th bit	6 th bit	5 th bit	4 th bit	3 rd bit	2 nd bit	1 st bit	HEX
0	0	1	0	0	1	0	0	24
0	0	1	0	0	1	0	1	25

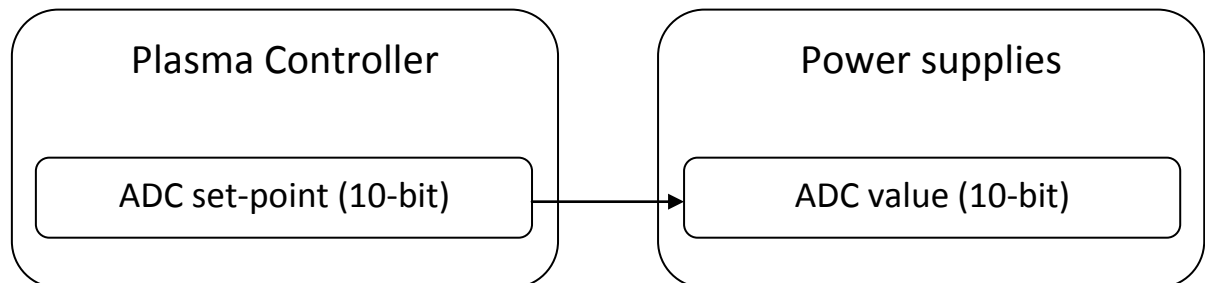
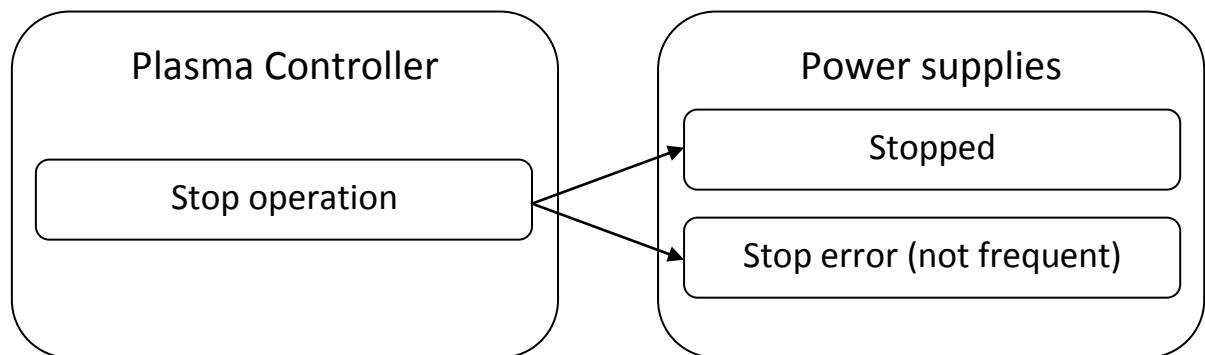
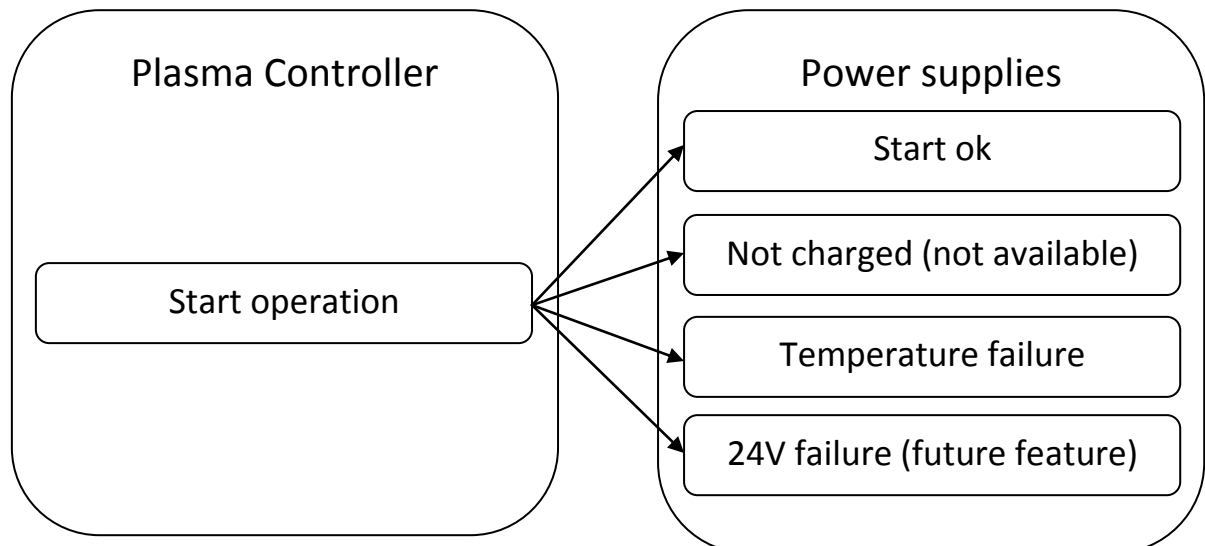
Comments: some error occurred during stop (not a problem the watch dog timer will reset the operation).

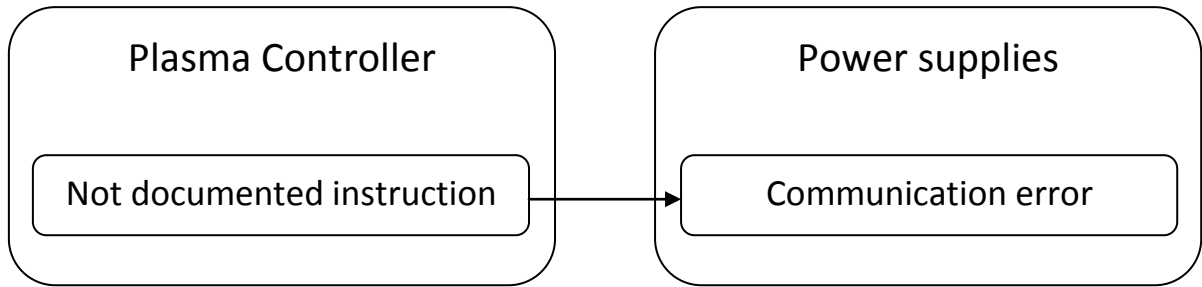
Communications error instruction:

8 th bit	7 th bit	6 th bit	5 th bit	4 th bit	3 rd bit	2 nd bit	1 st bit	HEX
1	1	0	1	1	0	1	0	DA
1	1	0	1	1	0	1	1	DB

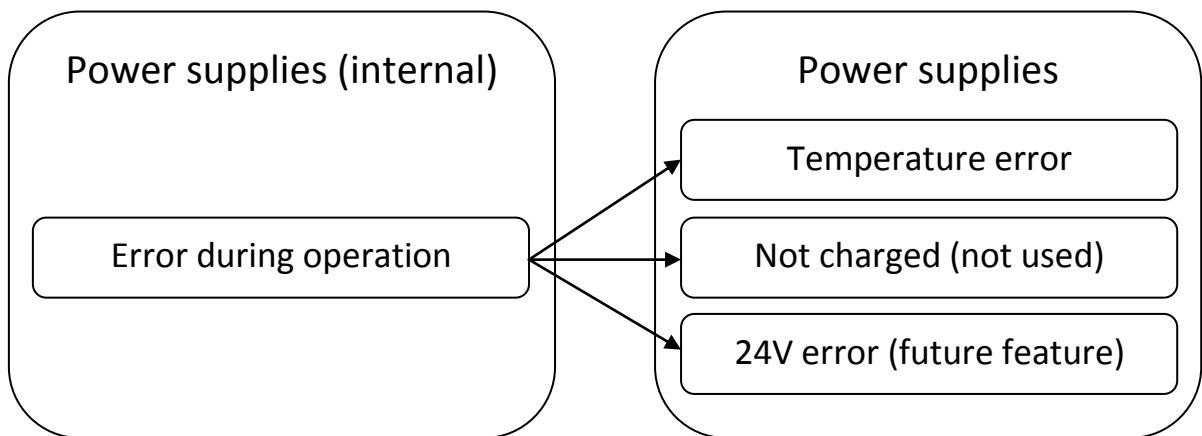
Comments: instruction was not recognized by the power supply controller.

Normal communication from Plasma position controller to power supplies:



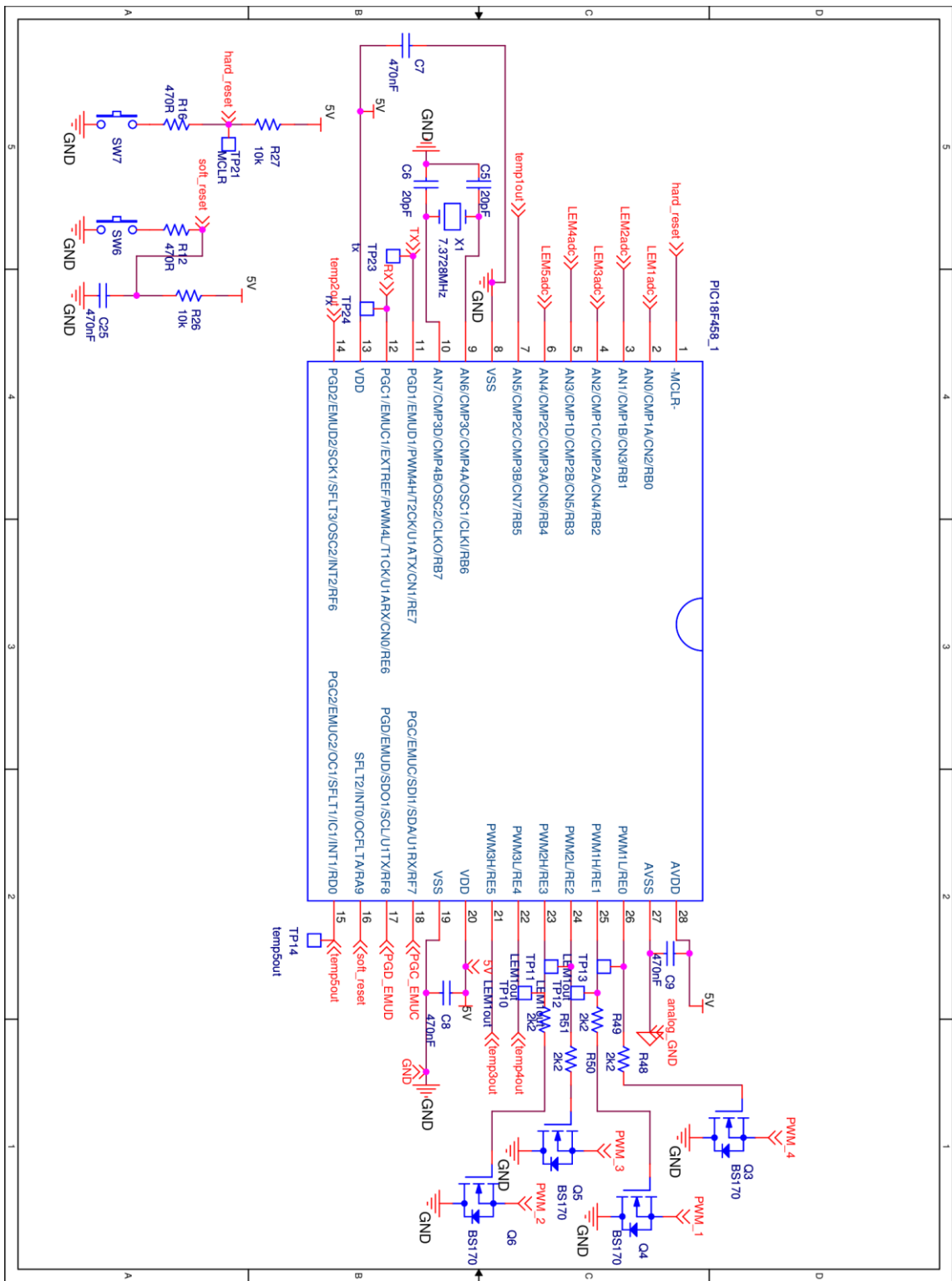


Exceptional communications from the power supplies:

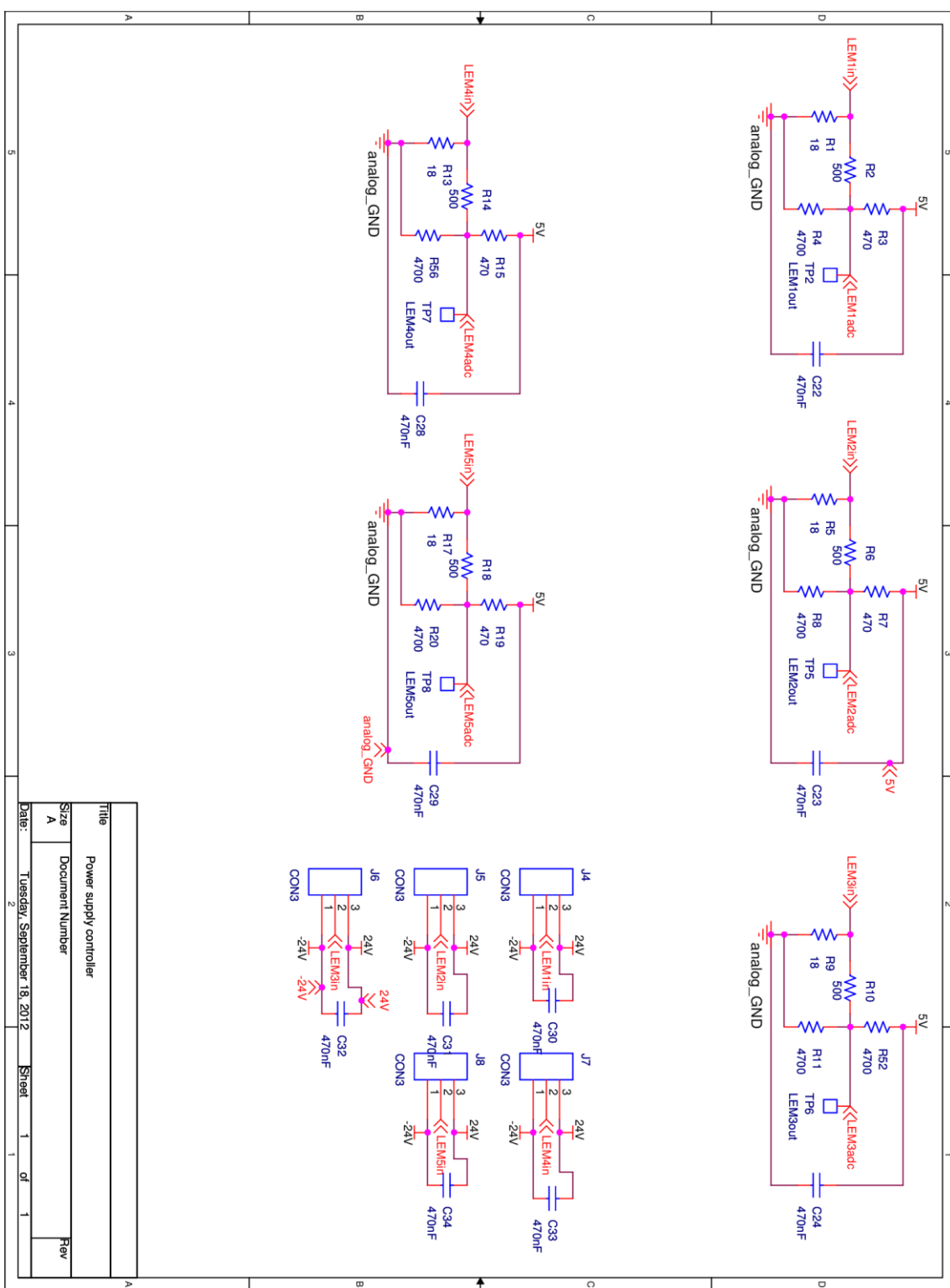


Schematics (power supplies controller)

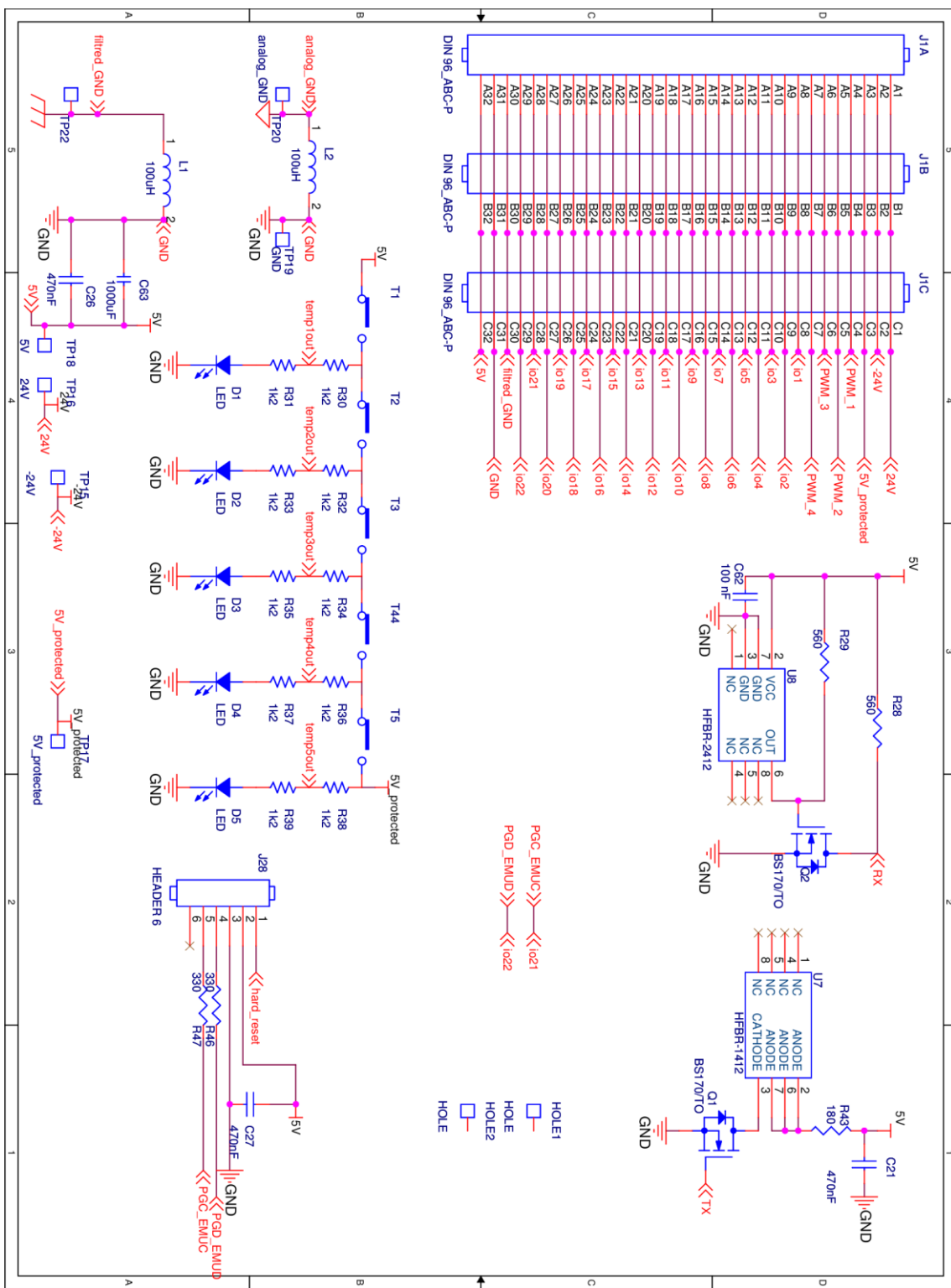
Controller board - 1



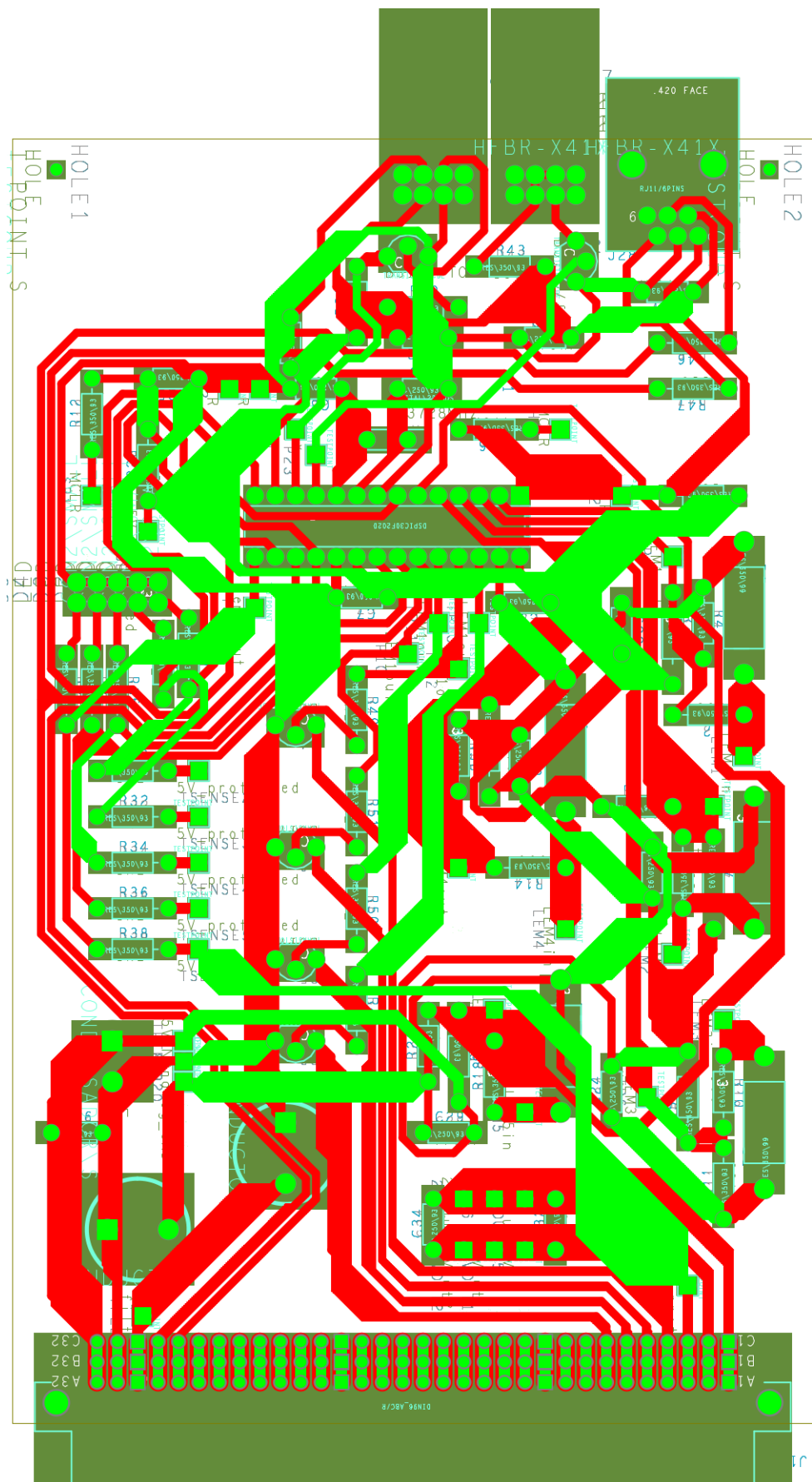
Controller board - 2



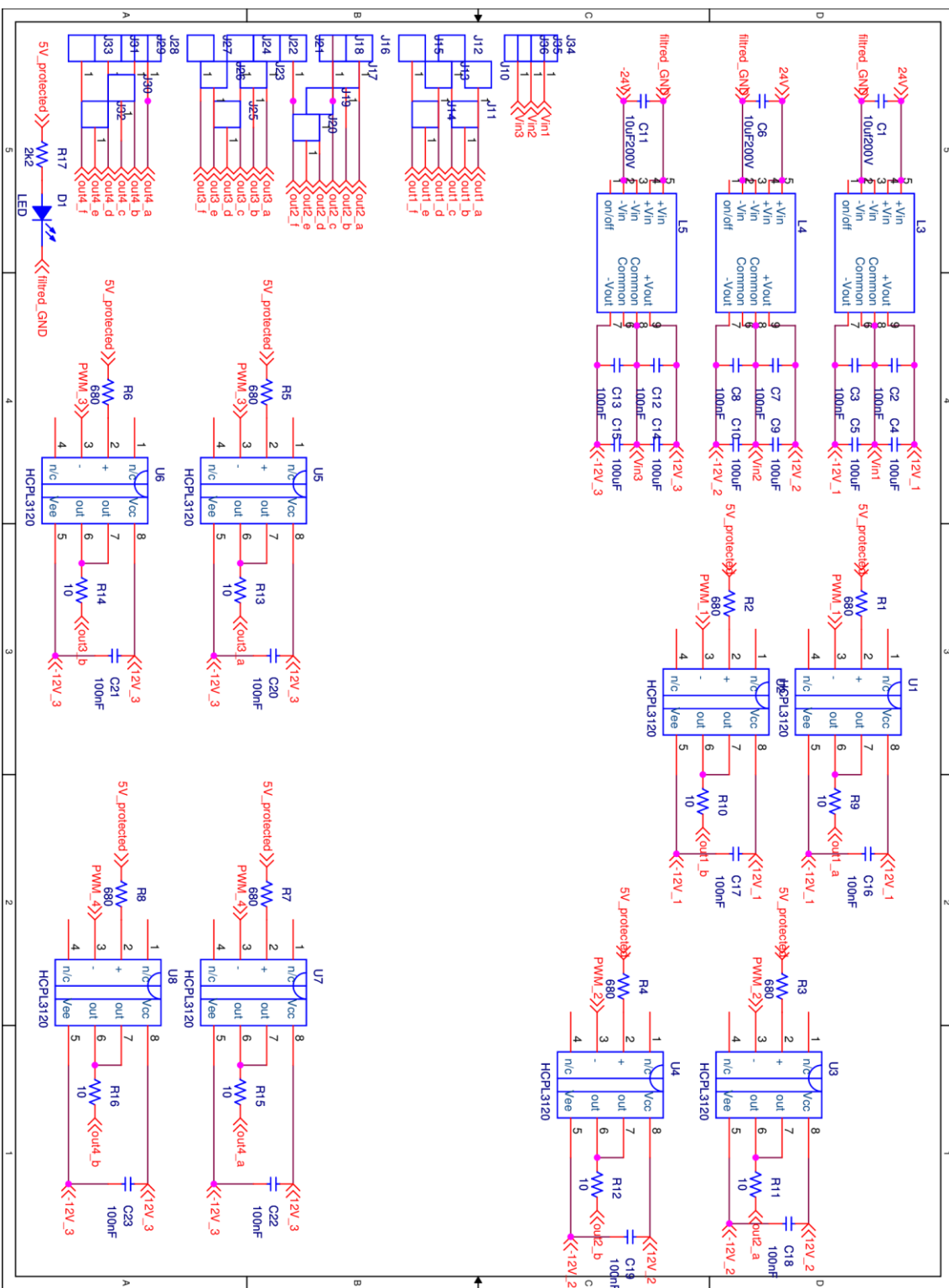
Controller board - 3



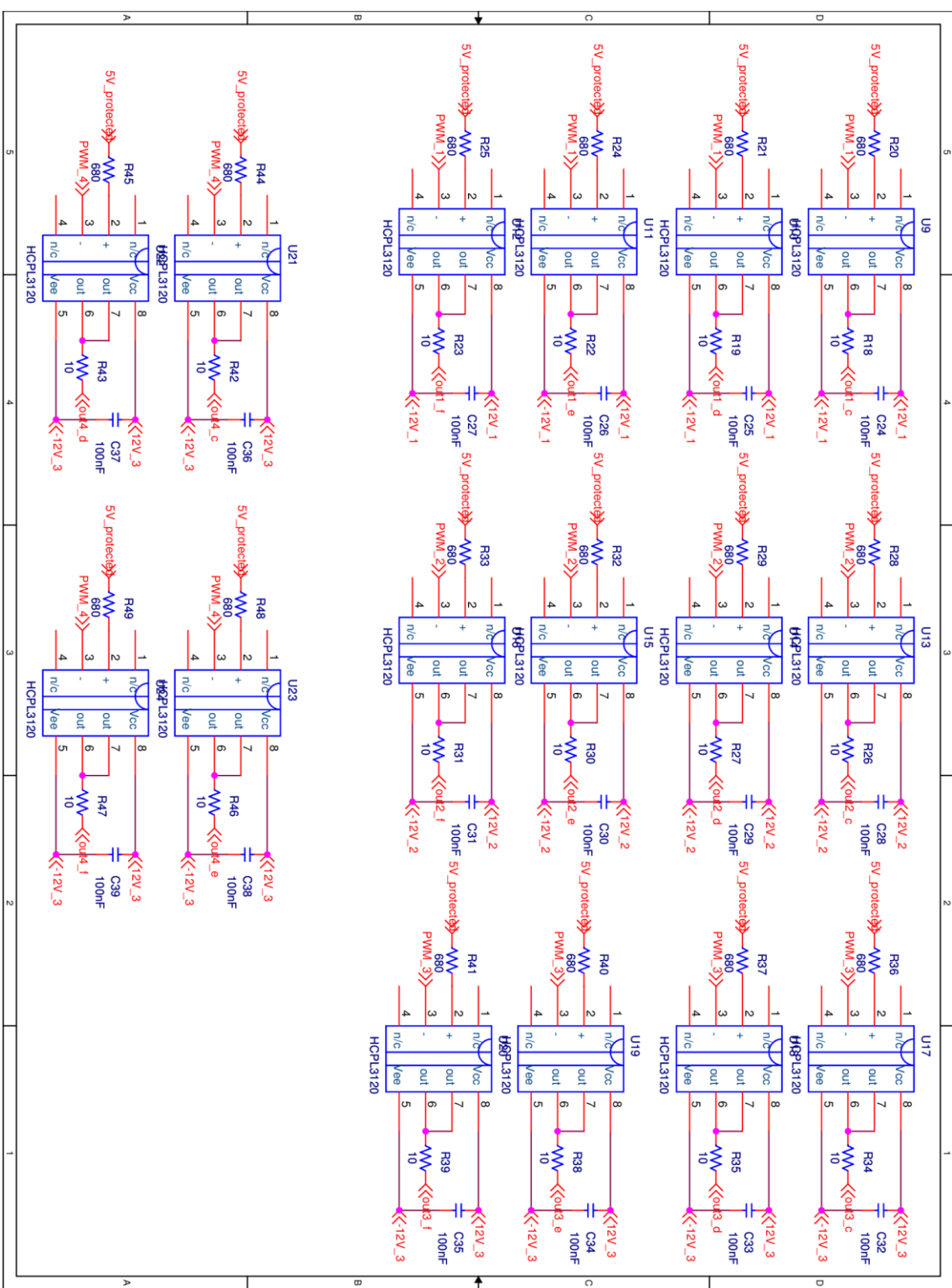
Controller board - PCB



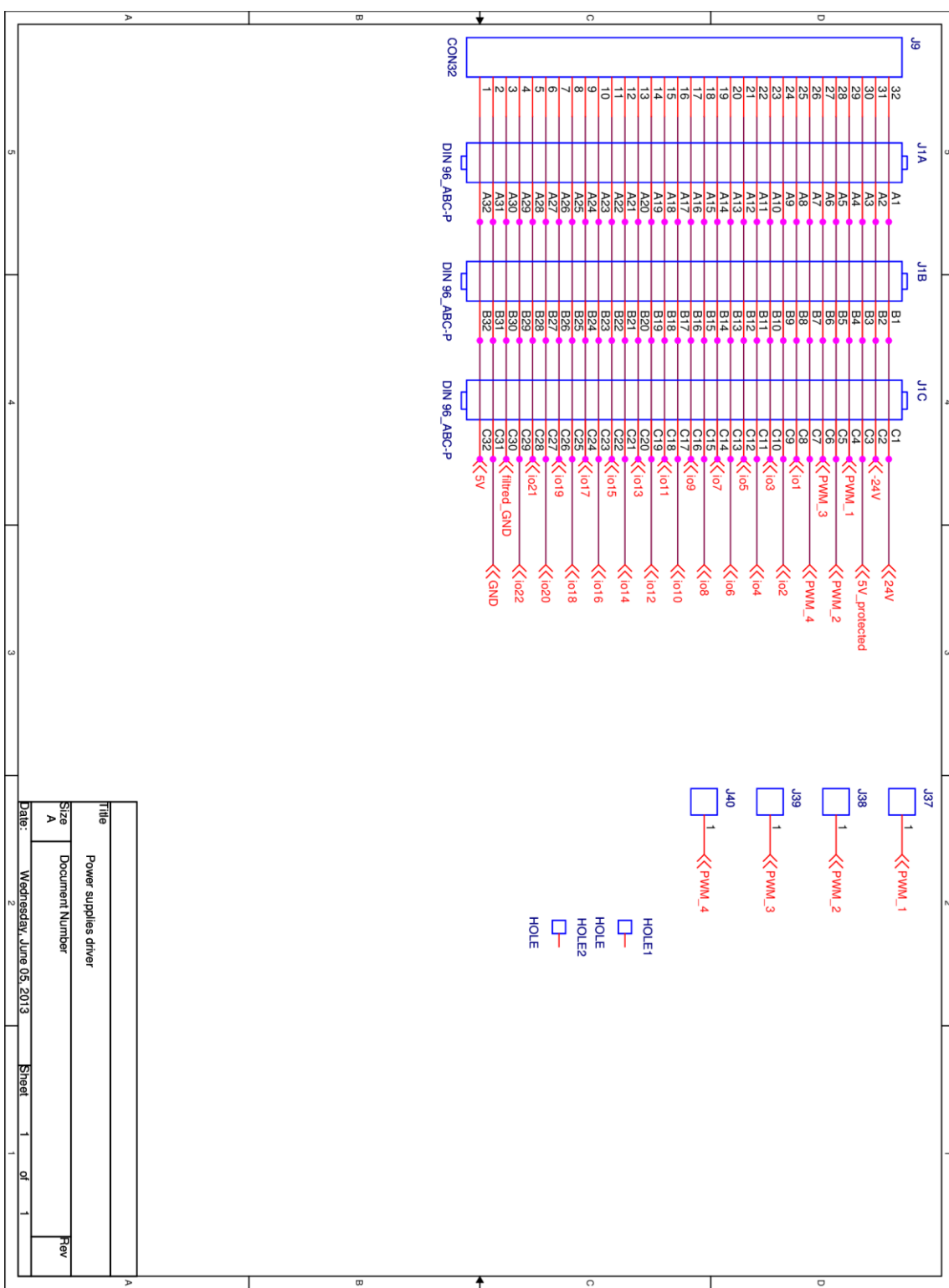
Driver board - 1



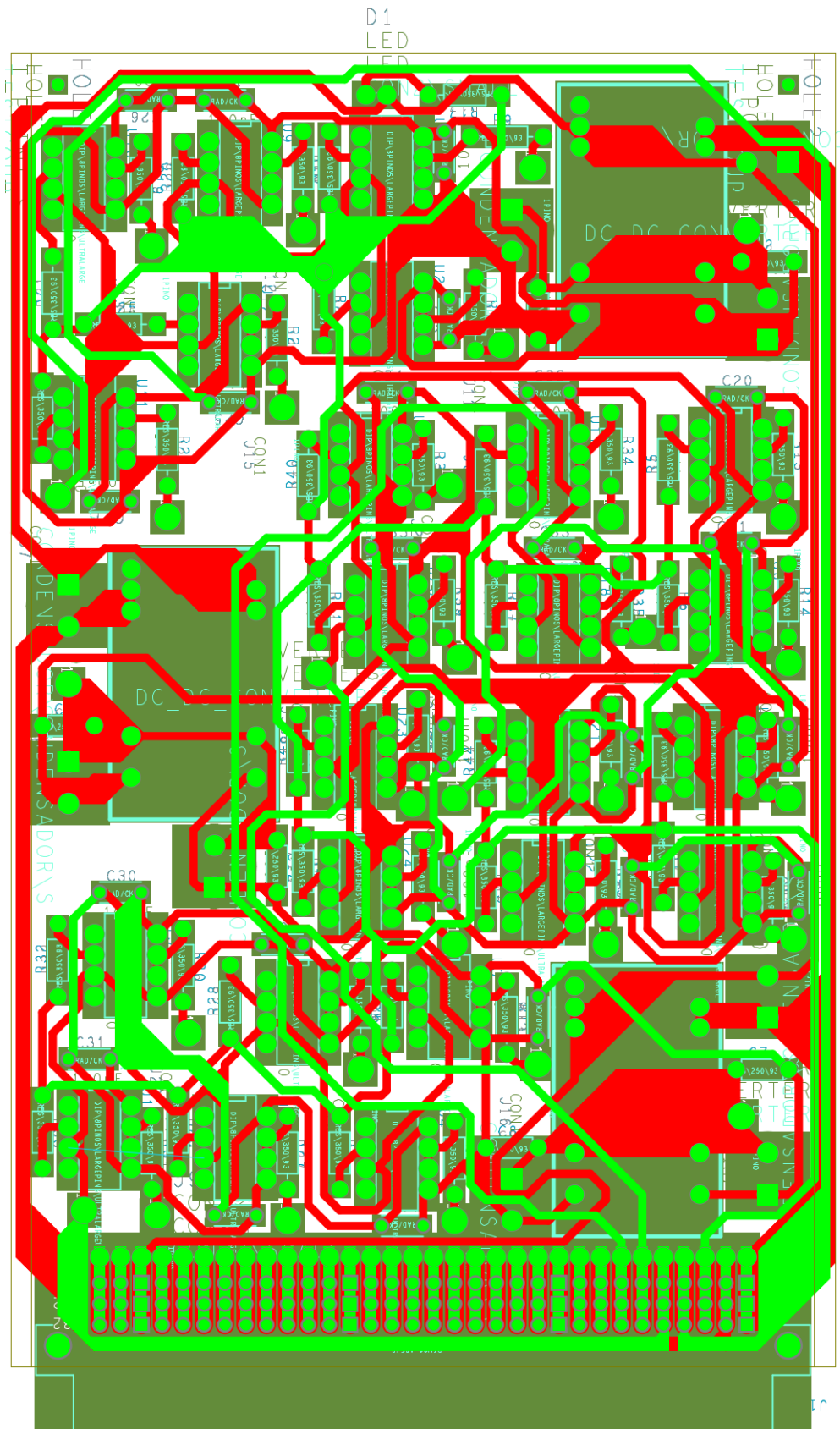
Driver board - 2



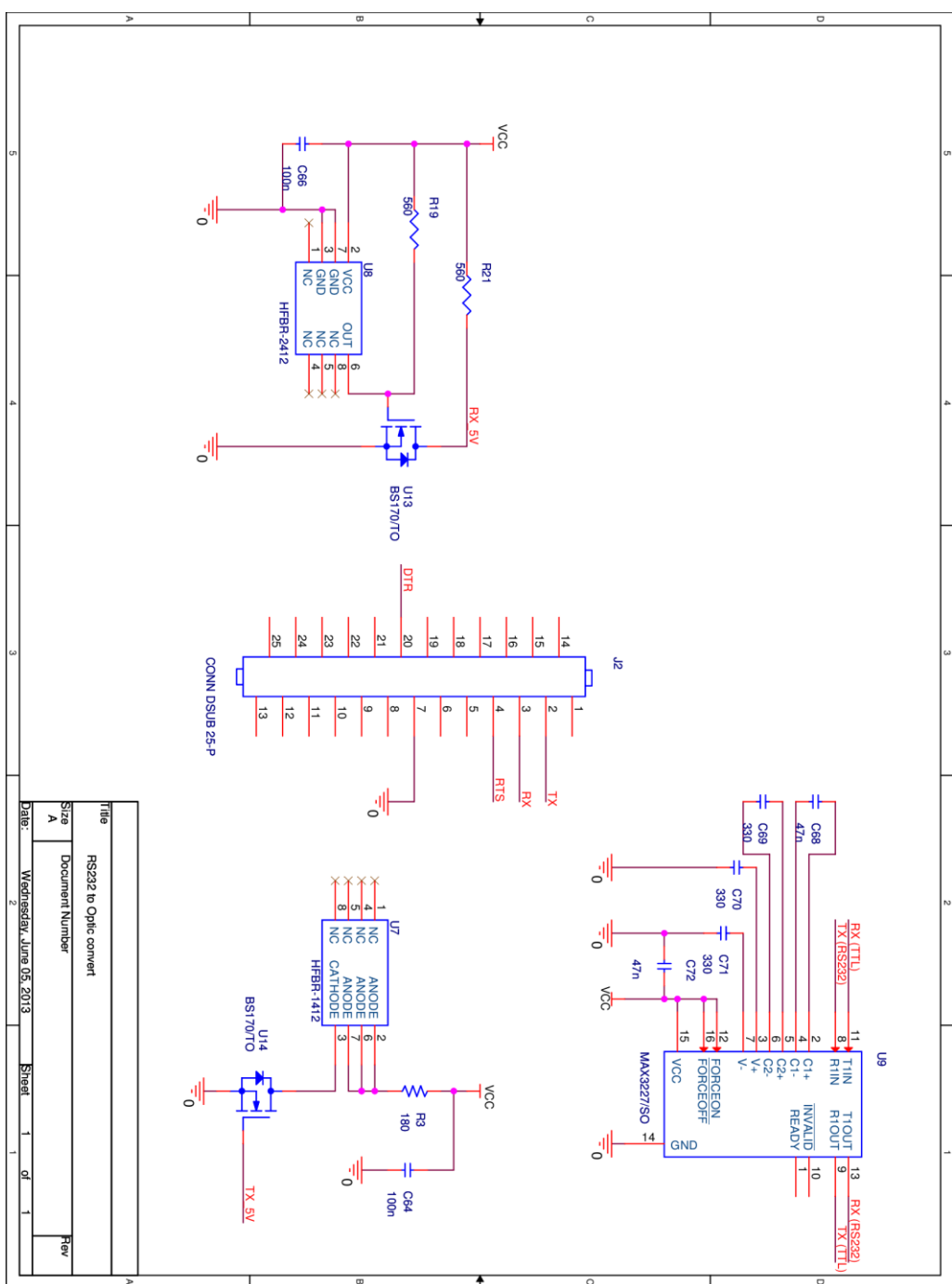
Controller board – 3



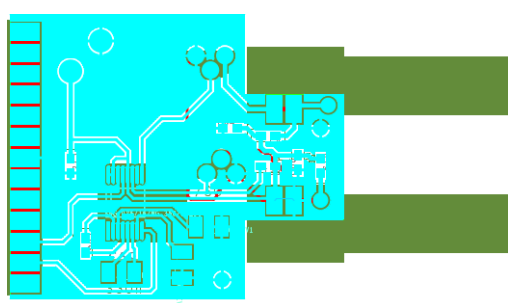
Driver board – PCB



Serial to optic board



Serial to optic board - PCB



Backplane board – PCB

